Development and Reduction of a Multicomponent Reference Fuel for Gasoline

Von der Fakultät für Maschinenbau, Elektro- und Energiesysteme
der Brandenburgischen Technischen Universität Cottbus - Senftenberg
zur Erlangung des akademischen Grades eines
Doktors der Ingenieurwissenschaften
genehmigte Dissertation

vorgelegt von
Dipl. Ing.
Lars Seidel
geboren am 8. Juli 1983 in Merseburg (Saale)

Vorsitzender: Prof. Dr.-Ing. Heiko Schmidt
Gutachter: Prof. Dr. Terese Løvås
Gutachter: Prof. Dr.-Ing. Fabian Mauß
Tag der mündlichen Prüfung: 4. Mai 2017

Jedesmal, wenn durch einen experimentellen Befund ein Widerspruch mit der bestehenden Theorie festgestellt ist, kündigt sich ein neuer Fortschritt an; denn dann wird eine Veränderung und Verbesserung der Theorie notwendig. Die Frage aber, an welchem Punkt und in welcher Weise diese Veränderung vorzunehmen ist, bietet oft große Schwierigkeiten.

Max Planck - Sinn und Grenzen der exakten Wissenschaft

Contents

1 Abstract - Objective of this thesis

Within this thesis, a detailed multicomponent gasoline surrogate reaction scheme was developed and reduced to a four component scheme of skeletal size. The main target is to cover the most important features for typical spark ignited (SI) combustion - flame propagation, emission formation and the tendency to auto ignite and subsequently cause engine knock. To achieve this a variable mechanism concept was developed to include sub models for different fuels as needed. Using this approach a detailed mechanism describing the oxidation of n-heptane, iso-octane, toluene and ethanol was compiled and compared against various experiments published in literature. Furthermore, correlations were developed to suggest four component gasoline surrogates based on typical fuel data sheets. The correlation method is validated against measurements in the Cooperative Fuel Research (CFR) engine from various groups and further compared against correlations between octane numbers (ON) and predicted 0D ignition delay times. These correlations are used to identify and discuss the impact of the uncertainty of two reactions on ignition delay time of a multicomponent fuel. To be able to reduce the detailed scheme in a time efficient way existing reduction concepts where improved and applied to different schemes and targets. Since various reduction techniques are available, an optimal sequence of those was worked out. Using this sequence of reduction steps two multicomponent schemes were compiled: one scheme for the prediction of laminar flame speeds and one for the prediction of major emissions and auto-ignition. To underline that the suggested reduction procedure is universal it was also applied to n-heptane as single fuel surrogate for diesel fuel and to a large two component fuel from another work group.

1.1 Publications related to this PhD thesis

At the time of submitting the PhD thesis I published several works in the field of combustion and chemistry modelling. While this thesis is written as autonomous monography the work is related to previous publications. The scheme presented herein is based on the work of Oßwald et. al. (2011), Schenk et al. (2013), Nawdiyal et al. (2015) and Seidel et al. (2015). A flow chart outlining the connection between those and previous works from other authors is shown in figure 13. All publications which are (co-)authored by myself are treated as any other publication.

Publications in reviewed journals and proceedings:

1. Oßwald, P., Kohse-Höinghaus, K., Struckmeier, U., Zeuch, T., Seidel, L., Leon, L., and Mauss, F., "Combustion chemistry of the butane isomers in premixed low-pressure flames", Z. Phys. Chem. 225, pp. 1029–1054, 2011

2. Schenk, M., Leon, L., Moshammer, K., Oßwald, P., Kohse-Höinghaus, K., Zeuch, T., Seidel, L., Mauss, F., "Detailed mass spectrometric and modelling study of isomeric butene flames", Combust. Flame 160, pp. 487-503, 2013

3. Seidel, L., Hoyermann, K., Mauß, F., Nothdurft, J., and Zeuch, T., "Pressure Dependent Product Formation in the Photochemically Initiated allyl + allyl reaction", Molecules 18 (11), pp. 13608-13622, 2013

4. Goos, E., Sickfeld, C., Mauß, F., Seidel, L., Ruscic, B., Burcat, A., and Zeuch, T., "Prompt NO formation in flames: The influence of NCN thermochemistry", Proc. Comb. Inst. 34, pp. 657–666, 2013

5. Nawdiyal, A., Hansen, N., Zeuch, T., Seidel, L., Mauß, F., "Experimental and modelling study of speciation and benzene formation pathways in premixed 1-hexene flames", Proc. Comb. Inst. 35, pp. 325-332, 2015

6. Seidel, L., Moshammer, K., Wang, X., Zeuch, T., Kohse-Höinghaus, K. , Mauss, F., "Comprehensive kinetic modelling and experimental study of a fuel-rich, premixed n-heptane flame", Combustion and Flame, Combust. Flame 162, pp. 2045-2058, 2015

7. Moshammer, K., Seidel, L., Wang, Y., Selim, H., Sarathy, S.M., Mauss, F., Hansen, N., "Aromatic ring formation in opposed-flow diffusive 1,3-butadiene flames" Proc. Comb. Inst. 36, pp.947-955 , 2017

8. Seidel, L., Netzer, C., Hilbig, M., Mauss, F., Klauer, C., Pasternak, M., Mastrisciano, A." Systematic Reduction of Detailed Chemical Reaction Mechanisms for Engine Applications" ASME. J. Eng. Gas Turbines Power. 139(9):091701, 2017

 Publications in conference proceedings with review (included in Scopus):

1. Tuner, M., Fröjd, K., Seidel, L., Mauss, F., "Diesel-PPC engine: Predictive Full Cycle Modeling with Reduced and Detailed Chemistry", SAE 2011-01-1781

2. Perlman, C., Frojd, K., Seidel, L., Tuner, M. and Mauss, F., "A Fast Tool for Predictive IC Engine In-Cylinder Modelling with Detailed Chemistry", SAE 2012-01-1074

3. Pasternak, M., Mauss, F., Matrisciano, A., Seidel, L., "Simulation of diesel surrogate fuels performance under engine conditions using OD engine - Fuel test bench", Proceedings of the 8th International Conference on Modeling and Diagnostics for Advanced Engine Systems, COMODIA 2012

4. Seidel, L., Netzer, C., Hilbig, M., Mauss, F., Klauer, C., Pasternak, M., Mastrisciano, A., "SYSTEMATIC REDUCTION OF DETAILED CHEMICAL REACTION MECHANISMS FOR ENGINE APPLICATIONS", ICEF2016-9304, Proceedings of the ASME 2016 Internal Combustion Fall Technical Conference, October 9-12, 2016, Greenville, SC, USA

2   State of the art

This chapter gives a brief overview about the state of the art in mechanism creation and reduction. The term mechanism or reaction scheme in this thesis is used for a set of elementary reactions describing the oxidation, decomposition and build up of hydrocarbon fuels. This reaction schemes are formulated in a computer readable standard format along with rate expression for each reaction included. This allows easy transfer of compiled reaction schemes and the use in different software solutions. For details the reader is referred to the literature cited within this chapter.

2.1   Mechanism creation

In the last decades hundreds or thousands reaction schemes for various applications were generated. Those schemes vary significantly in number of species and reactions, range of application, stiffness, structure, targets and much more features. However one observation can be made: reaction schemes for smaller fuels, usually up to C_3 or C_4 fuels, are composed of single reaction rates published in literature. A good overview for such elementary rates can be found in collection from the CEC group [1, 2, 3], Wing Tsang [4, 5, 6, 7] or with a limited focus on certain reaction types for example from Allara and Shaw, Badra and co-workers or Olzmann and Scherzer [8, 9, 10] to name only a few examples. However when larger molecules shall be modelled single reaction rates are often not known and the modelling community usually obtains the reaction rates via rate analogies which are than summarised to reaction classes. Already the modelling of the low temperate chemistry of propane relies on such analogies. The probably most cited example are the 25 reaction classes introduced by Henry Curran to model n-heptane [11] and than further applied by different groups to larger multicomponent schemes (see for example [12, 13]).

Even though those classes are widely accepted the degree to which species they are applied during the mechanism generation process differs. This becomes clear when we compare the detailed n-heptane scheme from Ahmed et al. with 246 species [14] with the aforementioned scheme from Curran [11] with 550 species. The major difference in number of species mostly results from the fact that Ahmed et al. applied the complete set of classes to the seed molecule only and a particular class (class 3) for the consumption of olefins. The fact that both reaction schemes are considered to be detailed illustrates that there is no clear definition when a scheme is detailed or reduced. Often a reaction scheme is considered to be detailed when all known major decomposition pathways are included and/or no reduction technique was applied yet. The fact that due to better experimental setups and measurement techniques the combustion community is able to identify more products and intermediate species which subsequently leads to more species and reactions included in reaction schemes. Sticking with the example of n-heptane as fuel, such steps where the determination of different furan species at low temperatures [15] and other findings lead to the formulation of new reaction classes [16].

To be able to handle larger schemes different tools for automatic mechanism generation

were developed within the community often with the goal to fully automise the generation procedure. This automation shall cover the application of reaction classes as well as the calculation of molecular properties of the individual species. Different numerical approaches were followed by researchers in the past. The major contribution in the field of automatic combustion modelling were done by the following authors (sorted by year of publication):

- Chevalier et al. in 1992 [17]

- Ranzi et al. in 1995 [18] including a post priori vertical lumping approach

- EXGAS in 2000 [19]

- Blurock in 2004 [20] with improvements by Moreac et al. in 2006 [21]

- RMG (Reaction Mechanism Generator) from van Geem presented in 2006 [22]

- A mechanism generator from Hilbig, Seidel and co-workers first presented in 2011 [23]

An extensive review of "best practices, recent advances and future challenges" in mechanism generation can be found in the overview article from van de Vijver et al. [24].

The wide range of different compilation methods and philosophies resulted in very different sizes for schemes modelling fuel oxidation relevant to in cylinder combustion. A good example for a very small reactions is the manual compiled n-heptane / iso-octane scheme from Tsurushima with 33 species / 38 reactions [25]. The automatic generated reaction schemes for methyl stearate and methyl oleate combustion from Naik et al. [26] represents the large schemes with about 3500 species and more than 17 000 reactions.

Both schemes, however can be further reduced by limiting its range of application and accepting deviations from its non reduced state.

The process of mechanism development is often supported by two very common tools: the flow and the sensitivity analysis. Both tools were used during the mechanism generation process leading to the publication listed above (see section 1.1) and the reaction scheme developed in this thesis. However both tools are only shown in a small extend, since this work does focus on reduction and the implications towards in cylinder combustion modelling.

2.2   Mechanism reduction

In the last decades computation power was rising significantly and the code base of chemistry solvers became more efficient. This allowed the generation of larger kinetic schemes and the use of more detailed computational (fluid dynamic) models. It can be expected that the increase in computational performance, hardware or software, will be used to increase the level of detail or solving chemistry in real time. Under these circumstances we can formulate a very clear target for mechanism reduction: The generation of small enough reaction schemes to be able to solve a task within a reasonable time frame and acceptable accuracy.

Reduction procedures can be separated into 2 major ideas:

1. Removing of species or reactions

2. Combination or lumping of species or reactions into new pseudo species or global reactions

3. Tabulation strategies.

The advantage of species or reaction removal is obvious, each reaction or species not included does not need to be considered by the solver or transported in the Computational Fluid Dynamic (CFD) calculation[1]. Therefore the question is how to identify species/reactions which can be removed? A series of different techniques were developed in the past to address this problem:

- Species elimination via trial and error: A random reaction or species will be removed and the solution of the reduced scheme will be compared against the solution of the original scheme.

- Unweighted and weighted graph based methods: The most common are

  - Necessity Analysis by Soyhan et. al [27]

  - Direct Relation Graph (DRG) introduced by Lu and Law [28] with further development to DRG with error propagation (DRGEP) [29] and DRG aided sensitivity analysis (DRGASA) [30] or DRG with expert knowledge.

Details and comparison of different reduction techniques can be found in the book from Turanyi and Tomlin [31]. At this point it is worth to mention that it is not always clear how those methods ensure that the reduced reaction scheme has a performance within certain thresholds in a given parameter range. It is clear that the comparison against the original scheme can be only done post-priory. This implies two important tasks which needs to be addressed before the start of the reduction procedure. On one hand side a clear range or set of inlet conditions needs to be defined for which the reduced schemes are validated against the detailed. On the other hand side it is of equal importance which kind of benchmarks are used for the validation of the schemes. Both points will be addressed in the mechanism reduction section of this thesis.

The advantage of combination and/or lumping of species / reactions is probably not that obvious. On the first view they do not show a good effort to removed species ratio. Some of those methods may be a lot of work and reduce the scheme only by small fractions. However they help to combine very similar pathways which contribute with small individual pathways. This supports further reduction by removal strategies. The most important among those methods are:

- Horizontal lumping of species

- Vertical lumping of species

---

[1]The author is fully aware of the fact that e.g. sparse matrix solvers do exist which do not need to solve for all species in each time step and scale linear with the number of species and (CFD) solutions exists which transport only selected species. However, those solvers will also benefit from the reduction.

- Vertical lumping of reactions

- Quasi steady state assumption.

The different reduction methods are explained in detail in chapter 10.

The tabulation of the combustion process and emission formation can be seen as the most efficient reduction method. Most of the combustion features (for in cylinder combustion) can be tabulated based on homogeneous reactors or flamelet approaches. Those reactor models are not computation expensive even for large schemes. Good results with tabulated chemistry can be achieved even for complex processes such as soot formation (see for example [32]). Since this tabulation needs to be done only once it may reduce the demand for reduced schemes in the future. The only exception is the tabulation of laminar flame speeds, which is computational expensive due to the large parameter range which needs to be covered by a flame speed table. Here the tabulation process can benefit significantly from reduced models.

3 Experimental setups and their representation in homogenous models

This chapter introduces the reader to the different experimental setups and their model representation. It further provides an overview of the underlying fundamentals.

3.1 Shock tubes

In the last years there are discussions within the community in which extend shock tubes are ideal or not ideal (see for example [33]). An ideal shock tube would show pressure and temperature traces as described by Zeldovich and Raizer in figure 1. Often, especially for long induction times a temperature and/or pressure rise can be observed before a clear ignition event is detected. This can be attributed to hydrodynamic effects, local pre-reactions or pre-ignition of the fuel due to small inhomogeneities (e.g. very mild low temperature) or reactions with residues in the wall. Both the temperature and the pressure rise before the ignition event will certainly shorten the ignition delay time. This is exemplary shown in a graph from Heufer et al. [34] for ethanol / air experiment in figure 2(a).

For inlet conditions with comparable long ignition delay times this may lead to a low temperature chemistry type of slope even for fuels which are known to have not low temperature chemistry. This is shown in two plots taken again from Heufer et al. [34] for ethanol (see figure 2(b)) and methane (see figure 2(c)). It is known that the dimensions of the shock tube can play an important role. Since all those factors are often unknown shock tubes are calculated as adiabatic homogeneous constant volume reactors. We have to keep in mind that measured ignition delay times at low temperature for fuels which are known to have no low temperature chemistry can be significantly influenced by non ideal conditions.

3.1.1 Accuracy considerations

Shock tube experiments are the major source for experimental obtained ignition delay times. Since the auto ignition characteristics of different fuels is the most important feature to consider in Diesel and Otto engines it is worth to discuss how measured ignition delay times translate into engine timings. The most simple way of comparing ignition delay timings with typical timings in engines is by calculating how much time is needed to turn the engine by one crank angle degree (CAD). Table 1 shows that this is dependent on the revolutions per minute which will strongly differ with the engine type and operating point. Since engines cover such a wide range of speeds[2], and subsequently time scales for the fuel to auto ignite, the necessary accuracy of shock tubes experiments differ with the engine type and operating point.

At this point only an estimation of the known uncertainty can be made. This is done in the following way: the difference in published ignition delay times measured at the same condition is translated to the amount of CAD this would cover at a given engine speed. The

---

[2]In the time a slow running ship diesel turned by one CAD a Formula 1 engine turned more than 180 CAD.
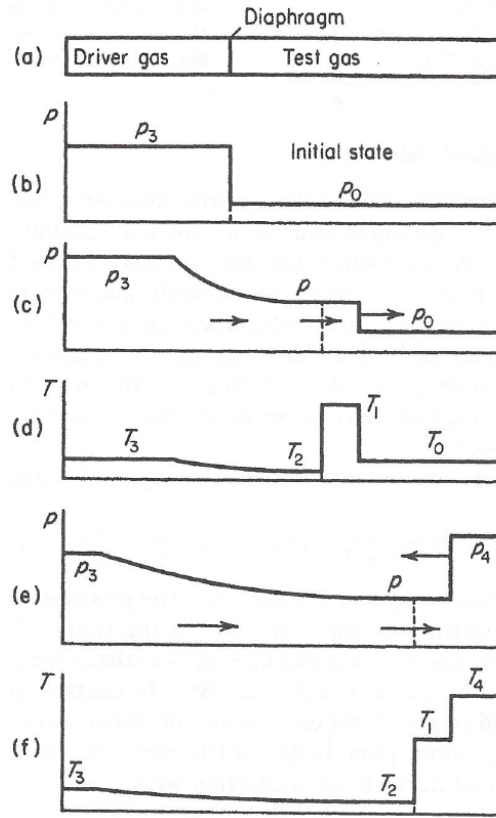
Figure 1: Depiction of an ideal, non reactive, shock tube by Zeldovich [35]: a) experimental setup before the diaphragm bursts and b) initial state, c) and d) propagation of the shock wave and e) and f) reflection of the shock wave.

obtained ignition delay can be either from one author or from different authors. The engine speed was chosen based on the correlations between RON / MON test conditions and initial conditions for 0D reactors suggested by different authors (see section 8). Four different sets of experimental data suitable for this study were found and they are summerised in table 2. From the few available experiment repetitions at engine relevant conditions it can be concluded that the experimental scatter is significant and correspond up to several CAD in engines. The largest uncertainty is found for the n-heptane / toluene mixture from Herzler [36] with about eight CAD at 900 rpm.

The demanded accuracy for ignition delay time determination can be estimated when the acceptable uncertainty in CAD is known for a given temperature and pressure at ignition onset:

$$Accuracy[ms] = \frac{166.7 \cdot \Delta CAD}{RPM}$$

This assumes the conditions (temperature, pressure and gas composition) at auto ignition onset / spark timing are the same as in the initial conditions in the shock tube experiment. Due to the transient and non homogeneous nature of engines this is a simplification.

(a) Measured pressure and photomultiplier signal at 20.5 bar and 880 K initial conditions.

(b) Measured ignition delay times for stoichiometric ethanol air mixtures.

(c) Measured ignition delay times for stoichiometric methane air mixtures.
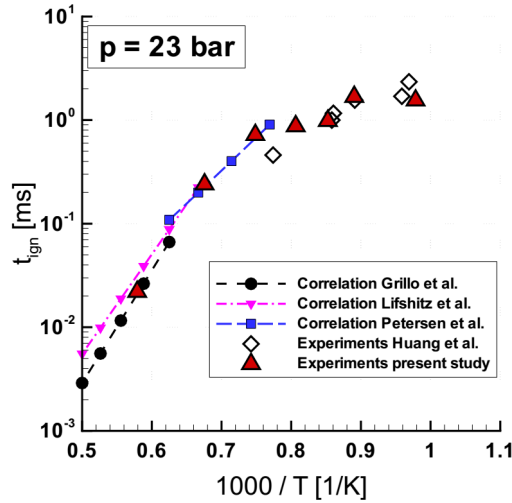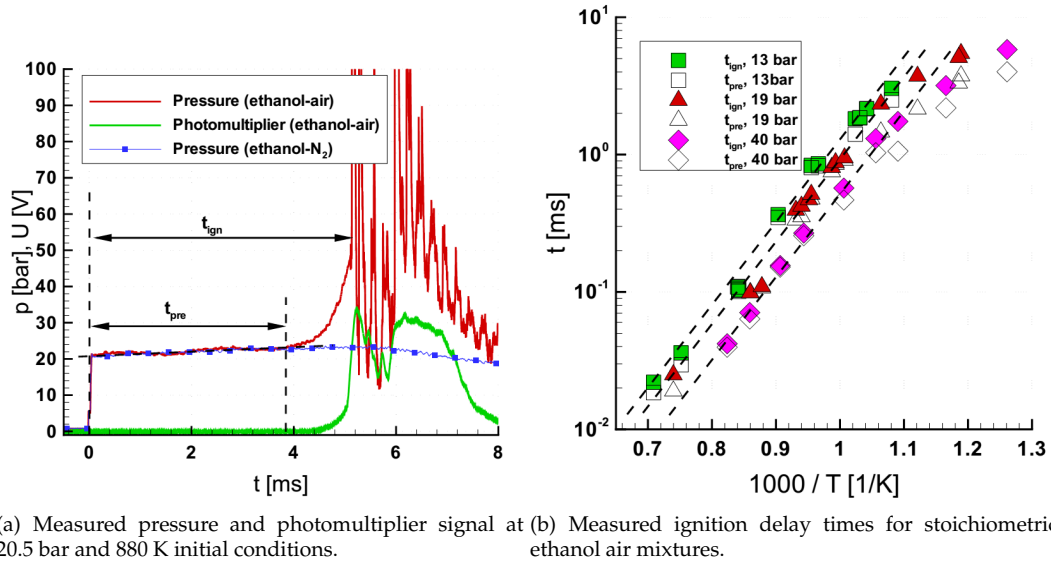
Figure 2: Different figures taken from the work of Heufer et al. [34] for fuels without a low temperature chemistry which show increased reactivity for long ignition delay times.

RPM	$[\frac{CAD}{s}]$	$[\frac{CAD}{ms}]$	$[\frac{ms}{CAD}]$	Engine type
100.0	600.0	0.6	1.667	Slow 2 stroke turbo charged marine Diesel
250.0	1500.0	1.5	0.667	Power peak of MAN DM 12 (1902)
500.0	3000.0	3.0	0.333	Diesel passenger car idle
600.0	3600.0	3.6	0.278	RON test conditions (see section 5.1.1)
900.0	5400.0	5.4	0.185	MON test conditions (see section 5.1.1)
1000.0	6000.0	6.0	0.167	Gasoline passenger car idle
1500.0	9000.0	9.0	0.111	Arbitrary engine case used for reduction validation
2000.0	12000.0	12.0	0.083	Power peak for Diesel truck engines
2500.0	15000.0	15.0	0.067	
3000.0	18000.0	18.0	0.056	
3500.0	21000.0	21.0	0.048	Power peak early VW Käfer
4000.0	24000.0	24.0	0.042	
4500.0	27000.0	27.0	0.037	
5000.0	30000.0	30.0	0.033	
10000.0	60000.0	60.0	0.017	Power peak for 4 Stroke, 4 cyl. sport bikes
20000.0	120000.0	120.0	0.008	Max. rpm Formula 1 in the 2000s
34000.0	204000.0	204.0	0.005	Max. rpm for glow plug engines

Table 1: Revolution per minute for different types of internal combustion engines and calculated time needed to turn one CAD.

Figure	Conditions close to	T [K]	τ_{min} [ms]	τ_{max} [ms]	Δ [ms]	CAD equiv.
41	MON (45bar / 980K)	≈ 980	0.53 (Hartmann [37])	0.78 (Fieweger [38])	0.25	1.35@900rpm
25	MON (45bar / 980K)	≈ 980	0.53 (Hartmann [37])	1.03 (Hartmann [39])	0.50	2.7@900rpm
46	MON (45bar / 980K)	≈ 980	0.43 (Hartmann [39])	0.57 (Fieweger [38])	0.14	0.76@900rpm
51	RON/ MON (25bar / 825K)	830	2.35 (Herzler [36])	3.45 (Herzler [36])	1.47	5.3@600rpm
						7.9@900rpm

Table 2: Largest experimental difference in ignition delay time and corresponding CAD covered at given rpm. Comparison at similar conditions for the same fuel and oxidizer.

3.2   Jet stirred reactors

Jet stirred reactors are simulated as perfectly stirred reactors in which the temperature is kept constant. It is kept constant because publication focusing on measurements often report that the temperature difference between inlet and outlet flow is typically only a few degree Kelvin and often reported to be below 10K (see for example Dagaut at al. and Moreac et al. [40, 21]).

3.3   Premixed burner stabilised flames

For the modelling calculation of the burner-stabilised flame, mixture average and thermal diffusion[3] is considered. If given in the experiment the measured disturbed temperature profile is used as input parameter. As described in 13.4.1 when no temperature profile is imposed it is calculated from the energy conservation equation, which considers the heat flux to the burner. For all major radicals we consider recombination at the burner surface. When a close agreement is found between the measured, the calculated temperature profile and the predicted major emission in equilibrium it can be assumed that the measurement is very accurate. This statement is based on the following consideration: the undisturbed flame stabilises above the burner through heat loss, which results from the temperature gradient at the burner surface. The heat loss determines the maximum flame temperature, which is below the adiabatic flame temperature. From flame theory it is known that the flame speed is proportional to the maximum flame temperature. Hence, the heat loss of the stable flame corresponds to a maximum flame temperature for which the burner exit velocity and the reduced flame velocity are equal. If the model can predict the laminar flame correctly it should predict very similar temperatures. Far away from the reaction zone we can rely on model prediction for the major species since rate kinetic data cannot influence the species concentrations at these heights and the thermodynamic data of these species are well known. If a strong deviation of predicted temperature and major species is observed in equilibrium, far away from the reaction zone, it means that either the species were not quantified correctly or the measurement of the temperature does not correspond to actual temperature during sampling. This may be the case when the temperature is measured with the rapid insertion technique and the sampling was done with comparable large probe which had a significant effect on the flow field and can cool the gas. For smaller flames this effect is more pronounced and we can expect a stronger deviation in atmospheric flames than in low pressure flames. The scheme used in this work was validated against several

---

[3]Hydrogen radical only.

low pressure flames [41, 42, 43] with a small deviation between predicted and measured species concentrations and temperature in equilibrium.

3.4   Laminar flame speed experiments

Laminar flame speeds are usually obtained in different experimental setups such as spherical bombs, counter flow burners, Mc Cenna burners or heat flux burners. It is assumed that in published data the stretch effects are correctly compensated and no effort was spent to investigate the reason for contradicting experimental flame speeds. Laminar flame speeds are calculated under the assumptions of ideal freely propagating flames as described in 13.4.1.1.

4   Fundamentals

This fundamental assumptions and equations used for modelling and mechanism analysis are described in Appendix I (see chapter 13). This is compiled from the different manuals of LOGEsoft 1.08 [44]. Even though parts of the manuals where written by myself the complete chapter should be regarded as citation since the reader may not have access to the manuals.

5 Gasoline Surrogate Fuels

5.1 Introduction

Todays commercial transportation fuels derived from fossil fuels are often complex mixtures of hundreds of components. A closer view of fuels for spark ignition engines reveals that the most common fuels are:

- Natural gas

- LPG (liquid petroleum gas) mixtures of propane and butane

- Pure ethanol

- Gasoline

- Gasoline / ethanol mixtures

The first three fuels are more or less composed of only a few components and can be described with a reaction scheme for C_1 to C_4 species chemistry (methane, ethane, propane, butane and ethanol). Gasoline on the other hand consists of several hundred species. Table 3 summarizes the major species identified in RD387 gasoline and the table 4 summarizes the composition of three different commercial gasoline fuels by species classes. It can be clearly observed that iso-paraffins and aromatics are the major fraction of commercial gasolines. Due to its complex composition it is not possible, and probably will never be possible, to compose a reaction scheme including all fuel components.

Component name	mol%
Cyclopentane	16.8
Toluene	9.7
Isopentane	7.8
meta-Xylene	4.9
3-Methylhexane	4.4
n-Heptane	3.6
2-Methylhexane	3.3
Ethylbenzene	3.2
n-Pentane	3.0
2,2,4-Trimethylpentane (iso-octane)	2.5

Table 3: RD387 gasoline major species composition taken from [45].

Component / Source	Kalghatgi [46]	Foong [47]	Anderson [48]
Napthenes	2.8	11.4	3.9
Paraffins (total)	15.3	48.9	64.3
i-Paraffins	29.5	35.3	48.3
Aromatics	37.4	31.7	26.0
Oxygenates (MTBE)	<0.01	-	-
olefins	2.6	8.0	5.8

Table 4: Gasoline compositions in volume % from different sources [46] [47] [48].

5.1.1   Primary Reference Fuel and Octane Numbers

The chemical composition is obviously not a sufficient way to describe the combustion performance of a commercial gasoline fuel. Already shortly after introduction of the SI engine in the beginning of the 20th century the compression ratio in SI internal combustion engines was increased by engineers to achieve more power per swept volume. This increase in compression ratio was, and still is, limited by unwanted knocking[4] and could rapidly destroy an engine. In the beginning the battery ignition system was thought to cause the knocking. Charles Kettering (the inventor of the electric ignition system) assigned Thomas Midgley to the task of finding the exact cause of the knocking [49]. He was able to demonstrate that it was caused by a violent pressure rise after ignition. As Graham Edgar pointed out in 1927 [50] *"To draw detonation specifications for fuels, a reproducible primary standard fuel must be developed and methods of comparing fuels must be agreed upon. The composition of gasoline is so complex and the knocking characteristics of its different constituents are so varied that great difficulty has been encountered in finding one or more hydrocarbons, the purity of which could be definitely established by test and which would thus be absolutely reproducible."* He suggested using two hydrocarbons as reference fuels to characterise gasoline. Those hydrocarbons needed to be produced in high purity and quantity. They needed to have similar volatility properties. Finally n-heptane and iso-octane (2,2,4-trimethylpentane) were chosen as those reference fuels and the mixtures of those are called Primary Reference Fuel (PRF). n-Heptane has a low antiknock value and iso-octane a high antiknock value. Graham demonstrated that all commercially available gasoline fuels at this time could be broken between 60:40 (40 octane) and 40:60 (60 octane). After the reference fuel was decided on, a lot of different engine test conditions appeared. Today only two test conditions are common for road bound engines: The Research Octane Number (RON) and the Motor Octane Number (MON). The RON represents a more mild driving with part load, while the MON represents high load driving (at that time). An overview of the test conditions is given in table 5 for the CFR engine. The outdated BASF / I.G. Farben engines are comparable and conclusion drawn from experiments using this engine (e.g. by Spausta [51]) are valid for todays octane number tests as well. The octane rating measures only one property: knocking in a limited area around the engine operating points. These ON is still in use in our daily life.

The advantage of describing the fuel quality with a single number is very clear and makes the choice of the appropriate fuel quality at the gas station very simple. However, there are several disadvantages of the PRF system:

- Today's commercial available fuels have a RON between 92 and 102[5] and therefore lay in upper 8% of the PRF scale or cannot be described at all.

- The RON and MON of the primary reference fuel are always the same number by definition. Real fuels however do usually have a MON which is lower than the RON (see for example table 11 for different batches of real fuels)

---

[4]Knocking in SI engines is an abnormal combustion phenomenon caused by autoignition in the unburned zone during flame propagation. The occurrence of knocking depends on the conditions in the unburned zone and the tendency of the fuel to auto ignite. The thermal efficiency of a SI engine is fundamentally limited by engine knock.

[5]e.g. Aral Ultimate 102

- The two alkanes do not reflect the high content of aromatic fuels in commercial gasoline.

- Mixtures of n-heptane and iso-octane can not capture most of the physical properties of gasoline such as lower heating value, density and H:C:O ratio.

During the years several attempts were made to introduce an alternative antiknock index. Most of them are based on mixtures containing toluene.

	RON	MON
Test Method	ASTM D2699	ASTM D2700
	DIN EN ISO 5164	DIN EN ISO 5163
Engine RPM	600 RPM	900 RPM
Intake air temperature	Varies with barometric pressure	38° C
Intake air humidity	3.56 - 7.12 g H_2O / kg dry air	equal to RON
Intake mixture temperature	52°C	149° C
Coolant temperature	100° C	100° C
Oil temperature	57° C	57° C
Ignition Advance	13° BTDC	varies with CR
Carburettor Venturi	Set according to engine altitude	14.3 mm

Table 5: Research methods for octane rating [51, 52].

5.1.2 Toluene Reference Fuel

Toluene as reference fuel component was already used in the 1920s. Mixtures of toluene with parafinic fuels were used to describe the highest compression ratio reachable in an engine before knock appeared. Detailed descriptions of this can be found in the book from Harry Ricardo (1926) [53] or Franz Spausta (1939/1956) [51]. In the beginning of the millennium a new two-component reference fuel was investigated. It was found in engine experiments that a mixture of n-heptane and toluene (often named "toluene number") is much more suitable to describe real gasoline in terms of RON and MON [54]. In the same year Gauthier and co-workers [45] compared the ignition delay times of gasoline RD387 measured in a shock tube with ternary mixtures of iso-octane, toluene and n-heptane. They could prove that such ternary mixtures have similar ignition delay times. At the same time Kalghatgi and others [46] proved that the primary reference fuel is not a suitable reference fuel to describe the knock resistance of various gasoline fuels in modern SI engines. They also suggested mixtures of iso-octane, toluene and n-heptane as the simplest non-PRF reference fuel [55]. They used the term "Toluene Reference Fuel" or TRF, which is also used in this work. This ternary reference fuel has several advantages over the primary reference fuel:

- The scale is extended to fuels with octane numbers above 100. The upper limit is defined by the ON of toluene which is about 120[6].

- Due to the higher density and lower heating value of toluene the physical properties of TRF mixtures are closer to real gasoline.

- Toluene represents the high content of (mono) aromatics in gasoline which is beneficial in terms of emission formation prediction.

---

[6]The RON / MON of toluene can only be determined by extrapolation methods or the use of octane enhancers such as tetraethyllead.

- The C/H ratio is close to commercial gasoline (see table 11).

- It is possible to formulate a single surrogate fuel which match RON and MON of real gasoline fuels very closely.

5.1.3   Ethanol Toluene Reference Fuel

Since the first SI engines were developed ethanol played an important role as knock resistant fuel (RON of about 109[7]). Henry Ford developed his Modell T for ethanol in the first place, but conventional gasoline became the more common fuel due to its availability in North America. In the Weimar Republic up to 10% of ethanol had to be added to the fuel. Even though ethanol was hardly used as fuel or fuel additive after the second world war it became an major fuel additive after the oil crisis in the '70s. In the USA the addition of 10% ethanol became mandatory and in (West) Germany 5% had to be added since the 1980s. Since 2010 up to 10% ethanol can be added to standard gasoline in Europe and some countries even sell gasoline with up to 85% ethanol. Due to its very different physical and combustion properties and its impact on emission formation [56] it needs to be considered as part of a surrogate fuel for gasoline.

At this point it can be concluded that surrogate fuel for today's common gasoline has to consist of at least four fuels: n-heptane, iso-octane and toluene to capture the most important characteristics of pure gasoline, as well as ethanol to take its high content into account. The table 6 summarises the most important properties of the four surrogate fuels.

Fuel	Formula	ρ	M	h_{298}	BP	LHV	LHV	RON	MON	C/H / C/O
Unit	[-]	[kg/m3]	[kg/mol]	[kJ/mol]	[K]	[MJ/kg]	[kWh/l]	[-]	[-]	[-] / [-]
n-Heptane	C7H16	683.81	0.10020	-225.9	371.8	44.566	8.41	0	0	0.44 / -
iso-Octane	C8H18	692.01	0.11423	-258.8	372.2	44.427	8.24	100	100	0.44 / -
Toluene	C7H8	866.89	0.09214	12.18	384.0	40.589	9.78	120	109	0.086 / -
Ethanol	C2H5OH	789.67	0.04607	-276.0	351.5	28.865	6.33	109	90	0.33 / 2
Methanol	CH3OH	791.01	0.03204	-238.4	337.8	19.9	5.55	109	89	0.25 / 1

Table 6: Properties of the four surrogate fuels at standard conditions. Most of the data are taken from the NIST database. BP - Boiling point. RON and MON are taken from [57] for toluene and from [58] for ethanol and methanol. Please note that RON and MON above 100 are blending numbers. h_{298} denotes the enthalpy at 298K; LHV denotes the Lower Heating Value.

5.2   Underestimation of fuel qualities in the MON test

There is clear evidence that the MON test systemically underestimates the antiknock qualities of certain fuels. A simple example are the MON of ethanol and methanol. In the last decades a MON of 90 for ethanol [58, 48, 47] and a MON of 89 [47] for methanol were reported. The highest number found suggests 98 for methanol and 99 for ethanol are considerably old [51]. These numbers are significantly lower than the MON of 100 for iso-octane.

---

[7]The RON / MON also needs to be determined by extrapolation methods.

There is no evidence that methanol or ethanol will ignite earlier than iso-octane under similar conditions (see for example correlations in figure 79). Both fuels do not show a low temperature chemistry (see figures 32 to 65 for validation of the developed mechanism in this work and discussion in chapter 3.1 why experiments may suggest a low temperature). A common conception about the octane measurements (RON and MON) is that they compare the knock resistance of different fuels and that fuels with higher ON are the better choices. Furthermore the MON test was designed to be closer to real driving[8]. The MON of those simple alcohol fuels would suggest that they are not a good choice and would actually perform worse than pure iso-octane in engines. At the same time we do know that methanol and ethanol fuelled engine are less prone to knock and can achieve much higher power per swept volume. This indicates that there is a systematic underestimation of anti knock qualities in the MON test.

A literature survey was performed to identify the origins of this underestimation:

1. Reason 1: Heat of vaporisation. Spausta [51] already summarises in his book from 1939 / 1953 that the MON method provides too low ON values for gasoline mixtures with high content of oxygenated fuels[9]. The main reason is that the MON test is carried out with preheated intake mixture. The mixtures is heated up to 149 Celsius, which is above the boiling point of C_1 to C_5 alcohols. Fuel with a high enthalpy of evaporation will significantly lower the intake temperature in the RON test or probably evaporate in the cylinder after intake valve closure. This cooling cannot take place when preheating is above the boiling point. This is underlined with data using the aviation method shown in section 5.2.1.

2. Reason 2: Fuel / Air ratio. MON and RON tests are not carried out at fixed fuel equivalence ratios. In fact the carburettor is set to reach a maximum knocking at fix compression ratio and spark timing (see discussions from Anderson et al [58]). Due to this setup is is not clear if the necessary fuel supply can be achieved with oxygenated fuels. It is further not clear if the same fuel equivalence ratios between the reference fuels (n-heptane / iso-octane) and oxygenated fuel are compared.

Both explanations are perfectly obvious for fuels with a boiling point below 149° Celsius and high heat of vaporisation and are partly discussed in studies focussing on alcohol fuels from Wallner [59]. This underestimation is clearly leading to the large fuel sensitivity S (S=RON-MON) assigned to methanol (S=20) and Ethanol (S=19). Actually a closer look to the data published by Wallner (table 7) reveals that fuel sensitivity decreases with the chain

---

[8]Even so it was designed in the 1930's it is more challenging than the RON test.

[9]Citation from page 93: Es hat sich gezeigt, daß Kraftstoffe für Otto-Motoren, die größere Anteile an sauerstoffhaltigen Komponenten von hoher Verdampfungswärme, z. B. niedere Alkohole, enthalten, bei der Prüfung nach der A.S.T.M.- oder der I.G. -Motor Methode zu ungünstig bewertet werden. Bei Anwendung dieser Methoden gelangen solche Treibstoffe bei der vorgeschriebenen hohen Ladegemischvorwarmung von 149° Celsius in praktisch vollständig vergastem Zustand in den Zylinder, während sie in der Praxis bei normaler Gemischvorwärmung wegen ihrer hohen Verdampfungswärme erst im Zylinder vollständig verdampfen und dabei dem Ladegemisch Wärme entziehen. Dadurch wird die Neigung zum Klopfen vermindert und eine höhere effektive Klopffestigkeit erreicht. Zur Bewertung solcher Treibstoffe für Automobile wurde deshalb in Ländern, in denen Alkohol als Zusatztreibstoff verwendet wird, an Stelle der in der Bewertung als zu scharf empfundenen C.F.R-Motor-, bzw. A.S.T.M.-Prüfmethode die (alte) Research Methode, der Vorläufer der C.F.R-Motoren-Methode, beibehalten, bei der eine niedrigere Drehzahl (600 statt 900 U/min) angewandt und auf eine besondere Ladegemischvorwärmung verzichtet wird. Diese Methode wird neben der A.S.T.M.-Methode auch etwa bei Klopffestigkeitsuntersuchungen an neuen Treibstoffarten und zu mehr wissenschaftlichen Zwecken angewandt.

length of primary alcohols. Unfortunately no octane numbers for a liquid fuel with a boiling point significantly higher the 149° Celsius was found.

The boiling point of 1-Hexanol is only slightly above the temperature of the preheater. An investigation with a fuel which cannot evaporate and has no low temperature chemistry would allow to determine if the sensitivity is mostly attributed to the preheating and/or to the different load point. However there is some evidence that the preheating (and therefore excluding the cooling effect) may play an important role:

- The RON and MON of methane are reported to be equal (120). Since it is a gaseous fuel with no low temperature chemistry, neither the heat of vaporisation nor ignition delay times could play a role. On the other hand RON 120 seems to be the limit of the American Society for Testing and Materials (ASTM) tests in CFR engines [51].

- Gaseous fuels (at room temperature) seem to show a smaller sensitivity than the liquid alcohols.

- The ASTM-CFR Aviation Method to determine octane numbers for aviation engines operates at different spark timing (30 CAD) higher RPM (1200) and coolant temperature (160° Celsius) with a slightly different cylinder geometry. For this test the mixture temperature is heated up to 104° Celsius. Barnett [60] determined a blending toluene number of about 117 for toluene with this method. We have to keep in mind that toluene has a boiling point of 110° Celsius (6° Celsius above the preheating temperature if atmospheric pressure is assumed) and may therefore evaporate after the preheater and be able to cool the charge. Even though this aviation targeted method operates at higher RPM it suggests an octane rating for toluene closer to the RON than to the MON where actually an ON around or below the MON would be expected.

Fuel	RON	MON	vapH [kJ/mol]	BP [K]	RON - MON
Methanol	109	89	35.21	337	20
Ethanol	109	90	38.6	351	19
1-Propanol	105	87	41.44	370	18
1-Butanol	98	85	43.29	390	13
1-Pentanol	86	76	44.4	411	10
1-Hexanol	70	64	61.2	430	6

Table 7: Fuel properties and octane numbers of different alcohols from [59].

To the best knowledge of the author it was never investigated in which extend the heat of vaporisation may impact the measured sensitivity of toluene as a fuel. It is evident that there is a significant difference in experimentally obtained RON and MON ratings for toluene:

- Spausta [51] collecting different sources: RON: > 100 and MON 104, 109, 110[10]

- Morgan et al. [57] using the data suggested by Heywood [52]: RON 120 and MON 109

- Knop et al. [61] using from different sources: RON 120 and MON 103.5

[10]Data from I.G. Farben and CFR engines

- Bruce Hamilton [62] citing an API project using mixing with a 60 RON fuel and gives blending numbers as follows: RON 124 and MON 112

- at the same time he also suggests blending numbers for modern fuels to be RON 111 and MON 94

- Haas and Dryer [63] respond to the publication from Knop et al. [61] arguing that a RON between 116 and 118 is more reasonable citing different sources.

This gives a wide spread of fuel sensitivity (RON - MON) reaching from 11 (Heywood) to 17 (Bruce Hamilton). This spread may be a result of the use of different base fuels when extrapolating the (blending) RON and MON of toluene. For a deeper insight the experimentally obtained sensitivity (RON-MON) from several n-heptane, iso-octane, toluene mixtures are summarised in table 10 and shown in figure 3. Until a toluene fraction of 75 volume percent (vol%) there is a linear trend pointing to a sensitivity of about 16 irrespective of the n-heptane or iso-octane fraction in the mixtures. Above 75 vol% toluene the experimentally obtained sensitivity drops dramatically. It is very unlikely that there is a non-linear behaviour in the gas phase chemistry which could explain this behaviour (see for example figure 120 for n-heptane/toluene and iso-octane/toluene mixtures in the appendix). It is rather likely that this behaviour is attributed to the fact that the RON and MON were never designed to determine octane ratings above 100, an octane rating often exceeded by mixtures with more than 75 vol% toluene. From these data (figure 3) it can be extrapolated that a sensitivity of pure toluene should probably be about 16 to 17.
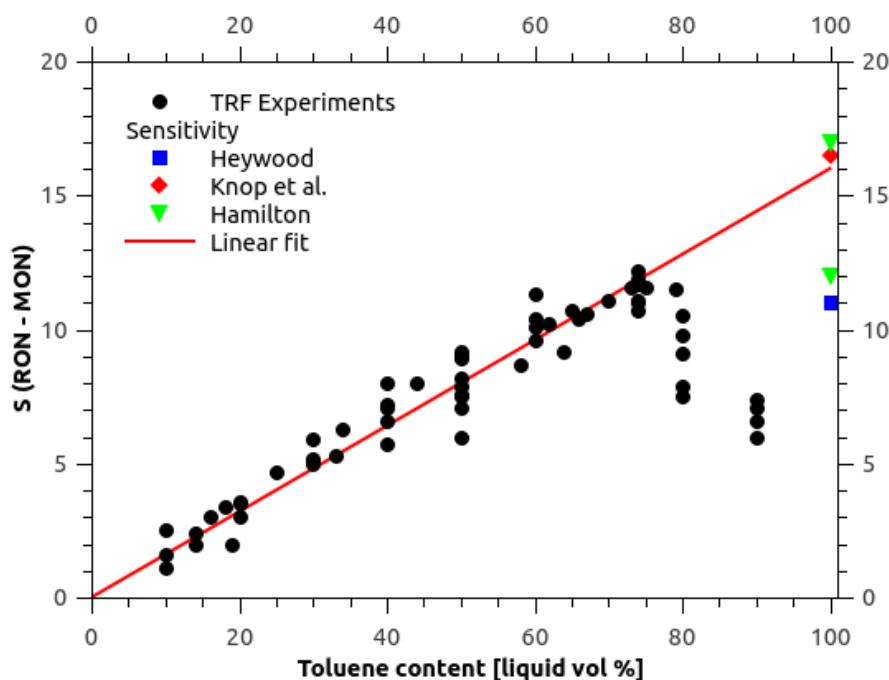

Figure 3: Measured fuel sensitivity (RON - MON) from table 10. Solid line: linear until 75 vol% toluene.

To assess to what extend the heat of vaporisation plays a role in the sensitivity, a set of fuel specific properties was compiled. This allows to compare the heat of vaporisation to the lower heating value of the individual reference component fuels. As summarised in table 8

a higher fuel sensitivity (a wider spread between RON and MON) is always associated with higher ratio of heat of vaporisation to lower heating value (LHV). If we further consider that we want to charge the cylinder with the same amount of energy during octane number determination[11] we should scale this factor to the LHV of iso-octane. This gives a ratio how much more "heat of vaporisation" would be "injected" to the cylinder if we would replace iso-octane by another fuel and adjust the amount of fuel at the same time to keep the amount of energy constant, assuming stoichiometric combustion. As shown in table 8 switching the fuel in the discussed way from iso-octane to methanol would provide 15 times more energy to cool the mixture. Even for toluene there is still a factor of 1.6 in comparison to iso-octane and a higher sensitivity correlates with higher scaled heat of vaporisation. This may indicate that the very high RON and comparably low MON is associated with the physical effect of mixture cooling. This effect is further explained in the following paragraph discussing experiments using the ASTM Aviation method.

In a similar fashion it could be argued that the PRF fuels are over rated for the MON simply by the fact that the rating is set to the octane fraction. This ignores the fact that the mixture preparation and engine load point will promote earlier ignition. Later on in section 9.2 it will be shown that by using a correlation with ignition delay times obtained in homogenous reactor simulations a MON of 80 for pure iso-octane would correlate much better with the ON of mixtures with non PRF fuels. However a different definition of the octane ranking for different test conditions is not usefull after using this number since decades.

Fuel	S (RON - MON)	Heat of vaporisation	$\frac{vapH}{LHV}$	Scaled to LHV of iO	Comparison to iO
Unit	[-]	[kJ/mol]	[J/J molar basis]		[-]
Methanol	20	35.21	4.84E-02	9.47E-02	15.62
Ethanol	19	38.6	2.91E-02	4.48E-02	7.38
Toluene	11 - 17	33.18	8.87E-03	9.71E-03	1.60
n-Heptane	0	31.77	7.11E-03	7.09E-03	1.17
iso-Octane	0	30.79	6.07E-03	6.07E-03	1.00

Table 8: Compilation of different fuel properties of different surrogate fuels related to heat of vaporisation. iO denotes iso-octane.

For sure this cooling effect needs to be considered when changing the fuel mixtures in engine operation or simulations. At this point it can be conclude that both the RON and MON have their limitations. Furthermore the MON test removes the effect of fuel vaporisation. Despite all the shortcomings they are still the only common fuel quality numbers used to characterise gasoline fuels.

5.2.1   The effect of internal coolants on knock-limited engine performance

This section does not deal directly with the RON/MON ratings common in road bound transportation, but with an aviation ON test. For aviations fuels the ASTM test is performed at more challenging conditions such as 2500 rpm and higher coolant temperatures. In a work carried out during the second world war by Bellman and Evvrad [64] the effect of

---

[11]This assumes that the maximum knock is associated with the same energy charge in the cylinder, which is probably not correct.

different preheating temperatures and different coolants (water and methanol/water mixture) on engine performance was investigated. The preheating temperature was varied by 100° Fahrenheit (about 60° Celsius) having different impact on the evaporation of the injected coolants and therefore the (knock limited) indicated mean effective pressure (IMEP). The coolant was injected at room temperature into the injection elbow into the preheated air, with a rate of 1/2 pound per pound fuel. This means that in the case of preheating to 150° Fahrenheit (figure 4), both coolants will enter the cylinder in liquid form (see appendix fig 121 and fig 122 for pressure dependent boiling points of the mixtures). In the case of 250° Fahrenheit (figure 5) it is very likely that the methanol (coloured in green) will enter the cylinder in a (mostly) gaseous state since its boiling point is in average 40 K below the preheating temperature at this pressure (see table 35 in the appendix for boiling points at different conditions). For the water (coloured in blue) fraction it is not clear if it will evaporate, its boiling point is at least a few Kelvin above the preheating temperature at the inlet pressures. Comparing the impact of water addition on the knock limited IMEP with the addition of water-methanol mixtures we can clearly see that the mixture with methanol shows a much higher sensitivity on the preheating temperature. Raising the preheating temperature above its boiling point lowers its efficiency at a certain fuel-air ratio (0.06) to nearly zero. This is while all other engine parameters are kept the same and would further suggest that the choice of the preheating temperature in the MON test is one of the main issues for the poor performance of some fuels in this test.

Figure 4: Fig 5c) from NACA Report 812 [64]. Colouring added by author for eye guidance. Original citation from [64]: *Effect of internal coolants 1,2, and 3 on knock-limited engine performance. CFR engine; fuel, AN-F-28, compression ratio 7.0; inlet-coolant temperature, 250° F; spark advance, 30° B.T.C.; engine speed, 2500 rpm. Variation of indicated specific fuel consumption and knock-limited indicated mean effective pressure with fuel-air ratio at inlet-air temperature of 150° F.*
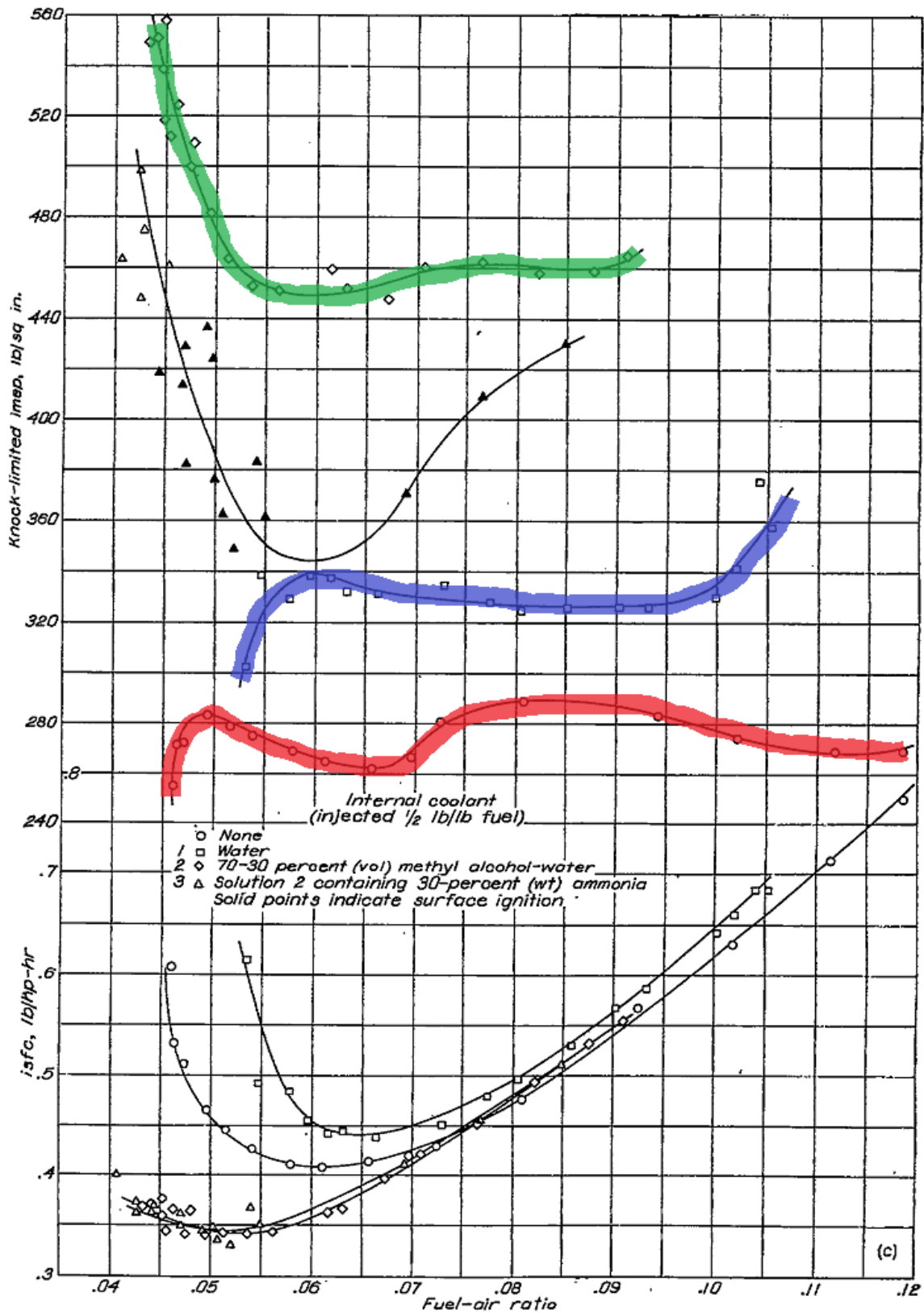
Figure 5: Fig 5a) from NACA Report 812 [64]. Colouring added by author for eye guidance. Original citation from [64]: *Effect of internal coolants 1,2, and 3 on knock-limited engine performance. CFR engine; fuel, AN-F-28, compression ratio 7.0; inlet-coolant temperature, 250° F; spark advance, 30° B.T.C.; engine speed, 2500 rpm. Variation of indicated specific fuel consumption and knock-limited indicated mean effective pressure with fuel-air ratio at inlet-air temperature of 250° F.*
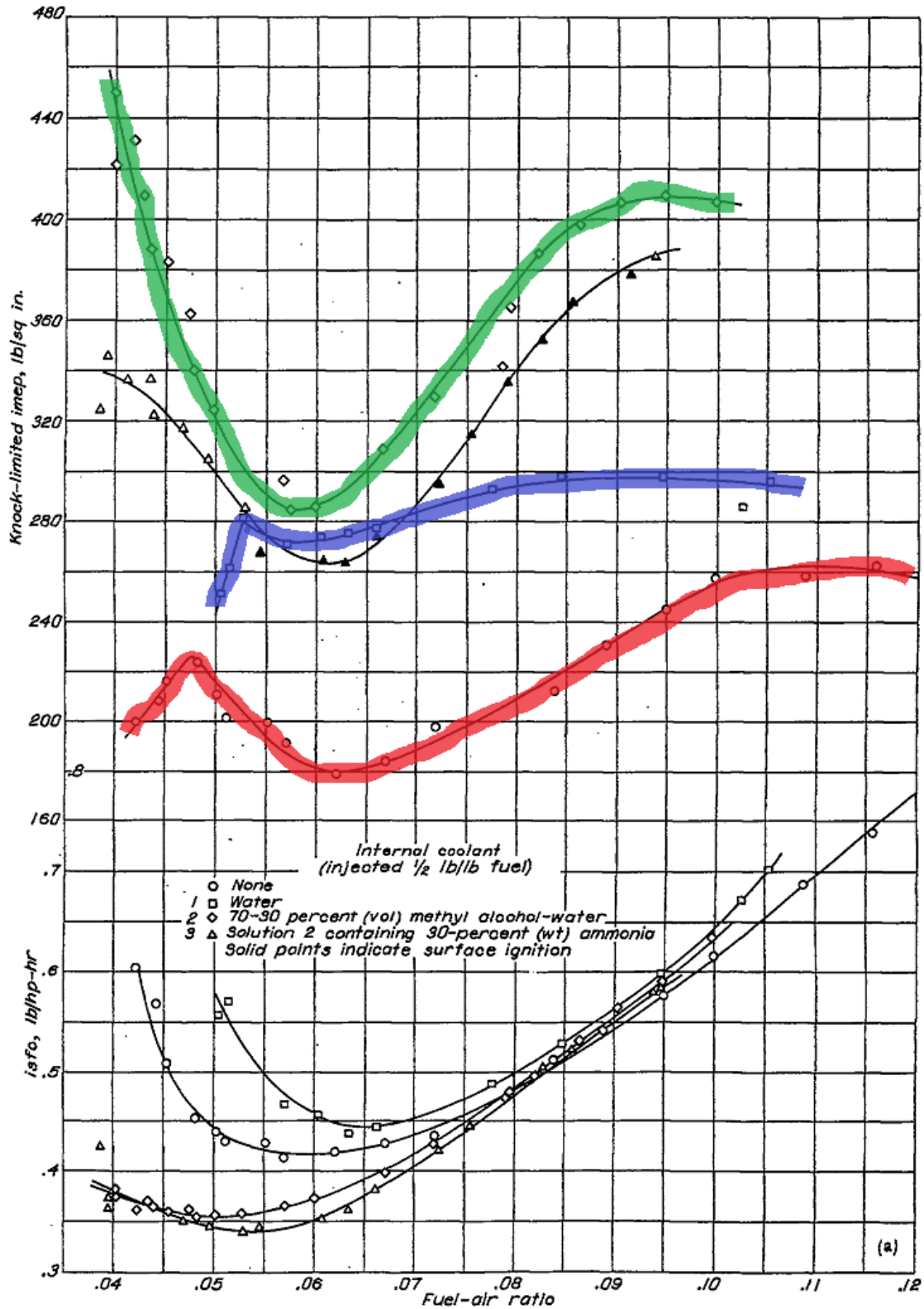
5.3 Blending rules and mixture formulation

The aim is to develop a tool which will suggest a ETRF surrogate on a minimal number of input parameters. First the applied blending rules are outlined and validated against measured RON and MON of TRF mixtures. In a second step ETRF surrogate mixtures are calculated for available commercial gasolines and its properties are compared.

As pointed out before toluene is the reference surrogate component representing the aromatics. Since the quantity of aromats is regulated in most countries its mixture fraction is stated in fuel data sheets. Further we often know the RON and ethanol content. The content of other components such as n- and iso-alkanes is often not known. This means that the ethanol and toluene content as well as the RON should be set as fix targets in the reference fuel composition. It will be shown that it is also necessary to make assumptions about the mean molecular density and molar mass of the gasoline. The calculation of a 4 component surrogate fuel for any gasoline containing up to 100% ethanol is done in two steps. Based on blending rules investigated by Morgan et al. [57] for gasoline / ethanol mixtures it is possible to calculate which RON the gasoline surrogate fraction needs to have to achieve the RON of the total mixture. Based on rules developed by Anderson et al. [58] the RON of the gasoline surrogate fraction and the target toluene content of the total mixture, the mixture fraction of iso-octane and n-heptane can be calculated. At this point the complete surrogate mixture is known and all other properties such as MON, density, C:H:O ratio and lower heating value can be calculated.

5.3.1 Blending rules for gasoline / ethanol mixtures

To the best knowledge there are no systematic studies of octane numbers of TRF - ethanol mixtures. At this point we rely on the investigations of Anderson et al. [58]. In their work they investigated the different blending rules for mixtures of gasoline and ethanol. The best agreement for RON/MON prediction was found for the linear molar based blending rule. It was further observed that the blending octane number of ethanol is equal to the octane number of the pure fuel. We assume a RON of 109 and a MON of 90 for pure ethanol.

5.3.2 Determination of the TRF surrogate mixture

The most crucial point is the correct prediction of the RON and MON for a given mixture of n-heptane, iso-octane and toluene. The calculation of other physical properties such as lower heating value and density is comparable easy. Already short after the testing conditions for RON and MON became common practise different methods to estimate those reference numbers for known fuel compositions were developed. Some early methods can be found in the work of Spausta [51] while the work of Knop et al. [61] gives an overview of different methods developed until today. In this work the "modified LbV response surface model" suggested by Morgan et al. [57] is used to determine the octane number of TRF mixtures:

$$ON = a_p p + a_{tol} + x_{tol} + a_{tol^2} x_{tol}^2 + a_{tol,p} x_{tol} p. \tag{5.1}$$

p is the re normalisation of the n-heptane / iso-octane (PRF) number from a value of 0 to 100 to a value between 0 and 1:

$$p = \frac{x_{io}}{x_{io} + x_{nh}}. \tag{5.2}$$

The coefficients used are those recommended by Morgan and co-workers and summarised in table 9. x_{tol}, x_{io} and x_{nh} are the molefractions of toluene, n-heptane and iso-octane.

Coefficient	a_p	a_{tol}	a_{tol^2}	$a_{tol,p}$
RON	100	142.79	-22.651	-111.95
MON	100	128.00	-19.207	-119.24
Sensitivity	0	14.79	-3.444	7.29

Table 9: Coefficients for equation 5.1 derived by Morgan et al. [57].

Since RON and toluene fraction are determined by the fuel data sheets we can calculate the n-heptane and iso-octane fraction needed to achieve the RON. At this point the complete surrogate mixture is known and all other properties such as MON, density, lower heating value and carbon to hydrogen ratio can be calculated.

In order to test this approach a literature survey was performed and table 10 summarises all data found for TRF mixtures. The first six columns state the composition of the fuel and the measured MON, RON and Sensitivity (S). All other columns state the predicted values using the approach outlined above. In contrast to the work of Morgan and co-workers the RON is not calculated, but together with toluene fraction set as target value. The equation is solved for n-heptane and iso-octane fraction, the MON and other physical properties are calculated from the obtained mixture. Since the volume fraction of ethanol and toluene is given, it is assumed that rest of the surrogate has the same density and molar mass as iso-octane. The error introduced by this assumption is small since n-heptane and iso-octane have similar properties (see table 6).

To estimate the accuracy of the developed method one has to know the experimental uncertainty of the determination of the RON and MON. One obvious uncertainty comes from rounded experimental data provided in the fuel data sheets (fuel fractions and sometimes octane numbers). This means a deviation below 0.5% volume fraction or 0.5 points in ON can often be ignored. The accuracy of the experimental uncertainty is hard to estimate. Merker [65] gives a general uncertainty of one point in the RON and MON determination, while Knopp et al. [66] suggest a different uncertainties for repeatability and reproducibility based on the actual octane number. The repeatability limit is given as 0.2 for the RON and for the MON up to 90 increasing to 0.6 for 105 MON. They further give a reproducibility limit for the RON of 0.7 up to 100 RON and increasing up to 3 for 115 RON. The reproducibility limit for the MON is given with 0.9 up to RON 90 increasing to 2 for RON 105. This is very much in line with the investigations summarised by Spausta [51] based on different studies carried out in the 1930s and 1940s.

Assuming that the average uncertainty in RON and MON is about 0.7 to 1.0 points for most of the mixtures summarised in table 10 the prediction is within this uncertainty. A strong

deviation of measured and predicted octane number is observed for the experiments of Kalgahatgi et al. from 2015 [67] with toluene fraction above 80 vol% (data set 55-59). Data for mixtures with such a high toluene fraction were not available when Morgan et al. [57] developed their correlation. Due to regulations it is very unlikely that comercial gasoline, and therefore the surrogate, will have such a high concentration of aromatics.

Figures 6 a) to c) show the calculated values for MON, n-heptane and iso-octane fraction vs. the experimental value. A line with a slope of 1 is shown illustrating a perfect agreement between prediction and measurement. In the plot for MON two dashed lines show an experimental uncertainty of 1 point in octane number. In general we see a very close agreement between the predicted values and the measured values.

In figure 6 d) and e) the deviation in MON is plotted over the input quantities RON and toluene fraction. It can be observed that most of mixtures are within the limit of 1 point deviation in MON. A larger deviation is found for higher toluene fractions and therefore higher RON. Here we have to keep in mind that most of the data sets are for surrogate mixtures above RON 90 and therefore most of the data sets are found in this region. However the correlation shows that most of the surrogates are within a deviation of 2 points in MON and therefore within the limit of reproducibility. Mixtures for which the prediction deviates more than 2 points often have toluene contents above 67 vol%. This would represent an aromatic content in real gasoline far above what is allowed by regulation in most countries. Excluding those experiments nearly all predicted motor octane numbers are within a deviation of 1 point.

| Nbr. Source	V_{io}	V_{nh}	V_{tol}	MON	RON	S	V_{io}	V_{nh}	MON	ΔV_{io}	ΔMON
		Measurement					**Prediction using correlation**			**Deviation**	
01 [67]	18	72	10	-	32	-	18.20	71.80	30.41	-0.2	-
02 [67]	16	64	20	-	42	-	14.80	65.20	38.90	1.2	-
03 [67]	14	56	30	48	53.2	5.2	13.10	56.90	48.66	0.9	-0.66
04 [67]	12	48	40	58	63.7	5.7	11.10	48.90	57.80	0.9	0.2
05 [67]	10	40	50	68	75.5	7.5	11.10	38.90	68.10	-1.1	-0.1
06 [68]	5	21	74	85.2	96.9	11.7	05.50	20.50	86.70	-0.5	-1.5
07 [68]	10	16	74	88.7	99.8	11.1	09.90	16.10	88.70	0.1	0
08 [67]	36	54	10	-	48	-	34.30	55.60	46.28	1.7	-
09 [67]	32	48	20	-	58	-	31.30	48.70	54.60	0.7	-
10 [67]	24	36	40	68	75.1	7.1	23.50	36.50	68.60	0.5	-0.6
11 [67]	20	30	50	76.2	83.8	7.6	20.50	29.50	75.77	-0.5	0.43
12 [67]	28	42	30	61	66.1	5.1	26.70	43.30	61.14	1.3	-0.14
13 [67]	54	36	10	64.4	66	1.6	52.60	37.40	64.12	1.4	0.28
14 [67]	48	32	20	70	73.6	3.6	47.40	32.60	69.92	0.6	0.08
15 [67]	36	24	40	79.6	86.2	6.6	35.50	24.50	79.10	0.5	0.5
16 [67]	30	20	50	82.9	92.1	9.2	29.90	20.10	83.38	0.1	-0.48
17 [67]	42	28	30	74	79	5	40.30	29.70	73.62	1.7	0.38
18 [67]	64	16	20	85.6	89.1	3.5	63.30	16.70	85.12	0.7	0.48
19 [67]	56	14	30	86.9	92.8	5.9	54.80	15.20	86.96	1.2	-0.06
20 [67]	48	12	40	88.7	96.7	8	46.90	13.10	89.05	1.1	-0.35
21 [67]	40	10	50	90.9	99.8	8.9	38.70	11.30	90.45	1.3	0.45
22 [67]	72	18	10	82	84.5	2.5	71.40	18.60	82.48	0.6	-0.48
23 [68]	0	42	58	66.9	75.6	8.7	00.50	41.50	66.90	-0.5	0
24 [68]	0	34	66	74.8	85.2	10.4	01.10	32.90	76.79	-1.1	-1.99
25 [68]	0	30	70	78.2	89.3	11.1	00.60	29.40	80.53	-0.6	-2.33
26 [68]	0	26	74	81.5	93.4	11.9	00.20	25.80	84.30	-0.2	-2.8
27 [67]	10	30	60	75.2	85.3	10.1	09.50	30.50	76.63	0.5	-1.43
28 [67]	20	20	60	83.7	95	11.3	21.30	18.70	85.04	-1.3	-1.34
29 [57]	17	64	19	37	39	2	13.10	67.90	36.09	3.9	0.91
30 [57]	0	50	50	57.7	65.9	8.2	00.20	49.80	59.30	-0.2	-1.6
31 [57]	33	33	33	70.9	76.2	5.3	33.50	33.50	70.49	-0.5	0.41
32 [57]	67	17	16	84	87	3	66.20	17.80	83.80	0.8	0.2
33 [57]	17	17	67	87.4	98	10.6	16.50	16.50	87.19	0.5	0.21
34 [61]	0	27	73	80.7	92.3	11.6	00.20	26.80	83.30	-0.2	-2.6
35 [61]	72	10	18	90.3	93.7	3.4	70.60	11.40	90.02	1.4	0.28
36 [61]	44	17	40	85.8	93	7.2	42.90	17.10	85.55	1.1	0.25
37 [61]	51	15	34	86.7	93	6.3	50.20	15.80	86.49	0.8	0.21
38 [61]	0	21	79	86.2	97.7	11.5	-01.80	22.80	88.65	1.8	-2.45
39 [61]	65	10	25	90.5	95.2	4.7	63.40	11.60	90.18	1.6	0.32
40 [61]	35	15	50	87.3	96.3	9	34.70	15.30	87.24	0.3	0.06
41 [61]	69	17	14	84.2	86.6	2.4	68.40	17.60	83.79	0.6	0.41
42 [61]	74	16	10	84.6	85.7	1.1	72.60	17.40	83.67	1.4	0.93
43 [61]	43	14	44	88.3	96.3	8	41.80	14.20	88.30	1.2	0
44 [46]	90	-	10	-	102	-	89.10	00.90	99.83	0.9	-
45 [67]	80	0	20	-	104.1	-	78.70	01.30	99.75	1.3	-
46 [67]	70	0	30	-	105.6	-	68.30	01.70	99.34	1.7	-
47 [67]	60	0	40	-	107.7	-	58.10	01.90	98.81	1.9	-
48 [67]	50	0	50	100.3	108.2	7.9	48.20	01.80	98.15	1.8	2.15
49 [67]	30	10	60	91.2	101.6	10.4	29.30	10.70	90.76	0.7	0.44
50 [67]	40	0	60	100.4	110	9.6	39.60	00.40	98.04	0.4	2.36
51 [67]	4	16	80	90.5	101	10.5	02.40	17.60	90.50	1.6	0
52 [67]	8	12	80	94	103.1	9.1	06.30	13.70	91.55	1.7	2.45
53 [67]	12	8	80	97.5	105.4	7.9	10.90	09.10	97.50	1.1	0
54 [67]	18	2	80	101	108.5	7.5	16.80	03.20	101.00	1.2	0
55 [67]	20	0	80	102.8	112.6	9.8	24.60	-04.60	102.80	-4.6	0
56 [67]	0	10	90	100	106	6	55.10	-45.10	59.30	-55.1	40.7
57 [67]	2	8	90	101.4	108	6.6	28.70	-18.70	78.68	-26.7	22.72
58 [67]	4	6	90	102.4	109.5	7.1	08.80	01.20	93.21	-4.8	9.19
59 [67]	6	4	90	104.4	111.8	7.4	-21.70	31.70	115.50	27.7	-11.1
60 [68]	15	11	74	92.6	103.3	10.7	15.20	10.80	91.08	-0.2	1.52
61 [68]	20	6	74	96.6	107.6	11	21.70	04.30	94.03	-1.7	2.57
62 [57]	17	17	67	99.3	110	10.7	32.30	00.70	96.85	-15.3	2.45
63 [52]	0	0	100	109	120	11	00.00	00.00	108.57	0	0.43
64 [69]	0	35	65	73.2	83.9	10.7	00.80	34.20	75.63	-0.8	-2.43
65 [69]	0	36	64	73.1	82.3	9.2	00.20	35.80	74.21	-0.2	-1.11
66 [69]	0	38	62	70.3	80.5	10.2	00.80	37.20	72.55	-0.8	-2.25
67 [69]	0	50	50	58.1	64.1	6	-01.90	51.90	57.70	1.9	0.4
68 [69]	0	25	75	82.6	94.2	11.6	-00.20	25.20	88.00	0.2	-5.4
69 [55]	63	17	20	85	88	3	62.20	17.80	84.05	0.8	0.95
70 [55]	69	17	14	85	87	2	68.80	17.20	84.18	0.2	0.82

Table 10: Experimental RON and MON for various published TRF mixtures along with the predicted octane numbers using the modified LbV response surface model. Data used by Morgen et al. [57] for the development of the correlation function are not included in this table. Fuel fractions are given in liquid volume fractions.
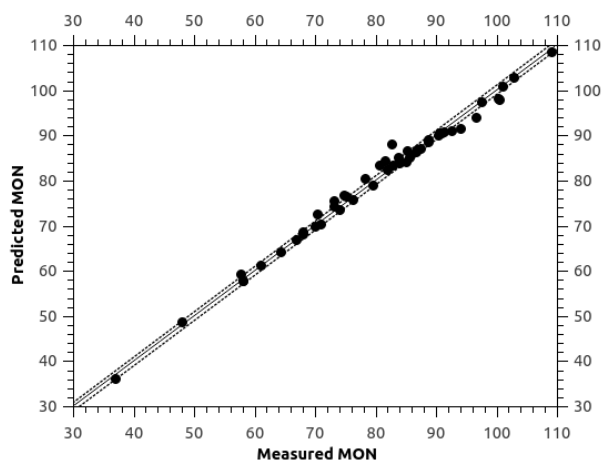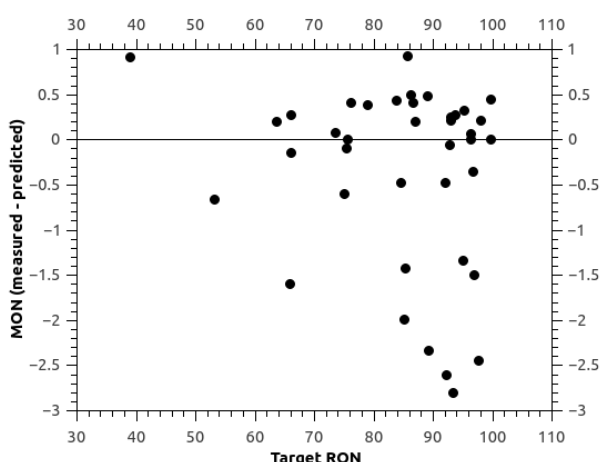
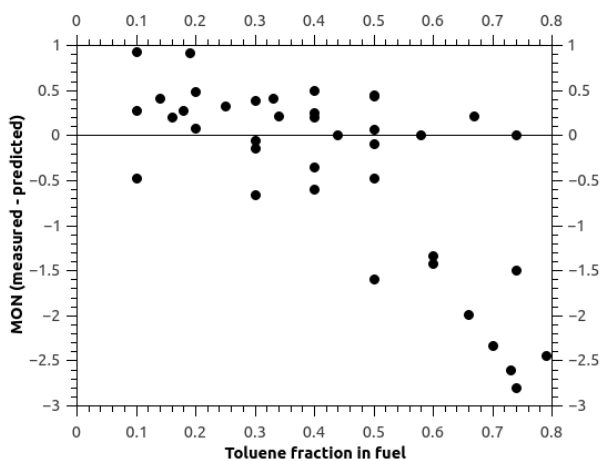(a) Predicted MON vs. measured MON
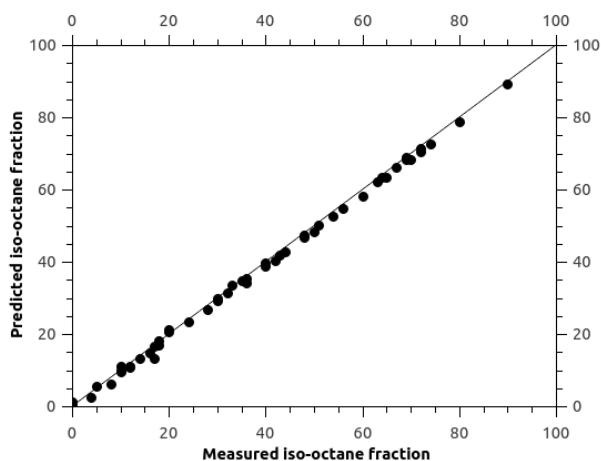
(b) Predicted vs. measured iso-octane volume fraction
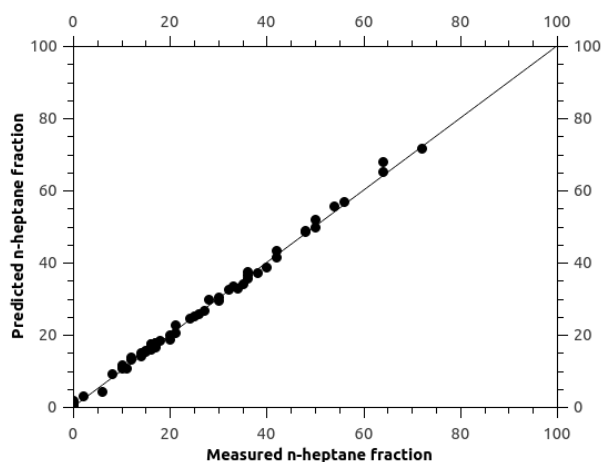
(c) Predicted vs. measured n-heptane volume fraction

(d) Target RON vs. deviation of predicted MON

(e) Target toluene fraction vs. deviation of predicted MON

Figure 6: Depiction of correlation between measured and predicted data from table 10. Mixture fractions are given in liquid volume fraction. Mixtures with 80 vol% and more toluene are not shown.

5.3.3 Graphical Representation of TRF Mixing Rule

As an example the calculation of the MON of a surrogate for gasoline (data sheet 3 in table 11) is outlined. As input a RON of 95.6 and an aromatic content of 22.8 vol% is given. The mixture can be deduced in several steps as shown in figure 7:

1. The crossing point of the surface for RON 95.6 and 22.8 vol% is searched.

2. This corresponds to 10 vol% n-heptane and 65 vol% in iso-octane.

3. At this point the mixture is known and we can read the MON from the plot from the ride side.

Fig. 2. A contour plot of RON in the tri-component mixture space generated using the 3-parameter MLbV model.

Fig. 3. A contour plot of MON in the tri-component mixture space generated using the 3-parameter MLbV model.

RON   MON
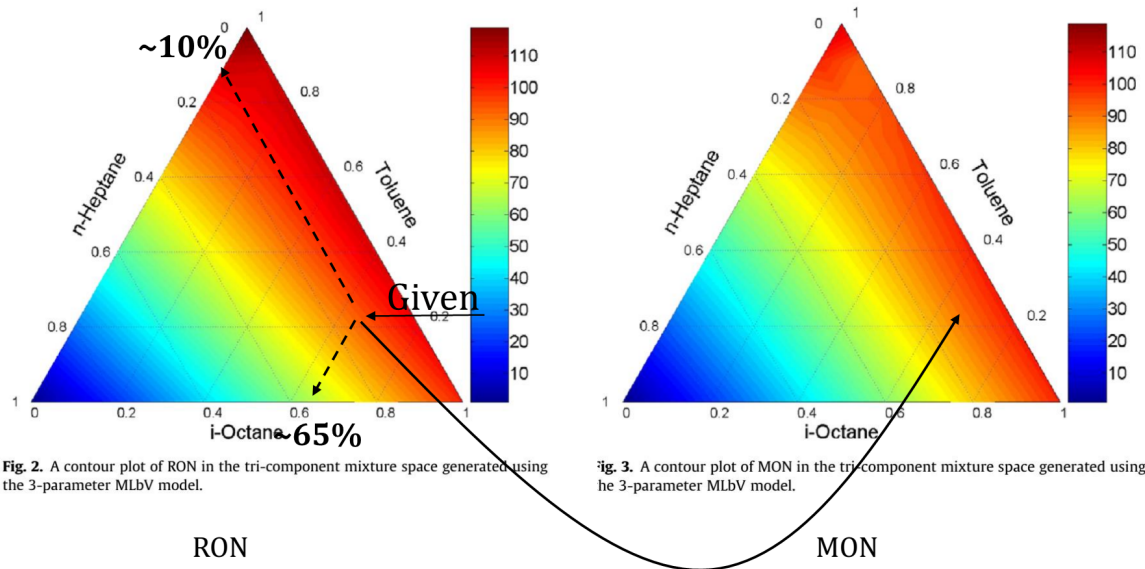
Figure 7: Deduction of a surrogate for gasoline with 22.8 vol% aromatic fraction and a RON of 95.6. Display of mixture triangles are taken from Morgan and co-workers [57].

5.4   Comparison of Calculated ETRF Surrogates against Commercial Gasoline

In this section the properties of commercial gasoline against the calculated TRF and ETRF surrogates are compared. The fuel certificates were mostly obtained from Total and their key properties are summarised in table 11. The RON, the aromatic and ethanol content from this data are used as input (see table 12). This input leads to the predicted surrogate fuel mixtures condensed in table 13 and the deviation between the fuel properties of the real fuel and the suggested surrogates is compared in table 14.

The MON is overestimated by the surrogate fuels by about four points in average. This is no surprise when considering that the two PRF fuels may overestimate the RON by default (see discussion in Section 5.2). The density is well matched and only underestimated by about 1% while C:H:O ratio and lower heating value is very well matched for all mixtures[12]. Overall it can be concluded that this is a very good agreement for three or four component surrogate fuels with those properties of real gasoline.

The boiling line of real gasoline can not be matched with a ETRF surrogates. As shown in table 11 the initial boiling point of gasoline is between 304 and 316 K. The four available surrogates have boiling points which are at least 35 K higher. For regular gasoline up to RON 98 the final boiling point is at least 48 K higher. Please note that the initial boiling point obtained is the EN-ISO 3405 or ASTM D86 test is not same as the boiling point of a pure substance. Due to the test setup both tests will very likely overestimate the initial[13] and the final boiling point by a few Kelvin and it can not capture the impact of very volatile fuel components. The boiling point of the three major surrogate components differs by about 12 K and it will not be possible to match the boiling line of commercial gasoline which often covers about 150 K. To be able to achieve a better match with the boiling lines of commercial gasoline fuels at least two components need to be added to the surrogate fuel: one with a low boiling point and one with a high boiling point. Possible candidates are a C_5 fuel (e.g. n-pantene with a boiling point at about 309 K) and a C_{10} to C_{12} fuel (e.g. n-decane with a boiling point at about 447 K). The selection of additional reference fuels should also take other properties into consideration such as: octane rating, availability as pure component, price, miscibility, toxicity, C:H:O ratio, and functional groups which need to be represented.

---

[12]Despite the uncertainty of fuel number 8. The C:H:O ratio would be closer when the unknown fraction is assumed to be water and not gasoline.

[13]Quote from the ASTM D86 procedure *initial boiling point (IBP), the corrected thermometer reading that is observed at the instant the first drop of condensate falls from the lower end of the condenser tube*. This temperature will be slightly higher than initial boiling point of most volatile species in the fuel. The impact of species which are highly volatile and do not condense can not be captured.

Data Sheet	RON [-]	MON [-]	V_a [-]	V_e [-]	Density [$\frac{kg}{m^3}$]	C [w %]	H [w %]	O [w %]	LHV [$\frac{MJ}{kg}$]	I_{BP} [K]	F_{BP} [K]
1	93.6	82.4	0.117	0.228	744	77.7	13.9	8.4	39.55	313.5	468.7
2	96.7	85.8	0.279	0.095	744	83	13.5	3.5	41.51	309.4	462.8
3	95.6	84.0	0.228	0	746	84.1	13.6	2.3	42.43	307.9	457.5
4	96.2	85.1	0.369	0	763.7	84.8	12.8	2.4	42.945	301.5	453.2
5	91.0	81.2	0.262	0	747.4	84.3	13.4	2.3	44.44	307.3	457.9
6	91.4	82.4	0.37	0	761.5	84.9	12.9	2.2	44.39	304.2	455.0
7	87.9	80.5	0.363	0	751.7	86.8	13.2	<0.2	NA	303.6	454.7
8	>95.0	>85.0	0.0	0.958	808	48.8	12.9	38.3	24.98	350.5	352.4
9	87.0	77.5	0.24	0	744.2	86.8	13.4	<0.2	43.155	308.0	457.5
10	90.1	80.2	0.263	0	753	86.7	13.3	0.0	43.12	316.2	441.2
11	94.0	80.9	0.262	0	750.6	84.4	13.2	2.4	42.02	311.4	461.0
12	106.9	95.3	0.352	0	756.2	84.1	12.7	3.2	41.26	306.4	394.2
13	91.0	82	0.149	0	744.2	86	14	<0.1	43.49	315.1	431.6
14	94.5	84.1	0.326	0	747.5	86.9	13.1	<0.2	42.94	308.0	435.6

Table 11: Data from the fuel specification sheets for the different commercial gasoline fuel batches. Please note that for the fuel number 8 the alternative is to assume that the mixture contains 95.8 vol% ethanol and the rest to be water - this would be in line with the measured lower heating value. With water the mixture would have a LHV of about 25.2 MJ/kg. The developed correlation cannot suggest mixtures containing water. V_a and V_e are the liquid volume fractions of aromatics and ethanol. I_{BP} and F_{BP} are the initial and final boiling point obtained in the EN-ISO 3405 or ASTM D86 test.

Batch Unit	RON [-]	V_a [-]	V_e [-]
1	93.6	0.117	0.228
2	96.7	0.279	0.095
3	95.6	0.228	0
4	96.2	0.369	0
5	91	0.262	0
6	91.4	0.37	0
7	87.9	0.363	0
8	108	0.0	0.958
9	87	0.24	0
10	90.1	0.263	0
11	94	0.262	0
12	106.9	0.352	0
13	91	0.149	0
14	94.5	0.326	0

Table 12: Data used as input the calculated the surrogate fuels for the different fuel batches derived from data summarised in table 11. V_a and V_e are the liquid volume fractions of aromatics and ethanol.

Fuel	X_e	X_{tol}	X_{io}	X_{nh}	L_e	L_{tol}	L_{io}	L_{nh}	Y_e	Y_{tol}	Y_{io}	Y_{nh}
1	0.435	0.114	0.321	0.13	0.232	0.11	0.484	0.174	0.25	0.131	0.457	0.162
2	0.202	0.319	0.37	0.109	0.096	0.276	0.497	0.131	0.101	0.32	0.46	0.119
3	0	0.311	0.585	0.104	0	0.228	0.666	0.106	0	0.271	0.631	0.099
4	0	0.47	0.411	0.119	0	0.369	0.501	0.13	0	0.424	0.459	0.117
5	0	0.349	0.495	0.156	0	0.262	0.576	0.162	0	0.309	0.542	0.15
6	0	0.469	0.365	0.166	0	0.37	0.448	0.182	0	0.425	0.411	0.164
7	0	0.46	0.342	0.199	0	0.363	0.419	0.218	0	0.418	0.385	0.197
8	0.985	0	0.006	0.009	0.961	0	0.017	0.022	0.966	0	0.015	0.019
9	0	0.322	0.486	0.192	0	0.24	0.562	0.198	0	0.284	0.531	0.184
10	0	0.35	0.485	0.164	0	0.263	0.565	0.172	0	0.31	0.532	0.159
11	0	0.348	0.526	0.126	0	0.26	0.61	0.13	0	0.306	0.573	0.12
12	0	0.457	0.523	0.02	0	0.352	0.626	0.022	0	0.405	0.575	0.02
13	0	0.211	0.653	0.136	0	0.149	0.717	0.134	0	0.18	0.693	0.127
14	0	0.423	0.447	0.13	0	0.326	0.534	0.14	0	0.378	0.495	0.127

Table 13: Calculated surrogate fuel based on the input in table 12. Mixtures are given in molar fraction (X), liquid volume fraction (L) and mass fraction (Y). The liquid volume fraction was calculated by using equation 14.1 stated in the appendix.

Batch Unit	M [$\frac{kg}{mol}$]	ρ [$\frac{kg}{m^3}$]	RON [-]	MON [-]	C [w%]	H [w%]	O [w%]	LHV [$\frac{MJ}{kg}$]	Δ MON [-]	Δρ [$\frac{kg}{m^3}$]	Δ C [w%]	Δ H [w%]	Δ O [w%]	Δ LHV [$\frac{MJ}{kg}$]
1	0.0802	746	93.6	83.47	76.97	14.35	8.68	39.50	-1.07	-2	0.73	-0.45	-0.28	0.046
2	0.0919	752	97.7	88.1	83.11	13.37	3.53	41.37	-2.3	-8	-0.11	0.13	-0.03	0.139
3	0.1059	730.55	95.6	90.97	86.02	13.98	0	43.30	-6.97	15.45	-1.92	-0.38	2.3	-0.87
4	0.1022	754.91	96.2	89.08	87.09	12.91	0	42.75	-3.98	8.79	-2.29	-0.11	2.4	0.194
5	0.1043	735.8	91	85.87	86.24	13.76	0	43.19	-4.67	11.6	-1.94	-0.36	2.3	1.243
6	0.1016	754.44	91.4	84.48	87.05	12.95	0	42.75	-2.08	7.06	-2.15	-0.05	2.2	1.635
7	0.1013	752.76	87.9	81.24	86.96	13.04	0	42.78	-0.74	-1.06	-0.16	0.16	0	NA
8	0.047	787.71	108	89.29	53.26	13.16	33.58	27.44	NA	20.29	-4.46	-0.26	4.72	-2.466
9	0.1044	731.5	87	82.36	86.03	13.97	0	43.29	-4.86	12.7	0.77	-0.57	0	-0.141
10	0.1042	735.85	90.1	84.98	86.24	13.76	0	43.19	-4.78	17.15	0.46	-0.46	0	-0.074
11	0.1048	753.84	94	88.83	86.27	13.73	0	43.20	-7.93	-3.24	-1.87	-0.53	0	-1.18
12	0.1039	753.29	106.9	99.6	87.07	12.93	0	42.80	-4.3	2.91	-2.97	-0.23	0	-1.543
13	0.1077	716.39	91	87.96	85.36	14.64	0	43.68	-5.96	27.81	0.64	-0.64	0	-0.193
14	0.1031	747.27	94.5	88.16	86.76	13.24	0	42.92	-4.06	0.23	0.14	-0.14	0	0.013
								ø:	-4.13	7.835				-0.25

Table 14: Left side: Predicted physical properties of the surrogate mixtures from table 13; Right side: difference to the actual real gasoline (measured - prediction) from table 11.

6 Detailed and Lumped Reaction scheme

The aim of the mechanism developed in this work is to provide a single scheme which can describe as much fuels as possible over a wide range of conditions and experiments. To be able to compile different multicomponent reaction schemes a new concept was developed. The principle idea of this "variable mechanism concept" is outlined in the next section. After this introduction the compilation of the detailed ETRF mechanism along with the lumping approach is explained. This lumped scheme is than validated and used for further investigations.

6.1 Variable Mechanism concept

The "variable mechanism concept" is an approach to compile reaction schemes from different sub-mechanism for different multicomponent fuel blends. The concept was designed and brought into application by the author of this thesis but never published as such. The approach is similar to the hierarchically organized mechanism from the CRECK Modeling group at Politecnico di Milano and fundamentally different to the other common approach to compile a new mechanism for each fuel / experiment which is studied.

It is comparable easy to generate chemistry models which work well for single fuels and limited application range (e.g. only prediction of ignition delay times). Developing a scheme for single fuels but for multiple applications, e.g. prediction of premixed flames, ignition delay and speciation in jet stirred reactors, is more demanding. Even more complicated is to capture the interaction of two or more fuels. The main issue one has to avoid is that the model combined of two or more chemistry sub-models predict a significant different combustion than the solely schemes.

All schemes must share the same "base" chemistry. The minimum number of species needed for this base chemistry can be estimated by a simple reasoning: It is known that large alkanes, starting from about five or six carbon atoms, show very similar combustion behaviour. Hence they can be described by site dependent rules (see also chapter 2). This further implies that all intermediates / products are covered by the reaction classes themself or are smaller than the fuel[14]. Therefor a base chemistry for n- and iso-alkanes should contain a well validated C_1 to C_5 chemistry. Further it can be assumed that cross reactions between large intermediate products formed by larger fuel molecules ($> C_6$) can be neglected - this assumption is based on two considerations:

1. The concentration of such species is very low in comparison to intermediates / products from the base chemistry up to C_2 formed during the oxidation process.

2. The lifetime of such species is usually very short.

With a determined covarage of the base chemistry and no cross-reactions to consider it is possible to develop the schemes (sub-models) for all larger fuels with the same base chem-

---

[14]This does not apply for typical build up chemistries such as the formation of poly-aromatic hydrocarbons (PAH). This is why the PAH chemistry is contained in an extra sub-model.

istry and combine those to more complex multicomponent schemes. The general approach is depicted in figure 8 and for the ETRF mixture in figure 9.
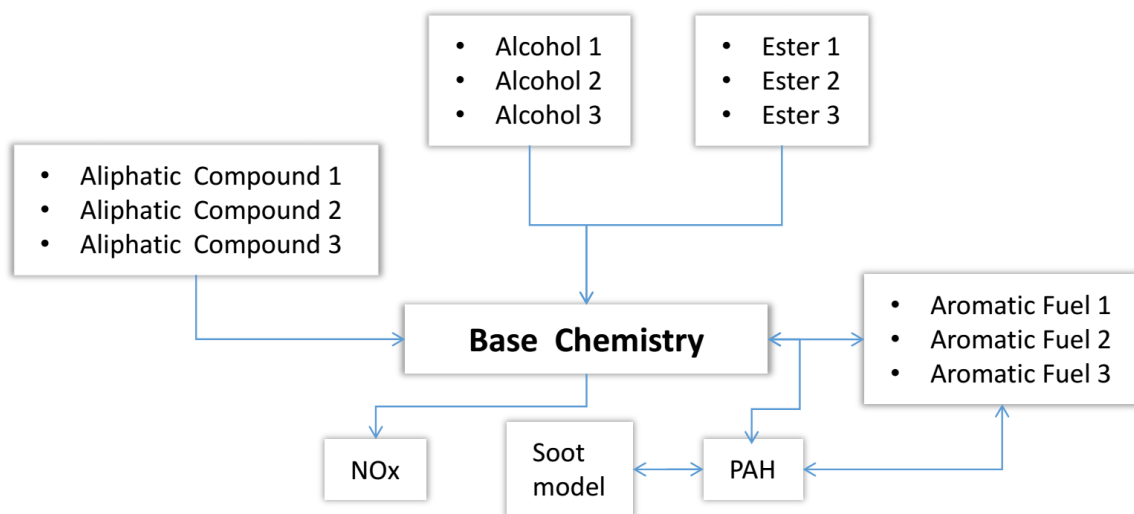
Figure 8: A general description of the variable mechanism concept.
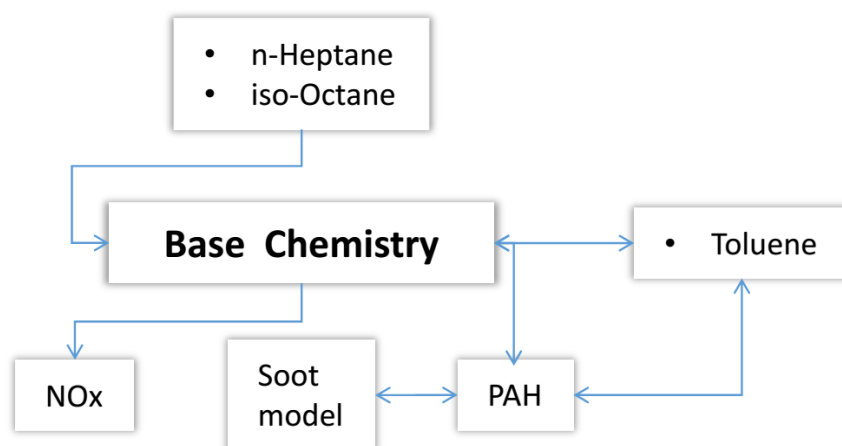
Figure 9: The compilation of the (semi) detailed gasoline reference fuel composed of the main fuels n-heptane, iso-octane, toluene and ethanol (part of the base chemistry).

To assure that the variable mechanism concept can work a few strict rules needs to be followed. Some of those rules may seem trivial, but they also explain why it is very demanding to combine reaction schemes from different sources (e.g. scientific publications) to a multicomponent mechanism. At least the following rules must be satisfied to combine (sub)mechanism:

- Same species need to have the same names in the base chemistry and in the sub mechanisms for larger fuels. Explanation: *Different names for the same species would lead to an inconsistent chemistry and very likely to dead ends and subsequently to reaction schemes which can never predict equilibrium condition / burn rates / hydrocarbon emissions.*

- Same species need to use the same physical properties (thermodynamic data and transport data). Explanation: *Major problem arise from thermodynamic data. Those are often needed to calculate the reverse reaction rates unless reverse reaction rates are stated explicitly. These reactions might be very sensitive. Since in the combined mechanism each species has only one set of thermodynamic data, depending on which values are used the reverse rates either in the base chemistry or the in sub mechanism for the larger fuels will change. Even if the reverse rate is written explicit the state function of the gas phase can slightly differ depending on the concentration of the species in question.*

- The sub-mechanisms for larger fuels shall not contain reactions already contained in the base chemistry. Explanation: *Each reaction can only exist once. If one reaction exists more than once using different rate expressions in the combined mechanism a decision has to be taken which reaction is valid. This will subsequently change the prediction of the base chemistry or the sub-mechanism for larger fuels.*

- The sub-mechanisms for larger fuels need to include decomposition pathways for all species which lead to species defined as products in the base chemistry. Explanation: *If an intermediate species has no pathway to decompose into species contained in the base chemistry they can become dead ends and subsequently the scheme cannot correctly predict equilibrium conditions / burn rates / hydrocarbon emissions.*

This set of rules and the fact that the sub-mechanisms for larger fuels need to be based on the same chemistry implicate that with any change to the base chemistry a validation of the other sub-mechanisms is necessary. There is an additional issue which needs to be made clear at this point. A good performance of each single fuel against experiments does not ensure that mixtures perform similarly well against experiments. In this approach cross reactions between large fuels are not considered, but still none linear effects can occur due to reactions with the same radical pool[15]. The radical pool may be formed in an early stage of the combustion by one fuel component and could than lead to an early H abstraction at another fuel molecule initiating an earlier fuel decomposition (see also discussion in chapter 9). Therefore multicomponent reaction mechanisms still need to be validated against experiments and a reasonable prediction for blends and pure fuels should be verified.

6.1.1 Verification of the variable mechanism concept

6.1.1.1 The impact of adding sub-mechanisms Figure 8 shows a general depiction of the variable mechanism concept and the representation for the gasoline reference fuel discused in this thesis is shown in figure 9. Figure 10 compares the predicted ignition delay times for pure n-heptane (see figure 10 a)) and iso-octane (see figure 10 b)) of two

---

[15]The term "radical pool" refers to the amount of different radicals in the gas phase. For chain explosion reactions, radicals are formed during the ignition delay period (also known as the induction time). Once the radical pool is large enough fuel is consumed at a high rate, ignition takes place and the temperature is rising rapidly. More detailed description can by found in the works from Coats et al. [70] or Warnatz et al. [71]. The discovery of the importance of a radical pool could be attributed to Nikolay Semenov and his investigations in the 1930 where he investigated chain reactions occuring in combustion. He and Norman Hinshelwood were awarded with a Nobel Prize in 1956 *"for their researches into the mechanism of chemical reactions"*. The importance of the radical pool is described in the Nobel lecture from Semenov [72].

schemes: the complete scheme (n-heptane and iso-octane) and the pure fuels only. No impact of adding / removing the sub-mechanism on ignition delay time is observed. A similar study was performed for laminar flame speed at atmospheric conditions shown in figure 11. Also for laminar flame speeds no difference between the schemes is observed. This leads to the conclusion that the addition of sub-models for larger fuels do not influence when the prediction of global combustion parameters the rules outlined above are respected.

(a) n-heptane
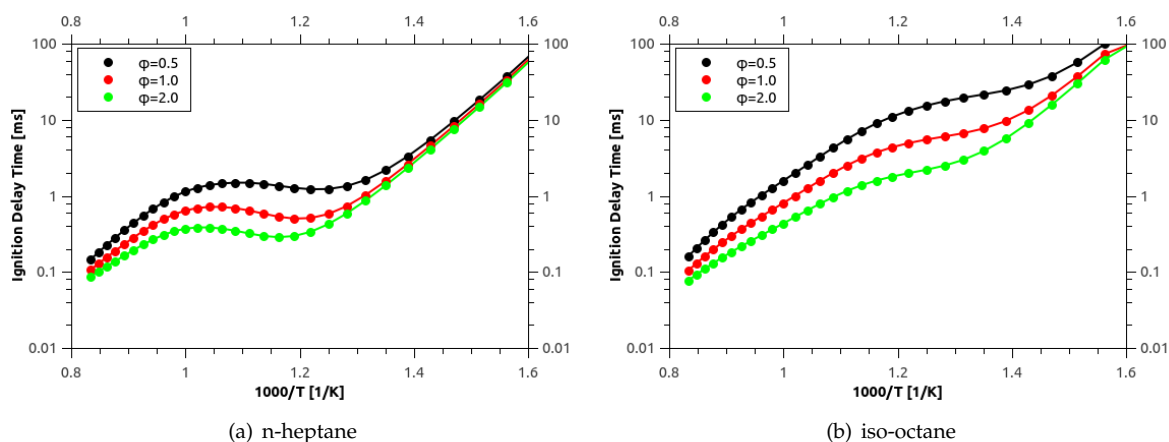
(b) iso-octane

Figure 10: Ignition delay times at 40 bar for n-heptane (left) and iso-octane (right) and different fuel/air ratios. Symbols: Simulation with complete lumped scheme; Lines: schemes without n-heptane (right) or iso-octane (left) sub-mechanism.

(a) n-heptane
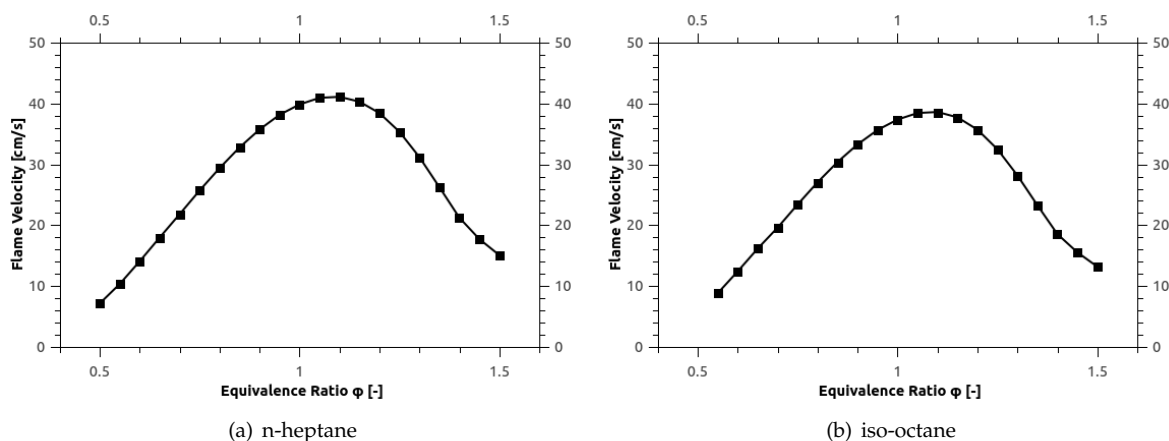
(b) iso-octane

Figure 11: Laminar flame speed at standard conditions for n-heptane and iso-octane and different fuel/air ratios. Symbols: Simulation with complete lumped scheme; Lines: schemes without n-Heptane or iso-octane sub-mechanism.

6.1.1.2 The impact of additional third bodies

C_1 to C_4 chemistry often contains many pressure dependent reactions with third body efficiencies. With the variable mechanism concept one question appears: Should the set of third bodies used in the base chemistry be extended by larger species when a sub-mechanism for a larger fuel is added? On the first glance it is quite feasible that large fuel molecules can act as significant third body since it appears in high concentration and is a comparably good energy carrier. A simple test was

performed to answer this question: In a reduced mechanism[16] for laminar flame speed prediction (with 49 species / 214 reactions developed in chapter 11.2) n-heptane was added as third body with an efficiency of 16.0. For example:

```
H+H+M=H2+M 1.800000E+18 -1.000000E+00 0.000000E+00
CO/ 0.75/CO2/ 1.50/H2O/ 6.50/O2/ 0.40/AR/ 0.35/N2/ 0.40/
```

was extended to:

```
H+H+M=H2+M 1.800000E+18 -1.000000E+00 0.000000E+00
CO/ 0.75/CO2/ 1.50/H2O/ 6.50/O2/ 0.40/AR/ 0.35/N2/ 0.40/ N-C7H16 / 16.0/
```

Assigning such a high third body efficiency (here about three times more effective than H_2O molecules) to all pressure dependent reactions would certainly overestimate efficiencies of the n-heptane molecule. The outcome of this analysis for predicted laminar flame speed at standard conditions is shown in figure 12. It can be observed that the scheme with the additional third bodies predicts a slightly faster laminar flame speed. The largest difference is found at the peak velocity of 39.57 cm/s vs. 39.83 cm/s[17]. This, clearly overestimated, difference of about 0.3 cm/s is far below today's accuracies achieved in experimental setups for laminar flame speed determination. It is therefore save to conclude that the list of third bodies does not need to be extended when adding an additional sub-mechanism for larger fuels to the base chemistry.
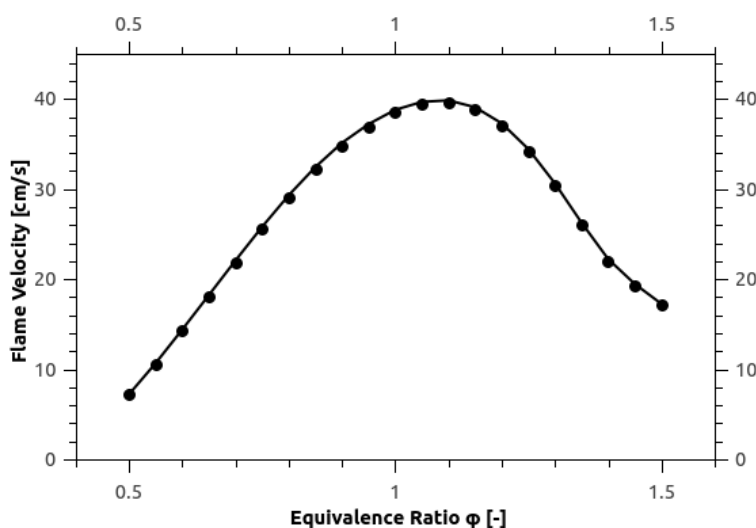
Figure 12: Predicted laminar flame speed at standard conditions with (solid line) and without n-heptane (symbols) as additional third body.

---

[16]A reduced mechanism was simply chosen for simplicity reasons, since less reactions had be altered than in a detailed scheme.

[17]Computed with a relative tolerance of 1E-8 which is 100 times stricter than the recommended tolerance. For the calculation with both schemes the same start profile was used.

6.2   Development of the Detailed Scheme

6.2.1   n-Heptane and base model

The published n-heptane scheme [43] (352 species and 3702 reactions) is used as detailed model for the fuel itself as well as for the base chemistry. The scheme is based on a series of published reaction schemes in collaboration with different research groups. The author of this thesis was directly involved in the mechanism development published in the work of Osswald et al. [41], Schenk et al. [42], Nawdiyal et al. [73] and Seidel et al. [43]. The development process towards the n-heptane scheme, the core model of this work, is illustrated in figure 13. Details regarding the reaction schemes are discussed in the publications and there supplements and only outlined briefly.

The first major development step was focused on butane isomers [41] and the reaction scheme for Hoyerman et al. [74][18] was extended. Subsequently the butene isomers were investigated in the work of Schenk et al. [42]. In 2015 a rich premixed n-heptane flame was investigated and a model developed in [42] were combined with the detailed scheme from Ahmed et al [14]. During the work on the n-heptane scheme several modifications were done to the scheme from Ahmed et al. [14] in terms of reaction rates and pathways. The PAH growth model from Nawdiyal et al. [73] and Mauss [76] was used, modified and updated based on measurements for C_6H_6 and $C_{10}H_8$. A sub-model for ethanol was already included in the scheme developed for the flames measured by Osswald et al. [41] and improved for the butene isomers [42]. The sub-model for ethanol was compiled by the author with a similar approach as published by Vourliotakis et al. [77] and is based on the work of Marinov et al. [78], Park et al. [79], Wu et al. [80] and Xu et al. [81].

6.2.2   iso-Octane model

The iso-octane mechanism was composed by using the 25 reaction classes first introduced by Henry Curran [11]. The rates and the concept of applying them only to the fuel molecule with and a depth of one (application only to the seed molecule) during all reaction classes introduced by Zeuch et al. [82] was followed. Mostly the rates introduced by Zeuch et al. were used. Revised reaction rates and classes developed for the butane and butene isomers as well for n-heptane were incorporated in the iso-octane model. If necessary rates were fitted to match the measured ignition delay time measured by Fieweger et al. [38]. Some of the changes were done directly in the lumped scheme.

6.2.3   Toluene model

The sub-model for toluene oxidation from Ahmed et al. [83] was revised with rates from different sources [2, 84, 85, 86]. During investigations carried out in this thesis it was found that a particular reaction pathway of the toluene decomposition has an strong impact on n-heptane / toluene mixtures. This is discussed in chapter 9 and an alternative scheme is suggested.

---

[18]The mechanism published by Hoyerman et al. is mainly based on the Ph.D. thesis from Thomas Zeuch [75].
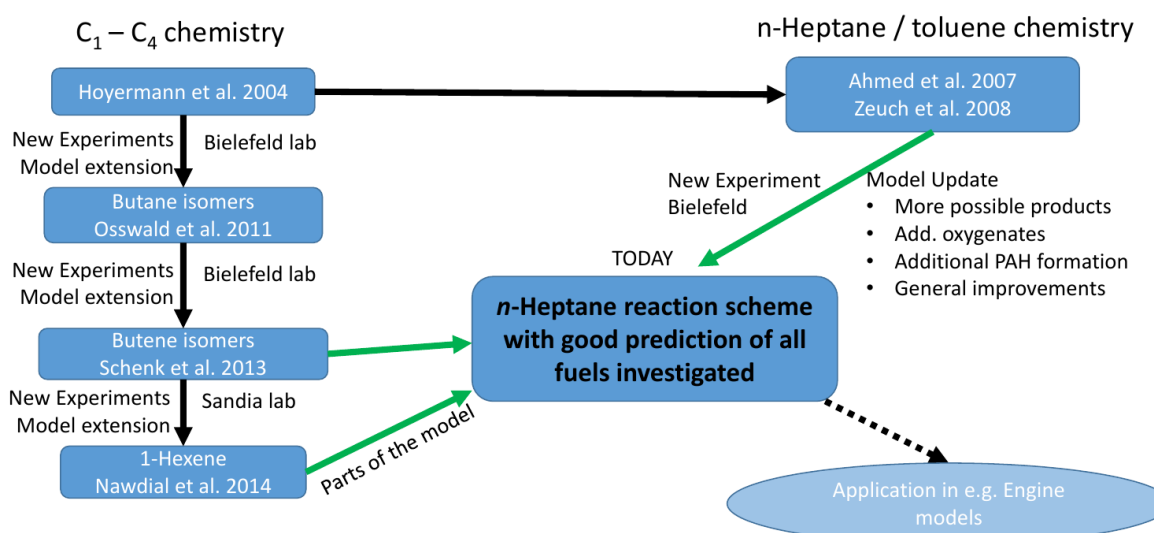
Figure 13: Series of development steps toward the n-heptane mechanism.

6.3 Lumping procedure

Species lumping is placed in this section since they differ from other reduction techniques. In difference to species or reaction removal lumping does not remove the pathways, it only merges them (see discussion in [14]).

An improved version of the chemical lumping introduced by Ahmed et al. [14] is applied [19]. In addition to the earlier work possible isomers to be lumped are identified from the thermodynamic data of the species rather than from the structure of the individual isomers. This concept was first presented by Andrea Matrisciano and the author of this work in 2015 [88, 89].

Firstly, all species with the same molecular formula are identified and their Gibbs free energies between 300 K - 3000 K are calculated. This is based on the assumption that isomers with similar structures have very similar Gibbs free energies and are found in comparable concentrations. In this work a threshold of 1 kJ is used. From this evaluation a list of potential candidates to be lumped into new pseudo species is obtained. Therefore lumping steps can be evaluated one by one. In general it was found that nearly all lumping steps were successfuly identified a priori and could be used as suggested by the evaluation of the thermodynamic data. The only exception was found for QOOH species, where the suggestion of Ahmed et al. [14] was followed where the isomers were sorted by ring size rather then via their Gibbs free energy levels.

The lumping of the species is done as follows: the resulting rate coefficients are weighted by the rates for the lumped isomers and the numbers of reactants and products in the reaction equation. If isomers with slightly different thermodynamic data are lumped these differences have been taken into account in the formulation of the calculated rate coefficients of the backward reactions. In the lumped scheme the total backward reaction is described as the sum of duplicate reactions with the different backward rate coefficients of the former

---

[19]The author needs to point out that this section was written (incl. the figures herein) before it was submitted to the ASME ICEF 2016 [87]. Even though the reader will find strong similarities this section and the reduction procedure for pure n-heptane shown in chapter 10 it may not be seen as citation.

isomeric species. Introducing one lumped species the source term for the differential equation is transformed from a single species $x = j$, via the isomers $x = l$ to the lumped species $x = L$ as follows:

$$\omega_j = \sum_{k=1}^{N_R}\left(\nu_{j,k}\prod_{i=1}^{N_S}(c_i{}^{\nu'_{i,k}})k_k\right) \tag{6.1}$$

$$\omega_l = \sum_{k=1}^{N_R}\left(\nu_{l,k}\prod_{j=1}^{N_L}(c_j{}^{\nu'_{j,k}})\prod_{i=1}^{N_S-N_L}c_i{}^{\nu'_{i,k}}k_k\right) \tag{6.2}$$

$$\omega_L = \sum_{l=1}^{N_L}\left(\sum_{k=1}^{N_R}\left(\nu_{l,k}\prod_{j=1}^{N_L}((c_l/N_L)^{\nu'_{j,k}})\prod_{i=1}^{N_S-N_L}c_i{}^{\nu'_{i,k}}k_k\right)\right) \tag{6.3}$$

$$\omega_L = \sum_{k=1}^{N_R}\left(\sum_{l=1}^{N_L}\left(\nu_{l,k}c_l{}^{\sum_{f=1}^{N_L}\nu'_{f,k}}\right)\prod_{i=1}^{N_S-N_L}c_i{}^{\nu'_{i,k}}k_k\prod_{j=1}^{N_L}(1/N_L)^{\nu'_{j,k}}\right). \tag{6.4}$$

With N_R denoting the number of reactions, N_S the total number of species, N_L the number of species lumped to L, c_x the concentration of species x, $\nu_{x,k} = \nu''_{x,k} - \nu'_{x,k}$ is the net stoichiometric coefficient of species x in reaction k where ν' indicates the reactants and the ν'' products, k_k the rate coefficient of reaction k. After lumping the new number of species is calculated together with the new rate coefficients and new stoichiometric coefficients of the lumped group:

$$N_S^* = N_S - N_L + 1 \tag{6.5}$$

$$k_k^* = k_k\prod_{j=1}^{N_L}(1/N_L)^{\nu'_{j,k}} \tag{6.6}$$

$$\nu_{L,k}^* = \sum_{l=1}^{N_L}\nu_{l,k} \tag{6.7}$$

$$\nu_{L,k}'^* = \sum_{l=1}^{N_L}\nu'_{l,k} \tag{6.8}$$

Equation (6.4) therefore reads as:

$$\omega_L = \sum_{k=1}^{N_R}\left(\nu_{L,k}'^*\prod_{i=1}^{N_S^*}(c_i{}^{\nu'_{i,k}})k_k^*\right) \tag{6.9}$$

where $\nu'_{i,k} = \nu'_{L,k}$ for $i = L$. Further lumping of species transforms the source term sequentially in this manner and thermodynamic data of the lumped pseudo-species are considered as the average of the isomers involved in the lump group.

During the lumping procedure deviations from the detailed scheme leading to a closer agreement with experimental ignition delay times, especially for rich mixtures were accepted. The idea behind this is that a reduction does not need to show a higher accuracy than available experimental data and the ignition timing in Diesel engines is dominated by
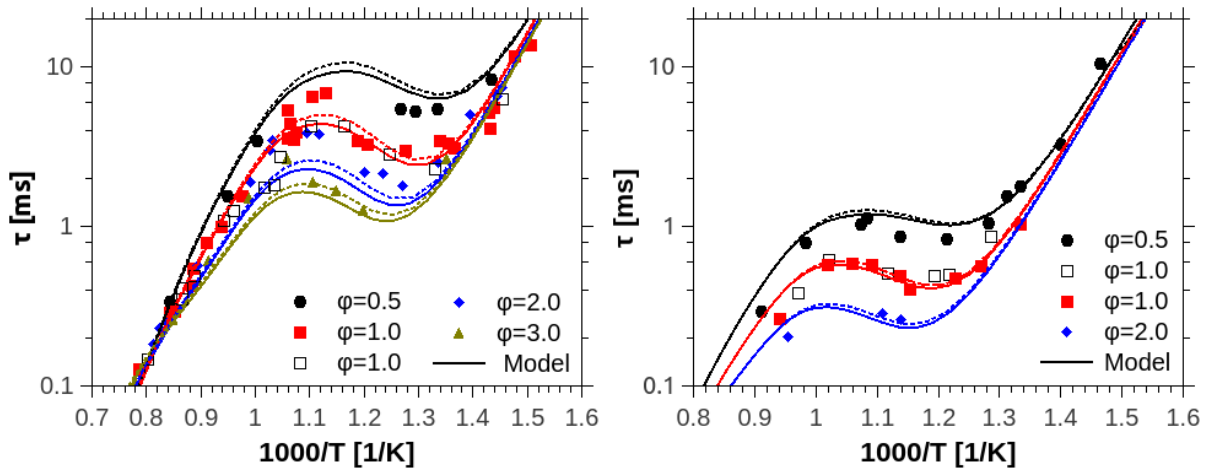
Figure 14: Ignition delay times (τ) for n-heptane/air in a shock tube. Left: experiments at 13.5 bar solid symbols [90]; open symbols [34]. Right: 40 ± 2 bar. Experiments: solid symbols for ϕ=0.5, ϕ=1.0 [38], and for ϕ=2.0 [90], open symbols [34]; solid lines: model predictions using detailed scheme, dotted line using lumped scheme.
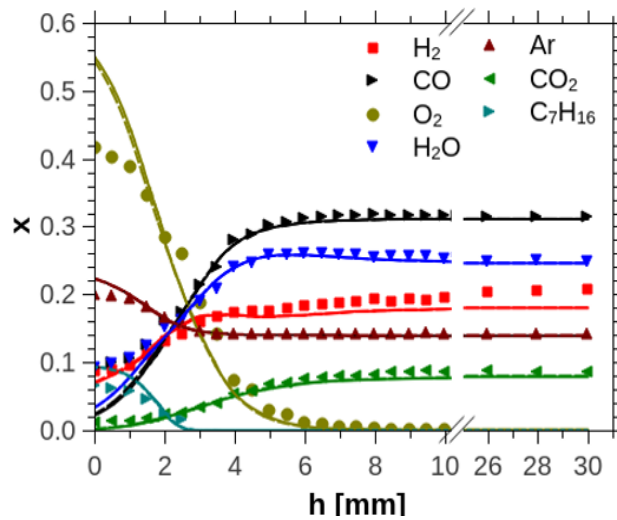
Figure 15: Molar fraction in a premixed fuel rich ($\phi = 1.69$) low pressure (40 mbar) flame [43]. Line: model prediction imposing experimental temperature profile. Solid lines: detailed scheme, dotted line using lumped scheme.

the rich zone with shorter ignition delay times. In the n-heptane scheme 24 representative pseudo species were identified and lumped from 44 species in total reducing the scheme to 308 species and 3680 reactions. The lumped scheme predicts slightly slower ignition delay times for n-heptane (Fig 14) and no observable difference for the major species profiles in the premixed flame (Fig 15).

7   Validation of the Lumped Scheme

7.1   n-Heptane

n-Heptane is the most common surrogate fuel. It is used as single fuel surrogate fuel for Diesel and is one of the components of the primary reference fuel for gasoline. Due to this frequent use a sufficient number of experiments do exist.

7.1.1   Ignition Delay Time
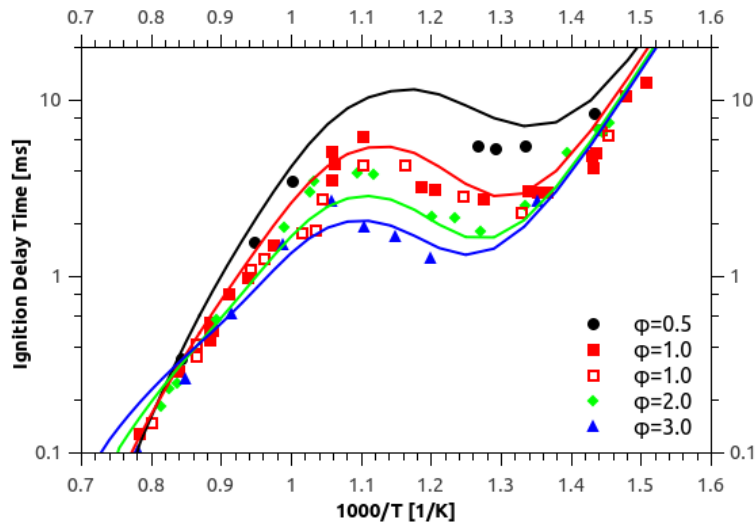
Figure 16: Ignition delay time of n-heptane / air mixtures at 13.5 bar. Experimental data from [38] (closed symbols) and [34] (open symbols).
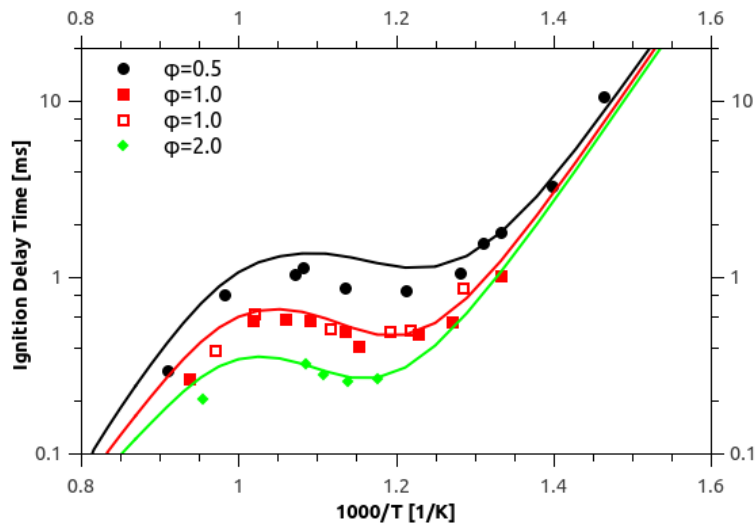
Figure 17: Ignition delay time of n-heptane / air mixtures at 40 bar $\pm$ 2 bar. Experimental data from [38], [90] (closed symbols) and [34] (closed symbols.)

7.1.2   Laminar Flame Speeds
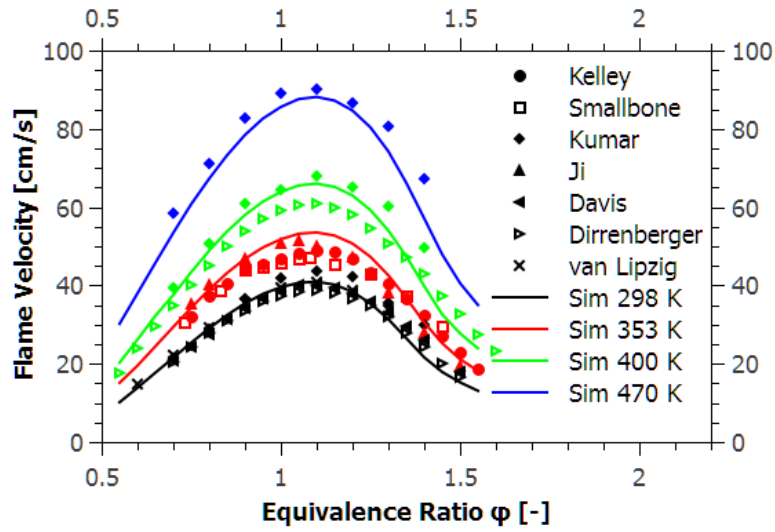
Figure 18: Laminar flame speeds for n-heptane / air mixtures at 1 atm and different inlet temperatures: 298 K (black); 353 K (red); 400 K (green) and 470 K (blue). Experimental data from [91], [92], [93], [94], [95] [96] and [97].
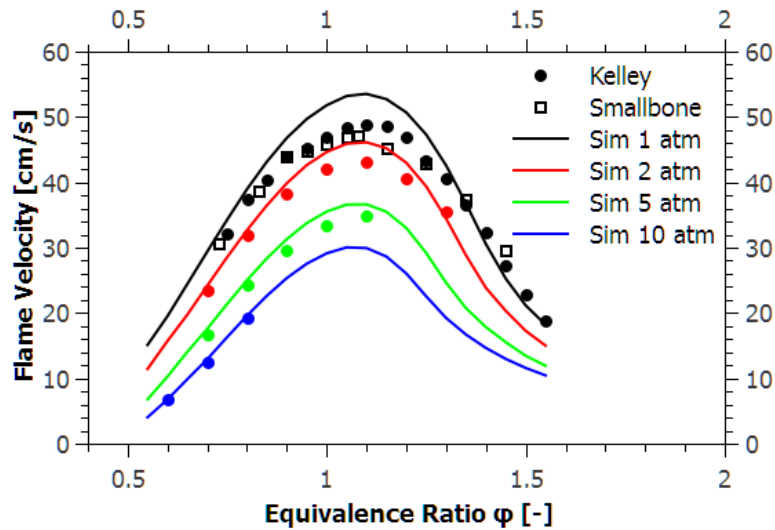
Figure 19: Laminar flame speeds for n-heptane / air mixtures at 350 K [91] / 353 K [92] different inlet pressures: 1 atm (black); 2 atm (red); 5 atm (green) and 10 atm (blue).
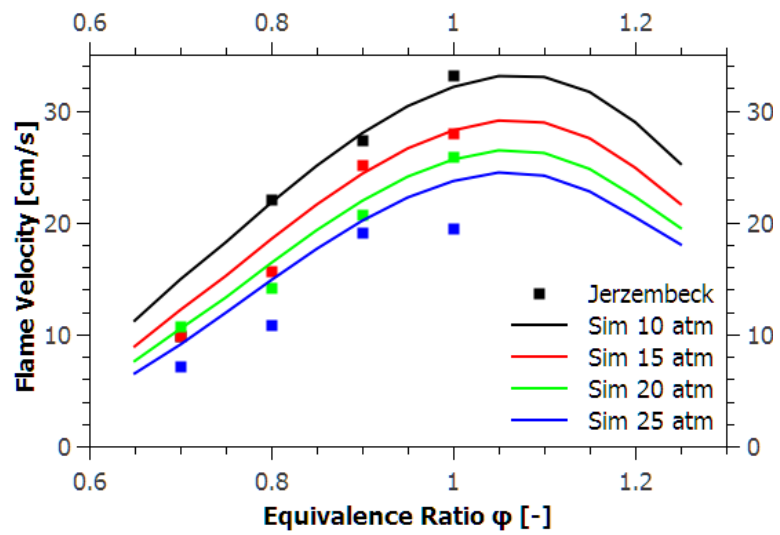
Figure 20: Laminar flame speeds for n-heptane / air mixtures at 373 K and different inlet pressures: 10 atm (black); 15 atm (red); 20 atm (green) and 25 atm (blue). Experimental data from [98].

7.1.3 Burner Stabilised Flame

The following plots show selected species profiles for a rich (ϕ=1.7) burner stabilised n-heptane flame at 40 mbar. All experimental data are from the publication of Seidel et al. [43], the experiments were carried out by Kai Moshammer.
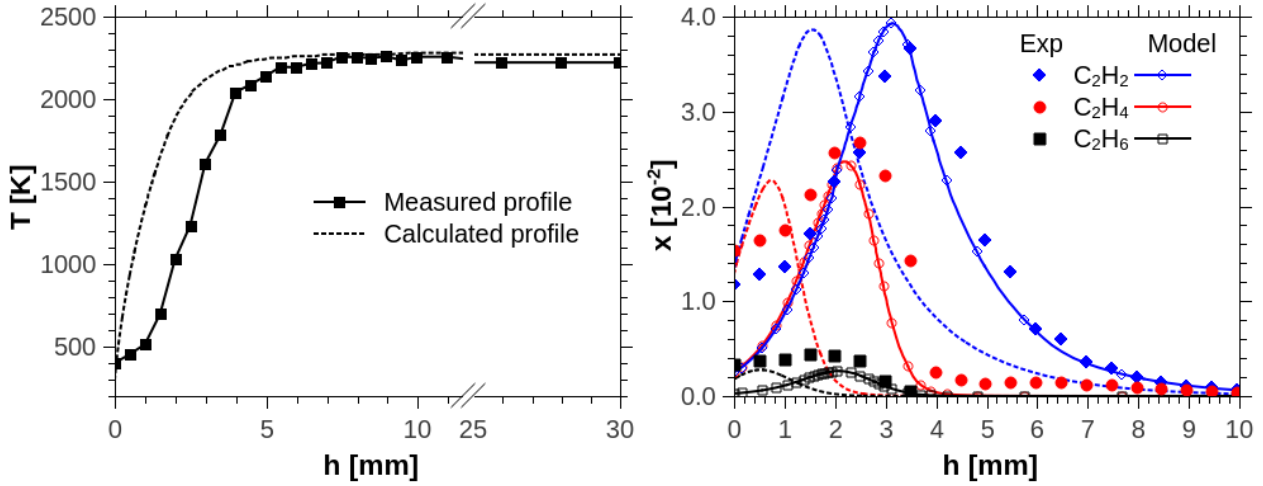
Figure 21: Left: Measured (disturbed) and calculated temperature profiles. Right: Experimental profiles for C_2H_2, C_2H_4, and C_2H_6 (filled symbols) and predictions using the simulated (solid lines with open symbols) and the disturbed temperature profiles (dotted lines). Conditions: Laminar flat premixed flame at 40 mbar with 10% n-heptane, 65% oxygen and 25% argon (molar) resulting in ϕ=1.7.
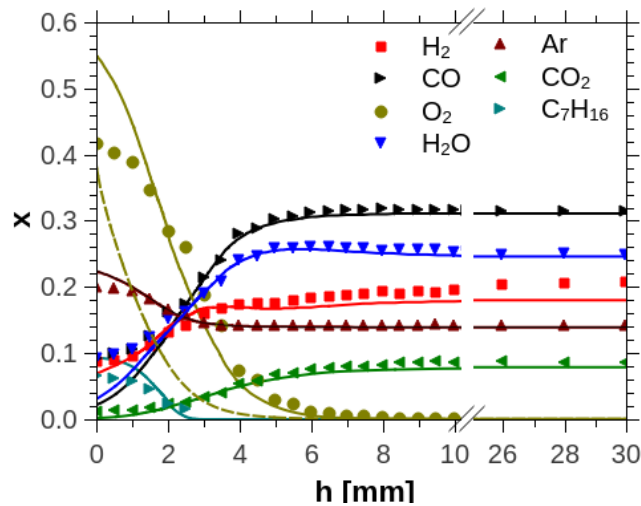
Figure 22: Mole fractions of major products. Symbols represent measurements; solid lines: model predictions using the measured temperature profile; dotted line: O_2 prediction from the energy conservation (without temperature profile). Conditions: Laminar flat premixed flame at 40 mbar with 10% n-heptane, 65% oxygen and 25% argon (molar) resulting in ϕ=1.7.
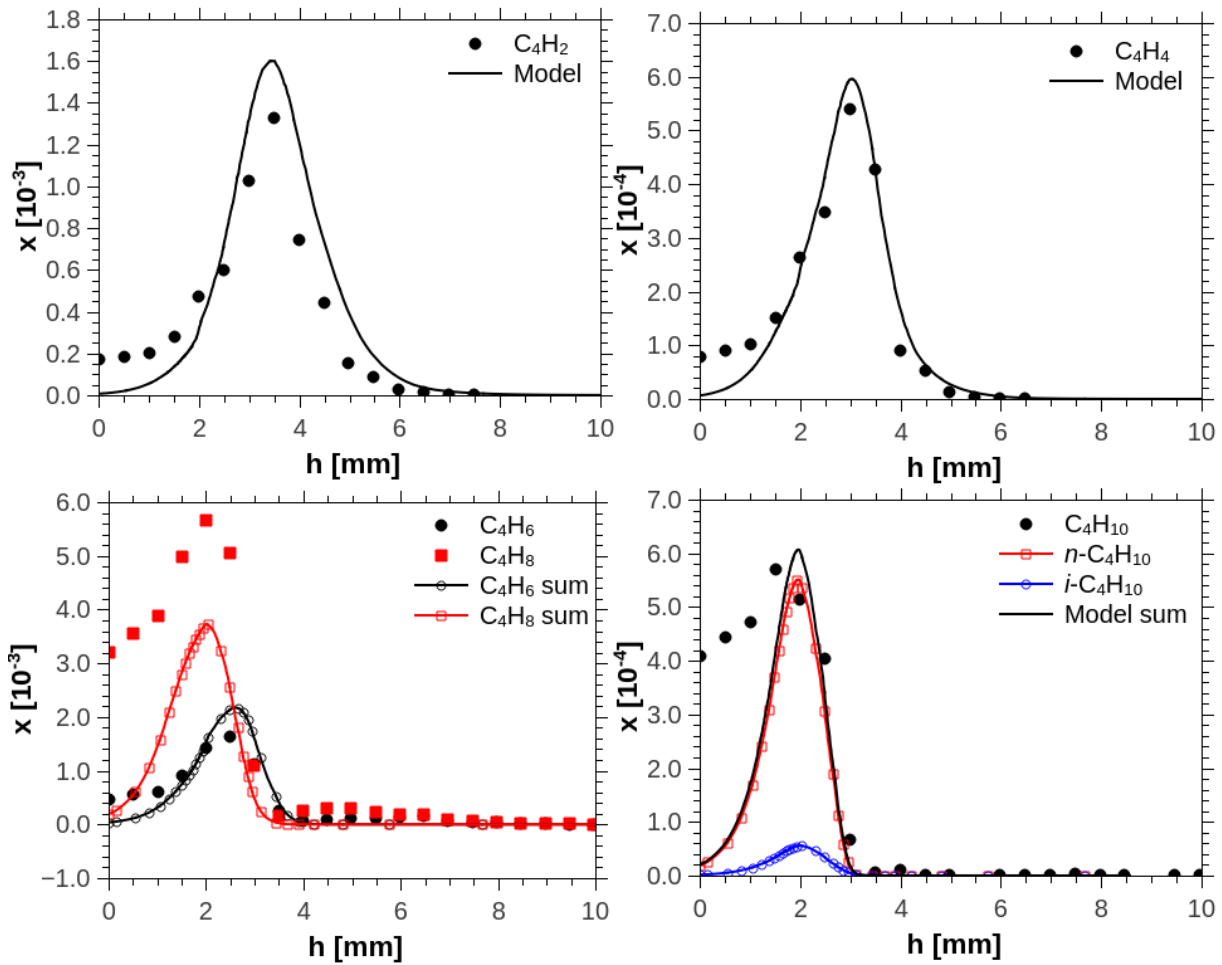
Figure 23: Experimental values for C_4 species (filled symbols) and model predictions (lines and lines with open symbols). C_4H_6 and C_4H_8 are only shown as sum of all isomers. Conditions: Laminar flat premixed flame at 40 mbar with 10% n-heptane, 65% oxygen and 25% argon (molar) resulting in ϕ=1.7.
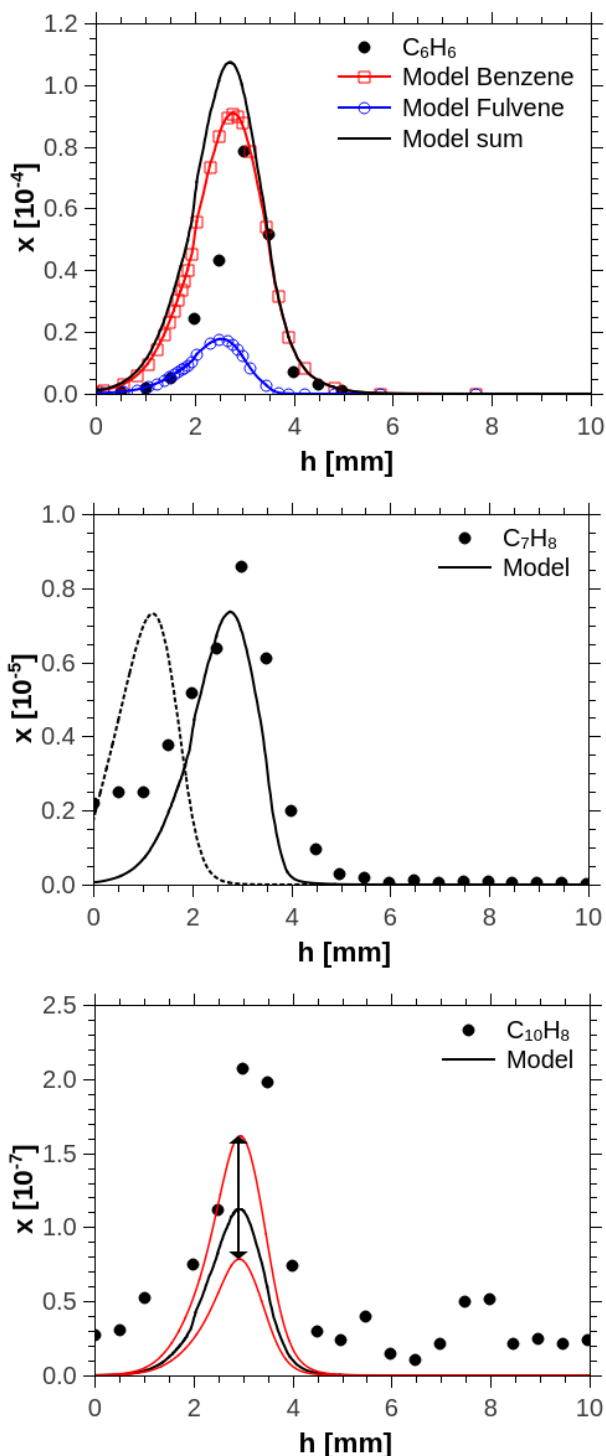
Figure 24: Measured values (filled symbols) and model predictions (lines and lines with open symbols) for aromatic species: Benzene and fulvene (C_6H_6), toluene (C_7H_8), and naphthalene ($C_{10}H_8$). The red lines indicate the effect of changing the flame stoichiometry through uncertainty in the oxygen supply by ± 5%. Conditions: Laminar flat premixed flame at 40 mbar with 10% n-heptane, 65% oxygen and 25% argon (molar) resulting in ϕ=1.7.

7.2   iso-Octane

7.2.1   Ignition Delay Time

Even though mankind uses more than 1 billion automobiles (not counting small motorcycles) world wide and the majority of those rely on gasoline engines we know surprisingly little about the combustion characteristics of the very important reference fuel iso-octane. To the best knowledge of the author the first shock tube experiments to determine the ignition delay time of iso-octane for conditions relevant to engine knock where performed by Fieweger et al. in 1997 [38], or 60 years after appointing iso-octane as the most important reference fuel in our daily life. More surprisingly those experiments were only verified one more time in a later work by Hartman and co-workers 2009 [39] and 2011 [37] which repeated the Fieweger and Adomeit experiments for stoichiometric n-heptane, iso-octane and PRF 80 air mixtures. Even though there is an extensive discussion about the repeatability in the work from Hartmann et al. it is worth to compare their measurements to those from Fieweger et al., in particularly because those ignition delay times will be used later on in correlations with octane numbers. From the comparison shown in figure 25 the following conclusion can be made:

- Hartman and co-workers extracted very similar ignition delay times for this set of experiments from the Fieweger et al. publication as done for in this thesis.

- For temperatures below 1000 K Hartmann and co-workers reported faster auto-ignition delay times, in particular when the mixture is prepared in the shock tube. Similar observations can be made for other other ignition delay times obtained by Hartmann et al.: They obtained shorter ignition delay times for n-Heptane (figure 45 and 46), for iso-octane (figure 47) and PRF 80 (figure 103) in comparison with other experiments.

A brief discussion about the implication on reaction rates and on the demanded accuracy can be found chapter 8 and section 10.2.2.
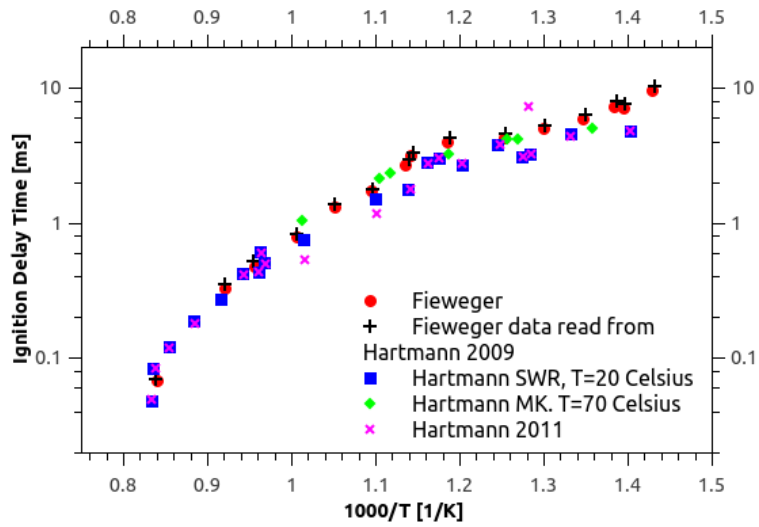
Figure 25: Measured ignition delay times from 2 different sources at 40 bar and ϕ=1.0 (in air). Data from [38] read from there work directly (red circle) and the Fieweger data read from the work of Hartmann [39] (black cross). Experiments from Hartmann 2009 [39] for mixture preparation in the shock tube at 20 Celsius (blue rectangle) and mixture preparation in a stirred reactor (green diamond). Magenta crosses are the ignition delay time published in 2011 [37].
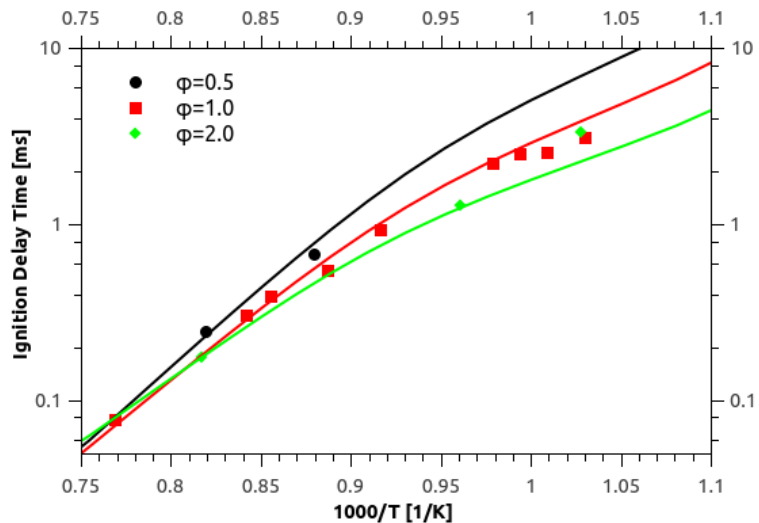

Figure 26: Ignition delay time of iso-octane / air at 13 bar. Experimental data from Fieweger et al. [38]
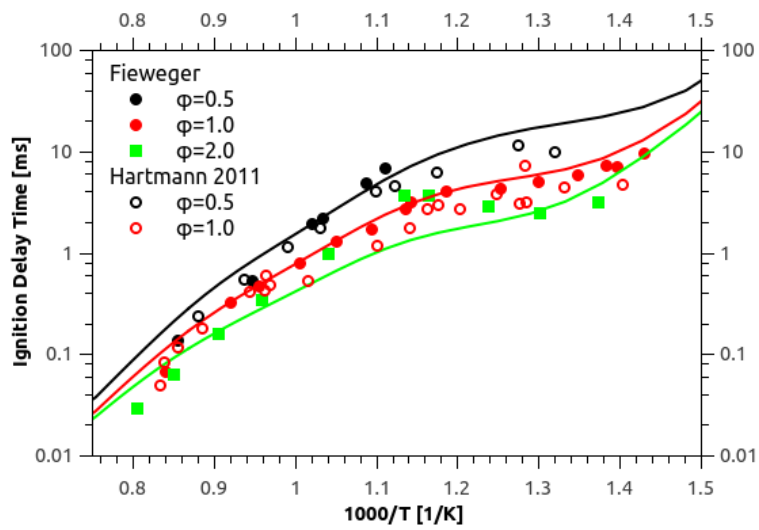
Figure 27: Ignition delay time of iso-octane / air at 40 bar $\pm$ 2 bar. Experimental data from Fieweger et al. [38] and Hartmann 2011 [37].

7.2.2 Laminar Flame Speeds
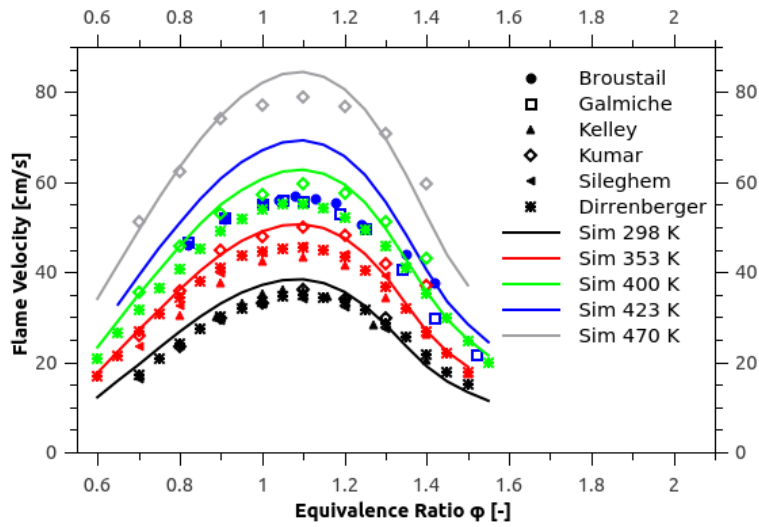
Figure 28: Laminar flame speeds for iso-octane / air mixtures at 1 atm and different inlet temperatures: 298 K (black); 353 K-360 K (red); 398 K-400 K (green); 423 K (blue) and 470 K (grey). Experimental data from [99], [100], [91], [93], [101] and [96].
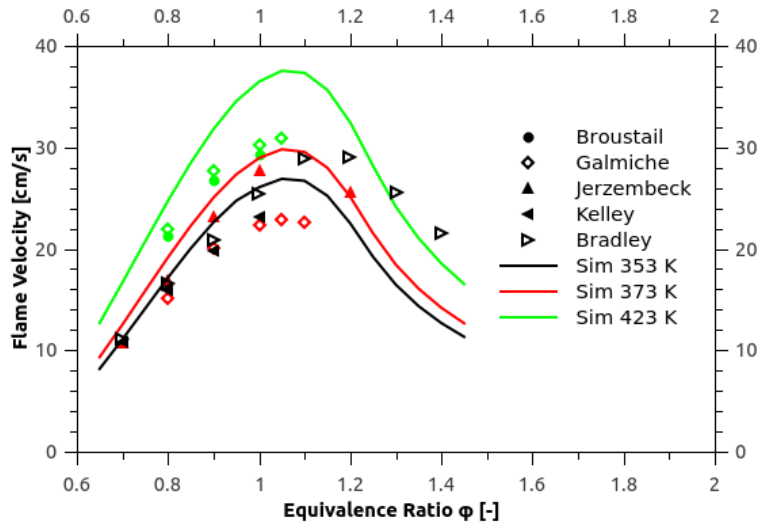
Figure 29: Laminar flame speeds for iso-octane / air mixtures at 10 atm and different inlet temperatures: 353 K-358 K (black); 373 K (red) and 423 K(green). Experimental data [99], [100], [98], [91] and [102].
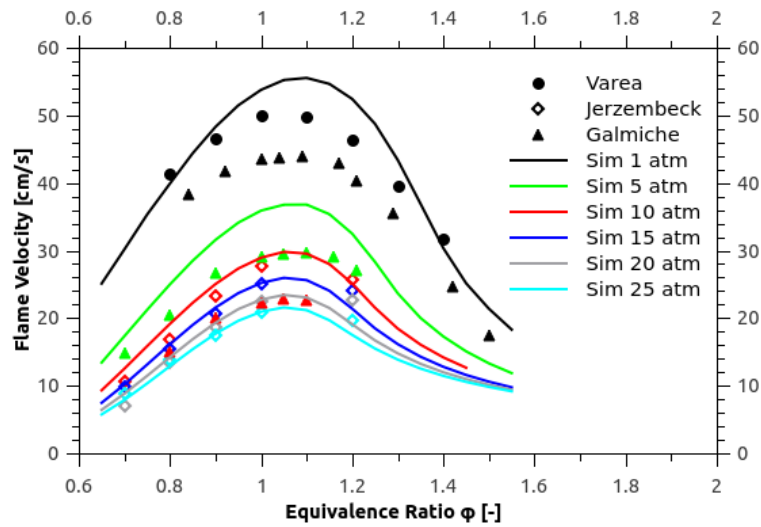
Figure 30: Laminar flame speeds for iso-octane / air mixtures at 373 K and different inlet pressures: 1 atm (black); 5 atm (green); 10 atm (red); 15 atm (blue); 20 atm (grey) and 25 atm (light blue). Experimental data from [103], [100], [98] and [100].
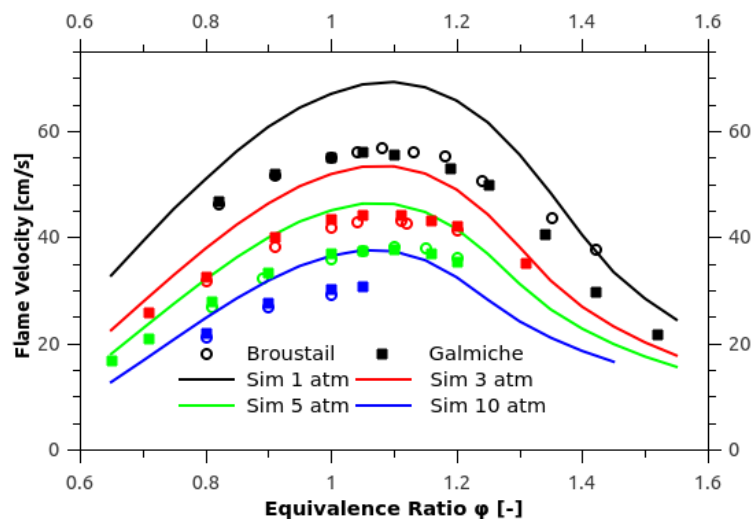
Figure 31: Laminar flame speeds for iso-octane / air mixtures at 423 K and different inlet pressures: 1 atm (black); 3 atm (red); 5 atm (green) and 10 atm (blue). Experimental data from [99] and [100].

7.3 Ethanol

7.3.1 Ignition Delay Time
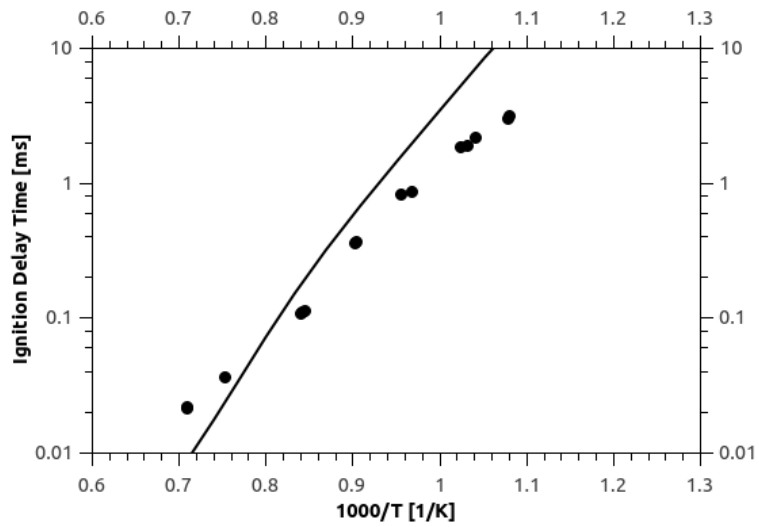
Figure 32: Ignition delay time of stoichiometric (ϕ=1.0) ethanol / air mixtures at 13 bar. Experimental data from [34].
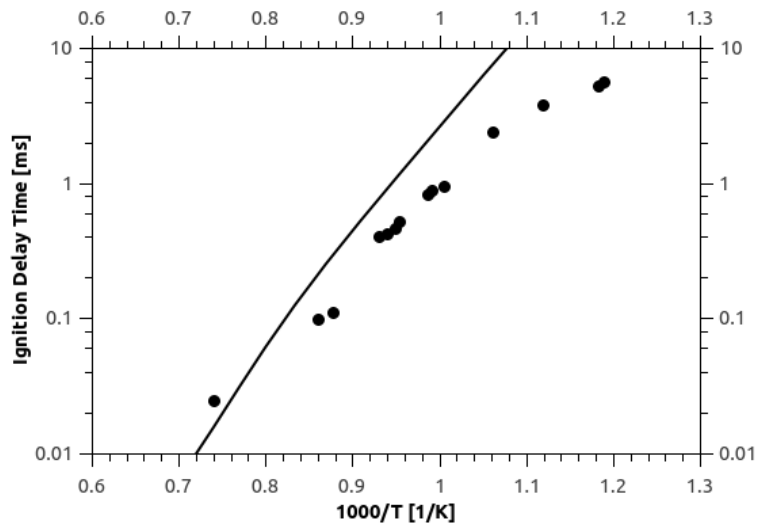
Figure 33: Ignition delay time of stoichiometric (ϕ=1.0) ethanol / air mixtures at 19 bar. Experimental data from [34].
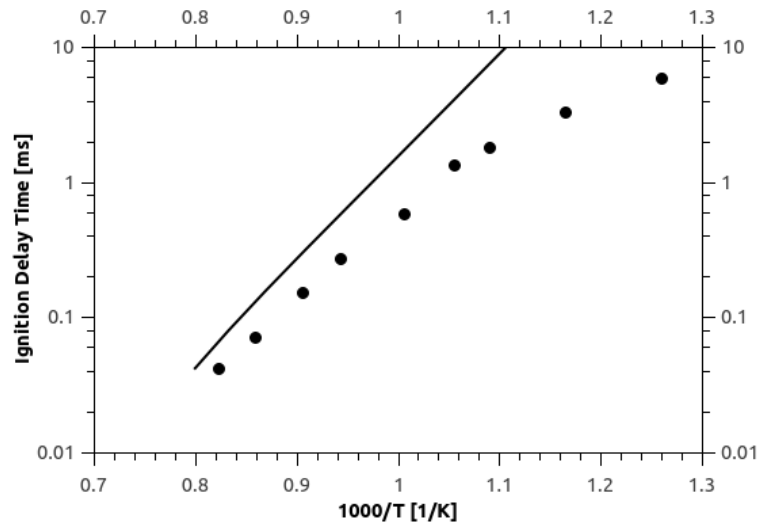
Figure 34: Ignition delay time of stoichiometric (ϕ=1.0) ethanol / air mixtures at 40 bar. Experimental data from [34].
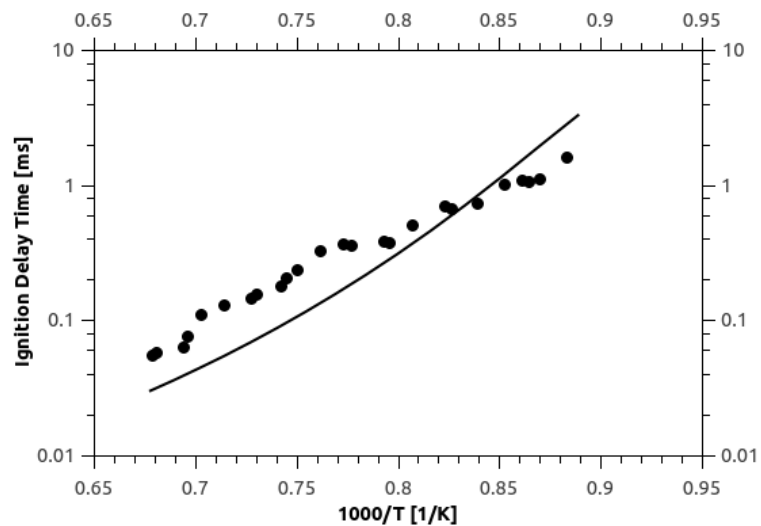

Figure 35: Ignition delay time of an ethanol / oxygen / argon mixture (1.25%/7.5%/91.25% (molar)) with ϕ=0.5 at 3.3 bar. Experimental data from [104] and [105].
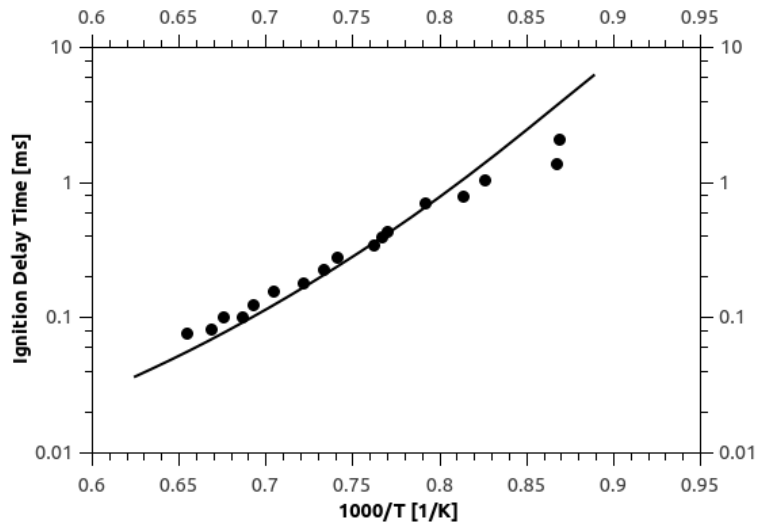
Figure 36: Ignition delay time of an ethanol / oxygen / argon mixture (1.25%/3.75%/95.00% (molar)) with ϕ=1.0 at 3.5 bar. Experimental data from [104] and [105].
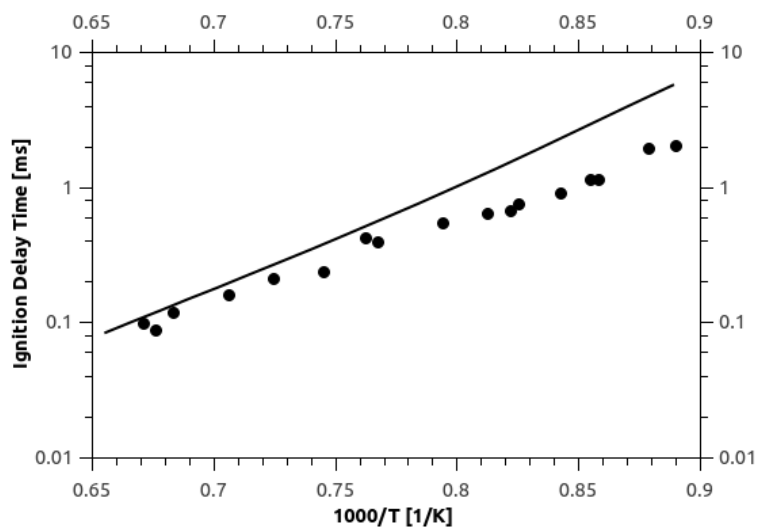

Figure 37: Ignition delay time of an ethanol / oxygen / argon mixture (2.5%/3.75%/93.75% (molar)) with ϕ=2.0 at 3.4 bar. Experimental data from [104] and [105].
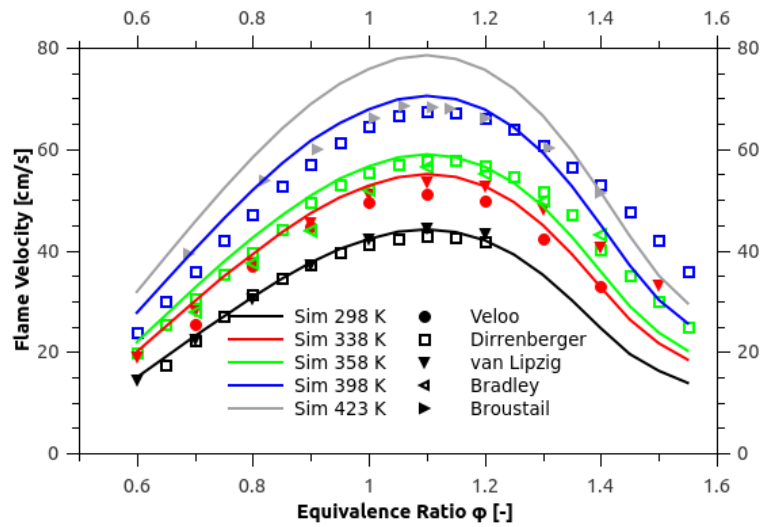
7.3.2   Laminar Flame Speeds

Figure 38: Laminar flame speeds for Ethanol / air mixtures at 1 atm and different inlet temperatures: 298 K (black); 338-343 K (red); 358 K (green) and 423 K (grey). Experimental data from [106], [96], [97], [107], [108].
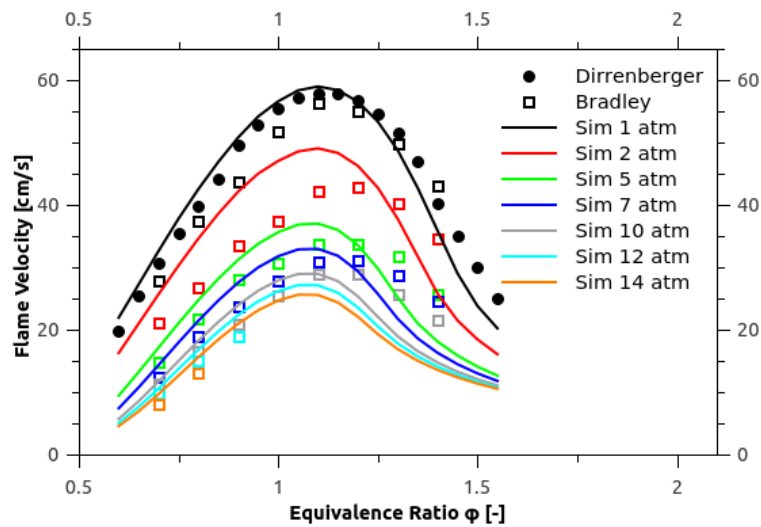

Figure 39: Laminar flame speeds for ethanol / air mixtures at 358 K and different inlet pressures: 1 atm (black); 2 atm (red); 5 atm (green); 7 atm (blue); 10 atm (grey) 12 atm (light blue) and 14 atm (orange). Experimental data [96] and [107].
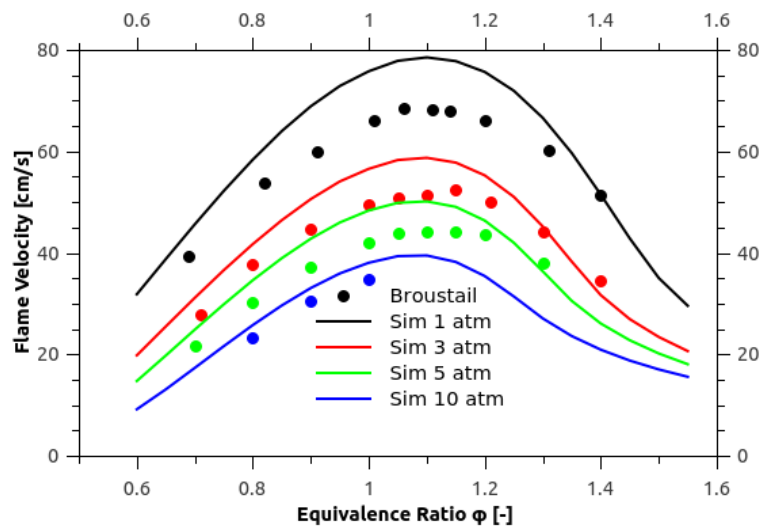
Figure 40: Laminar flame speeds for ethanol / air mixtures at 423 K and different inlet pressures: 1 atm (black); 3 atm (red); 5 atm (green) and 10 atm (blue). Experimental data from [108].

7.4   Toluene

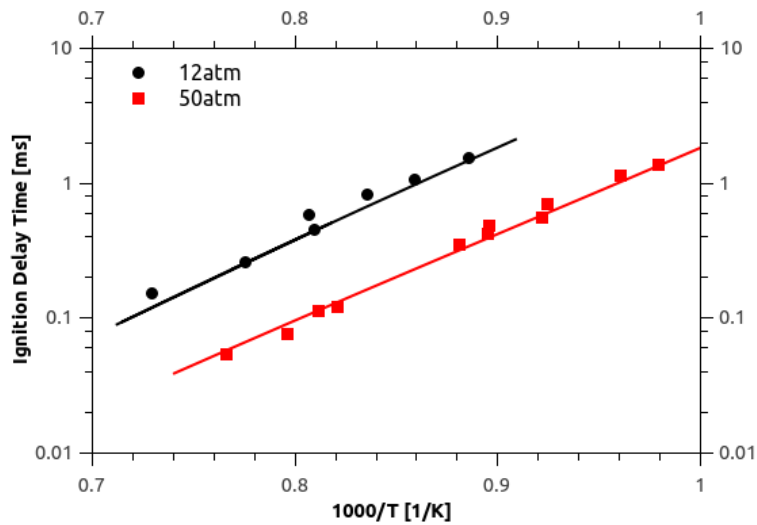### 7.4.1   Ignition Delay Time

Figure 41: Ignition delay time of stoichiometric toluene / air mixtures at 12 bar and 50 bar. Experimental points from [109]
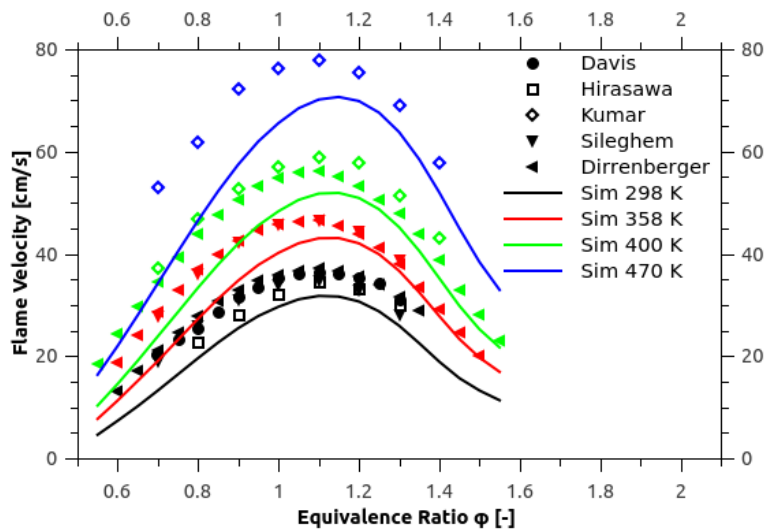
7.4.2   Laminar Flame Speeds

Figure 42: Laminar flame speeds for toluene / air mixtures at 1 atm and different inlet temperatures: 298 K (black); 358 K (red); 398-400 K (green) and 470 K (blue). Experimental data [110], [111], [93], [101] and [96].
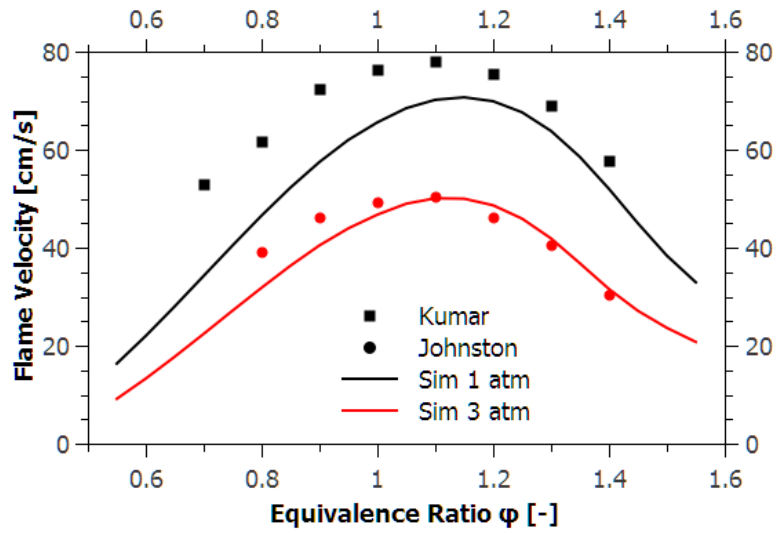
Figure 43: Laminar flame speeds for toluene / air mixtures at 450 K and 3 atm [93] and 470 K and 1 atm [112].

7.5 Fuel Mixtures

7.5.1 Ignition Delay Time
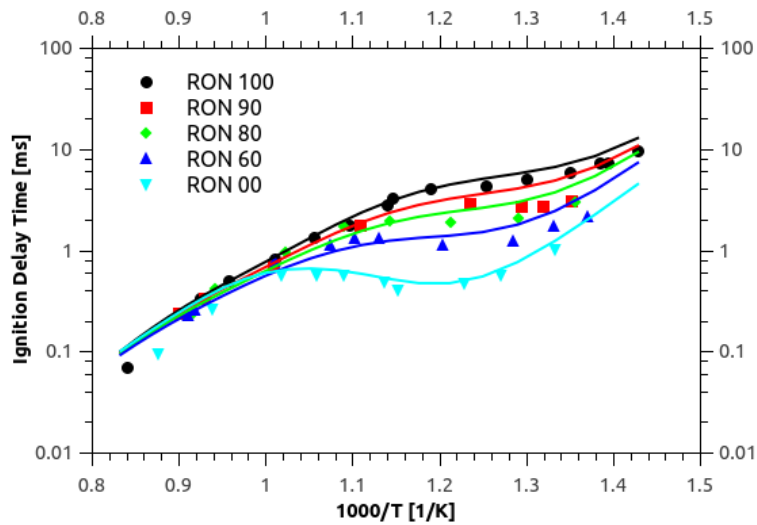
Figure 44: Ignition delay time of iso-octane/n-heptane mixtures at 40 bar, ϕ=1 with air as oxidizer. Experimental data from [38].
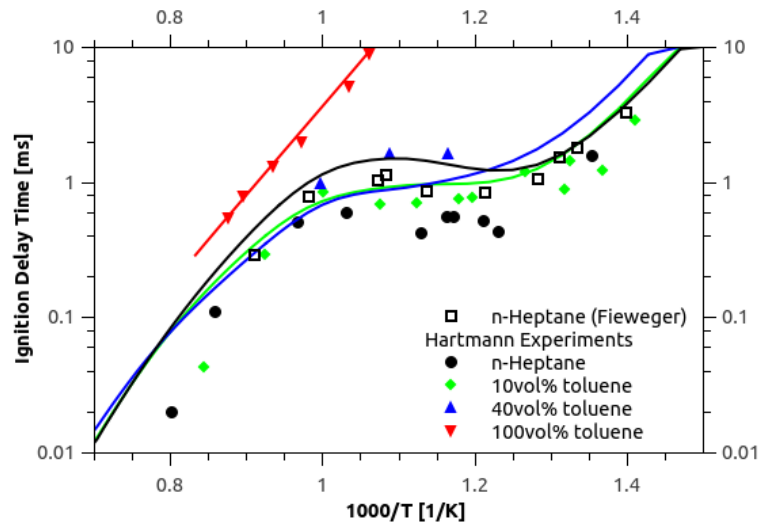
Figure 45: Ignition delay time for pure n-heptane and different n-heptane / toluene mixtures at ϕ=0.5 and 40 bar with air as oxidizer. Experimental data from Fieweger et al. [38] and Hartmann et al. [37].

Figure 46: Ignition delay time for pure n-heptane and different n-heptane / toluene mixtures at ϕ=1.0 and 40 bar with air as oxidizer. Experimental data from Fieweger et al. [38] and Hartmann et al. [37].
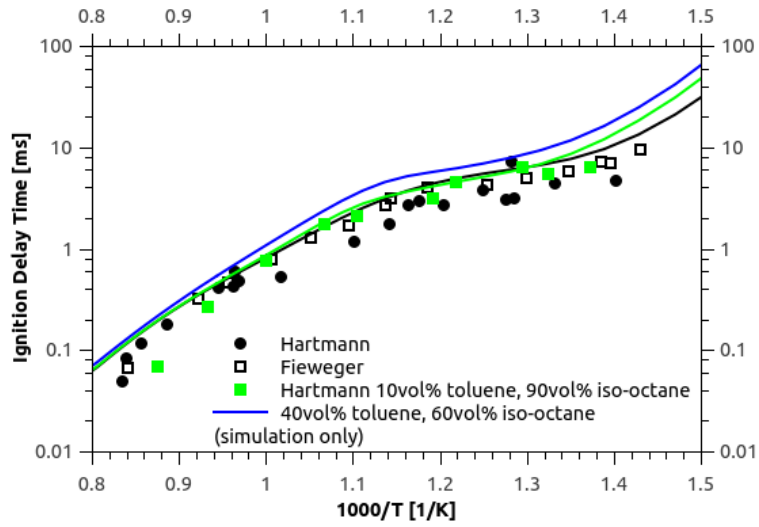
Figure 47: Ignition delay time for pure iso-octane and different iso-octane / toluene mixtures at ϕ=1.0 and 40 bar with air as oxidizer. Experimental data from Fieweger et al. [38] and Hartmann et al. [37].
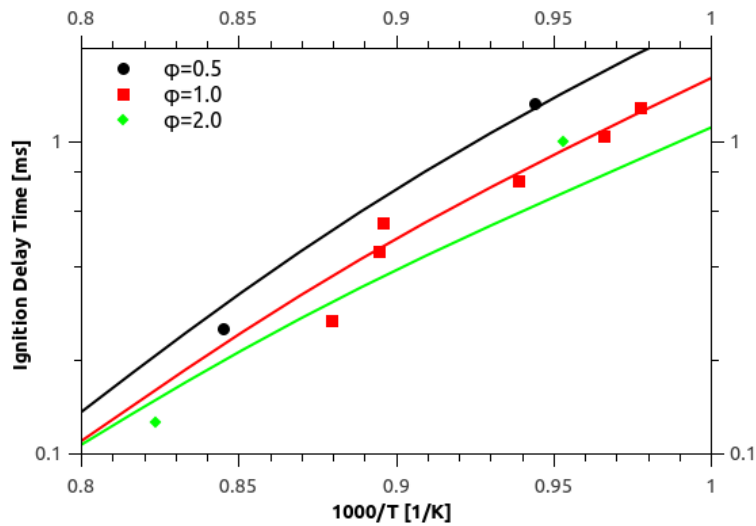
Figure 48: Ignition delay time for surrogate: 0.56 iso-octane, 0.28 toluene and 0.17 n-heptane (mole fraction) at 20 bar mixed with artificial air at ϕ=1.0. Experimental data from [45](Surrogate A). See publication for scatter in initial pressure.

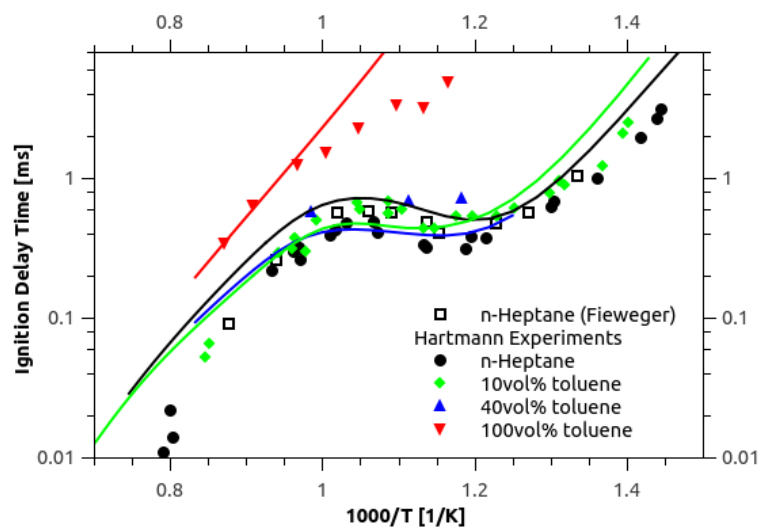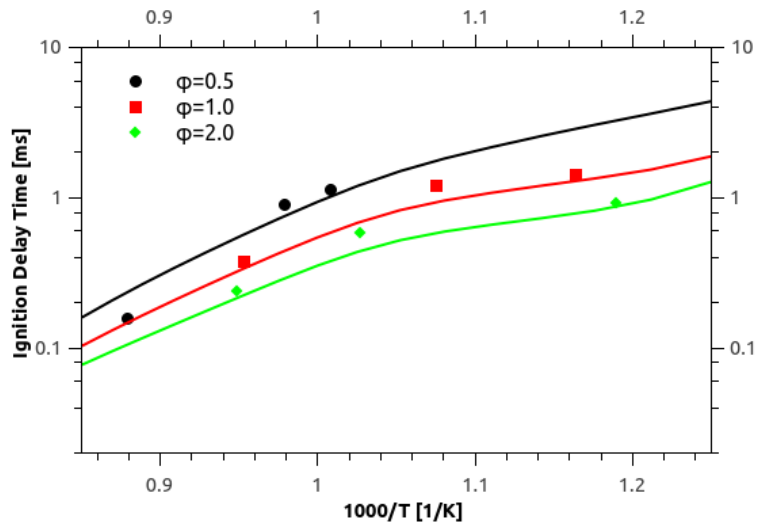Figure 49: Ignition delay time for surrogate: 0.56 iso-octane, 0.28 toluene and 0.17 n-heptane (mole fraction) at 52 bar mixed with artificial air at ϕ=1.0. Experimental data from [45] (Surrogate A). See publication for scatter in initial pressure.
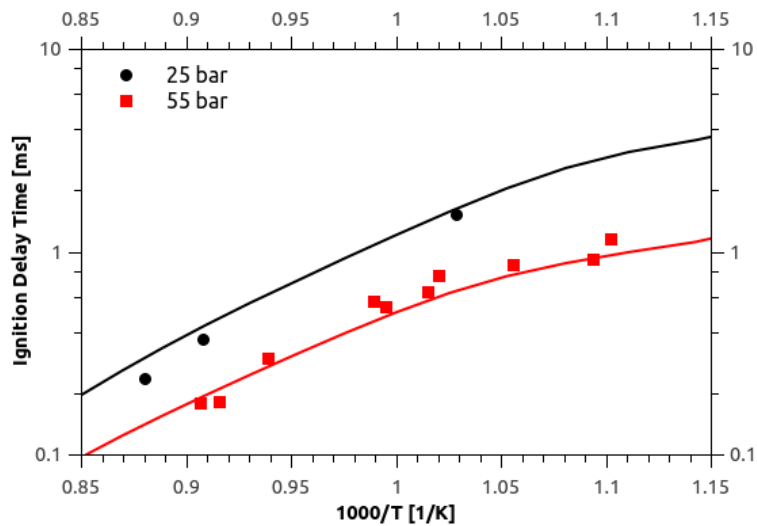
Figure 50: Ignition delay time for surrogate: 0.63 iso-octane, 0.20 toluene and 0.17 n-heptane (mole fraction) at 25 bar and 55 bar mixed with artificial air at ϕ=1.0. Experimental data from [45] (Surrogate B). See publication for scatter in initial pressure.
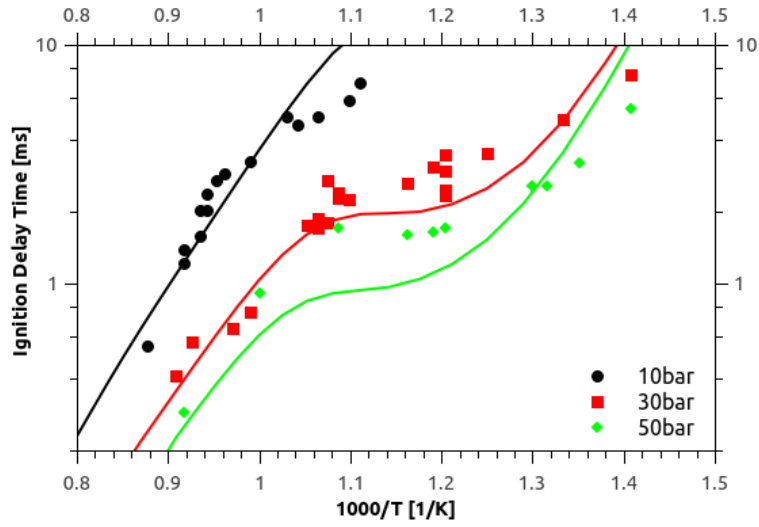
Figure 51: Ignition delay time for a mixture of 0.72 toluene and 0.28 n-heptane (mole fraction) at ϕ=1.0 and p=10, 30, 50 bar with air as oxidizer. Experimental data from [36].
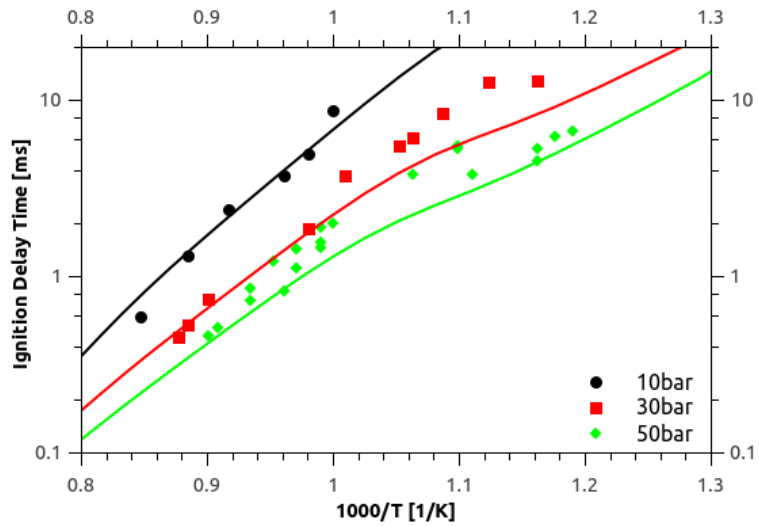
Figure 52: Ignition delay time for a mixture of 0.72 toluene and 0.28 n-heptane (mole fraction) at ϕ=0.3, p=10, 30, 50 bar with air as oxidizer. Experimental data from [36].
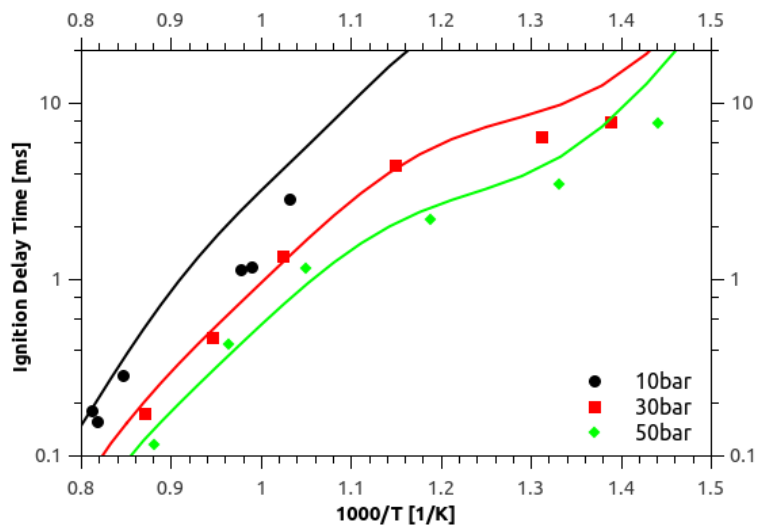
Figure 53: Ignition delay time for a stoichiometric mixture of 0.445 iso-octane, 0.41 ethanol and 0.145 n-heptane (mole fraction) with air as oxidizer at 10, 30, 50 bar. Experimental data from [113] (Fuel B).

7.5.2 Laminar Flame Speeds
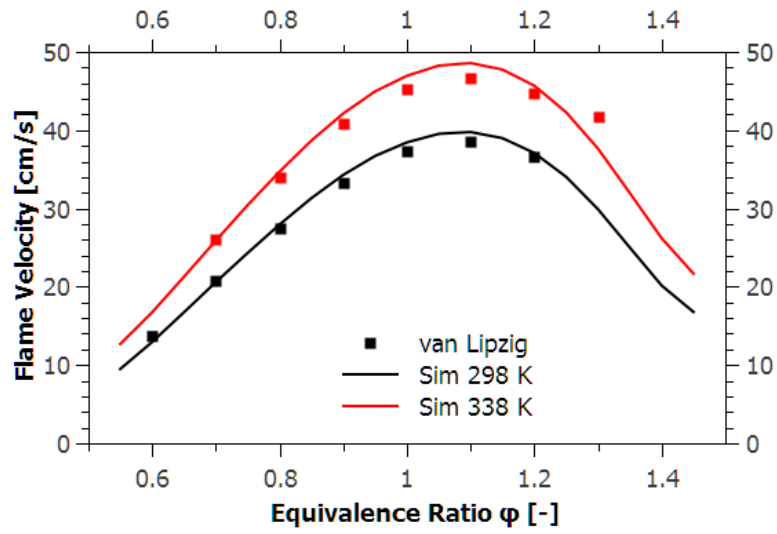
Figure 54: Laminar flame speeds for PRF 50 / air at 1 atm and different inlet temperatures: 298 K (black) and 338 K (red). Experimental data [97].
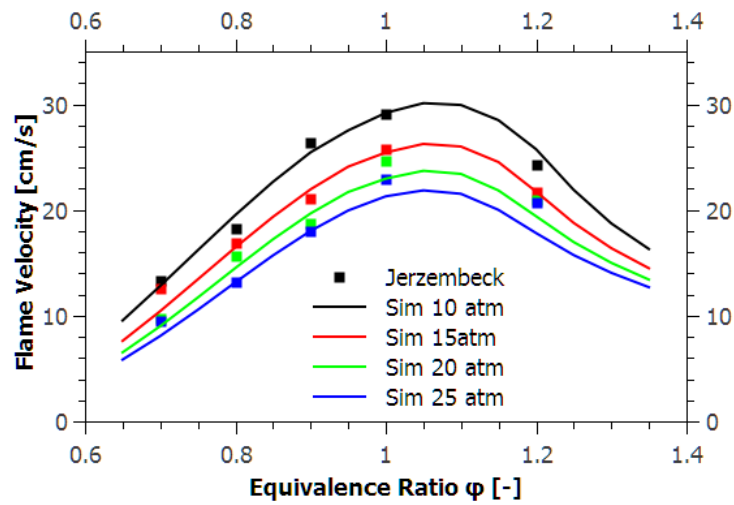
Figure 55: Laminar flame speeds for PRF 87 / air at 373 K and different ambient pressures: 10 atm (black), 15 atm (red), 20 atm (green) and 25 atm (blue). Experimental data from [98].
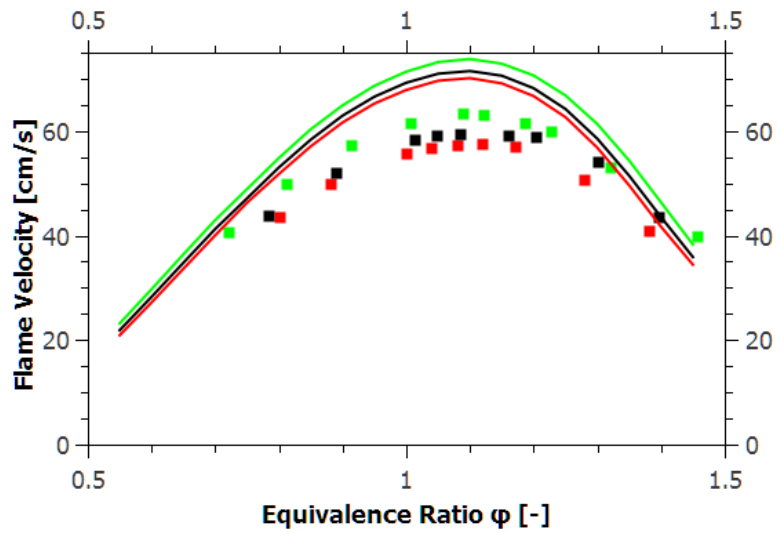
Figure 56: Laminar flame speeds for 3 different iso-octane / ethanol mixtures with 25% (red), 50% (black) and 75% (green) ethanol (liquid volume fraction). Air as oxidiser at 423 K. Experimental data from [108].
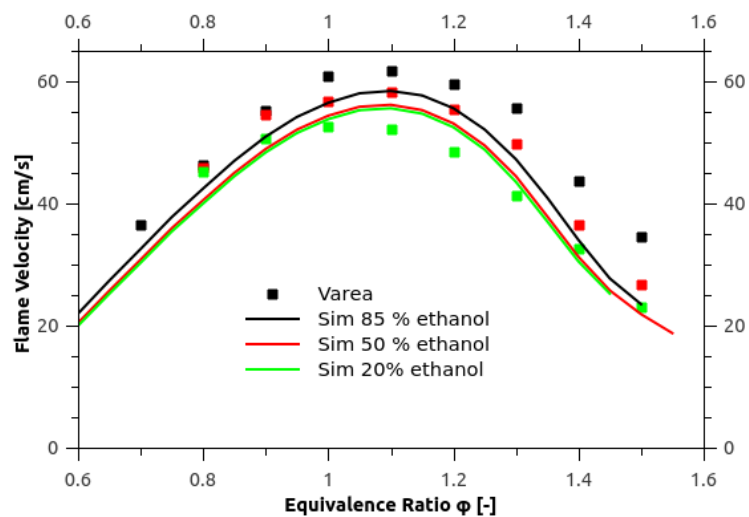
Figure 57: Laminar flame speeds for three different iso-octane / ethanol mixtures with 15% (green), 50% (red) and 80%(black) ethanol (mole fraction). Air as oxidiser at 373 K. Experimental data from [103].
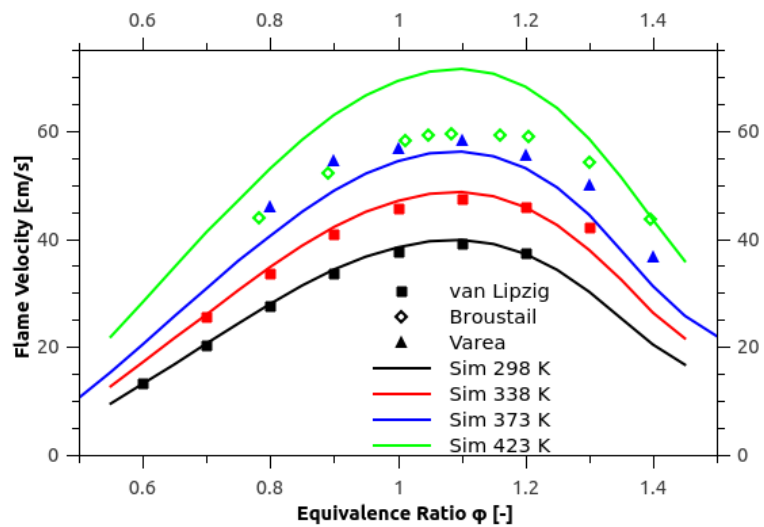
Figure 58: Laminar flame speeds for different iso-octane / ethanol mixtures with 50% ethanol (liquid volume fraction). Air as oxidiser at 1 atm and different inlet temperatures: 298 K (black); 338 K (red); 373 K (blue) and 423 K (green). Experimental data [103], [108] and [97].
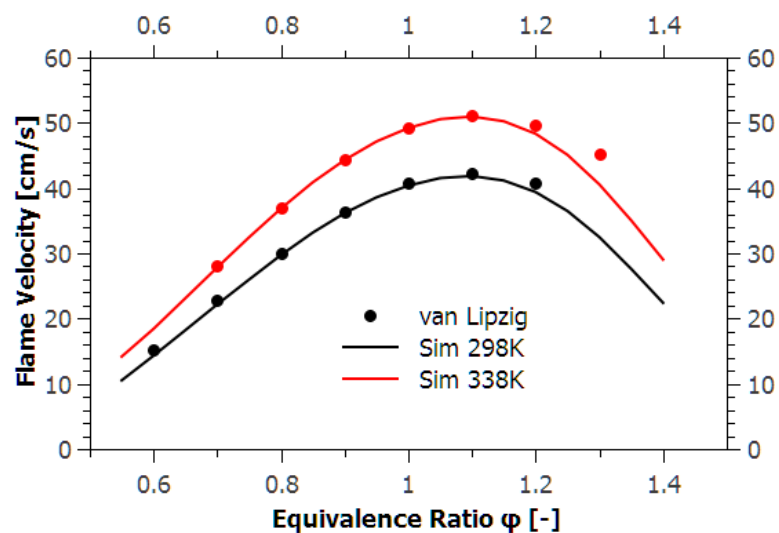
Figure 59: Laminar flame speeds for a mixtures of 50% ethanol, and 50% n-heptane (liquid volume fraction). Air as oxidiser at 1 atm and different inlet temperatures. Experiments from [97].
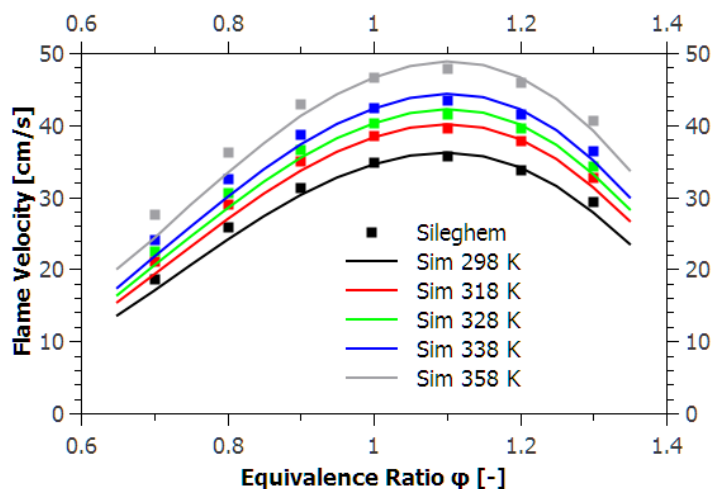
Figure 60: Laminar flame speeds for a mixture of 33.3% toluene, 33.3% iso-octane, 33.3% n-heptane (liquid volume fraction). Air as oxidiser at 1 atm and different inlet temperatures: 298 K (black); 318 K (red); 329 K (green); 338 K (blue) and 358 K (grey). Experimental data from [101].
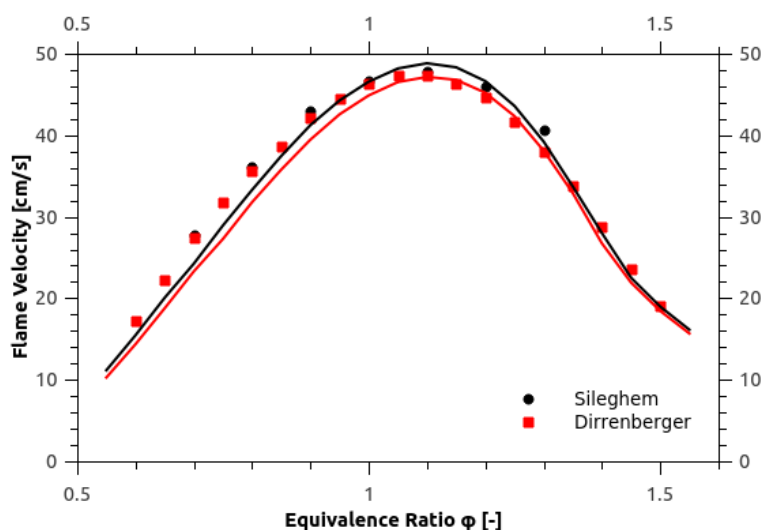
Figure 61: Laminar flame speeds at 1 atm and 358 K with air as oxidiser. A mixture of 33.3% n-heptane, 33.3% iso-octane, 33.3% toluene (liquid volume fraction) from Dirrenberger (red) [96] and a mixture of 13.7% n-heptane, 42.9% iso-octane, 43.4% toluene (liquid volume fraction) from Sileghem (black) [101].
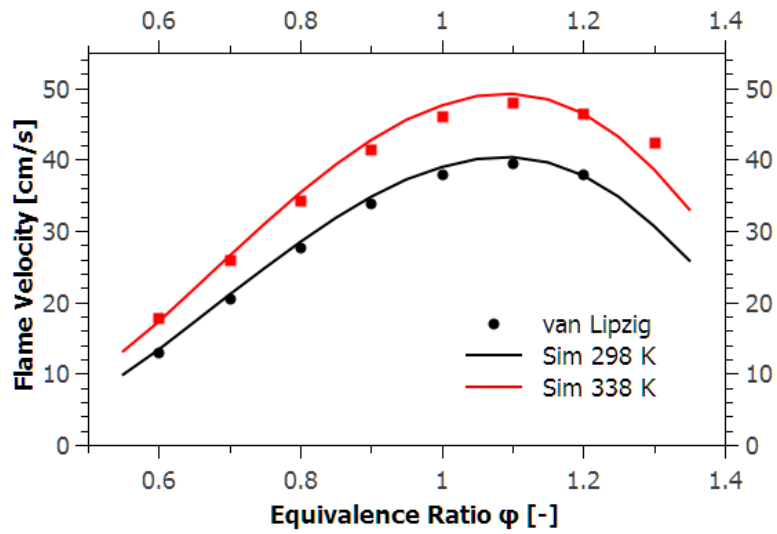
Figure 62: Laminar flame speeds at 1 atm and 358 K with air as oxidiser for a mixture of 33.3% n-heptane, 33.3% iso-octane, and 33.3% ethanol (liquid volume fraction) from [97].
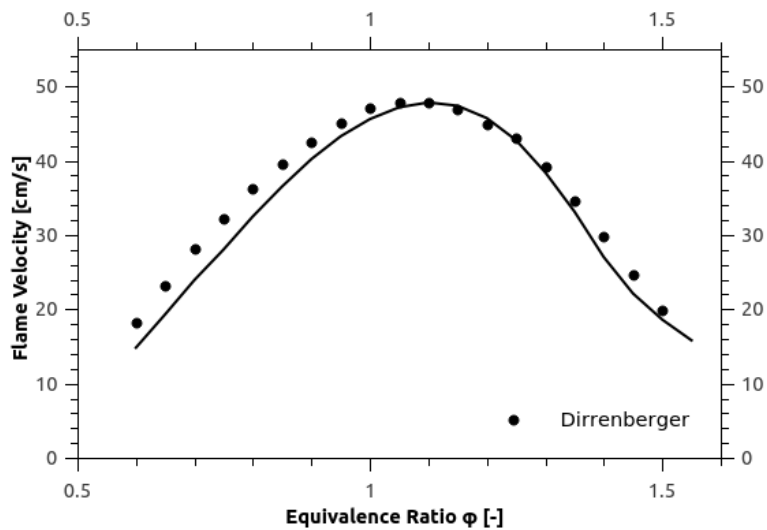
Figure 63: Laminar flame speeds at 1 atm and 358 K with air as oxidiser for a mixtures of 11.65% n-heptane, 36.47% iso-octane, 36.89% toluene and 15.0% ethanol (liquid volume fraction) from [96].

7.6   Other Fuels

7.6.1   Methanol
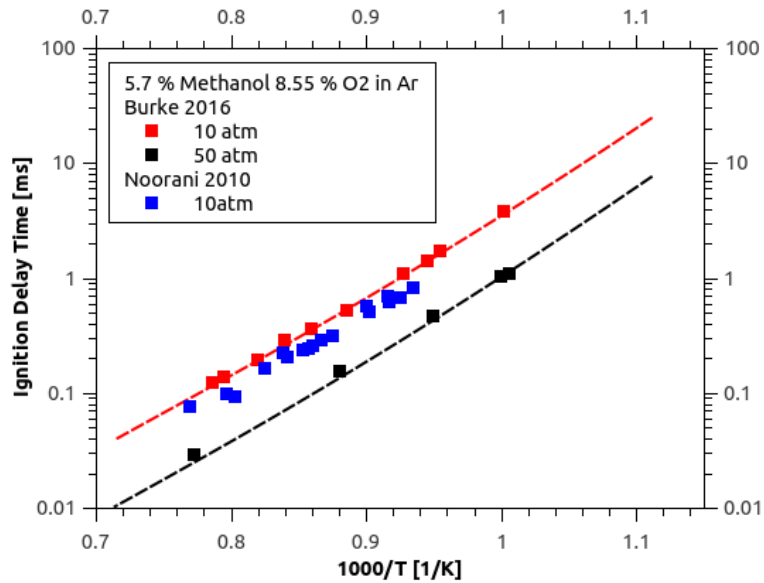
Figure 64: Ignition delay time for stoichiometric methanol mixture with argon as bath gas at different pressures. Experimental data from Burke et al. [114] and Noorani et al. [115].
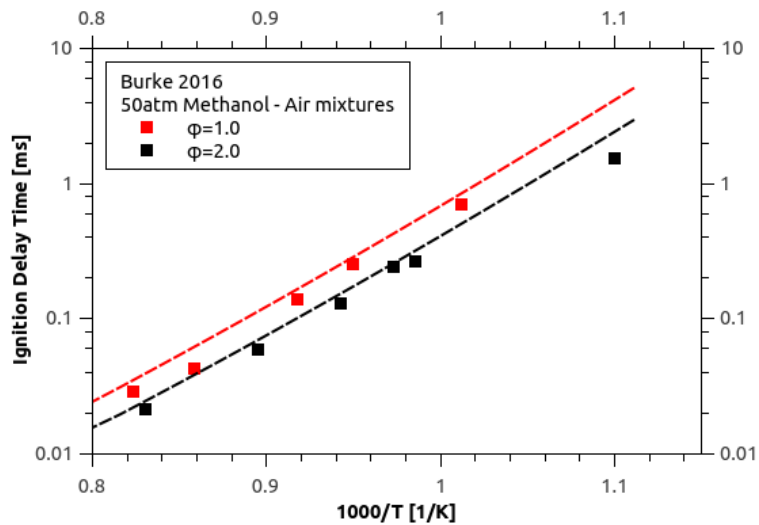
Figure 65: Ignition delay time for stoichiometric methanol mixture with nitrogen and argon as bath gas at 50 atm. ϕ=2.0 corresponds to a mixture of 21.882% methanol, 16.411% oxygen and 61.707% nitrogen. ϕ=1.0 corresponds to a mixture of 5.7% methanol, 8.55% oxygen and 85.75% nitrogen. Experimental data from Burke et al. [114].
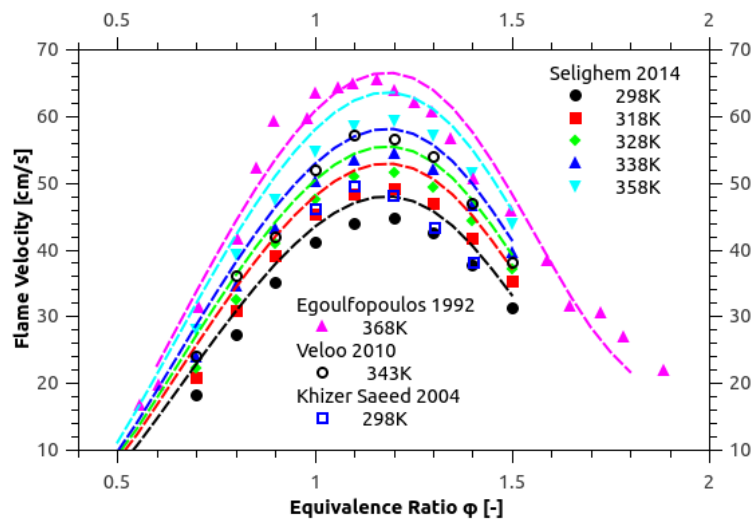
Figure 66: Laminar flame speed of methanol at atmospheric conditions and different inlet temperatures. Experimental data from Sileghem et al. [116], Veloo et al. [106], Egolfopoulos et al. [117] and Saeed et al. [118].

7.6.2   Laminar Flame Speeds
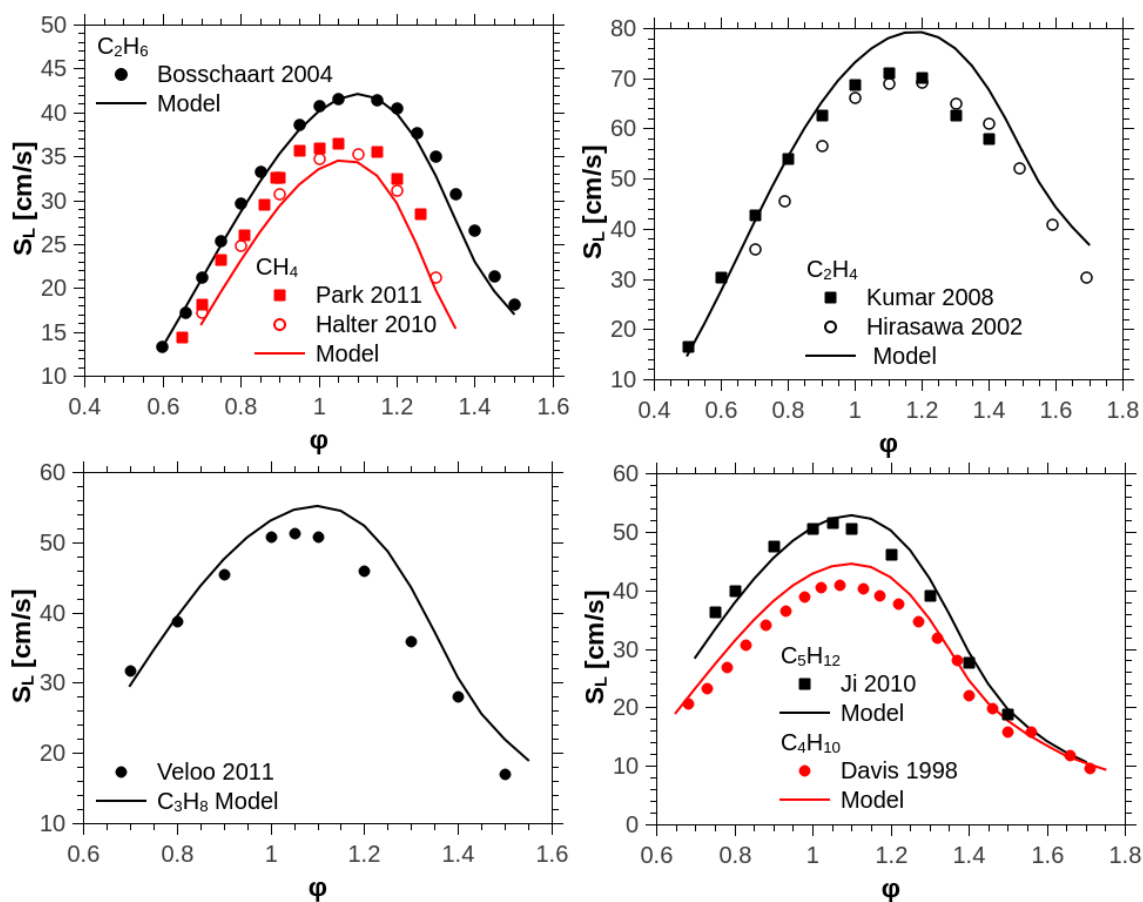
Figure 67: Comparison of measured laminar flame speeds for different fuels against model prediction (lines).
Top left: Methane at 1 atm and 298 K (red symbols); Experimental data from [119] and [120]. Ethane at 298 K and 1 atm (black symbols); Experimental data from [121].
Top right: Ethene at 1 atm and 298 K; Experimental data from [122] and [111].
Bottom left: Propane at 343 K and 1 atm; Experimental data from [123].
Bottom right: n-Butane at 353 K and 1 atm (red symbols); Experimental data from [94]. Butane at 298 K and 1 atm (black symbols); Experimental data from [110].
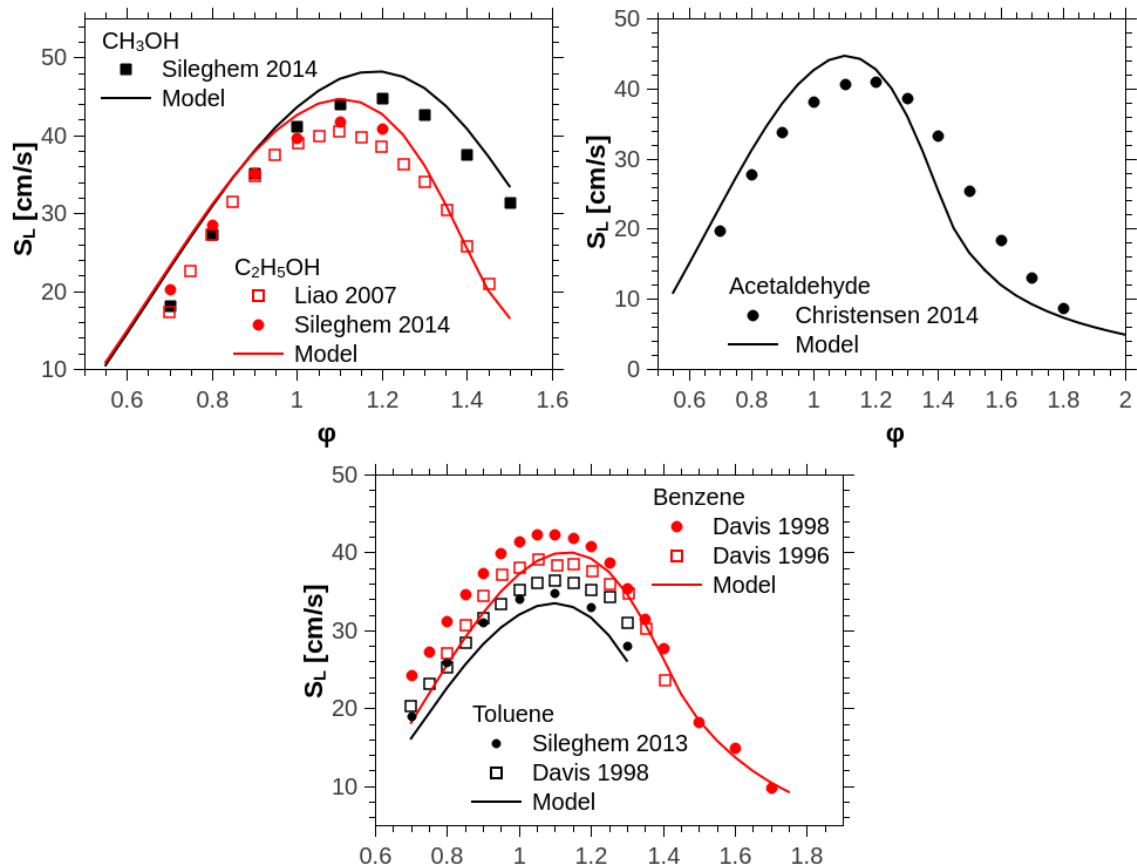
Figure 68: Comparison of measured laminar flame speeds for different fuels against model prediction (lines).
Top left: Methanol at 1 atm and 298 K (black symbols); Experimental data from [116]. Ethanol at 300 K and 1 atm (red symbols); Experimental data from [116] and [124].
Top right: Acetaldehyde at 1 atm and 298 K (symbols); Experimental data from [125].
Bottom: Benzene at 1 atm and 298 K (red symbols); Experimental data from [110] and [126]. Toluene at 1 atm and 298 K (black symbols); Experimental data from [126] and [101].

7.6.3   Burner Stabilised Flames
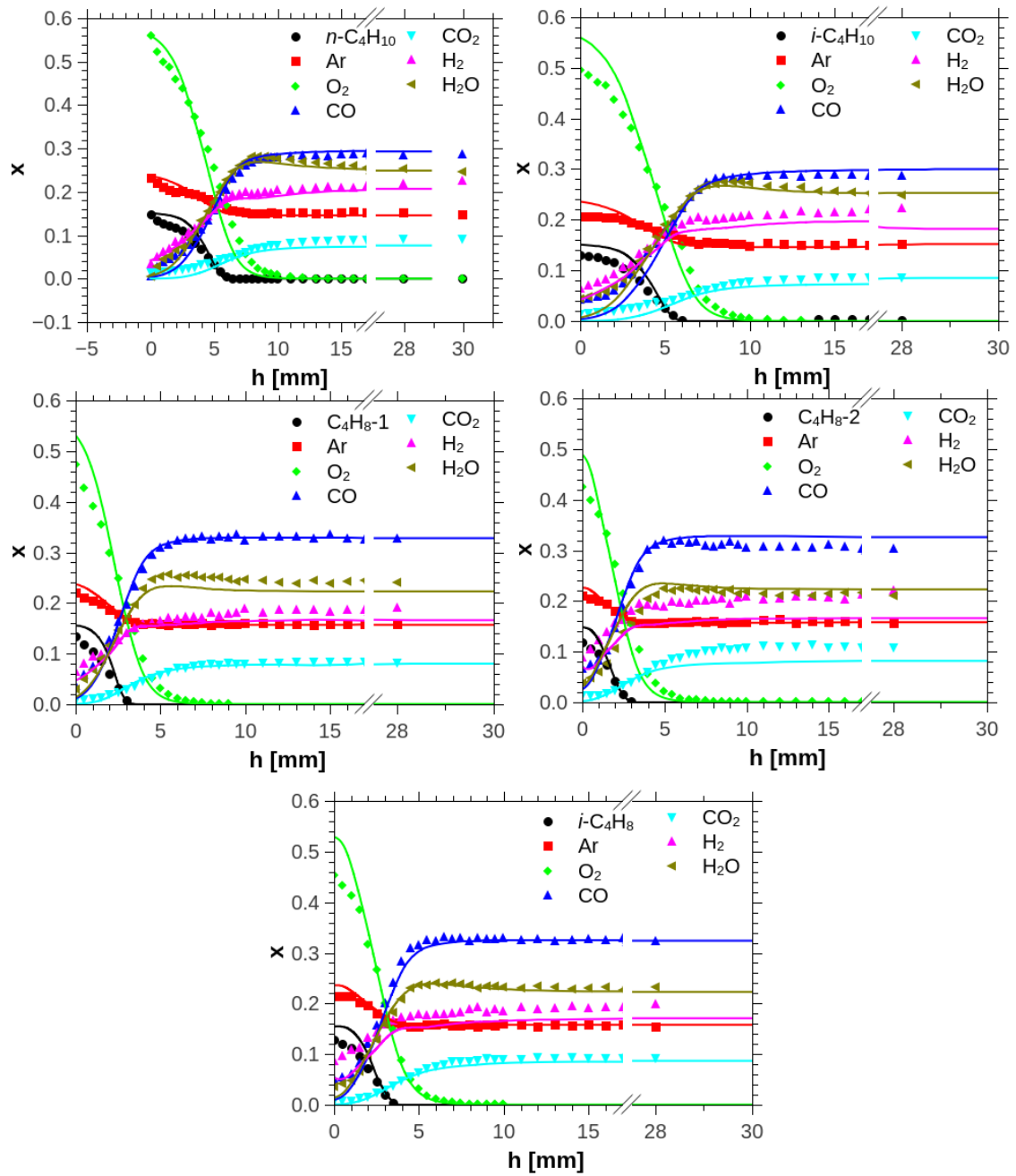
Figure 69: Validation of major species concentrations against burner stabilised C_4 flames at 40 mbar and ϕ=1.7. Top left: n-Butane [41]; Top right: iso-Butane [41]; Middle left: 1-Butene [42]; Middle right: 2-Butene [42]; Bottom: iso-Butene [42]. Conditions: 16.5% butene, 58.5 mol% oxygen and 25.0 mol% argon (molar) or 15.7% butane, 59.5 mol% oxygen and 24.8 mol% argon (molar) at 40 mbar and 300 K cold gas temperature.
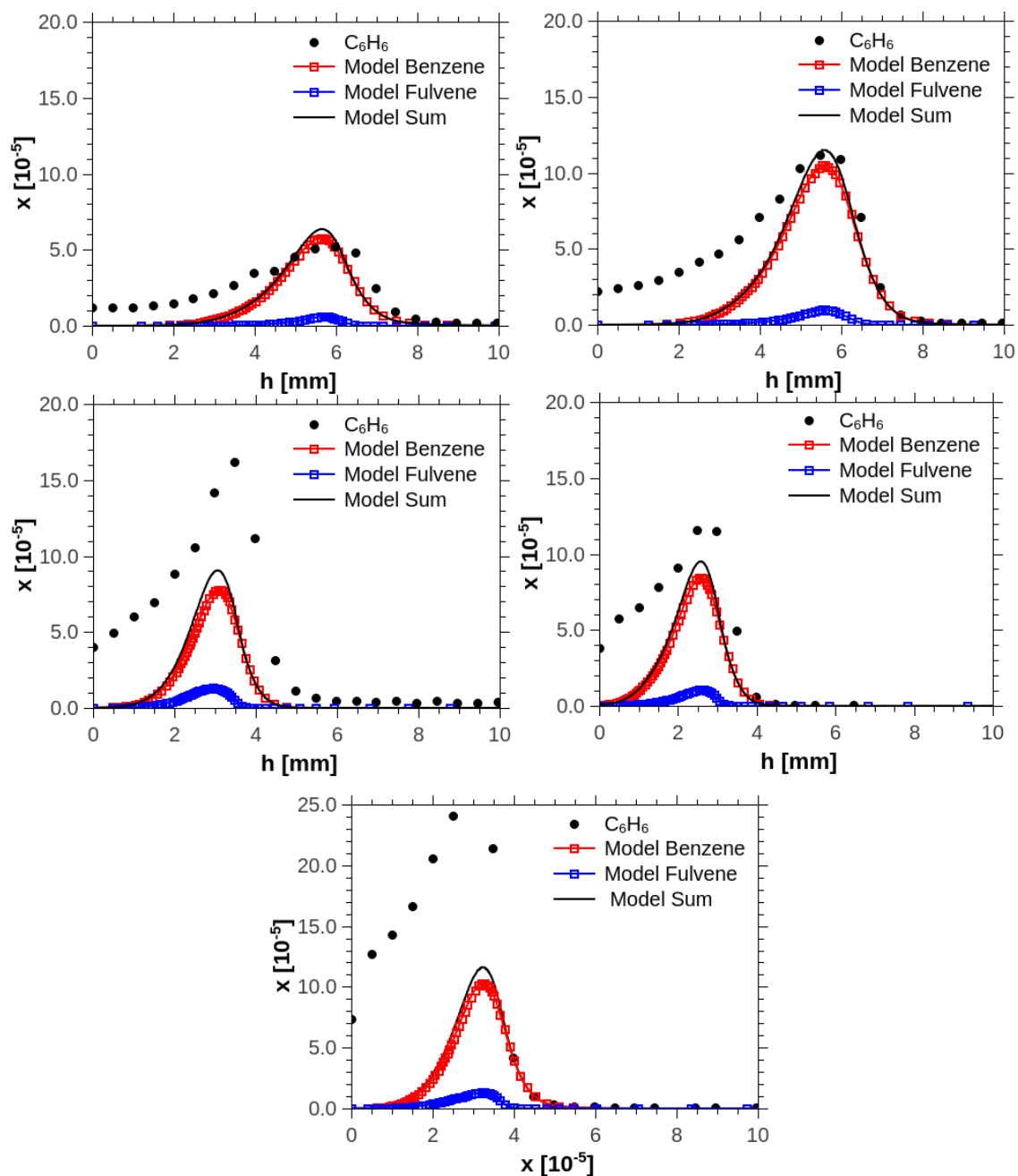
Figure 70: Validation of C_6H_6 concentrations against burner stabilised C_4 flames 40 mbar and ϕ=1.7. Top left: n-Butane [41]; Top right: iso-Butane [41]; Middle left: 1-Butene [42]; Middle right: 2-Butene [42]; Bottom: iso-Butene [42]. Conditions: 16.5% butene, 58.5 mol% oxygen and 25.0 mol% argon (molar) or 15.7% butane, 59.5 mol% oxygen and 24.8 mol% argon (molar) at 40 mbar and 300 K cold gas temperature.

7.7   Emissions

7.7.1   Different NOx models

To be able to model the formation and impact of NO addition different NOx sub-mechanisms were added to the detailed scheme. Four different schemes were chosen:

- The latest NOx model from Lamoureux and co-workers [127]. This mechanism is based on discussion within the combustion modelling community and implemented the latest findings. This sub-mechanism consists of 23 species.

- The complete NOx model from the GRI[20] 3.0 [128]. This is a very frequent used reaction scheme and is therefore used for comparison reasons here. This sub-mechanism consists of additional 17 species.

- The sub-mechanism for thermal NOx formation from the GRI 3.0. Since it is known that thermal NO formation is the major source for NO in engine combustion it is for chosen validation. This sub-mechanism adds three additional species.

- The NOx mechanism developed by Phillip Klaus and published in his Ph.D. thesis [129]. This sub-mechanism was chosen because it is based on an earlier version of the Warnatz combustion model and the core model of the reaction scheme presented here is largely based on Warnatz model as well. This sub-mechanism consists of additional 17 species, which were added.

The thermodynamic and transport data of additional species were used from the individual schemes to assure that in particular reverse rates are not altered.

First of all the impact of NO addition on fuel decomposition is investigated for different fuels. The investigation was carried out by simulating the experiments from Moreac et al. [21] for n-heptane (figure 71), methanol[21] (figure 72), toluene (figure 73) and iso-octane (figure 74).

For n-heptane (figure 71) the addition of NO retards the fuel decomposition at low temperatures and accelerates it at intermediate temperatures. The retardation effect below 650 K is best captured by the sub-mechanism from Klaus while both GRI sub-mechanisms cannot predict this behaviour at all. The Lamoureux sub-mechanism is the only scheme which captures the experimental observed fact that the addition of 500 ppm NO leads to disappearance of the negative temperature regime, observable in fuel concentration at about 750 K. The experiments for methanol (figure 72) suggest that any fraction of NO addition accelerates the fuel decomposition. The earlier onset is best captured by both GRI NO sub-mechanisms or the Lamoureux sub-mechanism. For toluene a similar increase of reactivity is observed in the experiment (figure 73), but none of the sub-mechanisms can capture this behaviour - all schemes predict a reduced reactivity. For iso-octane the experiment points (figure 74) suggest a slightly higher reactivity when 50 ppm NO are added. All schemes seem to overpredict this effect, although a few more experimental points would be helpful to evaluate

---

[20]Gas Research Institute
[21]Unfortunately no experiments for ethanol were carried out.

this properly. In general it can be concluded that in terms of NO addition either the NO sub-mechanism from Klaus or Lamoureux perform best.

Another important feature to be captured by NOx sub-mechanism is the formation of NO. This work focuses on the experimental investigations of Lamoureux an co-workers [127] for validation. They investigated a low pressure CH_4 flame to develope / verify the reaction scheme. The developed scheme from Lamoureux and co-workers [127] predicts most of the quantified species for lean (ϕ=0.8 - figure 75 (d)), stoichiometric (figure 76 (e), and rich methane flames (ϕ=1.25 - figure 77 (f)) well. The ETRF scheme combined with the different NOx sub-mechanisms does not achieve a similar good prediction. The only exception is the combination with the Lamoureux sub-mechanism for the rich flame. All other schemes underpredict all measured species for all flames[22]. It needs to be kept in mind that the NO formation is temperature dependent. This is illustrated by comparing predicted NO and CH profiles using the experimentally obtained temperature profile and the predicted temperature profile from LOGEsoft (figure 78). For the lean case the calculated temperature profile predicts two times more NO at a height of 20 mm above the burner in comparison the simulation with the imposed measured temperature profile. This is achieved even though the predicted temperature is below the measured temperature at this height. For this rich flame the predicted temperature profile is about 100 K hotter at the point where NO concentration reached an equilibrium. This difference of 100 K results in about 50% more NO in equilibrium.

The observations for NO addition and NO formation in premixed flames would suggest that there could be an significant difference in NO emission prediction in engine calculations using different NO-submodels. However engines operate at much higher pressure and different time scales. To investigate the impact of the different NO sub-mechanism the non knocking SI simulation set-up described in section 10.2.2 was used. Table 15 summarises the impact of the different NO models on CPU time and predicted engine out emissions. It can be observed that the large spread in NO_2 emissions are negligible in comparison to the predicted NO emissions. The engine out NO emissions differ between 2.9E-3 molar fraction for the complete GRI scheme and 3.4E-3 for the Lamoureux NOx sub-mechanism. All sub-mechanisms, except the complete GRI, predict nearly the same NO engine out emissions. The CPU times increase with the number of species and reactions and the largest scheme (Lamoureux) needs about two minutes (more than 10%) CPU time more than smallest (thermal GRI). This investigation suggests that engine out NO emissions are not as sensitive to the actual NO submechanism as the investigated premixed burner stabilised flames. The major reason for the comparable stable NO prediction is that the formation is dominated by the temperature in the engine. The temperature in a not knocking spark S.I. is determined by the flame propagation. S.I. engines mostly operate in conditions where thermal NO is formed, while the investigated flames show lower temperatures and the NO formation is dominated by the promp NO pathway. This small study suggests that a simple thermal NOx model would be sufficient when a short CPU time is an important target in the mech-

---

[22]Note that the species CN, HCN and NCO are not included in the thermal GRI mechanism. NCN is only included in the Lamoureux scheme.

anism development since it would cover the majority of NO formation.
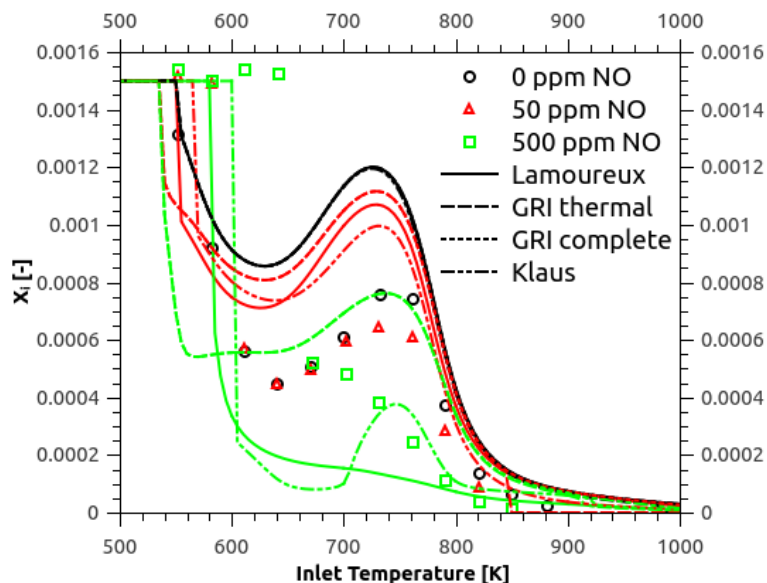
Figure 71: Measured n-heptane molar fractions at stoichiometric mixtures (0.15% n-heptane, 1.65% O_2) in nitrogen at 10 atm in a jet stirred reactor with a residence time of 1 s from Moreac et al. [21] Lines correspond to simulation with four different NOx sub-models. Black circles - no NO addition; red triangles - 50 ppm NO addition; green squares 500 ppm NO addition. Both GRI schemes predict the same combustion.
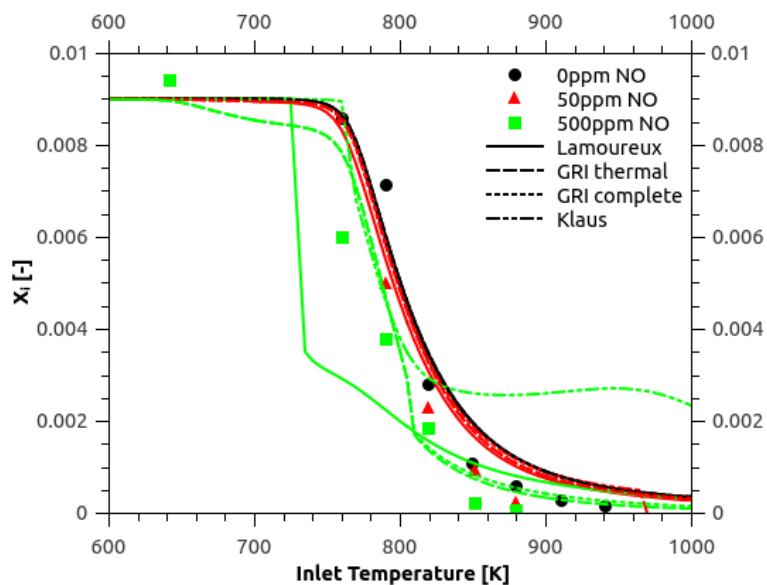
Figure 72: Measured methanol molar fractions at stoichiometric mixtures (0.9% methanol, 1.35% O_2) in nitrogen at 10 atm in a jet stirred reactor with a residence time of 1 s from Moreac et al. [21] Lines correspond to simulation with four different NOx sub-models. Black circles - no NO addition; red triangles - 50 ppm NO addition; green squares 500 ppm NO addition.
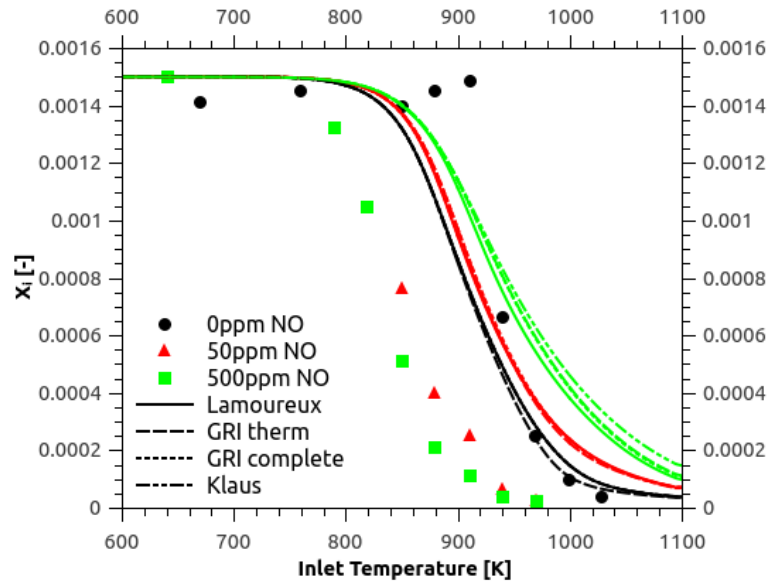
Figure 73: Measured toluene molar fractions at stoichiometric mixtures (0.15% toluene, 1.35% O_2) in nitrogen at 10 atm in a jet stirred reactor with a residence time of 1 s from Moreac et al. [21] Lines correspond to simulation with four different NOx sub-models. Black circles - no NO addition; red triangles - 50 ppm NO addition; green squares 500 ppm NO addition.
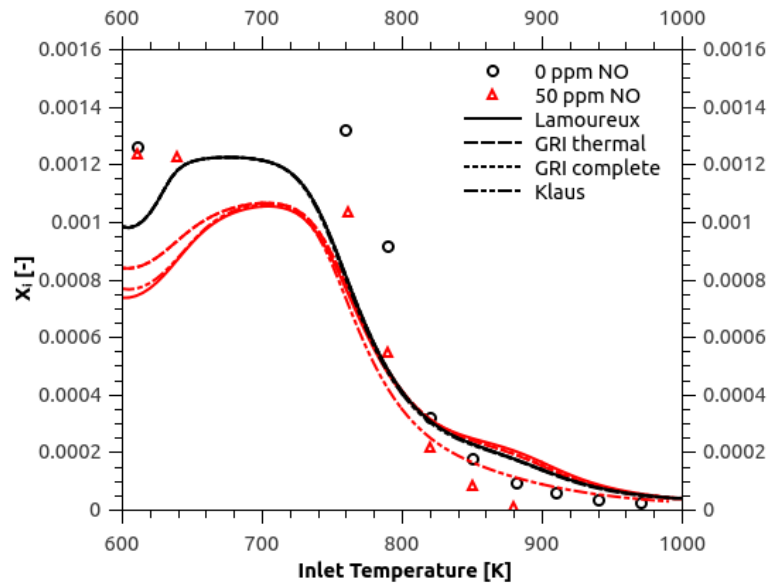
Figure 74: Measured iso-octane molar fractions at stoichiometric mixtures (0.15% iso-octane, 1.35% O_2) in nitrogen at 10 atm in a jet stirred reactor with a residence time of 1 s from Moreac et al. [21] Lines correspond to simulation with four different NOx sub-models. Black circles - no NO addition; red triangles - 50 ppm NO addition and green squares 500 ppm NO addition.

NOx sub model	Number of species	Number of reactions	CPU time (1 cycle) [s]	NO out	NO$_2$ out
Thermal GRI [128]	386	4511	910.0	3.37E-3	3.18E-7
Complete GRI [128]	401	4711	930.8	2.89E-3	2.81E-7
Klaus [129]	401	4771	980.4	3.26E-3	1.50E-7
Lamoureux [127]	407	4971	1029.0	3.40E-3	1.75E-7

Table 15: Obtained CPU times and engine out emissions using different NO sub-mechanisms for an arbitrary engine case (table 22 - non knocking). Emissions are average of 30 consecutive cycles in molar fraction.
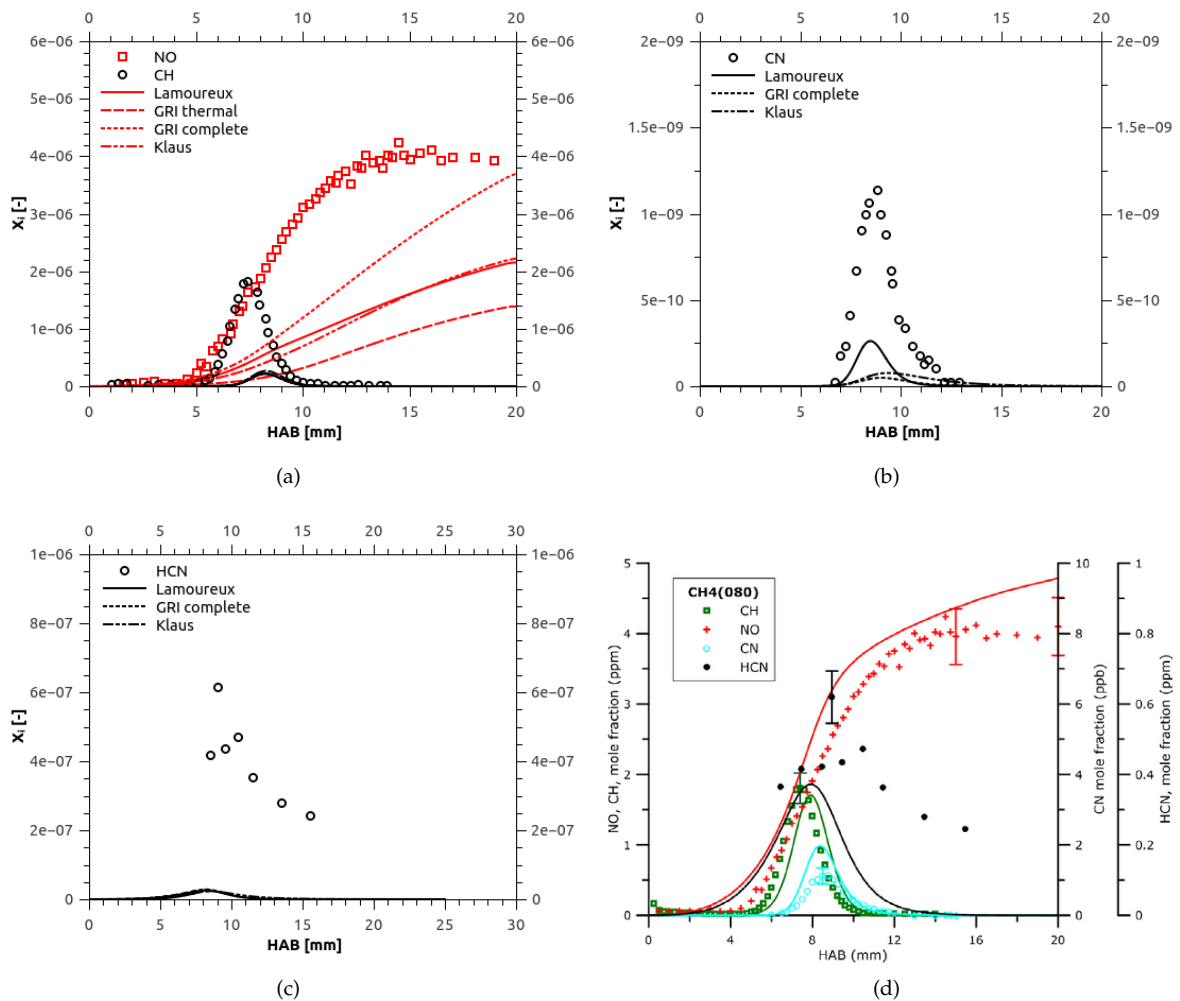
Figure 75: Prediction of NO and CH (a), CN (b) and HCN (c) using the lumped scheme with different NOx sub-models for a lean (ϕ=0.8) methane flame. Measurements are taken from Lamoureux et al. [127]. Figure (d) is taken from Lamoureux et al. [127].
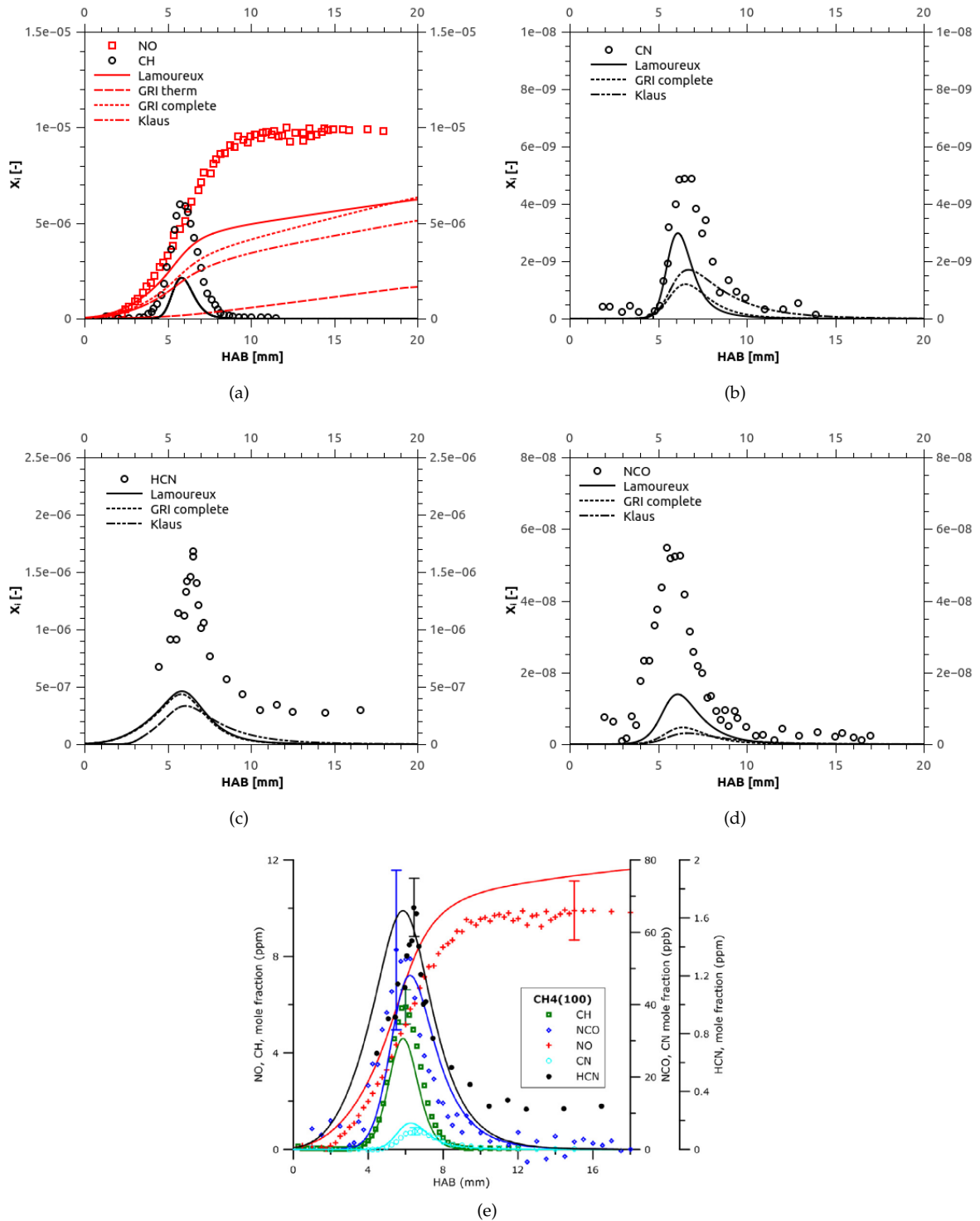
Figure 76: Prediction of NO and CH (a), CN (b), HCN (c), NCO (d) using the lumped scheme with different NOx sub-models for a stoichiometric (ϕ=1.0) methane flame. Measurements are taken from Lamoureux et al. [127]. Figure (e) is taken from Lamoureux et al. [127].
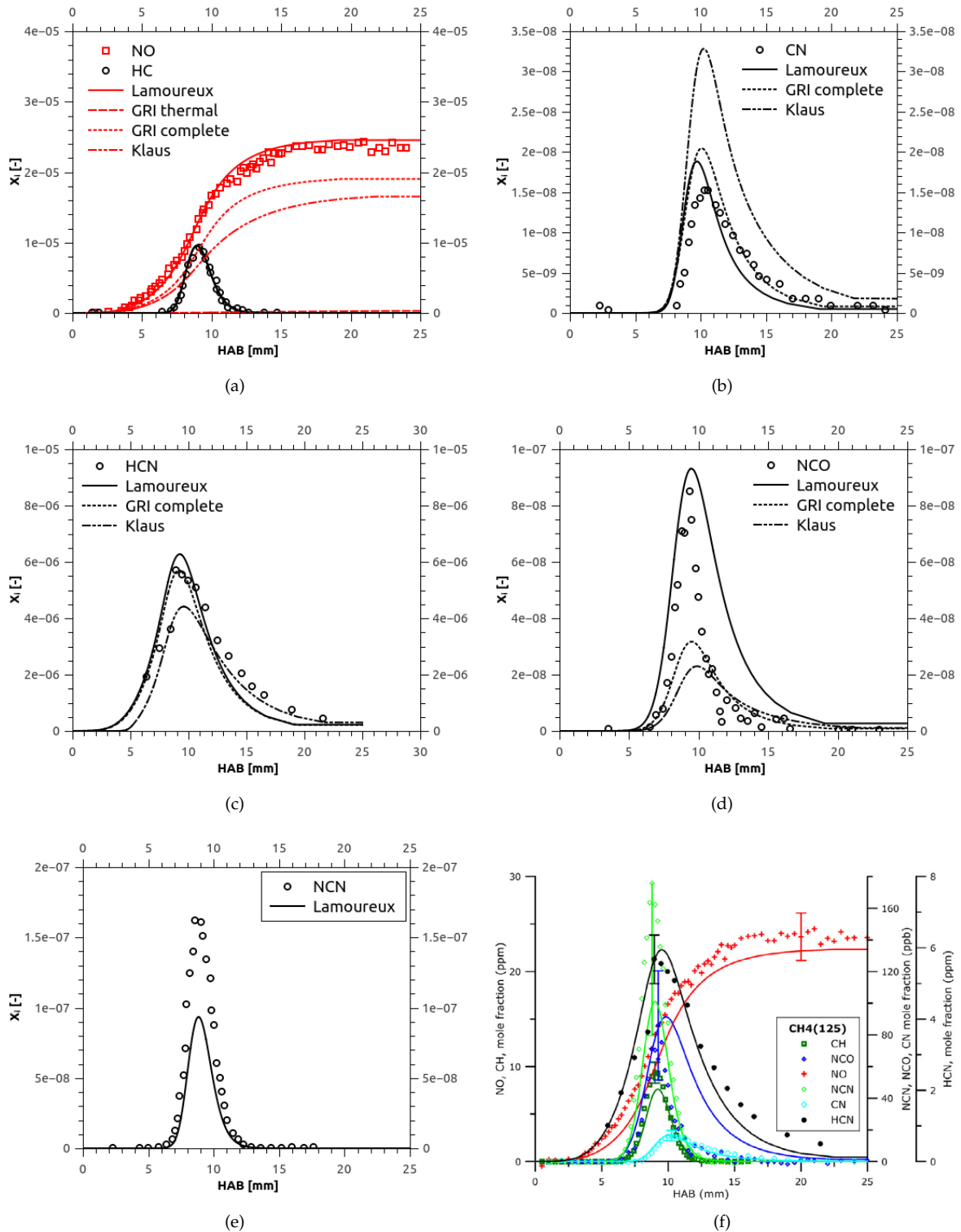
Figure 77: Prediction of NO and CH (a), CN (b), HCN (c), NCO (d), NCN (e) using the lumped scheme with different NOx sub-models for a rich (ϕ=1.25) methane flame. Measurements are taken from Lamoureux et al. [127]. Figure (f) is taken from Lamoureux et al. [127].

(a) $\phi = 0.8$

(b) $\phi = 0.8$

(c) $\phi = 1.25$

(d) $\phi = 1.25$
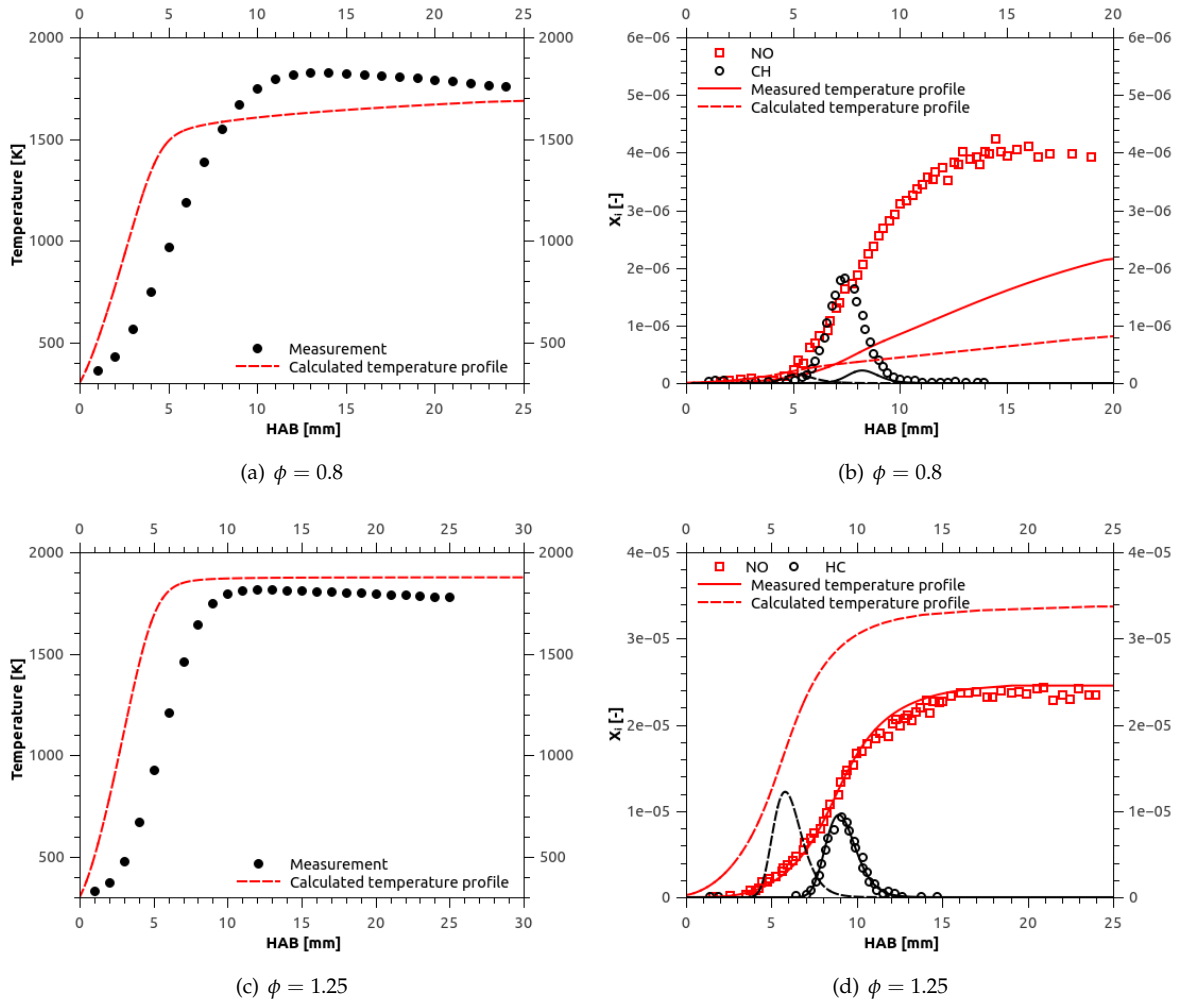
Figure 78: Impact of temperature profile on NO and CH formation for the lean (ϕ=0.8) and rich methane flame (ϕ=1.25). The calculated temperature profile refers to calculation without imposing the measured temperature profile.

8   Correlations of RON / MON with 0D calculations

As discussed in chapter 5 about mixture formulation each pure fuel or mixture has a RON and MON which is obtained in a test engine. There is clearly a correlation between ignition delay times and octane rating of the fuel. In the last five years different correlations between 0D ignition delay times and measured RON / MON values were suggested. The suggestions show a significant difference in initial pressure and temperature:

- Ahmed et al. 2015 [130]: 20 atm / 835 K for RON and MON

- Mehl et al. 2011 [131]: 25 atm / 825 K for RON and MON

- Badra et al. 2015 [9]: 45 atm / 980 K for MON

- Badra et al. 2015 [9]: 50 atm / 850 K for RON.

It needs to be kept in mind that such 0D and homogeneous correlations cannot cover real engines. A perfectly premixed S.I. engine would at least need the description of an unburned and burned zone. And in comparison to 0D reactors engines are transient, which means that they have a steady increase in temperature and pressure until top dead centre, even though no ignition event has occurred. Further one needs to consider that the unburned zone can show a heat release without a clear ignition event due to low temperature chemistry.

The suggested conditions are used to create plots comparing predicted ignition delay time (constant volume assumption) using the detailed scheme against measured RON and MON. Five pure fuels: n-heptane, iso-octane, toluene, methanol and ethanol are used for the comparison. Further ignition delay times for PRF 10, 50, 75, 90 and 95 are considered. Finally the computed ignition delay times for the TRF mixtures in table 10 are also included. Based on this correlations it will be tried to investigate two questions:

1. Do the correlations show a good and smooth (steady and monotonic) correlation between RON / MON and ignition delay times for

   - pure fuels and
   - multicomponent fuels

2. Which conditions are the best for RON or MON correlations?

Subsequently it will be evaluated if this correlation can be used for mechanism development or MON / RON determination of mixtures.

The ignition delay times for pure and PRF fuels illustrates the intrinsic problem with the MON / RON definition. As figure 79 a) c) and e-f) shows, the fuels n-heptane / iso-octane and its mixtures have the same ignition delay times for RON and MON due to its definition. The non PRF fuels, however have a significant lower MON at the same ignition delay time. This systematic difference results in a non smooth transition from PRF fuels and mixtures to the other pure fuels. It can be observed that the predicted ignition delay times for TRF mixtures follow the overall trend. However the scheme has the tendency to predict to short ignition delay times. Even though the lowest experimental RON is 32 and

(a) 20bar / 835K

(b) 20bar / 835K with TRF fuels

(c) 25bar / 825K

(d) 25bar / 825K with TRF fuels

(e) 45bar / 980K with TRF fuels (MON conditions)

(f) 50bar / 850K with TRF fuels (RON conditions)
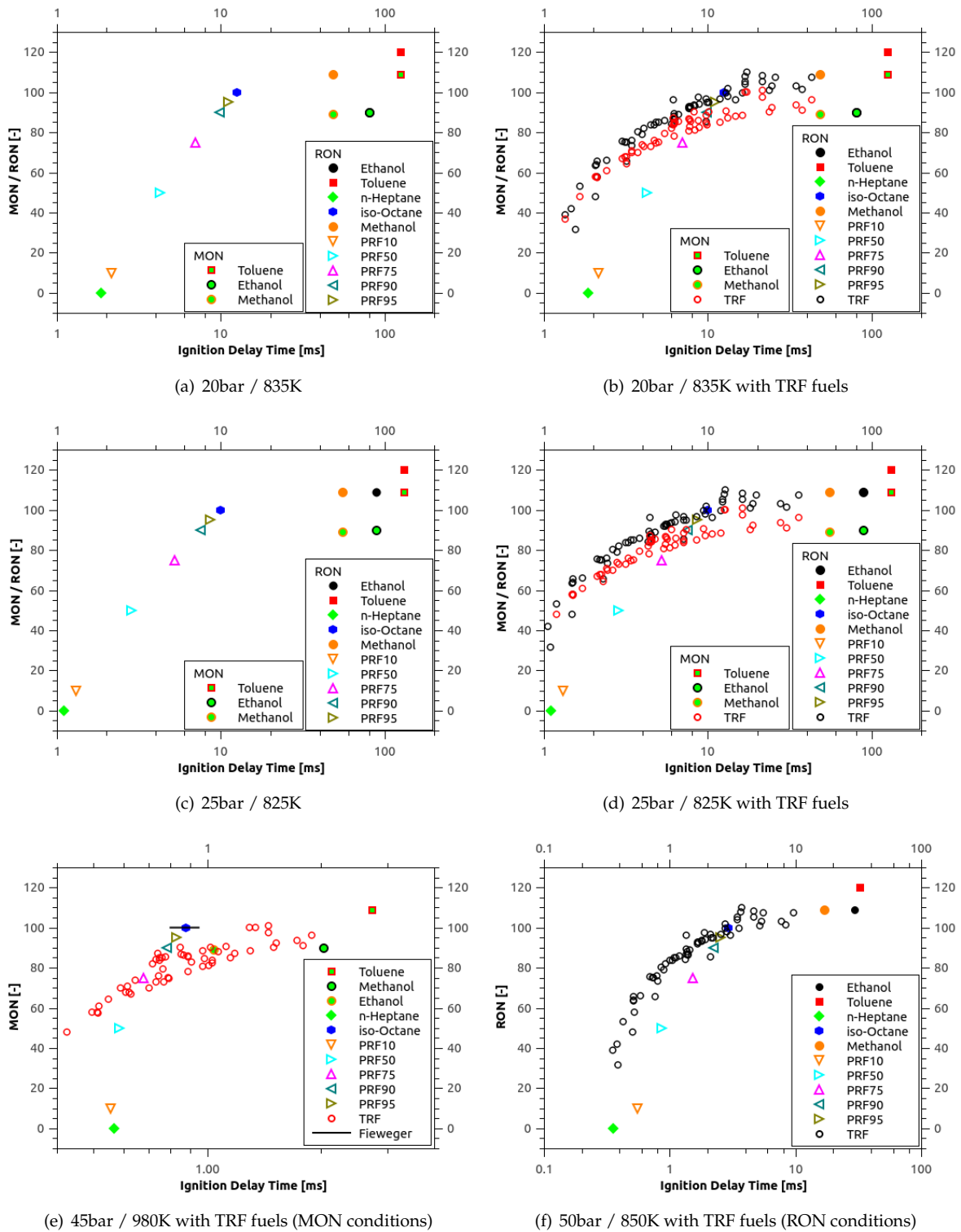
Figure 79: Plots correlating predicted ignition delay time to measured RON / MON in constant volume reactors.

the lowest MON is 37 some of the TRF mixtures show ignition delay times shorter than pure n-heptane (RON=MON=0). Even though it may be possible that small fractions of toluene can accelerate the combustion of the mixtures it is very improbable and the reason for this trend along with an updated scheme is discussed in the next chapter. After introducing the update to the scheme and a re-evaluation of the RON/MON correlation the questions raised

above can be answered. Before moving on it is worth to discuss the model and experimental uncertainties in this correlations.

8.1   Assessment of uncertainties

In this plots an uncertainty in measured octane numbers would be represented by a change in direction of the y-axis. Uncertainties in measured/predicted ignition delay time would result in a change along the x-axis. The uncertainty of octane rating determination is about 1 point for most of the mixtures as discussed earlier in section 5.3.2. This uncertainty is below the size of the symbols in figure 79. Determining the uncertainty of measured/predicted ignition delay is more difficult. Assuming the model is able to predict measured ignition delay times perfectly one still has to deal with the experimental uncertainty and the data transfer[23]. Some of the experimental data shown earlier in this work did show an significant scatter from the same experimental setup at the same temperature (see for example figure 51 at around 950 K). The only shock tube experiments which measured a ignition delay time for a fuel at a pressure used for the correlations was performed by Fieweger et al. [38] for 45 bar. To estimate the uncertainty of data extraction different people[24] were asked to read the ignition delay time for 45 bar / 980 K from the publication and the highest and largest value was discarded. This range is incorporated in figure 79 (e) and translate to a noticeable scatter in ignition delay time. The difference in ignition delay covers an equivalent of about $\pm$ 5 points in MON.

---

[23]The situation of data transfer is getting increasingly better with electronic supplementary material. In the past the typical way of data transfer was, or still is, that measured data are published in a plot and than be later extracted by the person who wants to use it.

[24]Engineers working in the field of combustion and beeing familiar with such plots.

9 The impact of the reaction Benzyl+Hydroperoxyl on ETRF mixtures

9.1 Reasoning and reaction modification

In the previous chapter different correlations between measured RON and MON against ignition delay times obtained in 0D calculations are shown. It was observed that some of the TRF mixtures show ignition delay times which are shorter than the ignition delay time of pure n-heptane. All mixtures with a very short ignition delay time contain toluene and n-heptane. Such a behaviour was not observed for binary mixtures of n-heptane and iso-octane or mixtures of iso-octane and toluene. This indicates that during the n-heptane decomposition intermediates are formed which will accelerate the combustion depending on the presences of toluene. Even though it is very likely that such a non linear effect does exist it may be overpredicted by the reaction scheme. At this point it is described by which series of reactions a small fraction of toluene, a fuel which hardly ignites below 1000 K, can accelerate the oxidation of n-heptane (the surrogate fuel with the shortest ignition delay time).

With the help of a sensitivity and flow analysis the following reactions where analysed to be responsible for the acceleration of the combustion when toluene is present in the fuel mixture:

$HO_2+A_1CH_2=>H+OH+A_1CHO$ and
$HO_2+A_1CH_2=>OH+CH_2O+A_1-$
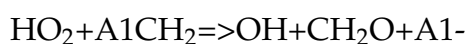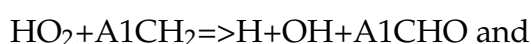
The early formation of HO_2 can be mainly attributed to the low temperature chemistry of n-C_7H_{16}. Most of the HO_2 is formed in reaction class 20 where QOOH decomposes into HO_2 and C_7H_{14}-olefins.
Another minor source is the oxidation of toluene: $O_2+A_1CH_3=HO_2+A_1CH_2$. The bimolecular reactions of HO_2 and A_1CH_2 form radicals (H, OH) which accelerates the decomposition of n-heptane and therefore shortens the ignition delay time of the fuel mixtures. There are indications that this reaction is sensitive. Since the major source of the acceleration mechanism for toluene / n-heptane mixtures is found it is worth to study the sensitivity of this reaction. In the derived mechanism the Arrhenius coefficients are chosen as follows:

$HO_2+A_1CH_2=>H+OH+A_1CHO$: 5.000E+12 0.00 2.000E+03
$HO_2+A_1CH_2=>OH+CH_2O+A_1-$: 5.000E+12 0.00 0.000E+00

Both Arrhenius rates are taken from the Group in Milano (e.g. in [132]). A literature review reveals that Hippler et al. [85] suggest a total rate of about 5.0E12 with an uncertainty of 3.0E12. Assuming that the branching ratio is similar to those of $O+A_1CH_2$ suggested from Emdee [86]) we obtain:

$HO_2+A_1CH_2=>H+OH+A_1CHO$: 3.800E+12 0.00 0.000E+00
$HO_2+A_1CH_2=>OH+CH_2O+A_1-$: 1.200E+12 0.00 0.000E+00.

This modification has little impact on the predicted ignition delay time (see figure 80) and laminar flame speeds of pure toluene (see figure 81 and 82). However the modification has the largest impact on the predicted ignition delay times in the low temperature regime of n-heptane / toluene mixtures (see figure 85), while typical TRF mixtures do show a smaller response on the modification as shown in figure 83 and 84.
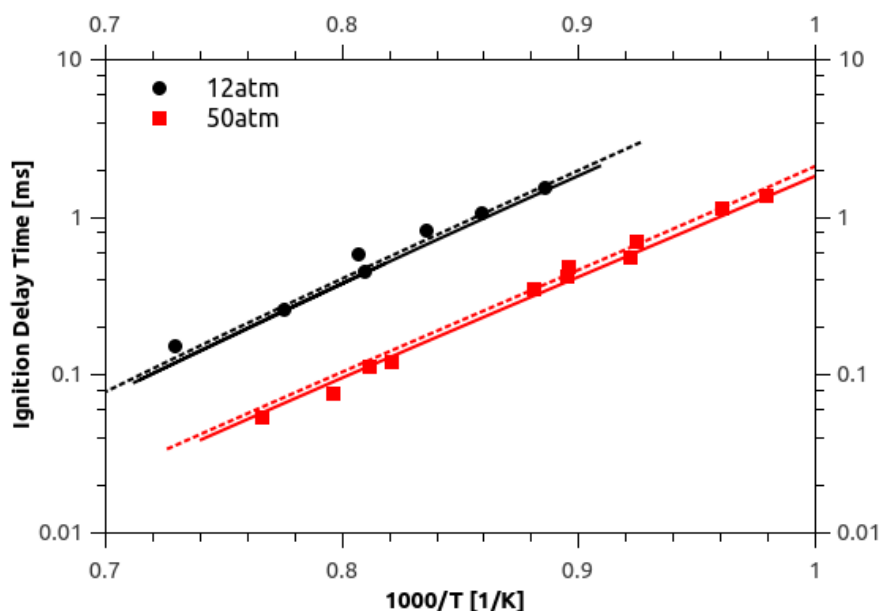
Figure 80: Ignition delay time of stoichiometric toluene / air mixtures at 12 bar and 50 bar. Experimental points from [109]. Solid line denotes the prediction using the unmodified scheme. Dashed line denotes the prediction using the modified scheme.
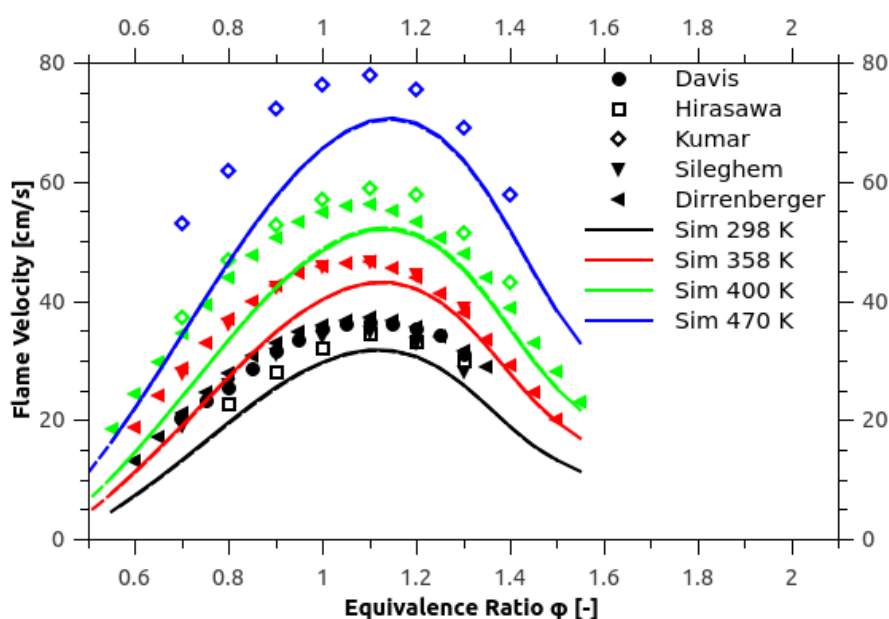
Figure 81: Laminar flame speeds for toluene / air mixtures at 1 atm and different inlet temperatures: 298 K (black); 358 K (red); 398K-400 K (green) and 470 K (blue). Experimental data [110], [111], [93], [101] and [96]. Solid line denotes the prediction using the unmodified scheme. Dashed line denotes the prediction using the modified scheme.
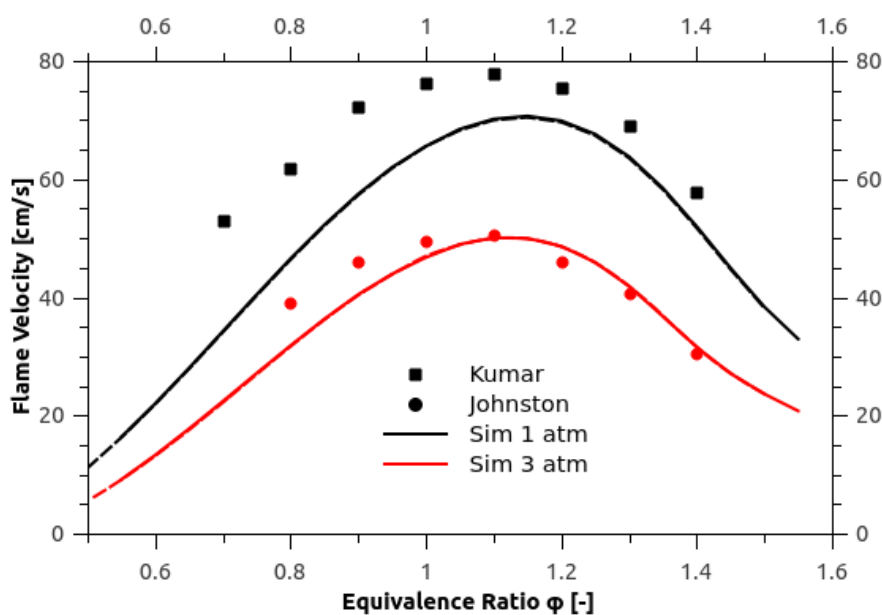
Figure 82: Laminar flame speeds for toluene / air mixtures at 450 K and 3 atm [93] and 470 K and 1 atm [112]. Solid line denotes the prediction using the unmodified scheme. Dashed line denotes the prediction using the modified scheme.
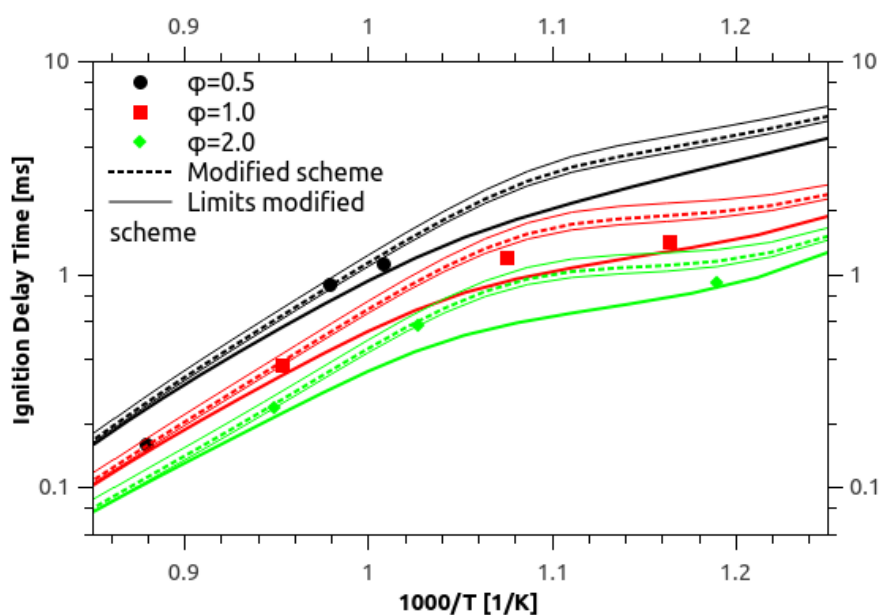
Figure 83: Ignition delay time for surrogate: 0.56 iso-octane, 0.28 toluene and 0.17 n-heptane (mole fraction) at 52 bar. Experimental data from [45]. Solid line denotes the prediction using the unmodified scheme. Dashed line denotes the prediction using the modified scheme. The thin solid lines are the prediction with the upper and lower end of the rate uncertainty suggest by Hippler et al. [85]

It needs to be mentioned that other decomposition pathways of the alkanes will also play a role. Especially the following major reaction classes may be of importance:

- Class 20: QOOH = QO + OH

- Class 1: H-Abstraction from the fuel via O_2 forming HO_2

- Class 2: H-Abstraction from the fuel and derived dienes via HO_2 consuming HO_2 and
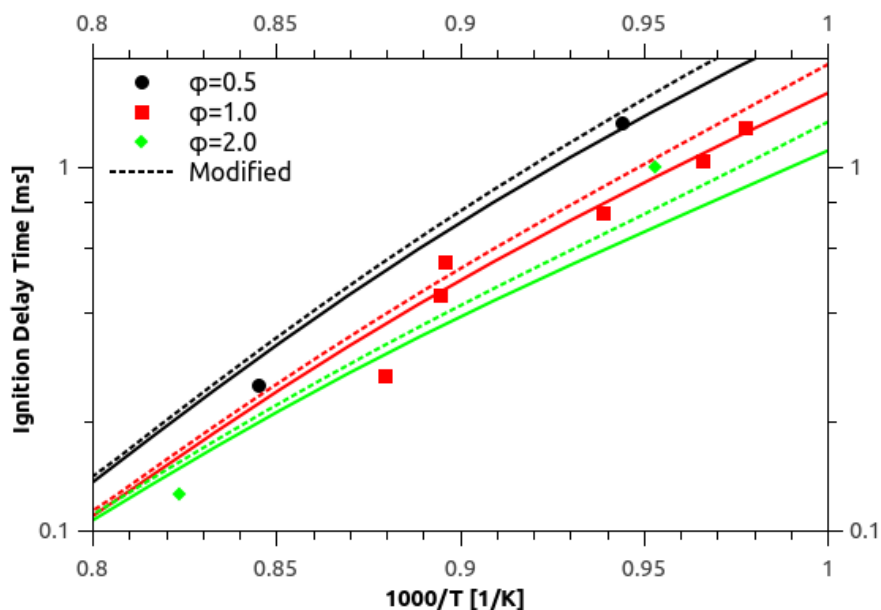
Figure 84: Ignition delay time for surrogate: 0.56 iso-octane, 0.28 toluene and 0.17 n-heptane (mole fraction) at 20 bar. Experimental data from [45]. Solid line denotes the prediction using the unmodified scheme. Dashed line denotes the prediction using the modified scheme.
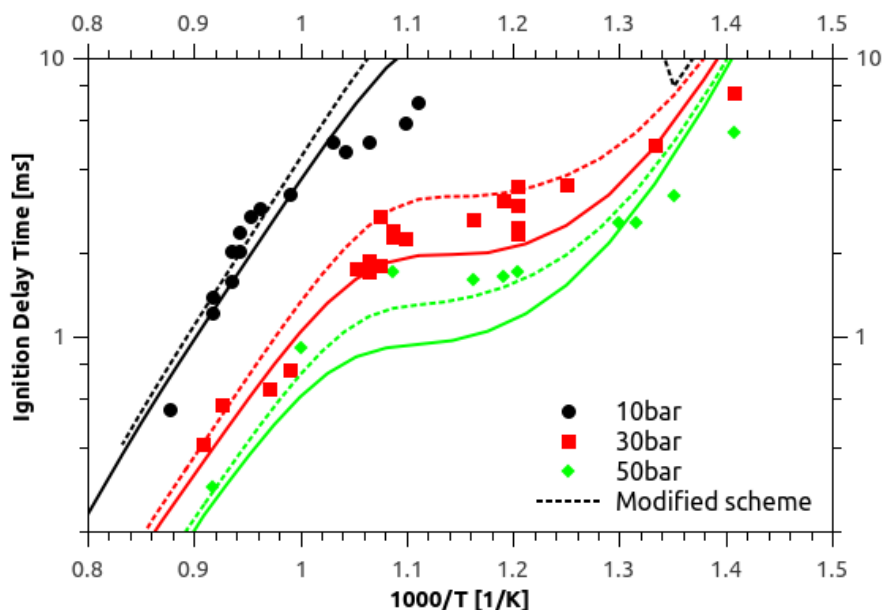
Figure 85: Ignition delay time for a mixture of 0.72 toluene and 0.28 n-heptane (mole fraction) at ϕ=1.0 and p=10, 30, 50 bar. Experimental data from [36]. Solid line denotes the prediction using the unmodified scheme. Dashed line denotes the prediction using the modified scheme.

forming H_2O_2

- Class 13: $RO_2 + HO_2 = RO_2H + O_2$.

Further the formation and consumption of HO_2 embedded in the base chemistry may also play a role. Due to the fact that those reaction classes where well balanced within their uncertainty by Curran [11] and Zeuch, Mauss, Ahmed and Moreac [14, 82]. A careful revision of the hydroperoxyl related decomposition pathways is not part of this thesis.
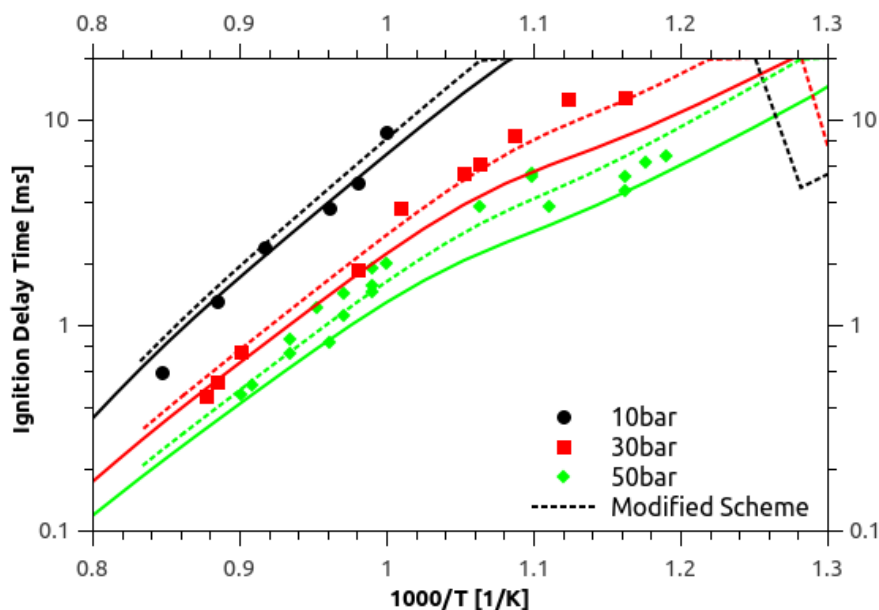
Figure 86: Ignition delay time for a mixture of 0.72 toluene and 0.28 n-heptane (mole fraction) at ϕ=0.3 and p=10, 30, 50 bar. Experimental data from [36]. Solid line denotes the prediction using the unmodified scheme. Dashed line denotes the prediction using the modified scheme.
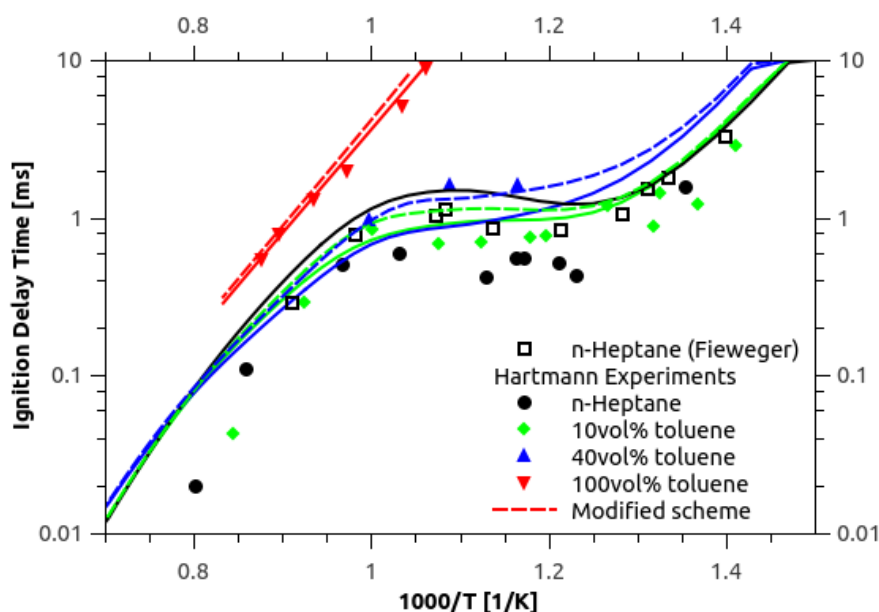
Figure 87: Ignition delay time for different n-heptane / toluene mixtures at $\approx$ 40 bar and ϕ=0.5. Experiments from Fieweger et al. [38] and Hartmann et al. [37]. Solid line denotes the prediction using the unmodified scheme. Dashed line denotes the prediction using the modified scheme.

Drawing a sound conclusion about the chosen rate looking only at validation against experimental data is rather difficult. One reason is that verified ignition delay times for fuel mixtures hardly exist. This dilemma is well illustrated when looking at the data shown in figure 85 which show a significant experimental uncertainty for ignition delay times at 30 bar. Looking at data for the addition of small toluene fractions to n-heptane in figure 87 and 88 reveals significant differences in experimentally obtained ignition dealay times. Here Hartmann and co-workers obtained faster ignition delay times for pure n-heptane as
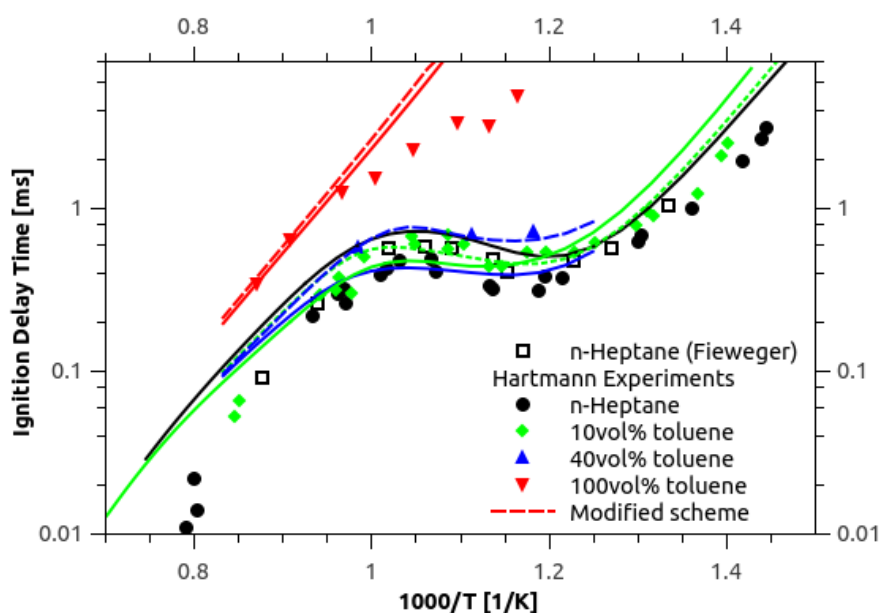
Figure 88: Ignition delay time for different n-heptane / toluene mixtures at $\approx$ 40 bar and ϕ=1.0. Experiments from Fieweger et al. [38] and Hartmann et al. [37]. Solid line denotes the prediction using the unmodified scheme. Dashed line denotes the prediction using the modified scheme.
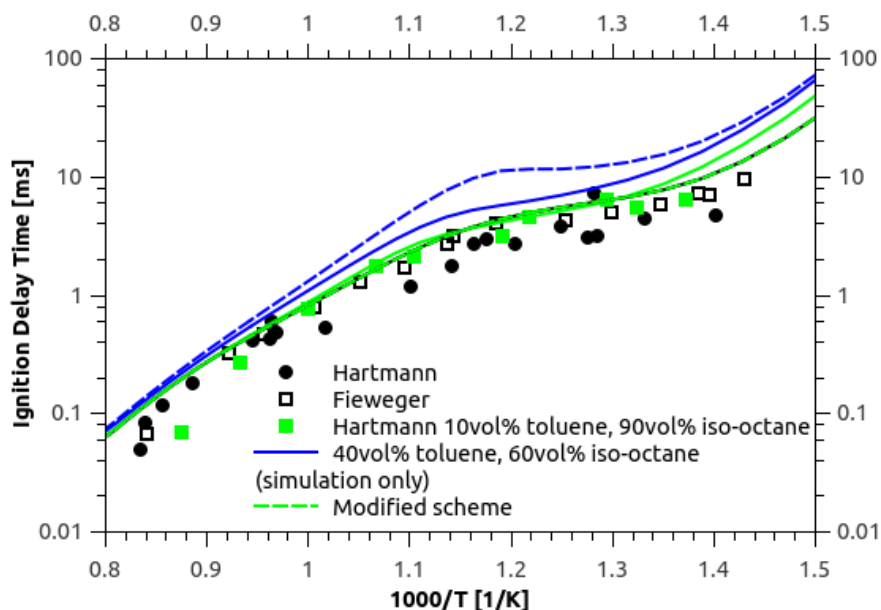
Figure 89: Ignition delay time for different iso-octane / toluene mixtures at $\approx$ 40 bar and $\phi = 0.5$. Experiments from Fieweger et al. [38] and Hartmann et al. [37]. Solid line denotes the prediction using the unmodified scheme. Dashed line denotes the prediction using the modified scheme. Please note that there are not published data for 40 vol% toluene addition and the simulation is only shown to visualise the impact of toluene addition.

Fieweger and co-workers reported earlier. The data from Hartmann reaches the same ignition delay time with 10 vol% toluene addition or more depending on the fuel equivalence ratio (figure 88 and 89). In general the modified scheme shows a good agreement with the measured ignition delay time from Hartmann and co-workers for 10 and 40% toluene addition in the temperature relevant for engine knock (800 K - 1000 K) for lean and stoichiometric

mixtures.

Assessing all experimental data the conclusion can be drawn that the modification is leading to a better overall prediction of ignition delay time. This will be more clear when looking at the correlation between 0D ignition delay times and octane numbers in the next section.

9.2   Impact on RON / MON correlations

As pointed out in the introduction of this chapter the correlation of RON / MON with 0D ignition delay times was leading to the investigations of the Benzyl + Hydroperoxyl reactions. Consequently the correlations are studied here again with the updated scheme. Figure 90 and 91 compare correlations of the unmodified (left side) with the modified scheme (right side). The outcome of the modification can be summarized as follows:

- The ignition delay time for PRF fuels and its mixtures are not effected by the modification.

- The oxygenated fuels are not effected by the modification.

- Toluene shifts to slightly longer ignition delay times at all conditions.

- All TRF mixtures show longer ignition delay times than pure n-heptane[25].

- The modified scheme somewhat follows a smother shape and fits much better to the PRF and oxygenated fuels correlation.

  It can be observed that for 20 bar / 835 K and 25 bar / 825 K the TRF mixtures with the highest octane number are close to the points of ethanol, however none of them can match the fuel sensitivity (RON-MON). Based on the discussion in chapter 5.2 a match in sensitivty is not expected.

  The correlation at 50 bar and 850 K for RON conditions shows a small variance between the PRF and the TRF mixtures after the modification. The suggested conditions for MON at 45 bar and 980 K show a significant deviation of the trend predicted by the PRF fuels and TRF mixtures. Similar observations can be made for correlations at 20 bar / 835 K and 25 bar / 825 K - the MON correlation shows a significant deviation from the PRF fuels while for very high octane numbers a better match is observed. At large is seems that none of the proposed correlations for MON conditions provides a good correlation over a wide range of octane ratings. To rate this finding one has to consider that 0D constant volume calculations are performed with gaseous fuels and therefore the cooling due to evaporation is excluded. This means that the simulation is actually closer to MON conditions with preheating and pre-evaporation of the fuel than to RON conditions. As briefly discussed in chapter 5.2 this would imply that the MON rating for iso-octane should be rated down to about 80. This is of course not how the MON is defined, but would result in a much more reasonable correlation with ignition delay times at the proposed conditions.

---

[25]Well, not entirely... One TRF mixture at 45 bar of indomitable TRF still holds against the correlation [133].

The best correlation for RON with this mechanism is found for ignition delay times calculated 50 bar and 850 K.

(a) 20bar / 835K (MON)

(b) 20bar / 835K (MON) modified scheme

(c) 25bar / 825K (RON)

(d) 25bar / 825K (RON) modified scheme
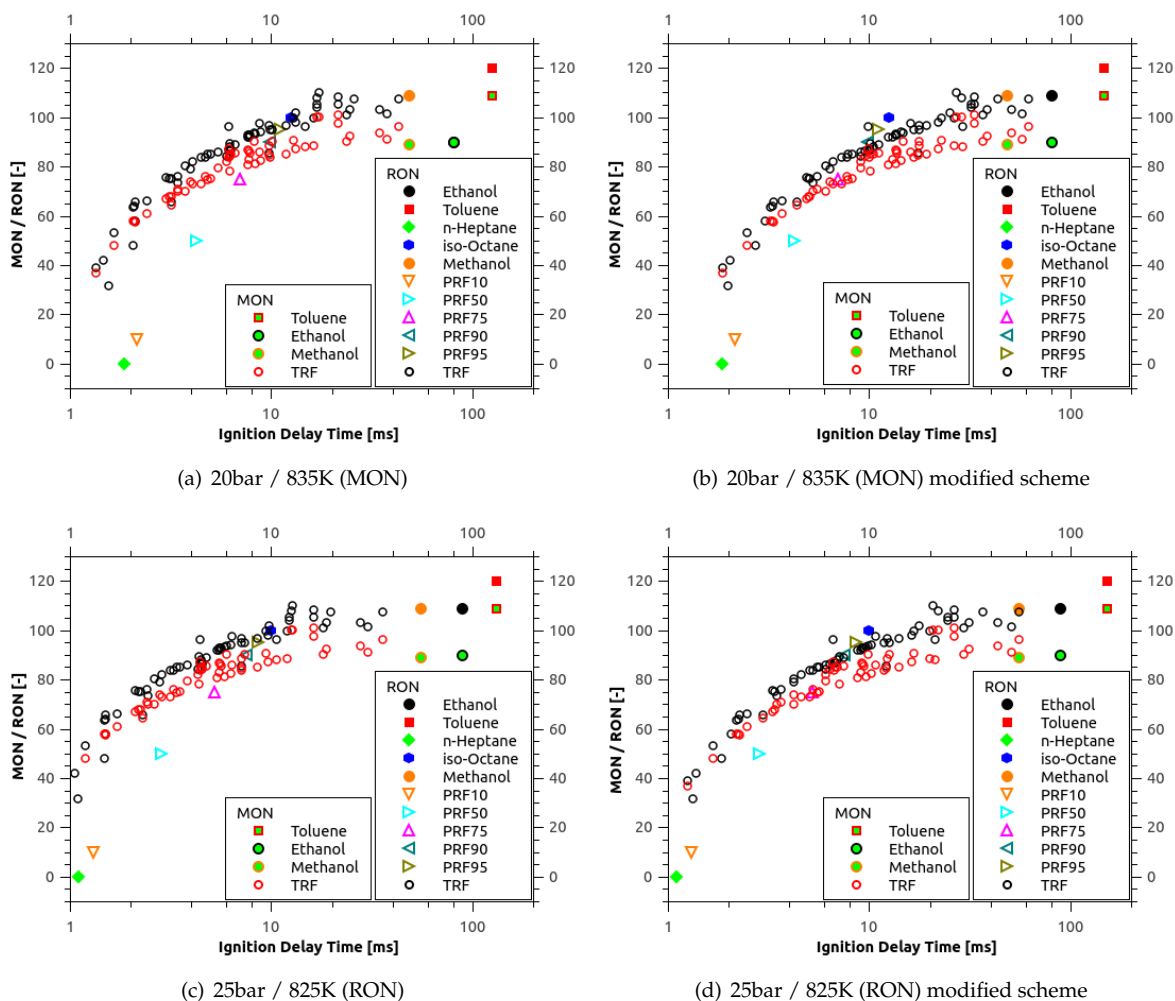
Figure 90: Plots correlating predicted ignition delay time to measured RON / MON in constant volume reactors. Left side: prediction using the unmodified scheme to determine the ignition delay times; right side: using the updated scheme.

(a) 45bar / 980K

(b) 45bar / 980K modified scheme

(c) 50bar / 850K

(d) 50bar / 850K modified scheme
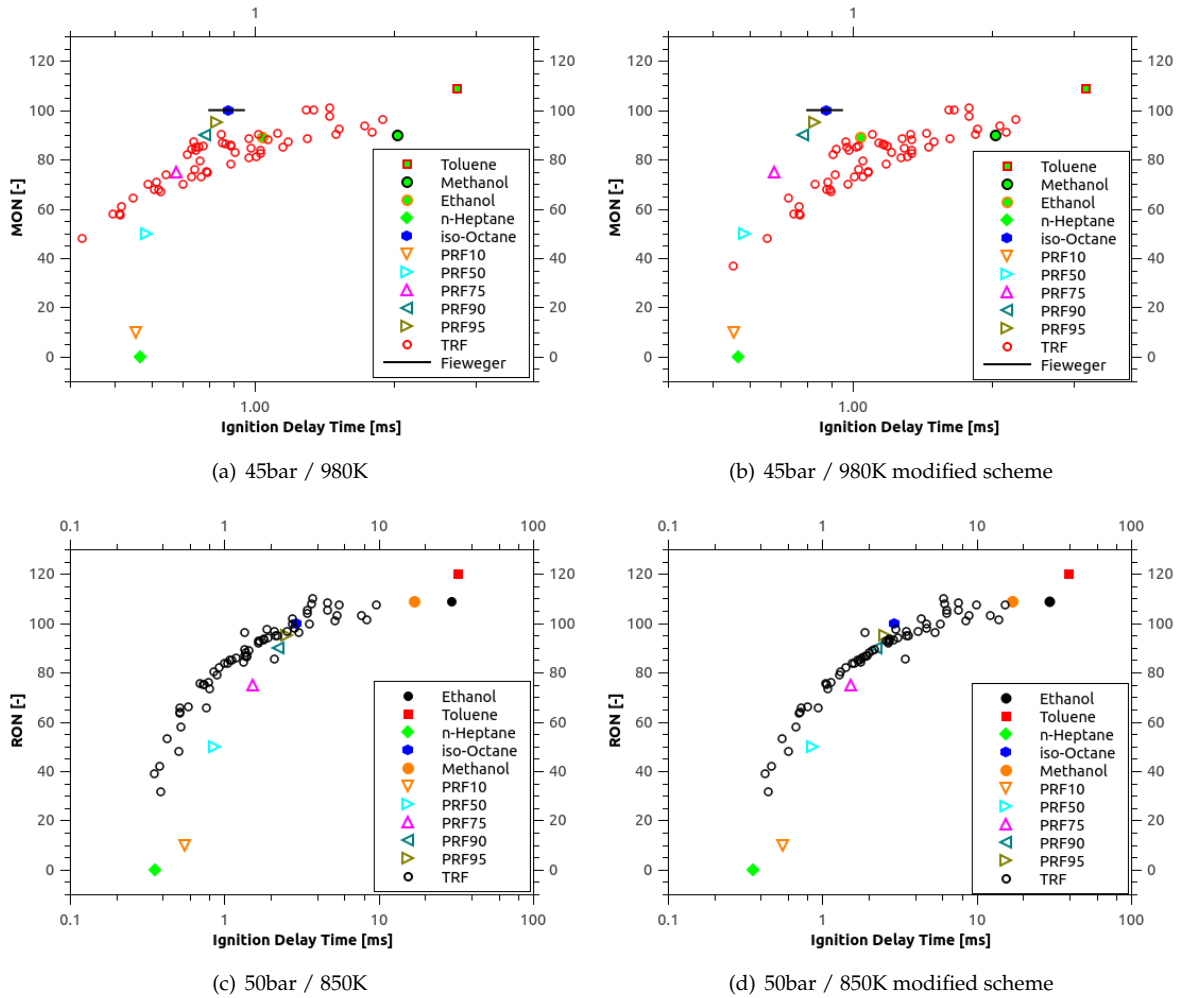
Figure 91: Plots correlating predicted ignition delay time to measured RON / MON in constant volume reactors. Left side using the unmodified scheme to determined the ignition delay times, right side using the updated scheme.

10   Reduction Methods used in this Work

A major demand on the reduction procedure is that the methodology needs to be applicable to any size of mechanism, for any kind of mixtures (single or multi-component fuel) and for a wide parameter range (i.e. pressure, temperature, equivalence ratio). Furthermore the reduction methods shall preserve certain features depending on the application and should not introduce artifacts such as quenching in the engine expansion phase. In addition users are often limited to the use of mechanisms in standard formats. To overcome this problem this work suggest to use a combination of 0D/1D reactors and a stochastic engine model for the mechanism reductions and apply them later in very time consuming CFD calculations.
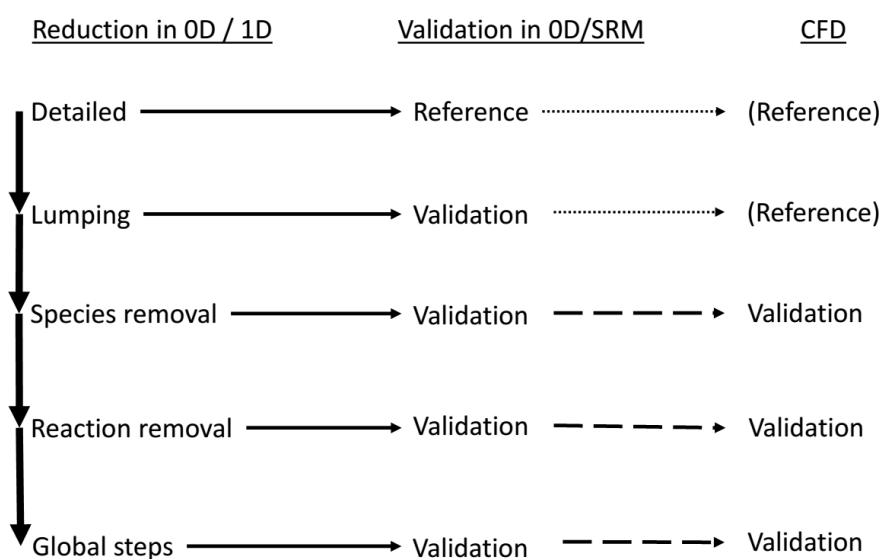
Figure 92: General reduction concept using 0D and 1D reactors for reduction, stochastic engine model for validation under engine conditions and final application of the reduced scheme in CFD modelling.

10.1   A Multi Purpose Mechanism Reducer

This section and the section describing the reduction of the n-heptane scheme[26] is in large parts similar to a manuscript submitted to the ASME 2016 Internal Combustion Fall Technical Conference [87]. The author of this thesis is first author of the submitted manuscript. It further needs to be mentioned that the major part of programming was done by Christian Klauer, while the major part of design, testing and application was done by the author of this thesis.

10.1.1   Species removal

The species removal is based on the concept of Chemical Guided Reduction introduced by Zeuch et al. [82]. Species will be removed based on an analysis in which a necessity value is assigned to each species. The necessity values are derived in a combined reaction flow and an optional sensitivity analysis as introduced by Soyhan et al. [27] and Løvås et al. [134] in

---

[26]The engine simulation (figure 95, 96 and 97) using the stochastic reactor model was performed by Michal Pasternak and the CFD calculations (figure 98) have been performed by Corinna Netzer.

2002. All calculations can be performed for a matrix of different inlet conditions (pressure, temperature, fuel/equivalence ratio, gas composition). Those range can be chosen related to the application target focusing on e.g. lean or rich conditions, a particular temperature or pressure range. Further it needs to be defined which reduction targets are of interest and the acceptable deviation from the detailed (not reduced) scheme needs to be set. In the proposed reduction concept it is possible to control ignition delay time, laminar flame speed and species profiles of any species in the reaction scheme based on statistical moments. Simulations are performed in parallel and evaluated for each reduction step.

10.1.2 Necessity analysis

The necessity analysis was introduced by Soyhan et al. in [27] and Løvås et al. [134]. The necessity $\bar{I}$ of a species i is calculated iteratively from:

$$\bar{I}_{i,k+1} = \max(I_{j,k} f_{i,j}^a, I_{j,k} c_{i,j}^a, I_{i,k}; \quad j = 1, N_S, a = 1, N_a) \tag{10.1}$$

where the initial value for I_i is calculated as

$$I_{i,0} = \max \left(\frac{S_{j,i}^S}{\max_{k=1,N_S}(S_{j,k}^S)}, B_i \right) \tag{10.2}$$

N_S and N_a are the total number of species and elements respectively, k denotes a species and B_i is 1 or 0 depending on if i was defined as necessary species or not. $S_{j,k}^S$ is the relative species sensitivity (in this work the sensitivity towards CO). $f_{i,j}^a$ is the weighted formation of species i from species j by element flux a from species j to species i over the complete simulation time (t_0-t_{end}) :

$$f_{i,j}^a = \frac{\int_{t_0}^{t_{end}} \left(\sum_{R=1}^{N_R} r_r(t) n_i^a \nu'_{jr} \nu''_{ir} \frac{1}{\Delta n_r^a} \right) dt}{\int_{t_0}^{t_{end}} \left(\sum_{r=1}^{N_R} r_r \nu'_{jr} \right) dt} \tag{10.3}$$

Similarly, $c_{i,j}^a$ is the weighted consumption of atoms from species i to species j:

$$c_{i,j}^a = \frac{\int_{t=0}^{t_{end}} \left(\sum_{r=1}^{N_R} r_r(t) n_i^a \nu'_{ir} \nu''_{jr} \frac{1}{\Delta n_r^a} \right) dt}{\int_{t_0}^{t_{end}} \left(\sum_{r=1}^{N_R} r_R \nu''_{jR} \right) dt}. \tag{10.4}$$

10.1.3 Moment based comparison of species profiles

The comparison of species profiles obtained from simulations or experiments can be a challenging task. In recent works Olm et al. [135] use distances to calculate the average absolute deviation and the average error function while Stagni et al. [136] are using normalised L^2 distances. Instead of calculating distances between data sets this work suggests to evaluate there individual moments. To achieve this, the species profiles of the detailed and reduced

reaction scheme are normalised:

$$\int_{-\infty}^{\infty} f(x)dx = 1. \tag{10.5}$$

Calculated moments are used to compare species profile shapes against the detailed solution. The first (expected value) and the second moment (variance) are evaluated:

$$E(X) = \int_{-\infty}^{\infty} xf(x)dx \tag{10.6}$$

and

$$Var(X) = \int_{-\infty}^{\infty} (x - E(X))^2 f(x)dx. \tag{10.7}$$

Since moments should be used to compare only the profile shapes the effect of different reaction onset times introduced by the reduction has to be eliminated. This is done by shifting all species profiles by the difference in ignition delay time (defined as maximum temperature slope) between the detailed scheme and the current reduction step. The maximum and the equilibrium values are evaluated as well. This way the relative position and shape of target species profiles are kept within a given error range. Figure 94 shows two exemplary species profiles of the original and a reduced mechanism with the calculated moments.

10.1.4   Species elimination process

In an initial step all reference values and the necessity is calculated using the detailed scheme. The most conservative necessity value over all calculated 0D reactors and targets is assigned to each species. The species with the lowest necessity, and all reactions associated with it, are removed. All reactors are recalculated with the reduced mechanism and species profiles and ignition delay times are compared. If all targets (ignition delay time, moments and concentrations) over all reactors in the matrix are within the given tolerance the reduction step is considered as valid. The next species with the lowest necessity value is removed and the performance of the new reduced scheme is validated. The necessity analysis will be repeated when an unsuccessful reduction step follows a successful one. The idea here is that as long there is a series of successful reduction steps the decomposition pathways did not change the flow considerably and an unsuccessful reduction step is a signal for changes in the flow patterns which demands an updated necessity analysis. All species which could not be removed before are considered as removable after a successful reduction step. The species removal stops when no further species can be removed. A flow chart of the proposed reduction procedure is shown in figure 93.

10.1.5   Reaction removal

After identifying and removing all unneeded species the reduction is continued by removing all reactions not needed within the given parameter and error range. Reaction removal is done in the same manner as species removal by controlling the same reduction targets. In contrast to species removal the reactions are picked randomly. No creteria was found which allows a time efficient evaluation of the importance of single reactions against multiple tar-
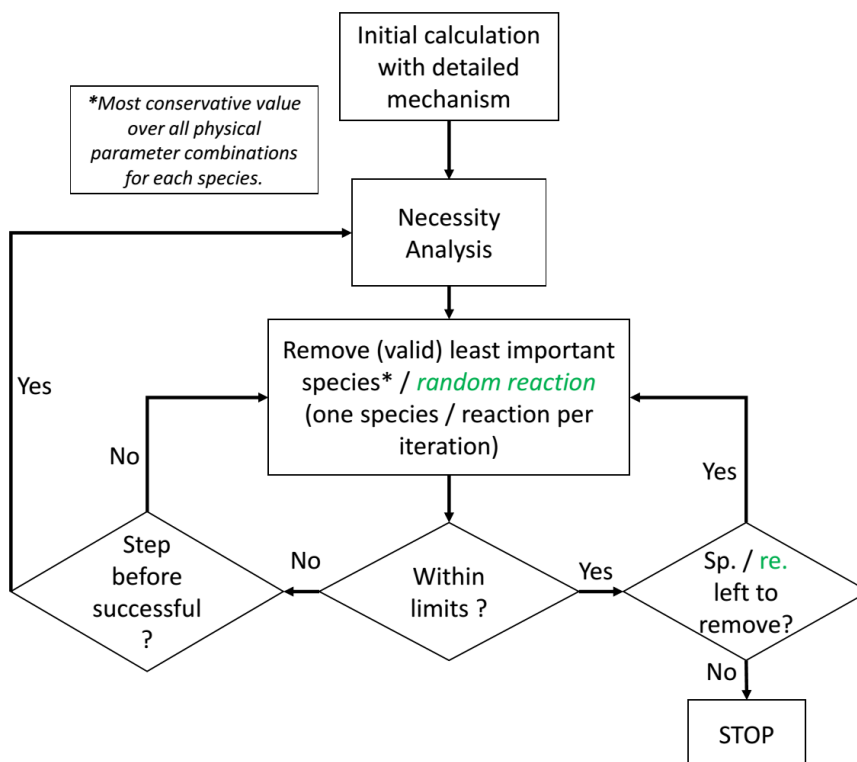
Figure 93: Flow chart depicting the loop for identifying and removing species and reactions.
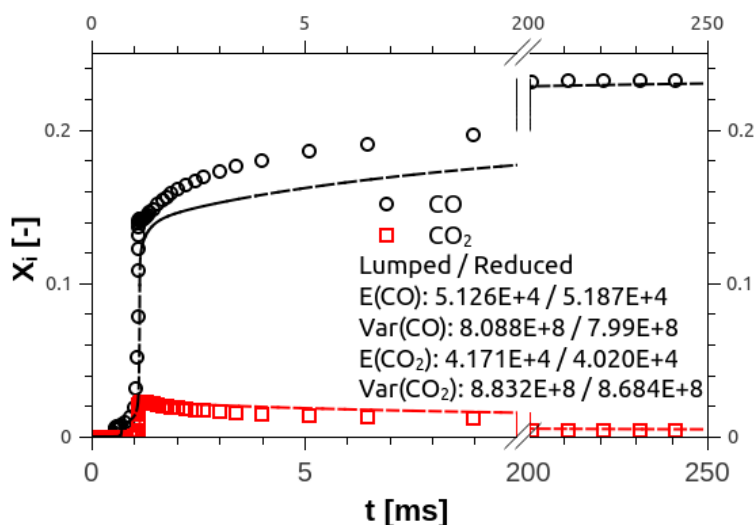
Figure 94: Predicted CO and CO_2 profiles using the lumped n-heptane scheme (symbols) and 78 species / 347 reaction n-heptane mechanism (lines). Simulation at 13.5 bar, 800 K and ϕ=3.0 using air as oxidiser in homogeneous constant volume reactor. The calculated expected value and variance for both schemes are given in the legend.

gets[27]. Due to the control of species profiles the major pathways are preserved. Furthermore it is possible to remove all slow and unimportant reverse reactions of those which are formulated in equilibrium.

---

[27]Evaluating the reation rate or the net atomic flow of a reaction can not capture the importance towards a set of different targets e.g. laminar flame speed and PAH production. Further more both creteria can not capture the impact the of reactions which produce a significant amount of radicals, but having an overall small flow / low reaction rate. The sensivity analysis needs severely more CPU time and would result in much more read/write processes in the current implementation. In addition a rating system for multiple targets would need to be introduced. In the complete reduction process oulined in this work, the reaction removal is the part where most of the enhancement in terms of total CPU time can be gained.

10.1.6   Chemkin type steady state and global steps

After all unimportant species and reactions are removed from the scheme it is possible to further reduce its size by identifying steady state species with a relative short lifetime. Once those species are identified they can be removed by introducing global steps. This can be done in standard format and the concept can be explained with a theoretical reaction chain: ... $\longrightarrow$ A $\longrightarrow$ B $\longrightarrow$ C where $[A] \cdot k_1 - [B] \cdot k_2 = 0$ can be written as: $[B] = \frac{[A] \cdot k_1}{k_2}$. The production rate of [C] can be calculated as:

$$\frac{\partial C}{\partial t} = [B] \cdot k_2 = \frac{[A] k_1 \cdot k_2}{k_2} = [A] k_1. \tag{10.8}$$

In order to identify species which can be set into steady state a life time analysis is carried out for all points. The chemical lifetime can be expressed as:

$$\tau_i = \frac{1}{\frac{\partial \omega_i}{\partial c_i}} = \frac{c_i}{\sum_{k=1}^{N_r} \left(v'_{i,k} - v''_{i,k} \right)} v'_{i,k} r'_k \tag{10.9}$$

where ω_i represents the species source term in terms of concentrations c_i, $v_{i,k}$ is the stoichiometric coefficient (prime - reactant and double prime - product values) and r_k is the reaction rate for reaction k. The most conservative value for each species over all inlet parameter combinations is considered. Once the species with the shortest lifetime are identified one can assume quasi steady state (QSSA) trying to replace it by its products. A possible truncation of the steady state assumption can be evaluated by investigating the consumption and formation pathways for the species. Putting this to example a reduction can look like this: the reaction is L12 $\longleftrightarrow$ OH + L18 + CH_2O where the life time of species L18 is short and L18 is only decomposed via the reaction L18 $\longleftrightarrow$ C_2H_4 + $C_2H_5COCH_2$. Once it is ruled out that both reverse reactions are important the reaction can writen as L12 $\longrightarrow$ OH + C_2H_4 + $C_2H_5COCH_2$ + CH_2O and the species L18 is removed. Since products are gradualy replaced in the process comparable long reactions are formulated: L11 $\longrightarrow$ OH + 0.75 CH_3 + 0.75 CH_2CO + 0.25 N$-C_3H_7CHO$ + 0.25 CO + 0.5 C_2H_4 + 0.5 C_2H_5CHO + 0.25 C_2H_5 + 0.25 CH_3CHO (example taken from the reduced n-heptane scheme in 10.2.1).

10.1.7   Validation in Stochastic Engine Model

As briefly discussed in the introduction, reaction schemes are nearly exclusively developed and/or reduced in premixed 0D/1D models. While in such models pressure and temperature will solely increase or remain constant, piston engines face a decrease in pressure and temperature in the expansion phase. This expansion can lead to quenching of species after top dead centre introduced by removing decomposition pathways relatively unimportant in 0D reactors but important in IC engines. Another issue is strong mixing in direct injection engines. Even though a wide parameter range is controled during the reduction in 0D reactors it cannot be certain that the scheme shows the expected performance during mixing

and in the expansion phase. Since it is not possible to validate reduced schemes in a time efficient manner in CFD calculations an engine model based on a stochastic reactor approach is used. This model is described in Ph.D. thesis (e.g. [137]) and numerous publications ([138, 139, 140, 141, 142, 143].

Engine calculations were carried out using the stochastic reactor model for direct injection (DI-SRM) [141, 142, 139] engines. Shortly: the SRM is a 0D model of physical and chemical processes occurring during an engine cycle. It is formulated within the PDF approach to turbulent reacting flows [144] that enables exact treatment of chemical reactions. The SRM considers gas inside the cylinder as an ensemble of notional particles. The particles can mix with each other and exchange heat with the cylinder walls. Each particle has a chemical composition, temperature and mass representing a point in phase-space. These scalars are treated as random variables and can vary within the cylinder. They determine composition of the gas mixture and are described with probabilities using PDF. The in-cylinder mixture is thus represented by a PDF in gas-phase space and the particles are realisations of the distributions. The solution for scalars, temperature and species mass fraction, is obtained from the PDF transport equation [145]. The changes of the PDF are due to chemical reactions, convective heat loss, volume changes due to piston motion, fuel injection and turbulent mixing. These processes are calculated sequentially using the Monte Carlo particle method [144] with the operator splitting technique. The in-cylinder mixture has been discretised into 1000 particles. Calculations were carried out with 0.5 CA time step. Mean in-cylinder performance parameters, such as pressure, rate of heat release (RoHR), and NOx concentration, were computed from 30 consecutive cycles. The mixing process is described using the Curl's model with a crank angle dependent mixing time profile, which was obtained as described in [140, 141] using the LOGEengine tool [145].

The experimental engine data where kindly provided by Volvo[28]. The engine was fueled by nearly aromat free (below 2.5 m%) Swedish commercial Diesel with a cetane number of 53.3, a lower heating value of 43 MJ/kg and 86 m% carbon. The n-heptane model described in 10.2.1 was used as single fuel surrogate in this work for two reasons. The properties of n-heptane in terms of lower heating value and cetane number are close to those of the Diesel used in the experiment. All verification calculations were done exemplary on a Volvo engine summarised in table 16. The problem during expansion is lined out by an example encountered during the reaction reduction of the pure n-heptane scheme where a scheme with 87 species / 345 reactions was generated as smallest set of reactions found during the reduction. As can be seen in figure 95 this scheme predicts the same pressure trace and and NOx emissions, but 3.5 times higher HC emissions. It was found that this additional HC emissions were caused by a quenched heptene isomer (C_7H_{14}) in the expansion phase while it was completely decomposed in homogeneous calculations. Since all successful steps are stored during the reduction the problem can be tracked back and the removal of the decomposition pathways necessary in the expansion phase can be prohibited. Than the reduction process can be continued from a point before the problem was introduced. This verification

---

[28]Dr. Ingemar Magnusson and Dr. Manus Christensen from AB Volvo Gothernburg (Sweden) are greatly acknowledged for providing the experimental engine data.

Bore [mm]	131.0
Stroke [mm]	158.0
Connecting rod [mm]	267.5
Compression ratio [-]	16.1
Engine speed [rpm]	1500.0
IMEP [bar]	12.0
EGR [m%]	28.0
ϕ [-]	0.267

Table 16: Engine specification and operating condition

in the SRM model prevented to find the problem later in a much more time consuming CFD calculation. In this manner three major reduction mile stones were derived which predict combustion within the given tolerance range in 0D and engine calculations. The combustion and emission prediction of those valid schemes can be found in figure 96, figure 97 and the CPU times are summarised in table 17. In a similar way SRM calculations can be used during the development process of the detailed scheme to identify species which can be affected by quenching in the expansion phase and revise there decomposition pathways accordingly.
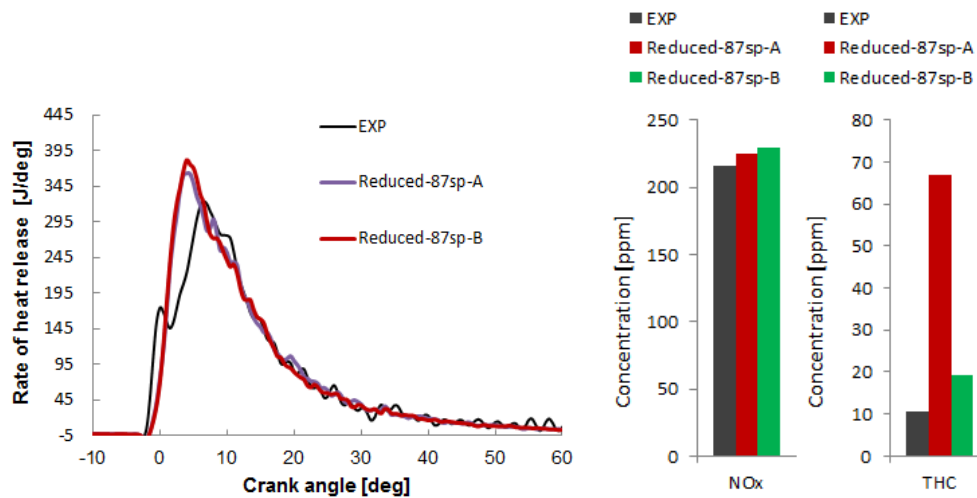
Figure 95: Comparison of predicted and experimental pressure trace using two mechanisms with 87 species / 345 reactions (A) or 347 reactions (B). Mechanism A was identified as failed reduction step not suitable for engine simulations and discarded.

10.1.8   Application in CFD Calculations

The reduced mechanism was used in the CFD setup for the engine calculations and compared against the detailed and lumped scheme using the same settings. For the reduced n-heptane reaction scheme (from 352 to 56 species) the total CFD CPU time is reduced by factor 2, whereas in the transient interactive flamelet (TIF) chemistry solver [146] a speed up of factor eight is achieved (see table 17). The major part of computational cost in the CFD calculations goes into the turbulence and spray calculation. The overall combustion prediction for the three used mechanism stages aligns well. Figure 98 (a) shows that the predicted ignition onset for the three stages is close, only minor deviations can be seen dur-
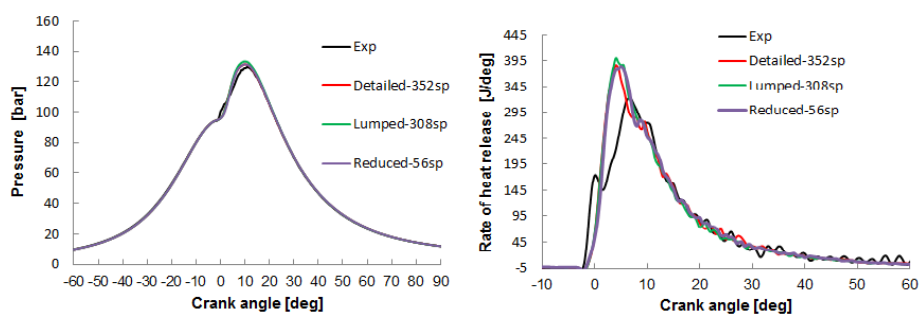
Figure 96: Predicted (SRM model) pressure trace and rate of heat release calculation using detailed, lumped and 56 species mechanism vs. experimental values.
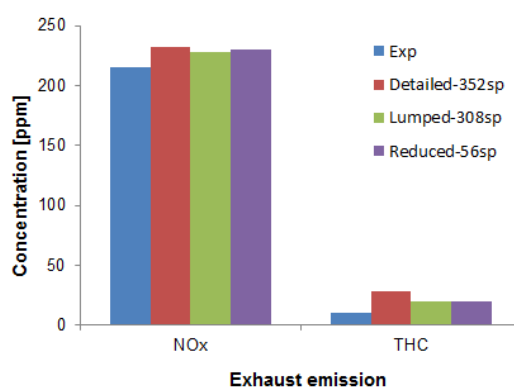
Figure 97: Predicted (SRM model) and measured exhaust out emissions using detailed, lumped and 56 species mechanism vs. experimental values.

ing the combustion progress. Also the CO_2 and CO traces (figure 98 (b)) align well. In the peak CO concentration the reduced reaction scheme differs slightly within the accepted deviation during the reduction procedure. The predicted NO_2 and NO traces[29] for the detailed and lumped scheme are very close (figure 98 (c)). Due to further species and reaction removal the predicted traces using the 56 species scheme differ to the ones obtained with the detailed reaction scheme. These species were not controlled during the reduction process, but anyhow the deviation is comparable small and acceptable. A large deviation of the predicted major hydro carbon species CH_4 and C_2H_2 between the detailed and 56 species scheme is observed. This is an expected behaviour since most of the decomposition pathways are lumped and removed during the reduction. Hence the same flow (from the fuel to mostly CO_2) is distributed over only a few species, which subsequently leads to higher peak concentrations. During the expansion phase those HC species are converted to CO and CO_2 and the traces assimilate again (figure 98 (d)). This is also strong indication that a reduction which would focus on certain/different species profiles of HC species would lead to a completely different mechanism.

Figure 98 (e) shows the predicted dry engine out mole fractions in comparison to the experiment. As a result of the reduction strategy the predicted CO_2 concentrations are for all three mechanism stages very close. To be able to compare the predicted CO_2 concentrations

---

[29]Using the thermal NOx from the GRI 3.0 mechanism.

Stage	Species / Reactions	SRM [s]	CFD tot. [h]	TIF solver [s]
Detailed	352 / 3702	1800	73.9	1910
Lumped	308 / 3680	1500	62.2	1530
Species removal	87 / 788	150	-	-
Reaction removal	87 / 347	110	-	-
Global steps	56 / 206	64	44.3	230

Table 17: CPU times for different reduction stages of the n-heptane scheme.

to the test data the dry CO_2 amount needs to be corrected by the difference in H:C ratio between the in the experiment used Diesel and n-heptane used in the simulations. After that correction the predicted CO_2 concentration matches the experiment very good.
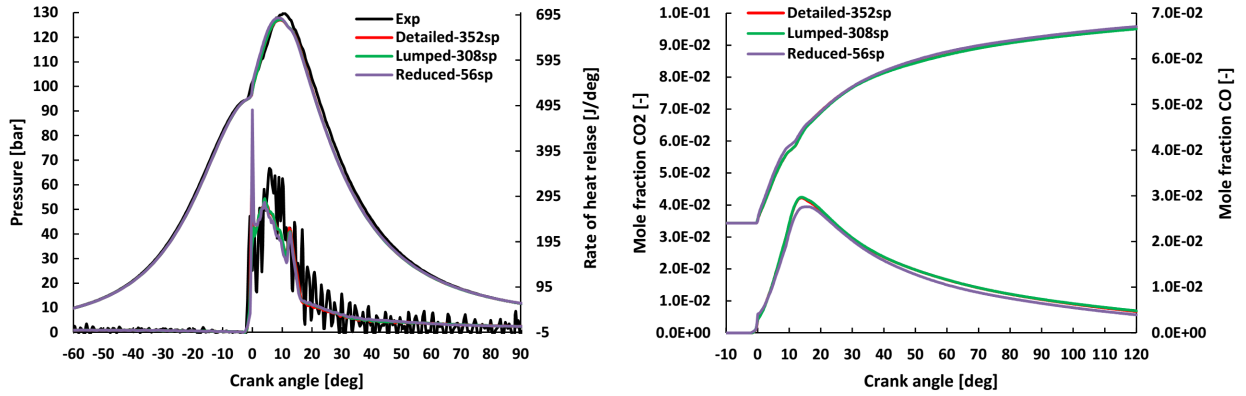
(a) Pressure trace (left axis) and rate of heat release (right axis)

(b) Predicted CO_2 (left axis, upper lines) and CO (right axis, lower lines)
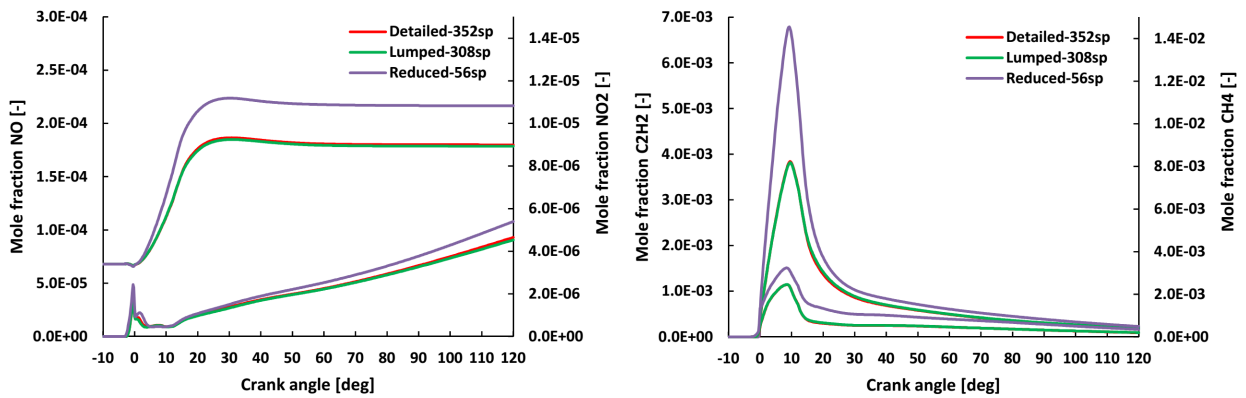
(c) Predicted NO (left axis, upper lines) and NO_2 (right axis, lower lines)

(d) Predicted C_2H_2 (left axis, upper lines) and CH_4 (right axis, lower lines)
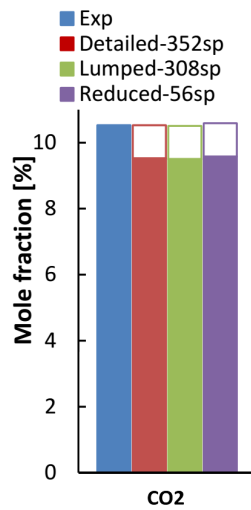
(e) Predicted (CFD) exhaust out CO_2 vs. experiment. Transparent bars show the CO_2 concentrations after the correction using the differences in H/C-ratio in experimental Diesel fuel and simulation

Figure 98: Predicted CFD results using the detailed, lumped and 56 species n-heptane mechanism vs. experimental values.

10.1.9   PAH Species for Soot Formation

One reason for using detailed chemistry to model in-cylinder combustion is the prediction of soot formation. The developed (detailed) n-heptane [43] mechanism contains an updated version of the PAH growth chemistry formulated by Fabian Mauß [76]. It therefore contains all species needed to apply the moment based method to calculate solid soot developed by Fabian Mauß and further maintained and improved in LOGEsoft, LOGEengine and LO-GECFD. This work will not focus on details of the soot model and the reader is referred to works from Mauß [76], Netzell [147] and others. Even without looking into details of the soot model it is apparent that the gas phase soot precursor species will determine the soot production. When all of those precursor species profiles (peak and equilibrium concentration, first and second moment) remain unchanged in the parameter range of question during the reduction the model will predict the same amount of soot[30]. Those precurser species cannot be removed if the reduced mechanism should be coupled with the soot model. The species necessary to calculate soot are:

- H (Hydrogen atom)

- OH (Hydroxyl)

- H2 (Hydrogen)

- CO (Carbon monoxide)

- O2 (Oxygen)

- CH2-1 (Methylene)

- CHO (Formyl)

- CHCO (Oxyethenyl)

- C2H2 (Acetylene (ethyne))

- H2O (Water)

- A3R5 (Acephenanthrylene)

- A3R5- (Acephenanthrylyne)

- A3R5CH3

- A3R5CH3-

- CH3 (Methyl)

- CH (Methine)

---

[30]Given that the combustion performance does not change.

10.1.10 Small Parameter Study

The reduction procedure itself is a very complex system and the outcome of a reduction is strongly influenced by several factors. The main factors clearly are: what is controlled (laminar flame speed, ignition delay time, species profiles, ...) and in which limits. At the same time the choice of the 0D/1D solver, the demanded accuracy and the reactor model will have an impact on the resulting mechanism. It is not possible to perform parameter studies for all possibilities, however a few interesting effects are briefly shown here to give the reader an insight in the performance and understanding which parameters may restrict the reduction. No general guide lines can be given, since the parameter range for the reduction depend on the targeted application.

10.1.10.1 Ignition Delay Species Profiles Control This test was carried out while developing the highly reduced PRF mechanism (see section 10.2.2). The reduction settings are the same as in table 22, but in addition species profiles were controlled within an allowed deviation of 15 % for the following major combustion products: CO_2, H_2O, N_2, O_2, CO, H_2, C_2H_2 and CH_4. In order to find at which point the reduction is limited by the preservation of the species profiles the acceptable deviation in ignition delay was increased starting from 1%. The reduction (species removal only) was started from the lumped ETRF mechanism. The table below summarises the outcome of this parameter study and it can clearly be seen that the control of the species profiles are the limiting factor. Further it can be observed that the reduction was not entirely deterministic - the reduction for 10% ignition delay time deviation limit do not yield the same result as the other limits. This shall not be mistaken as a non deterministic reduction procedure, the species removal is deterministic when solely based on the necessity values. However: small changes in the settings (parameter range and limits) may change the order in which species are removed leading to slightly different reaction schemes. It can be clearly seen that changing the tolerance for ignition delay has no impact beyond 5% and the reduction is limited by the species profiles which are controlled. Further reaction removal with 10% limits for species profiles and ignition delay time was carried out and only a few species were removed leading to a reaction scheme with 352 species (from original 386 species).

Tolerance ignition delay [%]	Number of species reached
1	284
5	258
10	257
15	258
16	258
20	258
50	258
100	258

Table 18: Obtained number of species using the reduction setting given in table 22 with different limits for deviation in ignition delay time.

10.1.10.2   The impact of the random reaction removal on mechanism sizes

As pointed out before the reaction removal is not designed as a deterministic process. The table below shows the reached number of species / reactions when performing a reaction removal during the compilation of a reduced PRF scheme. The reduction was started several times from the same 144 species mechanism (table 23) using the same settings a given in table 22.

Repetition	Number of species / reactions reached
1	124/371
2	133/427
3	139/494
4	130/414
5	138/476
6	131/423
7	130/422
8	134/471

Table 19: Obtained number of species/reactions using the reduction settings given in table 22 from several reaction removal repetitions.

10.2   Highly Reduced Special Purpose Mechanisms

This sections shows a few examples for ignition and emission targeted special purpose schemes for n-heptane as simple Diesel surrogate and n-heptane / iso-octane to model PRF fuel for SI engines.

10.2.1   Pure n-Heptane as Diesel Reference fuel

This mechanism was developed to be used as small and fast scheme for optimisations of Diesel engines. Therefore it should cover a wide range of fuel/equivalence ratios, temperature and pressure. Further a simple NOx model was included and special attention was paid to HC emission prediction. The reduction steps and the application of this scheme in engine simulations was already explained in the previous chapter. Here only the impact of the reduction steps on ignition delay times and premixed flames are shown. The plots are also included in the submitted manuscript to the ASME ICEF 2016. The reduction process was started from the detailed n-heptane scheme published by Seidel et al. [43]. Table 20 summarises the parameter range controlled during species and reaction removal. Table 21 shows the achieved mechanism sizes and CPU times. For the SRM engine calculations a speed up of factor 28 was achieved. For the CFD calculation a total speed up factor 1.7 was reached with the smallest scheme, where the speed up for the TIF solver was about factor 8.

During the lumping procedure deviations from the detailed scheme leading to a closer agreement with experimental ignition delay times were accepted, especially for rich mixtures. The idea behind this is that a reduction does not need to show a higher accuracy than available experimental data and the ignition timing is dominated by the rich zone with shorter ignition delay times. Finally 24 representative pseudo species were identified and 44 species were lumped in total reducing the scheme to 308 species and 3680 reactions. The lumped scheme predicts slightly slower ignition delay time (see figure 99 (a)) and no observable difference for the major species profiles in the premixed flame (see figure 101 (a)) or laminar flame speeds (see figure 102 (a)).

Species and reaction removal was leading to a mechanism with 87 species and 347 reaction. This scheme predicts ignition delay times close to the lumped scheme (see figure 99 (b)).

By introducing global steps 31 species were removed resulting in a reaction scheme with 56 species and 206 reactions. Larger deviations in respect to the detailed mechanism were accepted when they improved the prediction of ignition delay in comparison to experimental data. This scheme has a similar good agreement against experimental ignition delay times as the previous schemes (see figure 100). For the premixed flame the same emissions are predicted as by the detailed scheme and the predicted reaction zone is slightly shifted closer to the burner surface (see figure 101 (b)). Laminar flame speeds, which were not controlled during the reduction, are strongly over predicted at athmopheric pressure, but match the experiment and detailed mechanism very close at elevated pressure (see figure 102 (b)).

(a) Detailed (solid) and lumped (dotted)   (b) Lumped (solid) and reaction removal (dotted)
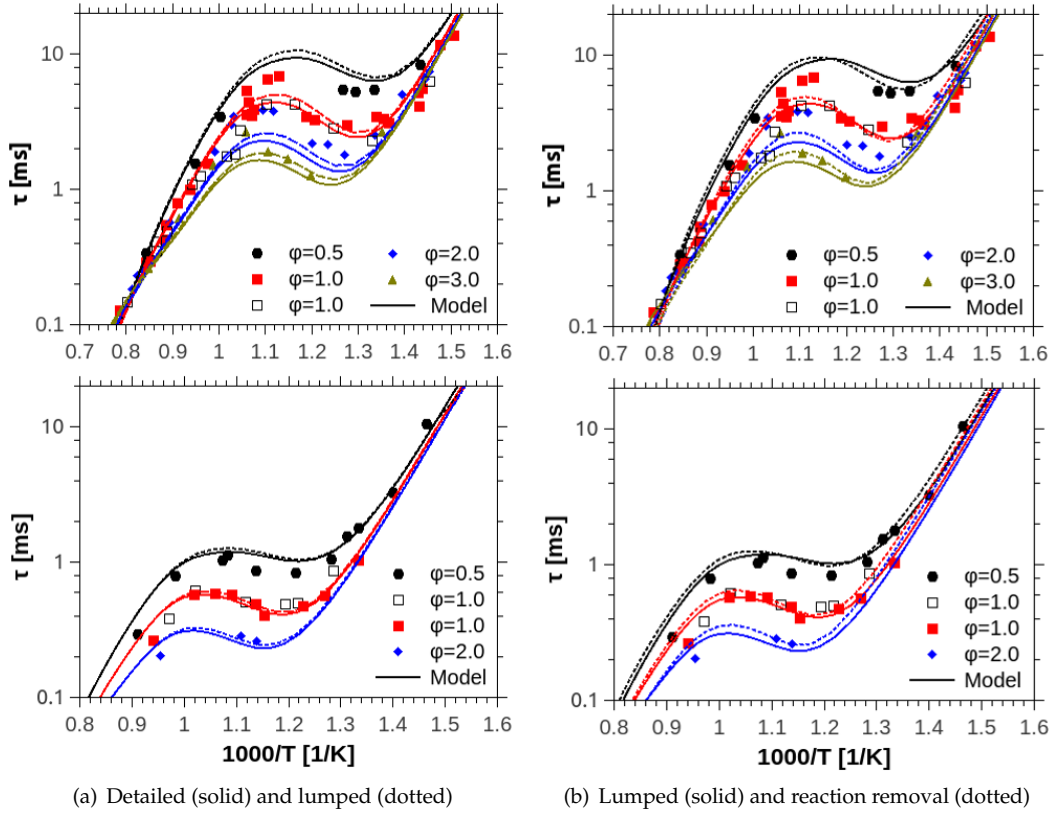
Figure 99: Ignition delay times (τ) for n-heptane/air in a shock tube. Upper: experiments at 13.5 bar solid symbols [90]; open symbols [34]. Lower: 40 ± 2 bar. Experiments: solid symbols for $\phi = 0.5$, $\phi=1.0$ [38], and for $\phi = 2.0$ [90], open symbols [34].

Parameter	Settings or limits
Fuel 1	n-Heptane
Oxidiser	artificial air
Inlet pressure [bar]	10, 25, 40, 65, 90
Inlet temperature [K]	650, 700, 800, 900, 1000, 1100, 1200
Inlet ϕ	0.5, 1.0, 1.5, 20, 3.0
Concentration control [%]	CO and CO_2 within 10
Auto ignition control [%]	20
Reactor model	Constant pressure

Table 20: Table with parameters for the reduction of pure n-heptane

Stage	Species / Reactions	SRM [s]	CFD tot. [h]	TIF solver [s]
Detailed	352 / 3702	1800	73.9	1910
Lumped	308 / 3680	1500	62.2	1530
Species removal	87 / 788	150	-	-
Reaction removal	87 / 347	110	-	-
Global steps	56 / 206	64	44.3	230

Table 21: CPU times for different reduction stages
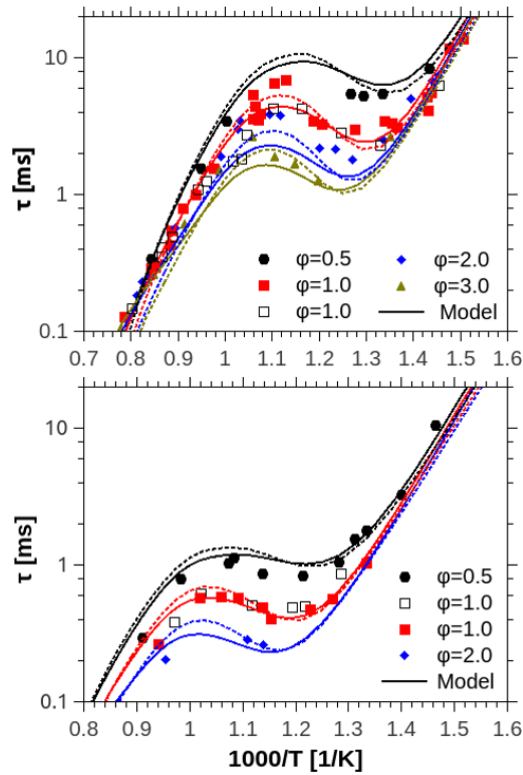
(a) Detailed (solid) and global steps (dotted)

Figure 100: Ignition delay times (τ) for n-heptane/air in a shock tube. Upper: experiments at 13.5 bar solid symbols [90]; open symbols [34]. Lower: 40 $\pm$ 2 bar. Experiments: solid symbols for ϕ=0.5, ϕ=1.0 [38], and for ϕ=2.0 [90], open symbols [34].

(a) Detailed (solid) and lumped (dotted)

(b) Detailed (solid) and global steps (dotted)

Figure 101: Mole fraction in a premixed fuel rich (ϕ=1.69) low pressure (40 mbar) flame [43]. Line: model prediction imposing experimental temperature profile.

(a) Detailed (solid) and lumped (dotted)   (b) Detailed (solid) and global steps (dotted)
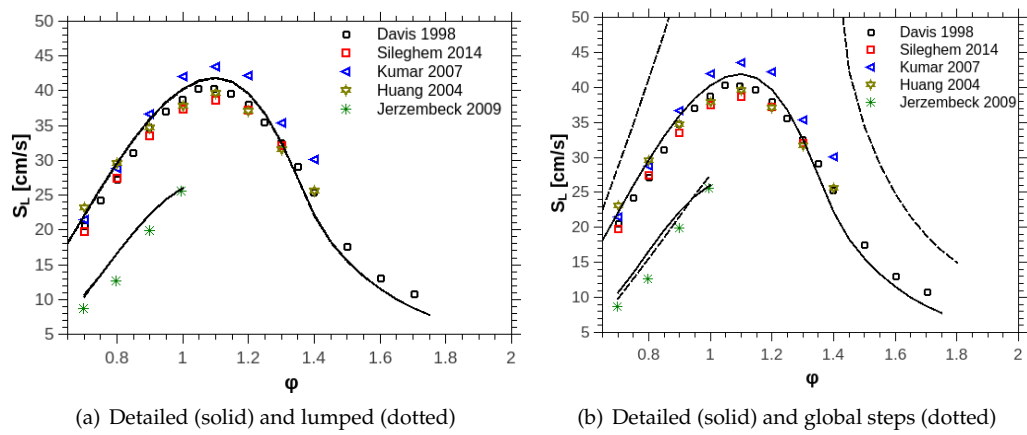
Figure 102: Laminar flame speeds for n-heptane/air mixtures. Open symbols: Experiments at 298 K and 1 atm [95, 116, 93, 124]; Asterisks: 19.7 atm and 373 K [98].

10.2.2 n-Heptane / iso-Octane PRF fuel

The aim of this mechanism reduction is to compile a scheme which can be used for fast simulation of gasoline engines. To minimise the size of the mechanism it was decided that the mechanism shall be valid in smaller range around stoichiometric mixtures than the Diesel reference fuel scheme. It was further decided that the two primary reference species (n-heptane / iso-octane) are suitable for simple engine optimisations. A special focus was given to major combustion products such as CO_2 and H_2O as well as on C_2H_2 and CH_4 as major representative for unburned hydrocarbons during species and reaction removal. The thermal NOx model from the GRI was added to the mechanism.

To be able to predict auto ignition in the unburned zone special attention was paid to the ignition delay times of different iso-octane / n-heptane mixtures below 1000 K inlet temperature. The settings for the reduction are summarised in table 22. It can be clearly observed in figure 103 (a) and (b) that the mechanisms generated by the automatic reduction procedure (lumping, species and reaction removal) are well within the predefined limits (see table 23 for achieved mechanism sizes). During further reduction by hand (introducing global steps, chemkin type steady state reactions, removing unimportant reverse reactions, ...) deviations from the original scheme which brought the model closer to the experimental values obtained in the old Aachen shock tube (Fieweger, Cienzki, Adomeit [90, 38]) were accepted. The experimental situation however is not that clear as shown in figure 103 (d) and (e). Unfortunately there are only few experimental data available for PRF mixtures at engine relevant conditions and they are not conclusive. The measurements from Hartmann and co-workers suggest shorter ignition delay times for PRF 100 (figure 103 (d)) and PRF 80 (figure 103 (e)). The Hartmann data [39, 37] correspond to ignition delay of mixtures with about 10 ON points lower. The Hartmann measurements for pure n-heptane are also slightly shorter than the Fieweger measurements. This Fieweger data however are backed up by Heufer et al. [34] . Based on this reasoning the author relies rather on the Fieweger data. Ignition delay times are overpredicted for temperatures below 760 K in the lumped and reduced scheme and there is a very good match for the engine relevant mixtures/conditions: RON between 90 and 100 temperatures above 825 K[31] (see figure 103 (d)).

The final mechanism consists of 66 species and is about 14 times faster than the original 386 species mechanism in 0D calculations [32].

To understand how this reduced mechanism performs in engine simulations the different reduction milestones were compared using the stochastic engine model. The arbitrary engine dimensions, operating point and simulation settings are summarised in table 24. A second operating point with strong auto ignition in the unburned zone was generated by raising the inlet temperature by 150 K. The simulations were performed on a Intel Core i7-3632QM at 2.9 GHz. All calculations were performed with ESM/ESSA Version LS1.08-4-g51539. It can be seen in figure 104 that the reduced 66 species scheme predicts the same combustion and engine out emissions as the lumped ETRF scheme for normal combustion.

---

[31]The lowest inlet temperatures for 0D RON - ignition delay time correlations is 825 K or higher. See chapter 8 for details.
[32]Determined in 0D constant pressure calculations for 825 K / 40 bar for PRF 90

Parameter	Settings or limits
Fuel 1	n-Heptane
Fuel 2	iso-Octane
Fuel 3	0.4 n-Heptane and 0.6 iso-octane
Oxidiser	artificial air
Inlet pressure (Fuel 1-3) [bar]	10.5, 40.0, 80.0
Inlet temperature (Fuel 1-3) [K]	600,700,800,900,1000
Inlet ϕ (Fuel 1-3)	0.6, 1.00, 1.4
Concentration control (Fuel 1-3) [%]	CO_2 and H_2O within 15
Auto ignition control (Fuel 1-3) [%]	0.16
Reactor model	const. pressure
Necessary species	i-C_8H_{18}, n-C_7H_{16}, CO_2, H_2O, N_2, O_2, CO, H_2, C_2H_2, CH_4

Table 22: Table with limits for PRF scheme

Reduction step	Number of species and reactions
Lumped	386 / 4511
Species removal	144 / 1295
Reaction removal	124 / 375
Global steps	66 / 187

Table 23: Milestones during the reduction of the PRF scheme

This is of course an expected result since combustion is completely dominated by flame propagation and the flame propagation model was not altered. For the operating conditions with higher inlet temperature shown in figure 105 all combustion takes place in the "unburned" zone by auto ignition before the flame front propagates into this region. The slightly faster ignition delay time predicted by the reduced scheme results in about 2 CAD earlier ignition onset (see figure 105 (a) and (b)). To rule out that this observation is due to the simulation of only 30 consecutive cycles the simulation was repeated with 100 cycles and no significant difference is observed. Due to the change in ignition onset there is also a difference in pressure slope. The main emissions are not effected due to reduction (figure 105 (c) - (d)).

Parameter	Values
Number of Particles	200
Number of consecutive cycles	30
Start of simulation (IVC) [CAD]	-119.66
End of Simulation (EVO) [CAD]	125.00
Mixing time	7.23E-04
Delta CAD	0.5
Heat transfer	Woschni Model
Engine Speed [RPM]	1500
Compression ratio	9.52
Bore [m]	0.0745
Stroke [m]	0.080
Connection Rod length [m]	0.08
EGR amount [%]	2
Wall temperature [K]	450
Spark timing (turb. θ) [CAD]	7.2
Flame speed table	Default
Fuel	95 % iso-octane (molar fraction)
Oxidizer	Artificial air
Pressure (IVC) [bar]	1.95
Temperature (IVC) [CAD]	360.428 / 510.428 (forced pre ignition)

Table 24: Setup parameters for the simulation of the arbitrary SI engine.
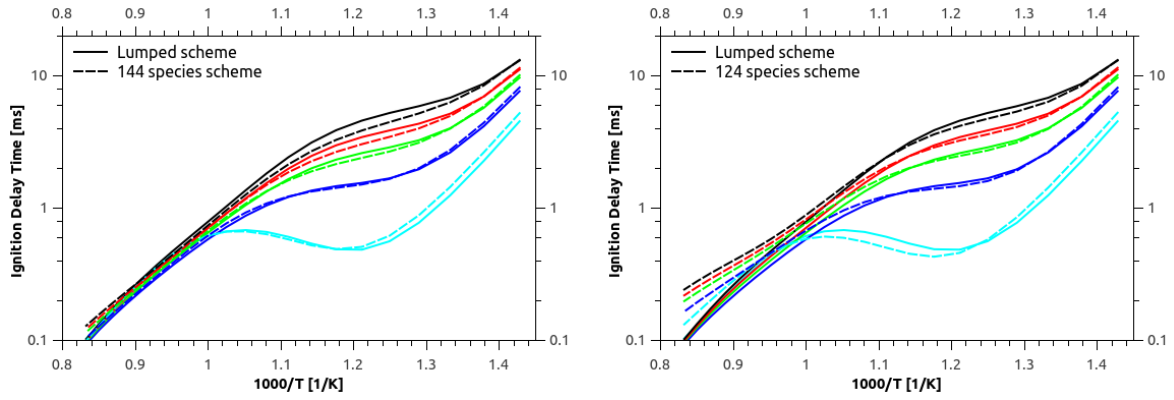
(a) Lumped ETRF and reduced mechanism obtained from species removal (144 species)

(b) Lumped ETRF and reduced mechanism obtained from reaction removal (124 species)
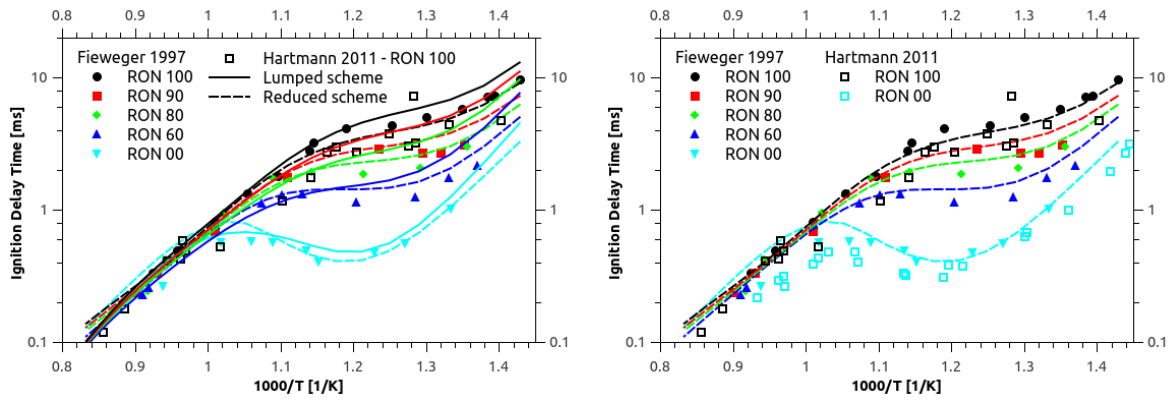
(c) Lumped ETRF and 66 species mechanism.

(d) 66 species mechanism without lumped scheme for better visibility
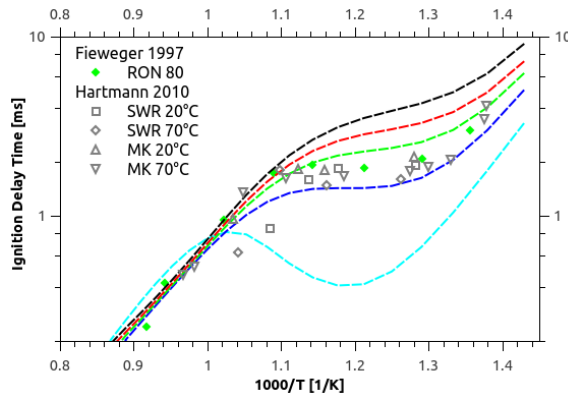
(e) 66 species mechanism with focus on RON 80 comparing different experimental sources. SWR: Mixture preparation in shock tube; MK: mixture preparation stirred reactor.

Figure 103: Simulation (lines) and experimental measurements (symbols) for different n-heptane/iso-octane mixtures at 40 bar, ϕ=1.0 in artificial air. Experiments from Fieweger et al. [38] and Hartmann et al. [39, 37]. Colouring: black: PRF 100; red: PRF 90; green: PRF 80; dark blue: PRF 60; light blue: PRF00

Mechanism	CPU time [s]
Normal combustion	
Lumped scheme	911.4
66 Species	47.0
Forced pre-ignition	
Lumped scheme	895.7
66 Species	45.7

Table 25: CPU times for different reduction milestones. CPU time is the average for one cycle.

(a) Pressure

(b) Mass fraction burned

(c) Major species

(d) NO and NO$_2$
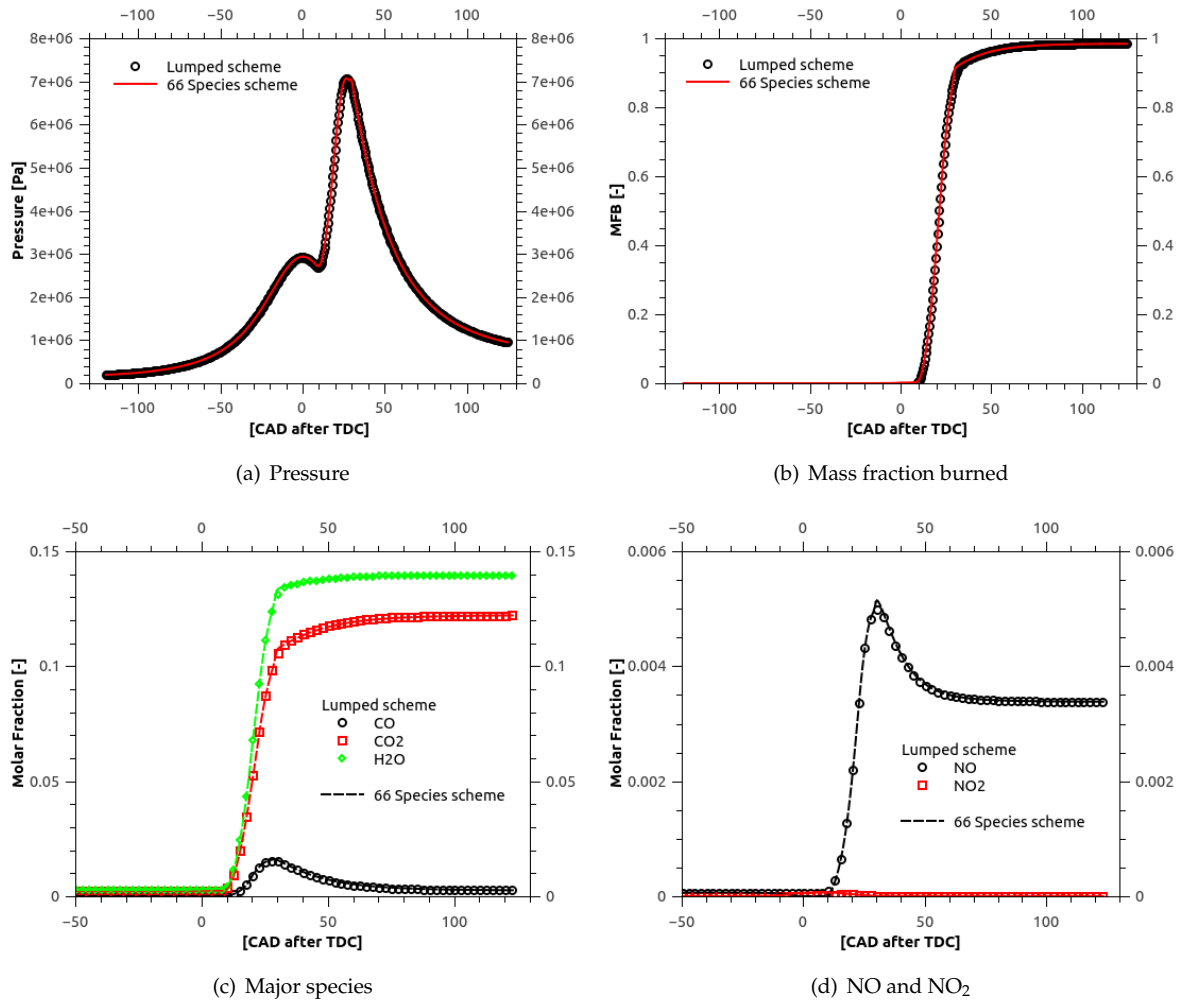
Figure 104: Comparison of combustion prediction using the lumped scheme (open symbols) and the reduced 66 species mechanism using the settings given in table 24.

(a) Pressure

(b) Pressure around the ignition event

(c) Mass fraction burned

(d) Major species

(e) NO and NO$_2$
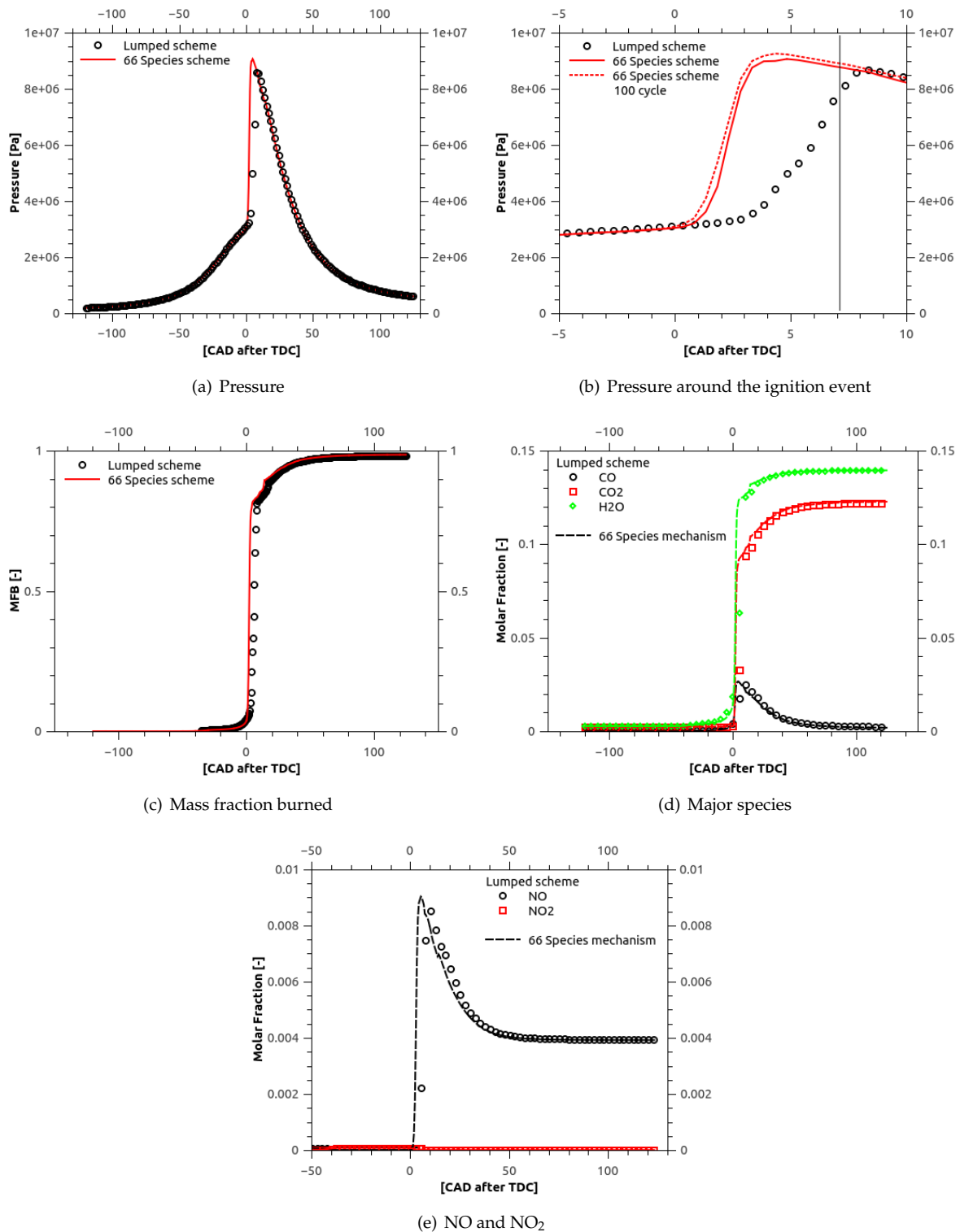
Figure 105: Forced pre ignition by using 150 K higher gas inlet temperature. Grey vertical line in (b) denotes ignition timing. Dashed red lines in (b) denotes calculation with 100 cycles.

10.3   Comparison of the Proposed Reduction Method with the DRG Method

So far the reduction procedure was only applied to variations of similar reaction schemes in this work. In order to prove that the reduction method can be applied to other schemes as well, it was decided to reduce the 2-component surrogate scheme from Pei et al. [148]. Pei and co-workers suggested a mixture of n-dodecane and m-xylene as Diesel surrogate and compiled a reaction scheme with 2885 species / 11754 reactions to model the fuel. The mechanism was then *"reduced to a skeletal mechanism consisting 163 species and 887 reactions for 3D diesel engine simulations. The mechanism reduction was performed using directed relation graph (DRG) with expert knowledge (DRG-X) and DRG-aided sensitivity analysis (DRGASA) at a fixed fuel composition of 77% of n-dodecane and 23% m-xylene by volume. The sample space for the reduction covered pressure of 1–80 bar, equivalence ratio of 0.5–2.0, and initial temperature of 700–1600 K for ignition."* as stated by the authors in the abstract of the journal contribution [148]. A validation of the reduced 163 species mechanism against the detailed mechanism along with the validation presented in the publication is shown is figure 106. The reduction procedure proposed in this work was applied to the same detailed mechanism to investigate if a similar skeletal mechanism can be generated.

10.3.0.1   Reading the Mechanism   While reading the mechanism a few modification were done in thermodata file to ensure the use of the NASA format and species containing special characters were renamed. Reading the mechanism in LOGEsoft revealed that about 40 species in the species list are inert (not counting N_2). LOGEsoft counts the mechanism to have 2846 species and 11754 reactions (or 20142 reactions when forward and backward are counted as individual reactions). In this work the detailed reaction mechanism is referred to have 2846 species.

10.3.0.2   First Lumping Attempt   352 possible lumped species were identified when using a maximum threshold of 10 Joule of the Gibbs free energy [33]. One has to keep in mind that the NASA polynomials only contain informations about thermodynamic states and the sum formula of the molecule. No informations about the structures are include and it is nearly impossible to reconstruct all isomer configurations in a mechanism of this size. With this limit in Gibbs free energy and the sum formula it was possible to reduce the size of the mechanism to 1207 species and 20022 reactions. Unfortunately the lumped scheme does show a bad performance (see figure 107 d) and it was not possible to find the reason for this at this stage. In a similar way as done by Pei et al. [148] the lumping step was applied in a later reduction stage.

10.3.0.3   Species and reaction removal   The reduction limits and parameters were set to be as close as possible to the parameter range considered by Pei et al. [148] . It is not clear how to translate the reduction settings of the DRG method to the method proposed in this work. Therefore the same parameter ranges in fuel equivalence ratio, pressure and tem-

---

[33]Which means all isomers using the same thermodynamic data were lumped.

perature were chosen and ignition delay and major species were controlled in best practise limits (see table 26). Table 27 gives an overview about the achieved reduction steps along with the CPU times for 0D calculation at 800 K, 10 bar and ϕ=1.0. Most of the species are removed by species removal reducing the size by more than factor 10 and the CPU times by more than 30 times. From this 220 species mechanism additional 35 species were removed via reaction removal and the number of reactions was reduced by factor three. This 185 species / 630 reaction mechanism is comparable in terms of CPU time to the mechanism derived by Pei et al. (see table 27). The derived schemes shows a good agreement with the detailed mechanism over the complete parameter range (see figure 107).

Parameter	Settings or limits
Fuel 1 (m/m)	77% NC12H26, 23% MEC6H3CH3
Oxidiser	artificial air
Inlet pressure	1.0, 5.0, 10.0, 20.0, 40.0, 80.0 bar
Inlet temperature	600, 700, 800, 900, 1000, 1100, 1200, 1400, 1600 K
Inlet ϕ	0.5, 1.00, 2.0
Concentration control	CO_2 and H_2O within 15%
Auto ignition control	0.16%
Reactor model	const. pressure
Necessary species	CO_2, H_2O, N_2, O_2, CO, H_2, $NC_{12}H_{26}$, $MEC_6H_3CH_3$

Table 26: Table with limits for the reduction

Reduction step	Number of species and reactions	CPU time 0D [s]
Detailed	2846 / 20142	170.26
Lumped (failed)	1207 / 20022	-
Species removal	220 / 1843	5.31
Reaction removal	185 / 630	2.80
Lumping	152 / 624	2.27
Global steps	127 / 497	1.62
Pei et al.	163 / 1674	2.91

Table 27: Milestones during the reduction of the 2-component surrogate scheme from Pei et al [148]. The CPU time are for calculations at inlet conditions of 800 K, 10 bar and ϕ=1.0

10.3.0.4 Second lumping attempt

Pei and co-workers carried out a lumping step after reducing the mechanism to 227 species (via DRG-X and DRGASA). The lumping step reduced the mechanism in there work to 202 species. In a similar fashion it was tried to apply the horizontal technique to the reaction mechanism obtained via species and reaction removal. It needs to be clearly stated that the author of this thesis is convinced that the lumping should be done before removing a species. Based on a maximum deviation of 1 J in thermodynamic properties eight possible isomers were identified. It turned out that lumping all C12OOH isomers into one lumped species caused a significant deviation in ignition delay time in the NTC. This problem could be solved by lumping only species with the same ring size[34]. Remarkably this is exactly what was found by Ahmed et al. [14] for a very different n-alkane mechanism compiled with a different concept. The lumping step reduced the mechanism to 152 species and 624 reactions. As shown in figure 108 the

---

[34]Based on the thermodynamic data the following species should have been lumped: C12OOH6-8 C12OOH6-4 C12OOH5-8 C12OOH5-7 C12OOH5-3 C12OOH4-7 C12OOH4-2 C12OOH3-6 C12OOH3-5 C12OOH2-4 .
A good result was achieved by lumping C12OOH6-8, C12OOH6-4, C12OOH4-2, C12OOH2-4, C12OOH5-7, C12OOH5-3 into one species and C12OOH5-8, C12OOH4-7, C12OOH3-6 into an other species.

(a) ϕ=0.5

(b) ϕ=1.0

(c) ϕ=2.0

(d) Validation plot for the reduced scheme from Pei et al. [148] for ϕ=2.0
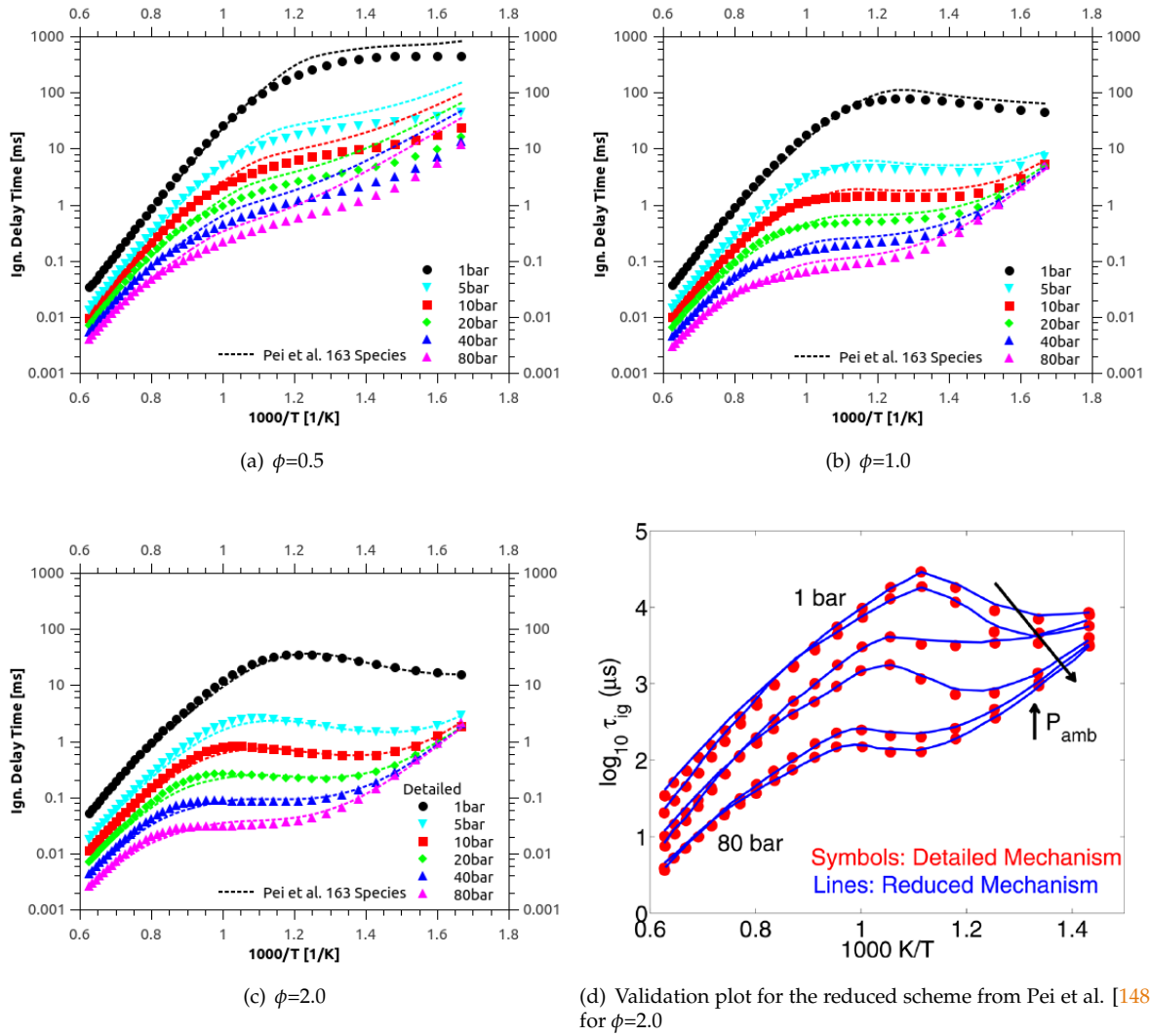
Figure 106: Figure (a)-(c) Comparison of predicted ignition delay times of the detailed (symbols) and reduced 163 (lines) species mechanism derived by Pei et al.

lumping step introduces a small deviation from the detailed scheme at high pressure over the complete range of fuel equivalence ratio and a small reduction in CPU time was achieved (see table 27). The overall deviation against the detailed mechanism is below those achieved by Pei and co-workers [148].

10.3.0.5   Further reduction The mechanism was further reduced by hand by introducing global steps, removing slow reverse reaction etc. . This reduced the mechanism to 127 species / 497 reactions resulting in a nearly factor two faster CPU times as achieved by Pei et al.. The predicted ignition delay times show the same small deviation from the detailed scheme as the scheme obtained by lumping (see figure 109). It is worth to note that the reduction procedure was stopped here and a further reduction would have been possible with more effort, but is not the scope of this work.
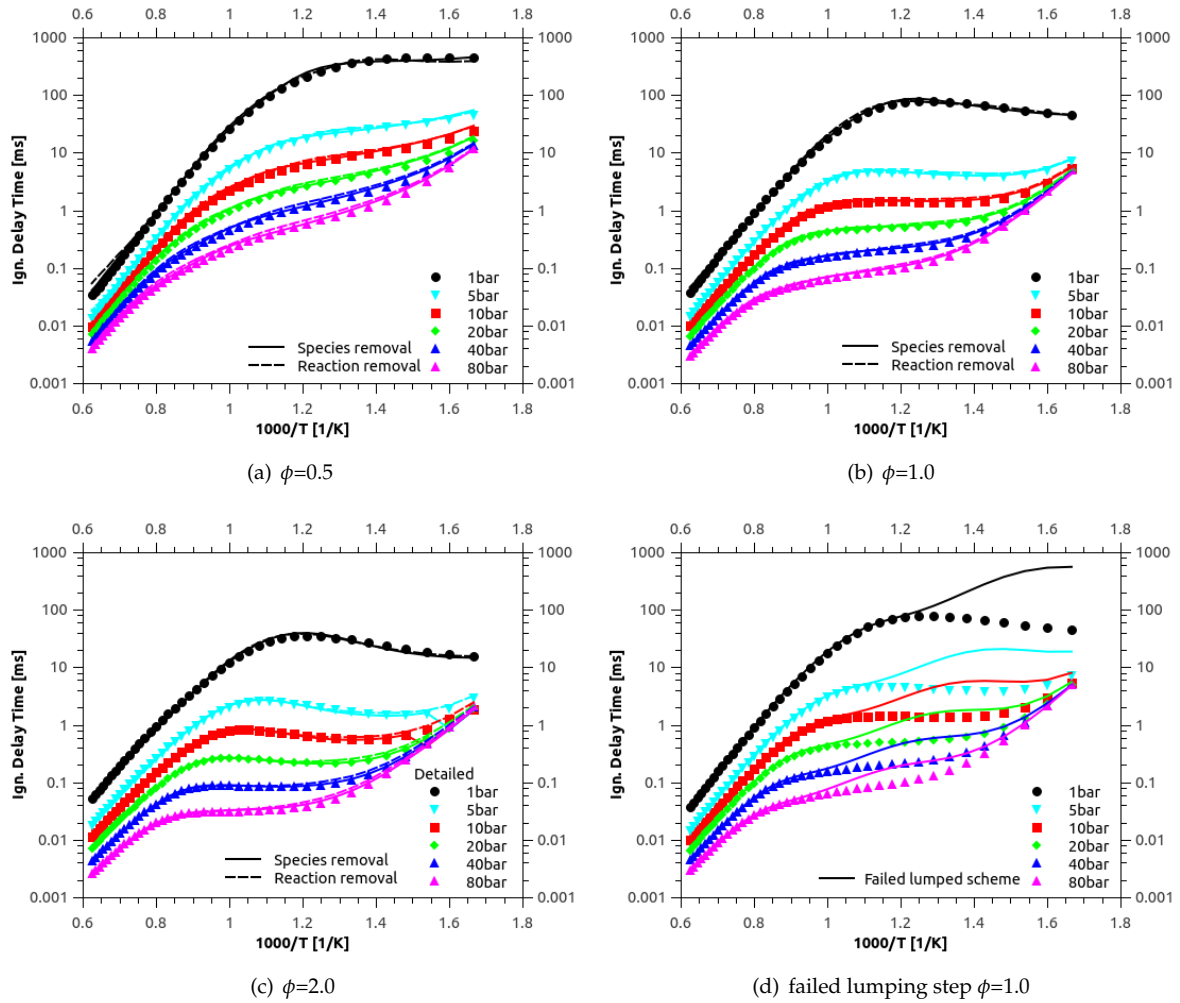
Figure 107: Comparison of predicted ignition delay times of the detailed (symbols) and reduced obtained via species removal (solid lines) and reaction removal (dashed line) derived in this work. Figure (d) shows the ignition delay times predicted by the failed lumping step.

(a) ϕ=0.5

(b) ϕ=1.0

(c) ϕ=2.0
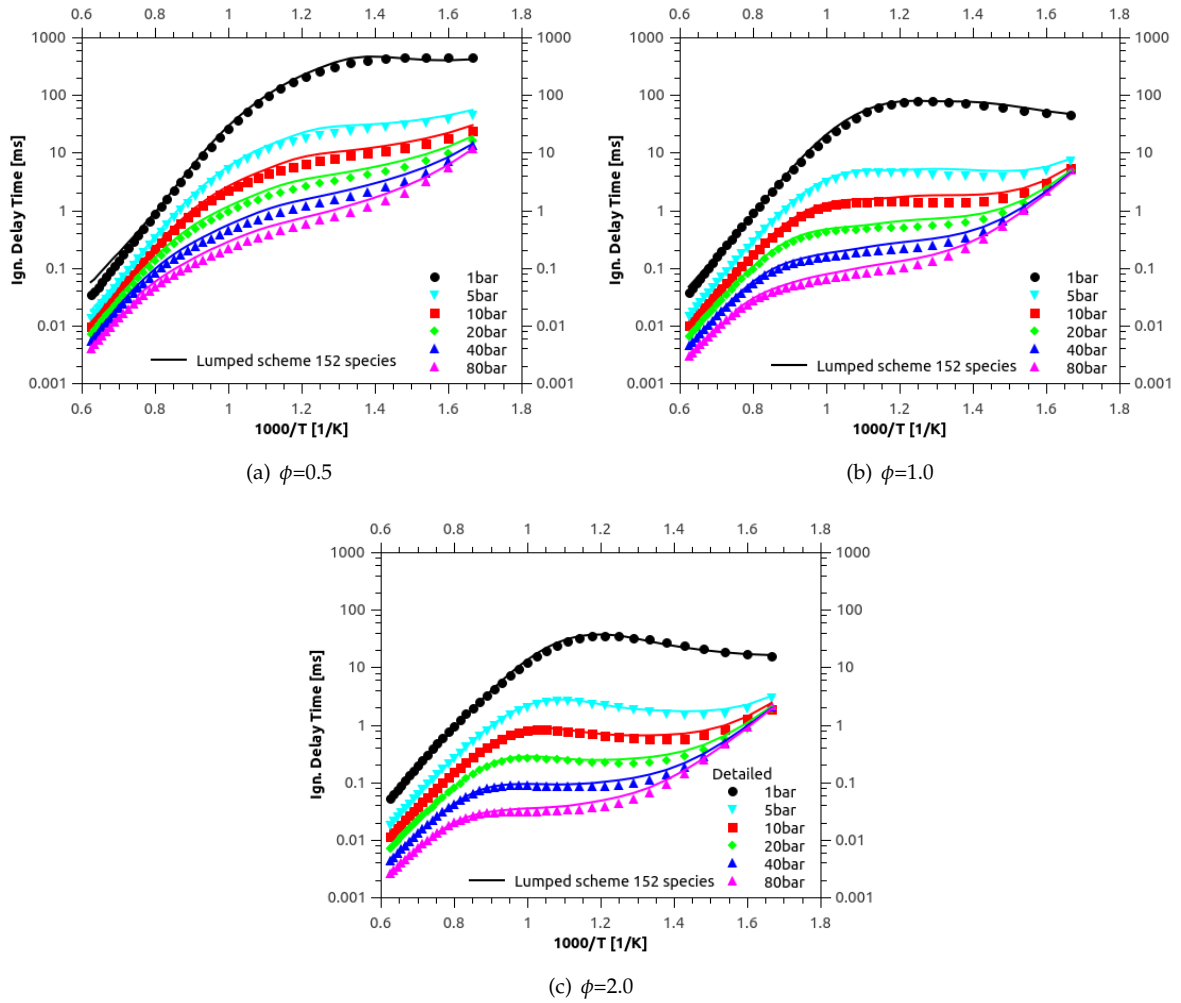
Figure 108: Comparison of predicted ignition delay times of the detailed (symbols) and lumped scheme (applied to reaction removal step - (solid line)) derived in this work.

(a) ϕ=0.5

(b) ϕ=1.0

(c) ϕ=2.0
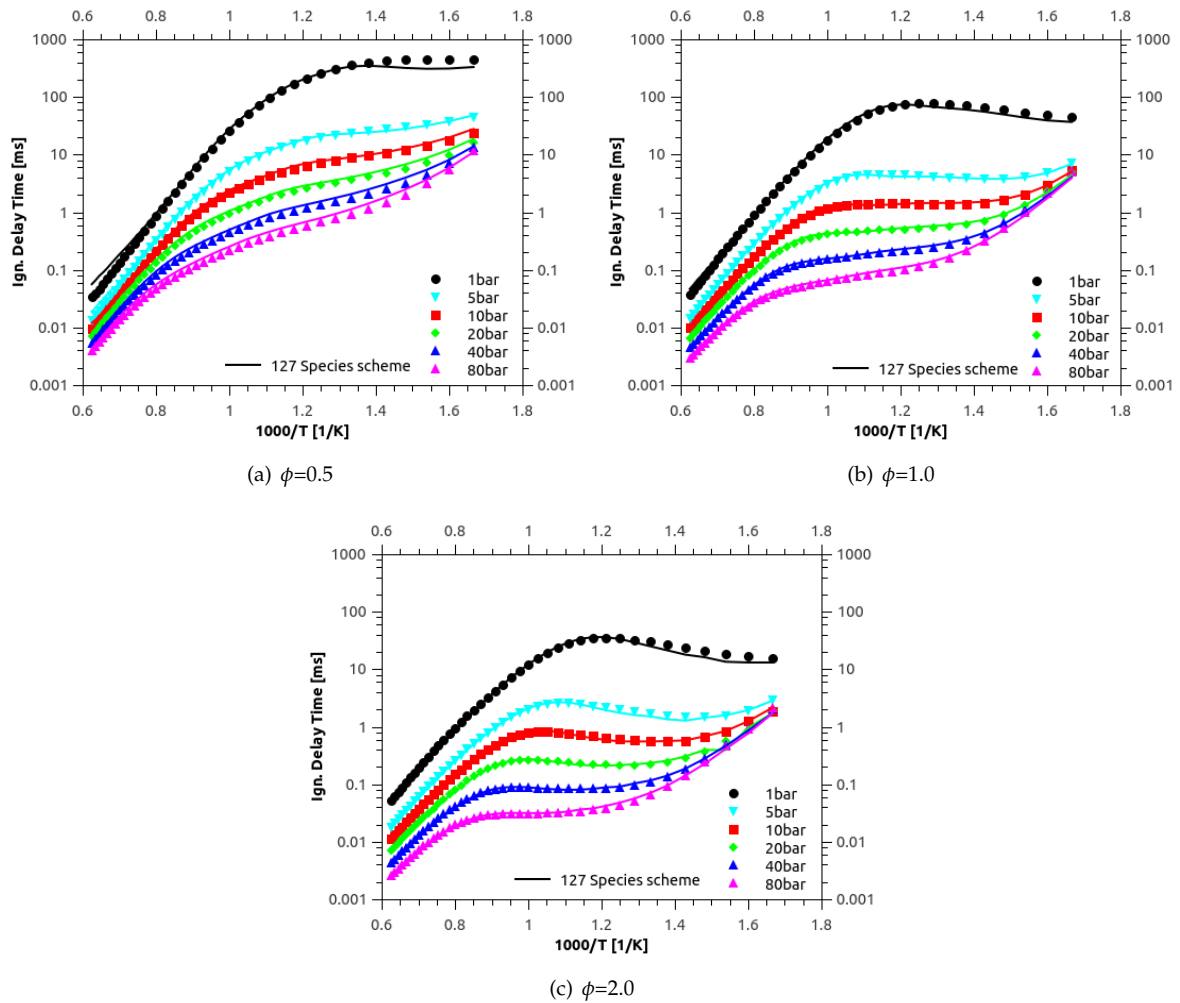
Figure 109: Comparison of predicted ignition delay times of the detailed (symbols) and 127 species and 497 species mechanism (solid line) derived in this work.

10.4   Pathway preservation

It is clear that a mechanism reduction needs to reduce the number of decomposition pathways of fuels and intermediate species. A complete preservation of all pathways and intermediates would result in the fact that none or only a few species and reactions could be removed. A closer look to the applied reduction steps in this work reveals that they will effect the decomposition pathways in a different extend:

- Horizontal lumping: The decomposition pathways are preserved by definition. No reaction is removed or added. Species are only lumped in new pseudo species. The radical pool is not influenced.

- Species removal: The removal of species has the strongest impact on the fuel decomposition pathways. Every removed species will remove at least one decomposition pathway (for hierarchical designed reaction mechanisms), but very likely more. The necessity based species removal should ensure that the most unimportant species are removed first. Further the control of major combustion products, ignition delay time and important intermediates leads to a distribution resulting in a similar radical pool.

- Reaction removal: Every removed reaction will at least remove one decomposition pathway for a single species. For duplicate reactions which cannot be summarised the total decomposition rate is reduced. The radical pool may be influenced, radicals of lower importance for the combustion process may be removed.

- Introduction of global steps: The introduction of global steps will not have an impact on the global decomposition pathways, only intermediate species with a short live time will be removed. The radical pool will be influenced since short lived radicals for which the steady state assumptions holds can be replaced by there products. This will lead to different peak concentrations of radicals. Very likely the most import radicals will show slightly higher concentrations.

Based on the considerations above it can be concluded that the proposed reduction sequence will preserve the major decomposition pathways. Figure 112 and 113 show the evolution during combustion of the fuel and radical concentrations for different reduction steps of the n-heptane scheme. It can be seen that the assumptions made about the impact of the reduction on the radical pool are valid for 0 dimensional homogeneous reactors and the major difference has its origin in the sligly different ignition delay times. The conservation of the radical pool in engine simulations using the ETRF reaction scheme is shown by comparing concentrations predicted by the detailed and the 130 species mechanism for the case discussed in the next chapter. The case with forced auto ignition was chosen for this evaluation. Figure 114 compares the average concentration of 100 consecutive cycles for the four fuels and selected radicals. The predicted shape and total concentration match well within the stochastic variance among both schemes.

In which extend the decomposition pathways are preserved is based on set reduction targets (controlled species profiles, error margin for species profiles, accepted deviation in

ignition delay time and laminar flame speed). Due to the lack of a numerical expression for pathway preservation the comparison of flow graphs shall serve as prove that the reduction sequence developed in this thesis will preserve pathways. Figure 110 shows the carbon flow from n-heptane to CO_2 using the lumped scheme (see table 21) for a stoichiometric n-heptane / air mixture at 800 K and 40 bar. Only the upper 5% of the largest carbon flow is shown. Figure 111 shows the carbon flow at the same conditions using the 87 species / 347 reaction scheme derived by species and reaction removal (see table 21). It can be clearly observed that major pathways from the fuel to the CO and CO_2 are kept and more carbon is flowing through the remaining pathways. The proposed reduction strategy can preserve the major decomposition pathways, in particular when the reduction is performed with tight tolerances and controlling major combustion products within a wide parameter range.
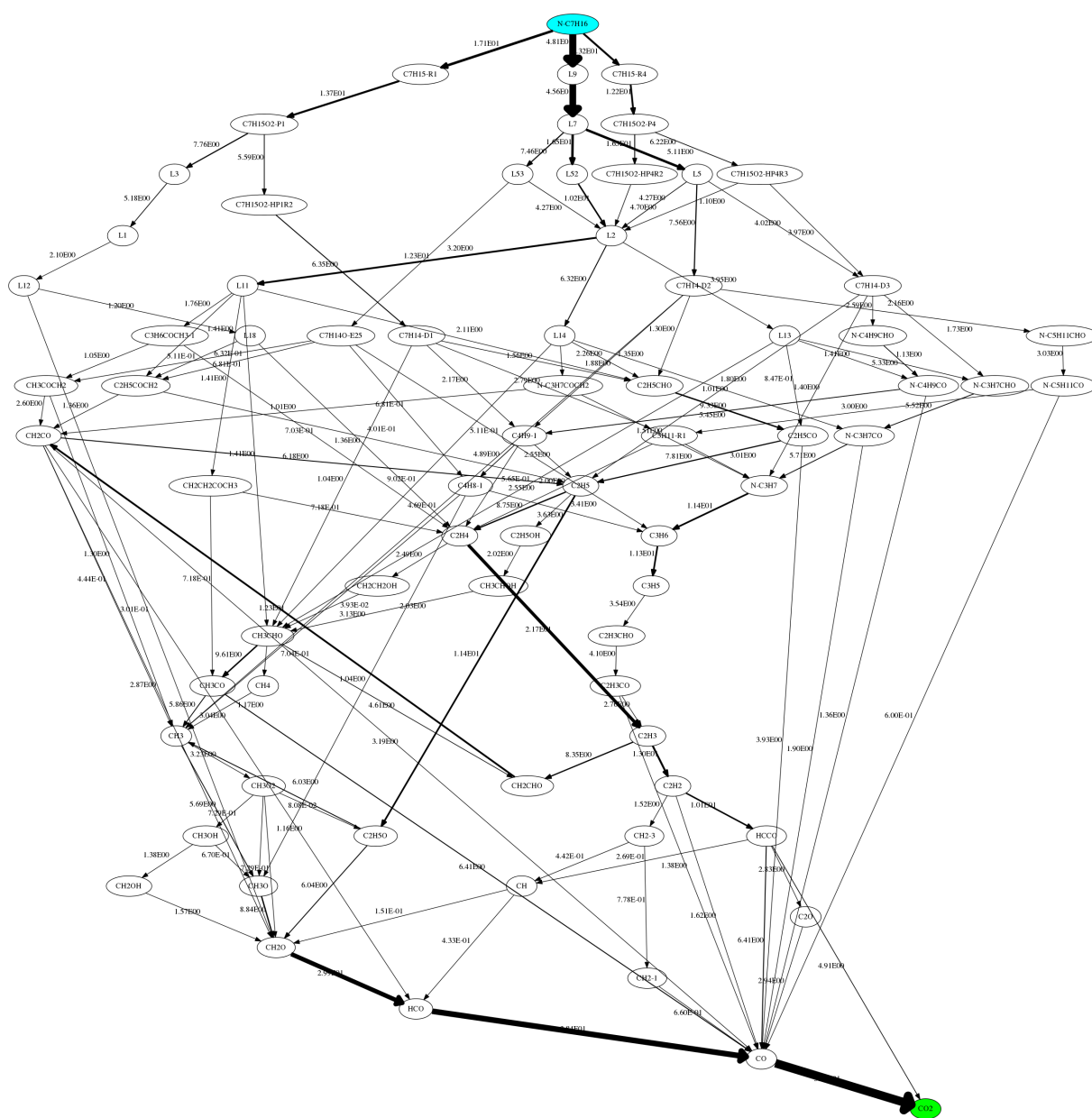
Figure 110: Carbon flow for a stoichiometric n-heptane / air mixture at 800 K and 40 bar in a constant volume reactor using the lumped n-heptane scheme. The flow is given in $\frac{mol}{m^3}$ and limited to the upper 5% of the maximum flow.
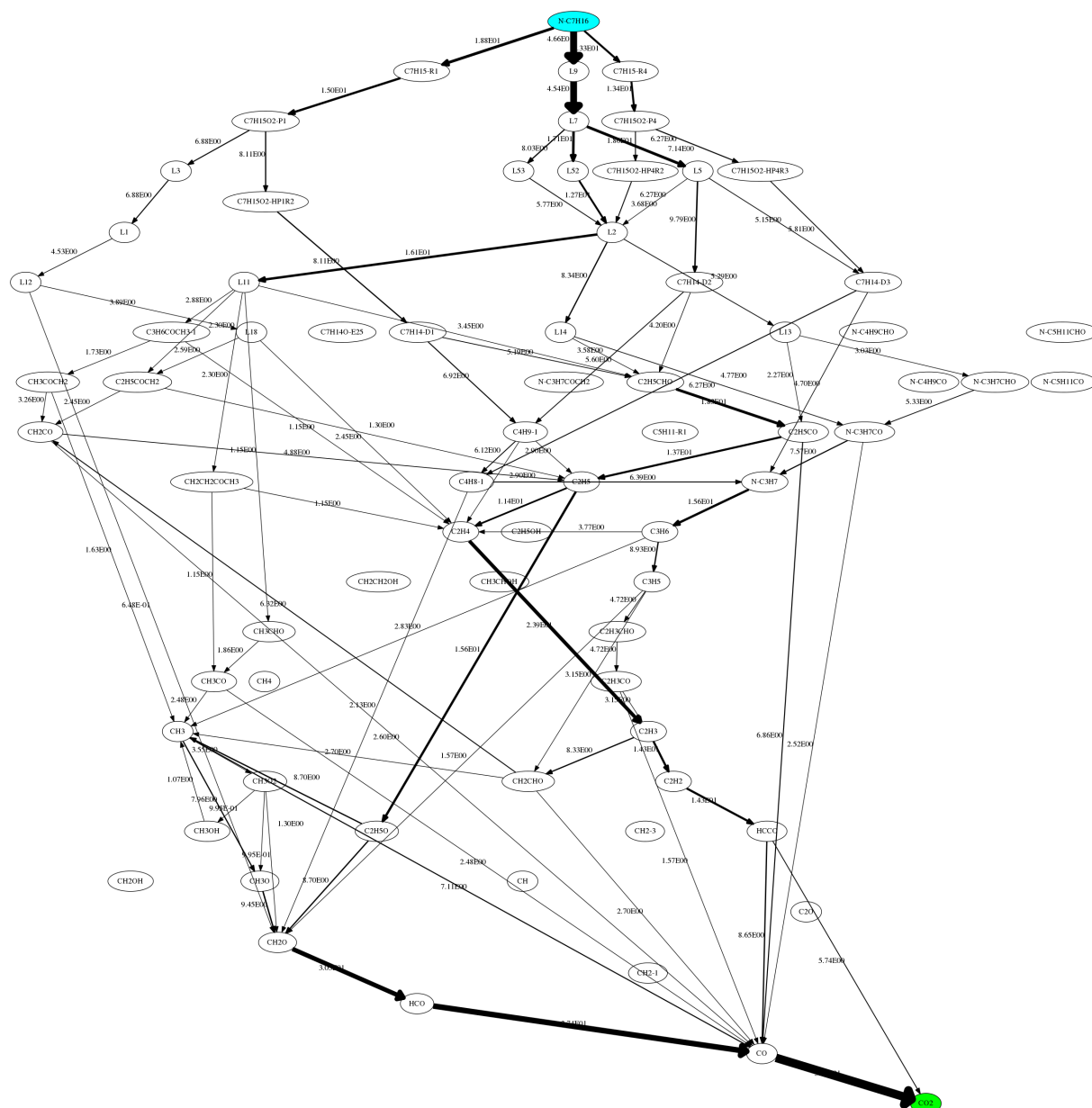
Figure 111: Carbon flow for a stoichiometric n-heptane / air mixture at 800 K and 40 bar in a constant volume reactor using the reduced n-heptane scheme (87 species / 347 reactions) derived by species and reaction removal. The flow is given in $\frac{mol}{m^3}$ and limited to the upper 5% of the maximum flow. Species which are not connected with arrows are removed in this scheme, but are included in the flow analysis using the lumped scheme.

(a) Temperature

(b) n-Heptane

(c) H_2O_2

(d) H

(e) CH_3O_2

(f) O
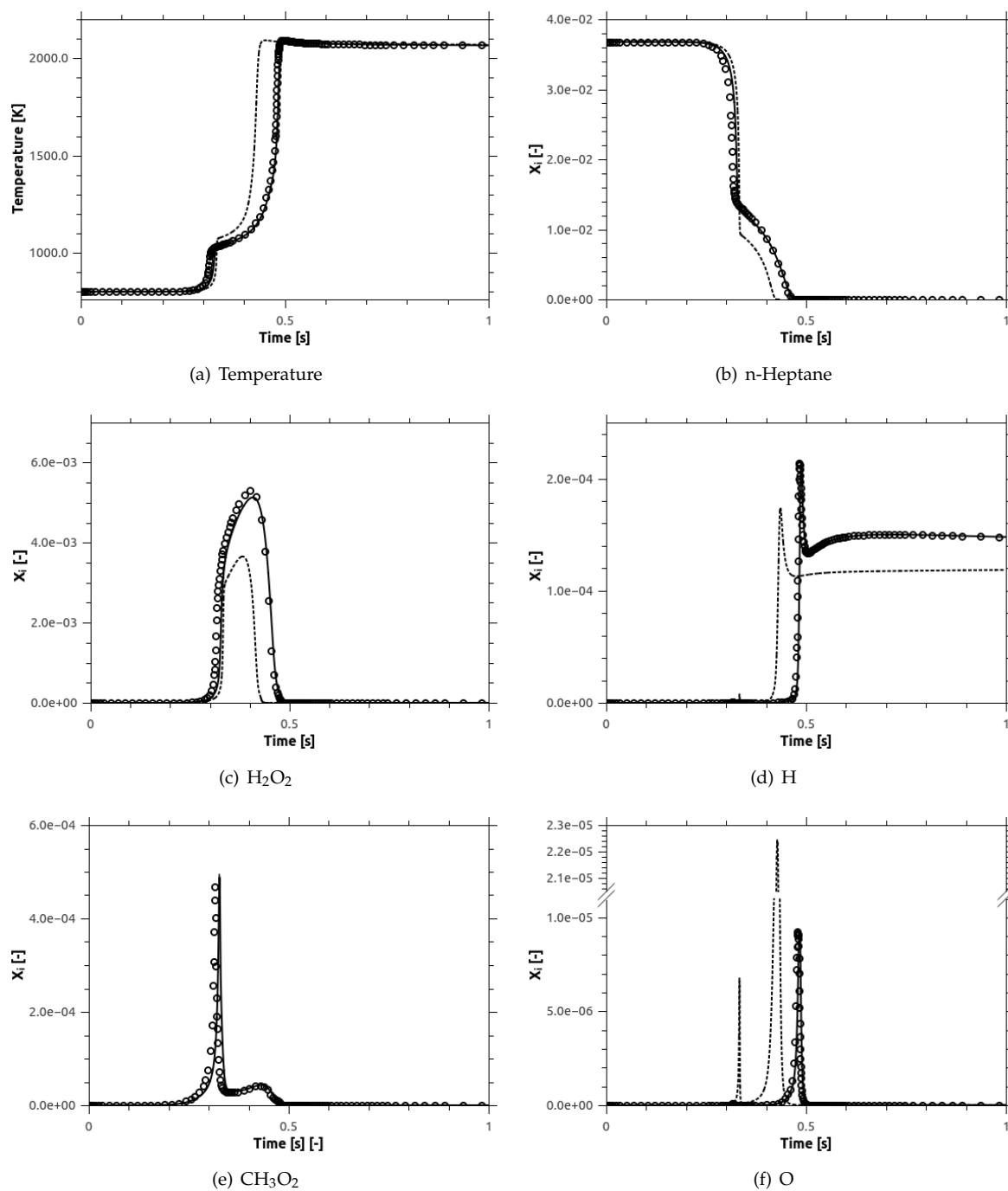
Figure 112: Temperature profile as well as the molar fraction of the fuel (n-Heptane), hydrogen peroxide and selected radicals in a homogeneous constant pressure reactor. Inlet conditions: 40 bar and 800 K with air as oxidizer ϕ=2.0. Open symbols: detailed scheme; solid line: lumped scheme; dotted line: 56 species mechanism.

(a) n-Heptane

(b) C_2H_3

(c) C_2H_5

(d) CH

(e) CH_3

(f) CH_3O
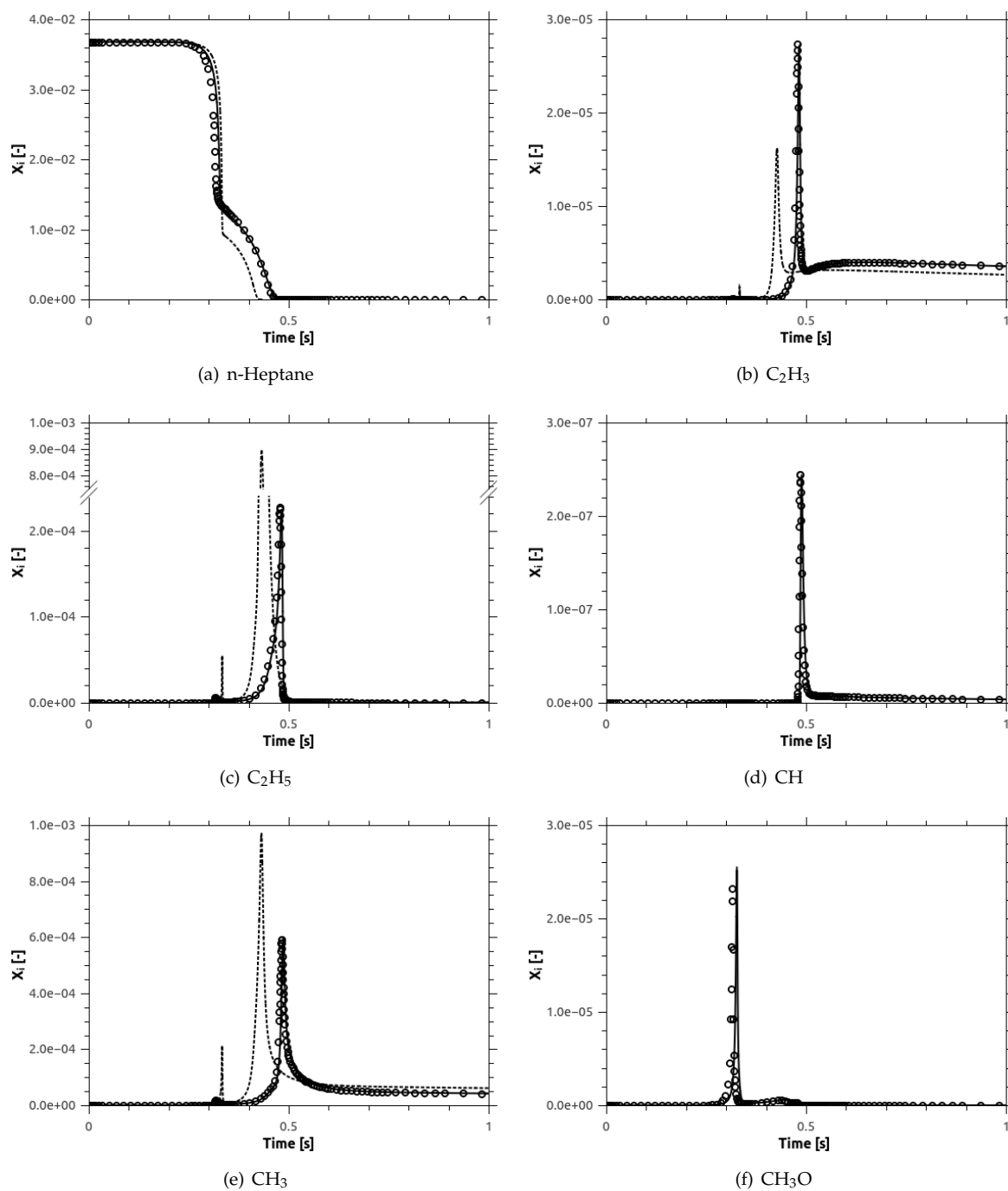
Figure 113: Molar fraction of the fuel (n-Heptane) and selected radicals in a homogeneous constant pressure reactor. Inlet conditions: 40 bar and 800 K with air as oxidizer at ϕ=2.0. Open symbols: detailed scheme; solid line: lumped scheme; dotted line: 56 species mechanism.

(a) Fuels

(b) OH

(c) H

(d) CH$_3$

(e) CH$_3$O
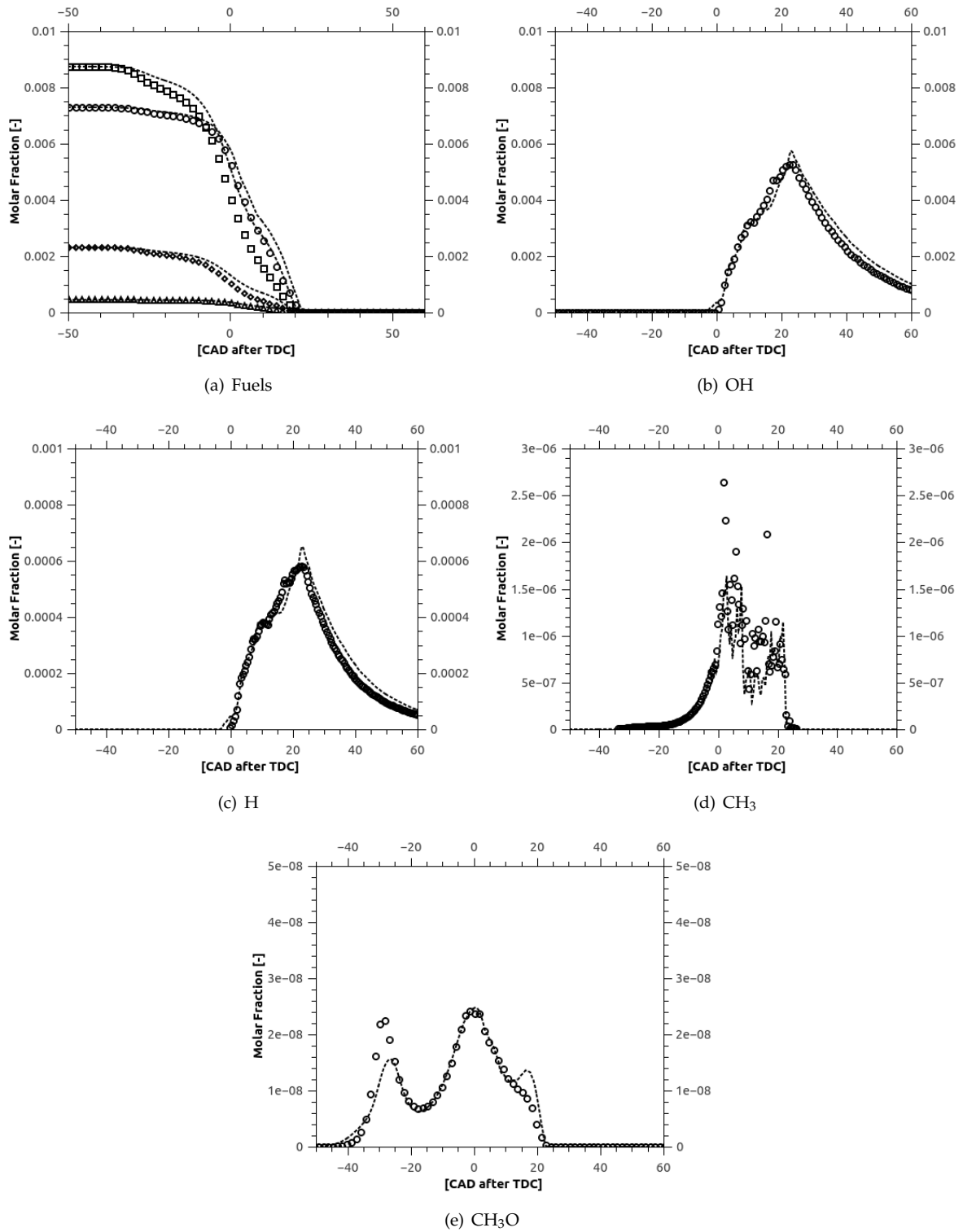
Figure 114: Average concentration of selected radicals of 100 consecutive engine cycles for the four component ETRF fuel.

11   Reduction of a ETRF Reference Fuel for Engine Conditions

The reduction of the ETRF mechanism is separated into two branches: a mechanism for prediction of laminar flame speeds and a mechanism for prediction of auto ignition and major emissions. This is based on the reasoning that normal combustion in SI engines is driven by propagation of the flame front which is initiated from a flame kernel generated by the spark plug. In engine simulations the turbulent flame speed is often derived from tabulated laminar flame speeds or correlation functions. Thus subsequently means that the reduced mechanism is predominantly used to predict auto ignition in the area which was not reached by the flame front and major emissions. This reduced mechanism can be used to model major combustion in a time efficient manner for a variety of operating points and surrogates. The lumped scheme can be used to study emission formation including build up of PAH species and solid soot.

11.1   Mechanism for auto ignition prediction

The fuel composition and parameter range controlled during the reduction is given in table 28. For this reduction a comparable wide range in pressure and fuel equivalence ratio was controlled. The inlet temperature was controlled up to 1400 K for fuels without low temperature chemistry and up to 1200 K for fuels with low temperature chemistry. In contrast to the reduced PRF scheme (see section 10.2.2) the ETRF scheme should cover a wider range to resolve local inhomogeneities in mixture composition and local air / fuel ratios in particular in CFD calculations. The reduction was started from the modified 386 species mechanism (see section 9). Due to the wide range of fuel composition and inlet conditions considered during the reduction the resulting mechanisms are larger than the special purpose schemes introduced earlier in this work.

The species removal reduced the mechanism by 205 species down to 181 species / 1856 reactions resulting in a reduction of CPU time of about factor 3.5 (see table 29). Note that in addition to the automatic reduction the only reaction forming naphthalene: CYC5H5- + CYC5H5- => A2+H+H was removed by hand. This was done since all other decomposition for naphthalene were removed before, the only remaining reaction was leading to a high concentration of naphthalene in the burned gas and has not effect on predicted ignition delay time. By applying the reaction removal the mechanism was reduced to a size of 179 species and 931 reactions which shortened the CPU time again by nearly 20%. The further reduction by hand (introduction of global steps and other techniques described in section 10.1.6) was leading to a reaction scheme with 130 species and 648 reactions. This step reduced the CPU time again by about 40% resulting in a total speed of factor 7 compared to the original scheme in the stochastic engine simulation.

The different reduction mile stones are compared using the stochastic engine setup given in table 24 and in 0D constant pressure calculations. The fuel mixture was calculated as described in chapter 5.3 for a RON 95 fuel containing 30 vol% aromatic species and 10 vol%

Parameter	Settings or limits
Fuel 1	ethanol
Fuel 2	toluene
Fuel 3	n-heptane
Fuel 4	iso-octane
Fuel 5	25% (molar) of each fuel
Oxidiser	artificial air
Inlet pressure (Fuel 1-5) [bar]	1.0, 5.0, 10.0, 40.0, 80.0
Inlet temperature (Fuel 1 and 2) [K]	1000.0, 1200, 1400
Inlet temperature (Fuel 3 - 5) [K]	600.0, 700.0, 800.0, 900.0, 1000.0, 1200.0
Inlet ϕ (Fuel 1 - 5)	0.3, 1.00, 1.5, 2.0, 3.0
Ignition delay time control (Fuel 1-5) [%]	15
Reactor model	constant pressure
Necessary species	$i\text{-}C_8H_{18}, n\text{-}C_7H_{16}, A_1CH_3, C_2H_5OH, N_2, O_2, CO, CO_2,$ $H_2, H_2O, CH_3, H, OH, O, HCO, N, NO, NO_2$

Table 28: Table with reduction settings for the ETRF scheme targeted on prediction of auto ignition and major emissions.

Reduction step	Number of species and reactions	CPU time (SRM) [s]
Lumped	386 / 4511	878.8
Species removable	181 / 1856	246.5
Reaction removal	179 / 931	202.6
Global steps	130 / 648	122.2
Cai et al.	335 / 2629	654.3

Table 29: Milestones during the reduction of the four-component ETRF scheme. CPU is the average time needed for one engine cycle with normal combustion.

ethanol. This represents an average European E10 fuel. The calculated surrogate fuel composition is given in table 30 and its properties are given in table 31. This four-component mixture differs significantly from the mixture controlled during the reduction which is composed of 25% (molar) of each fuel component. As shown in figure 115 (e) and (f) all reduction steps are close to the original reaction scheme for both four-component mixtures. It can be concluded that it is sufficient to control one multicomponent fuel in addition to the pure fuels. To underline the accuracy of the reduction procedure fuel equivalence ratios and a pressure was chosen which was not controlled during the reduction. It can be seen that for the pure fuels n-heptane, iso-octane, toluene and ethanol (see figure 115 (a) - (d)) neither the species removal nor the reaction removal introduced a noticeable deviation. The only noticeable deviation from the original scheme was introduced for pure toluene and pure iso-octane at high temperatures. Also slightly shorter ignition delay times for the lean ($\phi = 0.5$) four-component mixtures (quaternary and European E10) are observed.

To understand in which extend the deviation in ignition delay time can effect the combustion predictions in engine simulations the European E10 surrogate is used as fuel for the operating point summarised in table 24 with a realistic inlet gas temperature of 360.4 K resulting in normal combustion driven by flame propagation and artificial high inlet temperature of 510.4 K resulting in auto ignition in the unburned zone which was not reached by the flame front.

It is worth to point out that the modified mechanism shows a significant scatter in the cycle to cycle variation of the fuel burn rate (see figure 117 (d)) for the higher inlet temperature ranging from nearly complete combustion even before spark timing up to regular combustion only by flame propagation. This large cycle to cycle variation of the ignition onset in

the unburned zone is a crucial test for the proposed reduction procedure.

It can be observed in figure 116 that different reduction steps predict exactly the same combustion and emissions for the operating point with normal combustion (360.4 K inlet temperature).

For the more challenging task (see discussion in section 10.2.2) of auto ignition prediction in the unburned zone a difference between the various reduction steps can be observed. First of all the four schemes predict the same engine out emissions for the major species CO, CO_2 and H_2O and for NO and NO_2 as shown in figure 117 (e) and (f). This proves that the reduction kept all main fuel decomposition pathways. The averaged ignition onset of 30 cycles shows a stronger variation for each reduction milestone. As shown in figure 117 (a) and (b) the pressure trace for the 181 mechanism obtained via species removal is very close to the 30 cycle average of the lumped scheme. The reaction schemes with 179 and 130 species show a more unsteady combustion behavior. This is depicted in figure 117 (b) by plotting two times the 30 cycle average for the 130 species scheme. The average over 100 cycles (red dotted line) using the 130 species mechanism is closer to the predicted pressure trace (figure 117 (b)) and burn rate (figure 117 (c)) of the lumped scheme. The largest observed difference based on a 30 cycle average between the lumped scheme and 130 species is about three CAD using the pressure onset in figure 117 (b). Based on 100 cycle averages for the lumped and 130 species scheme the difference in pressure onset is below two CAD and nearly not observable. The combustion duration, defined here as distance from 10% mass fraction burned (MFB) to 90% MFB, shows no observable difference. Based on this it can be concluded that the reduced schemes are suitable to predict the same auto ignition or knock in SI engine simulations as the lumped scheme.

In this context the comparison of the predicted combustion for the operating point with 510.4 K inlet temperature using three different reaction schemes can help to classify the difference introduced due to reduction. Compared are the lumped reaction scheme, the modified lumped scheme introduced in section 9 and the published skeletal ETRF surrogate reaction scheme from Cai and Pitsch [149] with 335 species. The reaction scheme from Cai et al. needs the expected CPU time for one cycle as summarised in table 29. For the engine operating point with the higher inlet temperature shown in figure 118 (a) auto ignition is observed for all three schemes while the mechanism from Cai et al. shows the most early auto ignition followed by the original (not modified) lumped scheme derived in this work. For the operating point with the cooler gas inlet temperature shown in figure 118 (b) no auto ignition is observed using the both schemes derived in this work. The mechanism from Cai et al. on the other hand predicts auto ignition for this operating point. The tendency for auto ignition clearly follows the trend observed for the predicted ignition delay times for the ETRF mixture shown in figure 118 (c). Here a significant difference between the three schemes for stoichiometric and rich mixtures and temperatures below 1000 K is observed. The difference in predicted ignition delay time among those reaction schemes covers a range of about 20 CAD and is therefore much larger deviation than introduced by the proposed reduction method in this work.
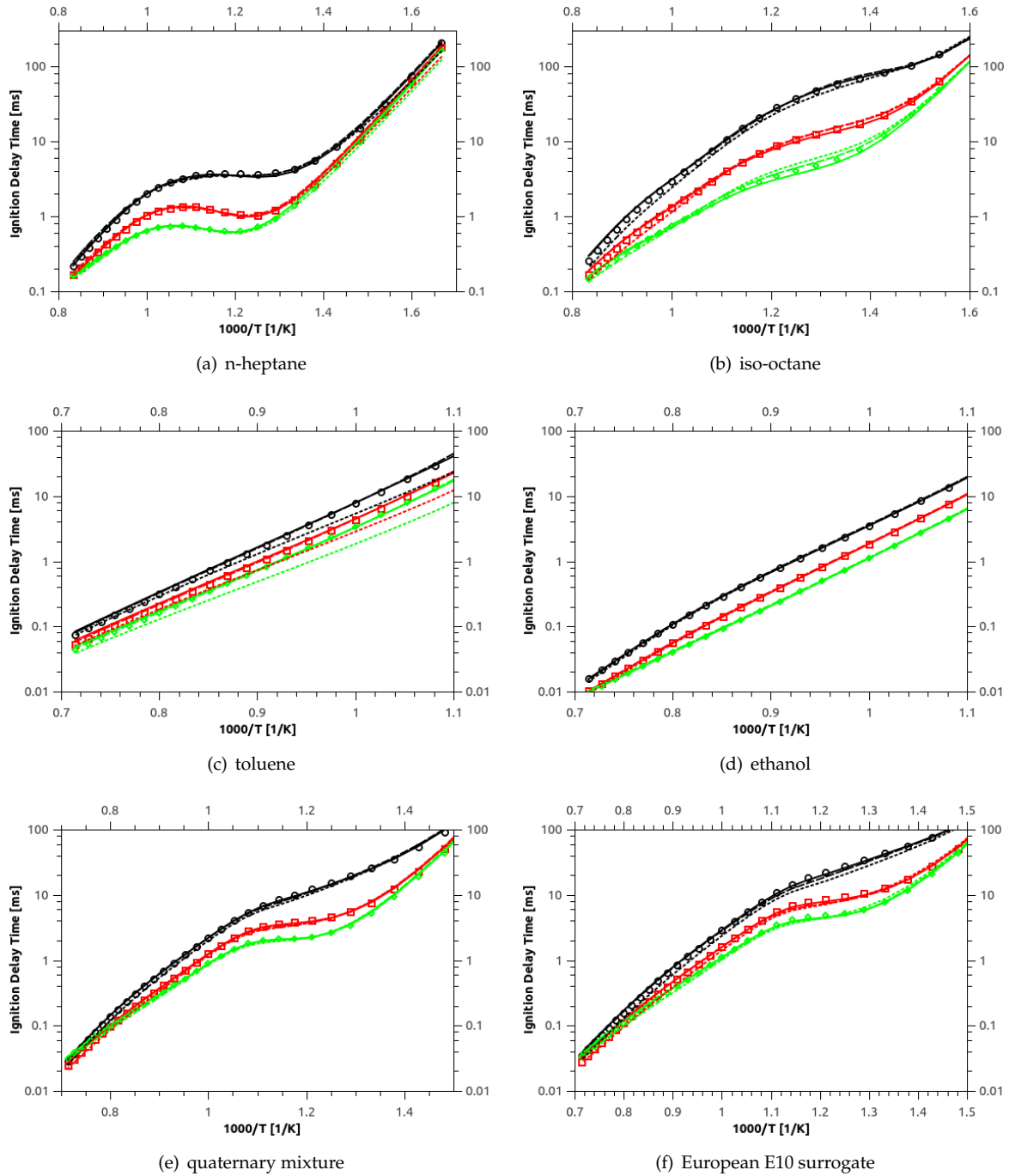
Figure 115: Predicted ignition delay for different fuel air mixtures at 30 bar. Black: ϕ=0.5; Red: ϕ=1.2; Green: ϕ=2.5. Open symbols: lumped scheme; solid line: species removal (181 species); dashed line: reaction removal (179 species); dotted line: further reduction by hand (130 species).

Fuel component	Molar fraction [-]	Liquid volume fraction [-]	Mass fraction [-]
Ethanol	0.024	0.010	0.011
Toluene	0.388	0.300	0.350
iso-Octane	0.465	0.558	0.519
n-Heptane	0.123	0.132	0.120

Table 30: ETRF mixture representing a European E10 gasoline surrogate fuel used for verification of reduction steps in stochastic engine model.

Property	Value
Avarage molar mass	0.1023
Density	744.37 $\frac{kg}{m^3}$ at 20° C
RON	95.00
MON	88.74
LHV	42847.14 $\frac{kJ}{kg}$

Table 31: Calculated properties of the surrogate fuel given in table 30.

(a) Pressure

(b) Pressure around the ignition event

(c) Mass fraction burned using the lumped scheme

(d) Major species

(e) NO and NO$_2$
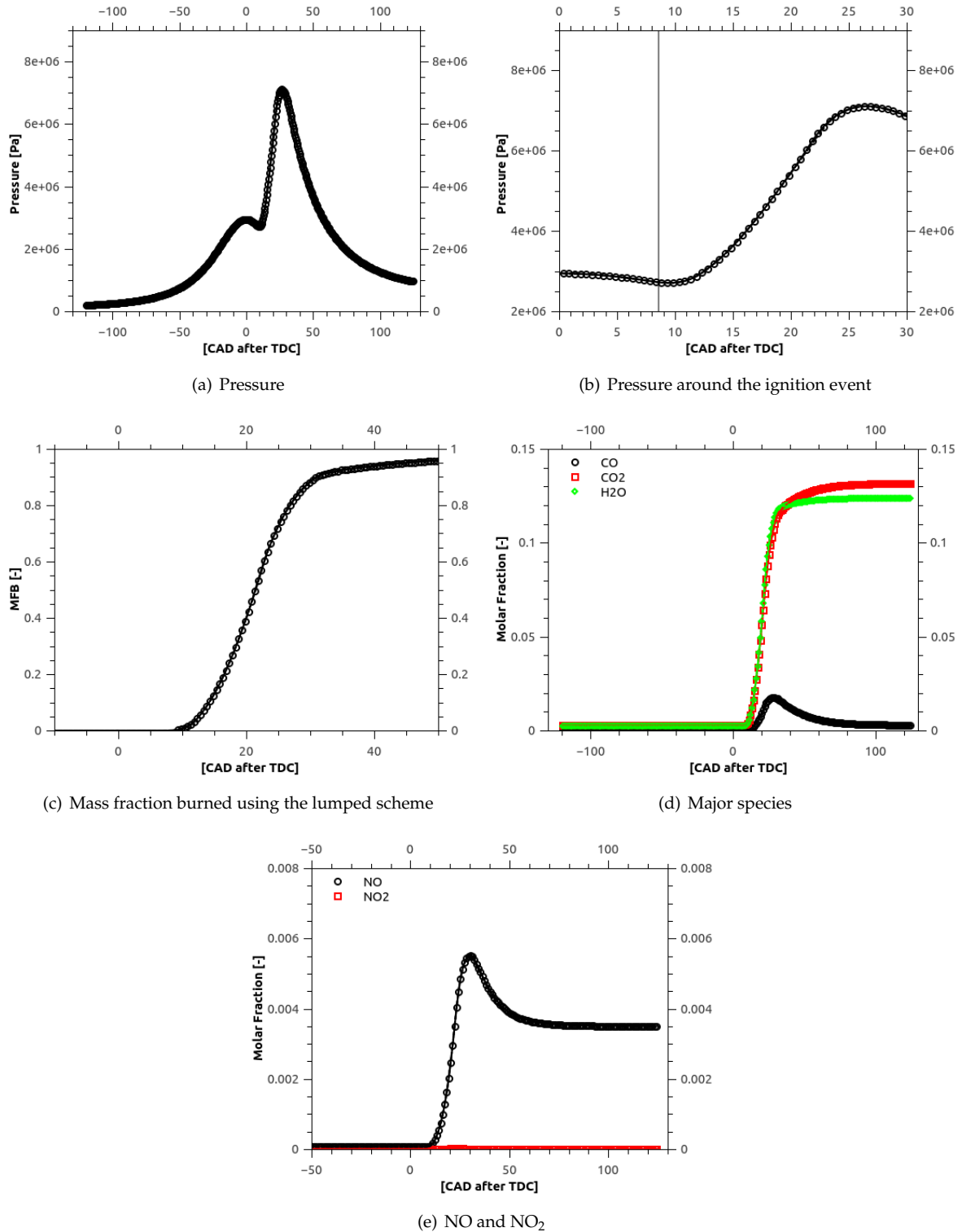
Figure 116: Comparison of combustion prediction (360.4 K inlet temperature) with different reduction stages using the settings given in table 24 and the fuel composition from table 30. Open symbols: modified lumped scheme; solid line: species removal (181 species); dashed line: reaction removal (179 species); dotted line: further reduction by hand (130 species). Vertical line denotes spark timing (turb. θ).

(a) Pressure

(b) Pressure around the ignition event

(c) Mass fraction burned

(d) Mass fraction burned around the ignition event

(e) Major species

(f) NO and NO$_2$
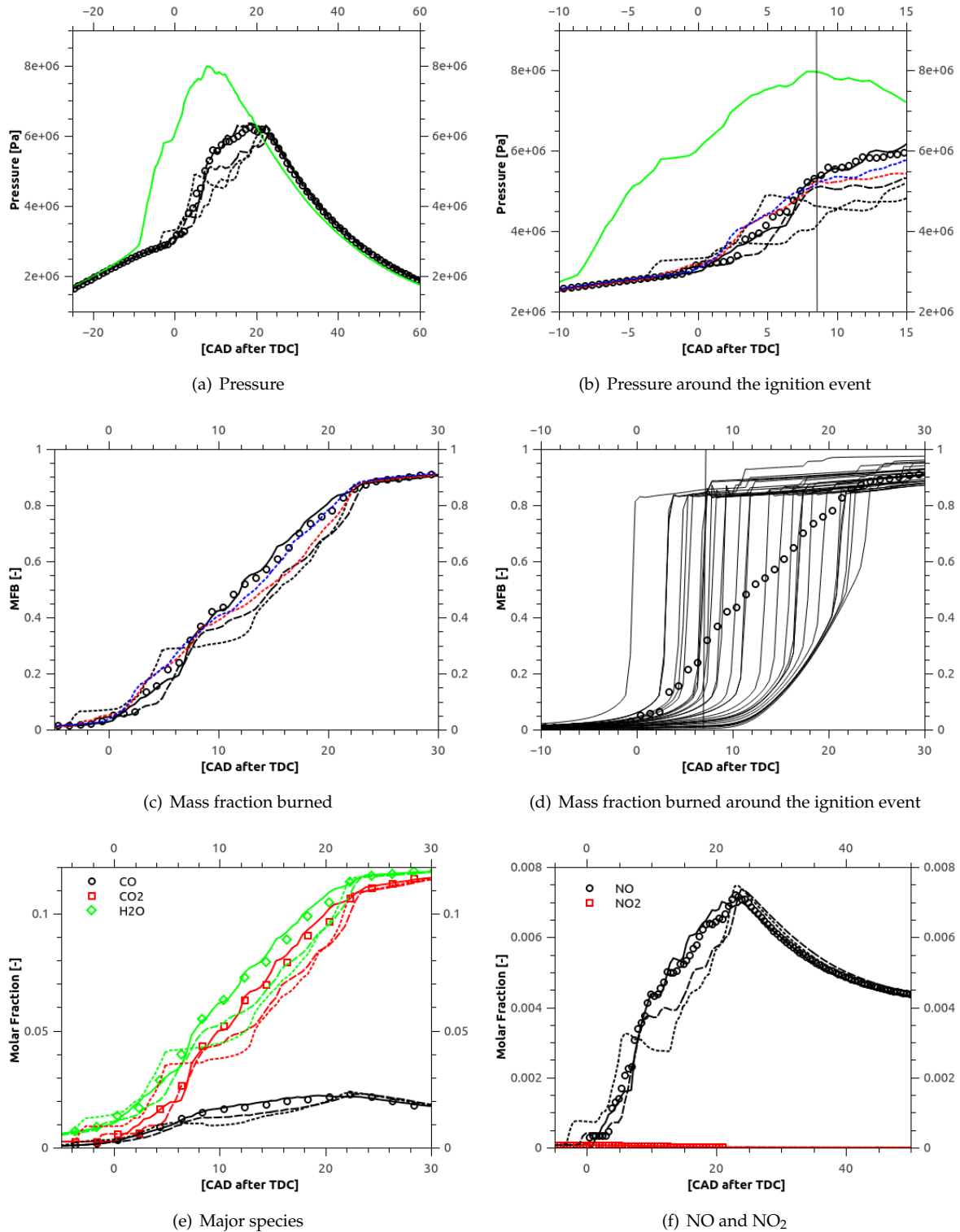
Figure 117: Comparison of combustion prediction (510.4 K inlet temperature) with different reduction stages using the settings given in table 24 and the fuel composition from table 30. Open symbols: modified lumped scheme; solid line: species removal (181 species); dashed line: reaction removal (179 species); dotted line: further reduction by hand (130 species). Solid green line in (a) and (b) is the prediction using the not modified scheme. Dotted red line in (b) and (c) is the average of 100 cycle using the 130 species mechanism, the dotted blue line is the avarage of 100 cycles using the modified lumped scheme. Vertical line denotes spark timing (turb. θ).
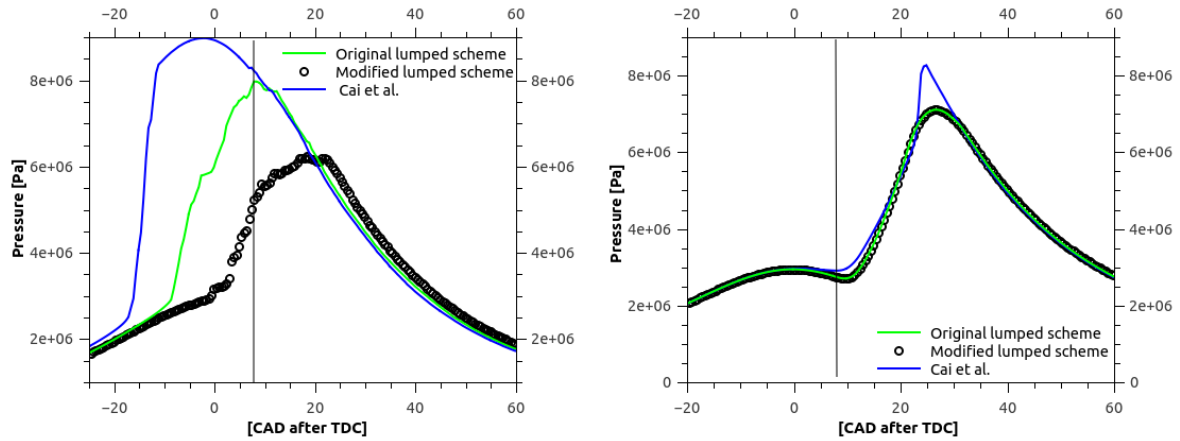
(a) 510.4 K inlet temperature

(b) 360.4 K inlet temperature
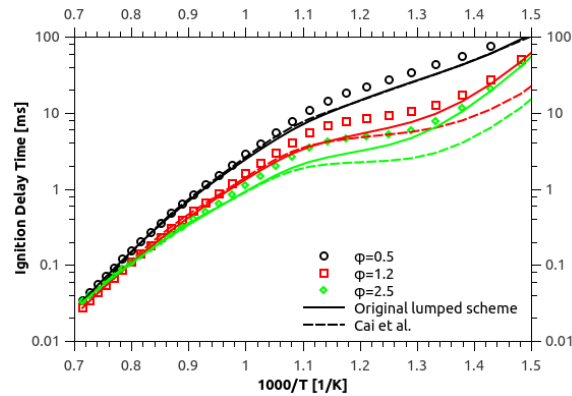
(c) Ignition delay time for E10 surrogate. Open symbols: prediction using the modified lumped scheme.

Figure 118: Comparison of combustion prediction with three different mechanisms. Settings are given in table 24 and the fuel composition from table 30. Figure (a) and (b): Open symbols: modified lumped mechanism; green line: not modified lumped mechanism; blue line: reaction scheme from Cai et al. [149]. Vertical line denotes spark timing (turb. θ).

11.2   Mechanism for flame speed prediction

The mechanism reduction targeted solely on flame speed prediction was carried out in the proposed way. The reduction settings and controlled parameters are given in table 32. Since flame calculations are more computational expensive than 0D calculation much less parameter combinations are controlled in each reduction step. The species removal reduced the scheme by more than 300 species reducing the CPU time by more than a factor of 10 (see table 33). Thereafter the reaction removal reduced the CPU time by factor eight. Finally the introduction of global steps and application of other reduction techniques (removing unimportant reverse reactions, introducing global steps,...) by hand reduced the CPU time demand by factor two. This 49 species / 214 reaction mechanism is about 170 time faster calculating a stoichiometric iso-octane flame at 600 K and 20 bar than the original mechanism. As shown in figure 119 all reduced schemes show a very close agreement with the original scheme. The fact that laminar flame speed is also well predicted for inlet temperatures of 600 K indicates that is seems to be sufficient to control only two points in inlet temperature to capture the response on temperature change.

Parameter	Settings or limits
Fuel 1	ethanol
Fuel 2	25% (molar) of each fuel
Fuel 3	iso-octane
Fuel 4	n-heptane
Fuel 5	toluene
Oxidizer	artificial air
Inlet pressure (Fuel 1-5) [bar]	1.0, 10.0, 25.0
Inlet temperature (Fuel 1-5) [K]	350.0, 450.0
Inlet ϕ (Fuel 1)	0.7, 0.9, 1.1, 1.3
Inlet ϕ (Fuel 2 - 5)	0.6, 0.9, 1.1, 1.3, 1.5
Concentration control (Fuel 1-5)	CO_2, CO and H_2O within 20%
Laminar flame speed control (Fuel 1-5)	6%
Reactor model	Freely propagating flame
Necessary species	$i-C_8H_{18}$, $n-C_7H_{16}$, A_1CH_3, C_2H_5OH, N_2, O_2, CO, CO_2, H_2, H_2O, CH_3, H , OH, O

Table 32: Table with reduction settings for the scheme focused on laminar flame speed prediction.

Reduction step	Number of species and reactions	CPU time [s]
Lumped	386 / 4511	1284.7
Species removal	78 / 849	112.9
Reaction removal	74 / 321	14.2
Global steps	49 / 214	7.5

Table 33: Milestones during the reduction for prediction of laminar flame speed only. CPU time denotes the computational time for simulating a stoichiometric iso-octane flame at 600 K / 20 bar from scratch using the different schemes.

(a) n-heptane

(b) iso-octane

(c) toluene

(d) ethanol

(e) 4 component mixture
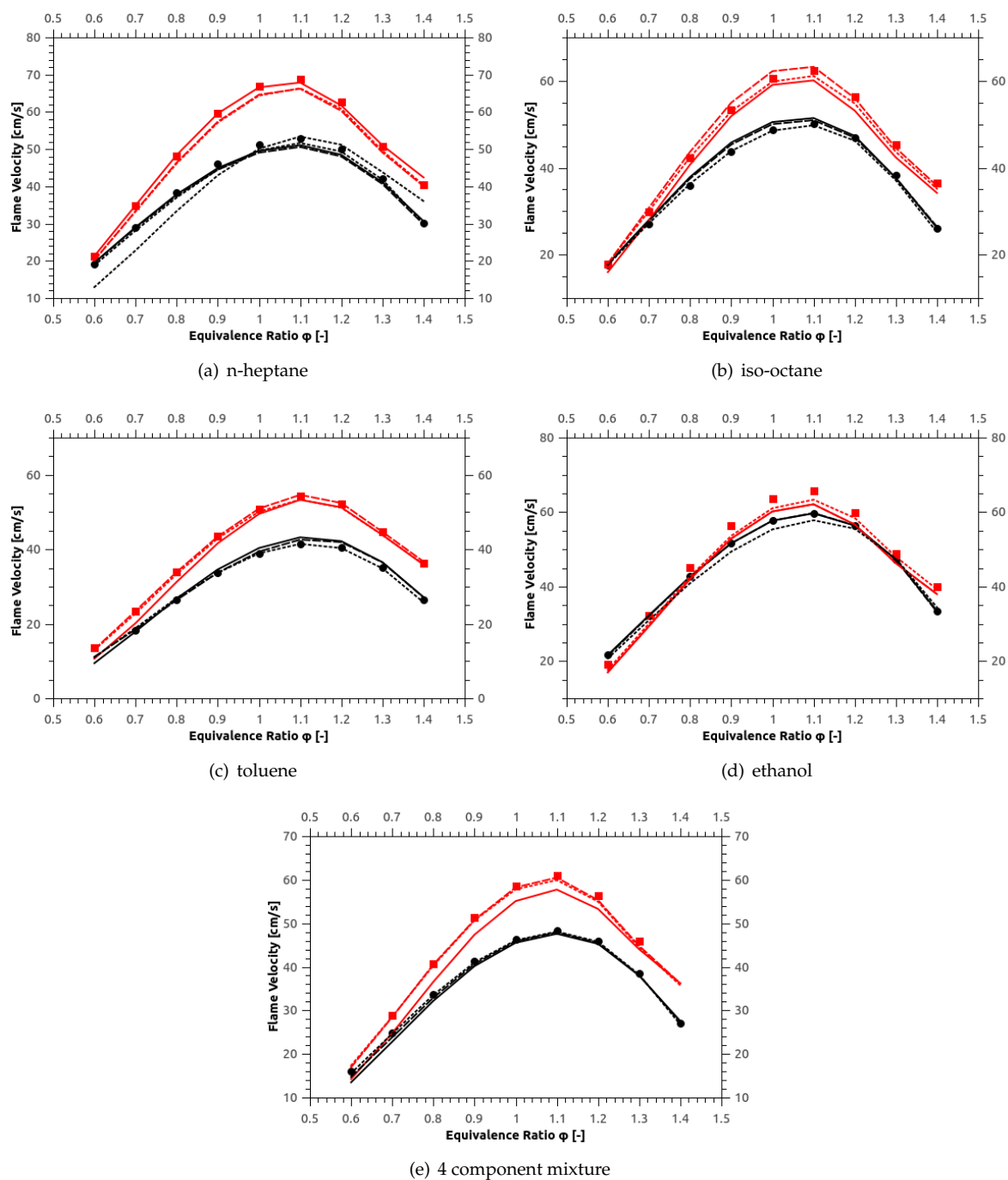
Figure 119: Laminar flame speeds for all four pure fuels and a quaternary mixture (25% (molar) each fuel) at 1 bar / 350 K (black) and 20 bar / 600 K (red). Symbols: 386 species mechanism; Dotted lines: 78 species mechanism (species removal); Dashed line: 74 species mechanism (reaction removal); Solid line: 49 species mechanism (introduction of global steps).

12   Conclusions and Outlook

In this work a novel sequence of mechanism reduction techniques along with a new method for quality control was applied to a newly developed ETRF gasoline surrogate mechanism. The detailed reaction scheme was developed based on publications in collaboration with different research groups and further validated against experiments published in literature. The mechanism is able to predict combustion in a wide range of pressure, temperature and fuel equivalence ratio for pure components and multi component mixtures. The scheme is able to predict aromatic species up too a size of two rings and is compatible with published models to calculate the formation of soot. This scheme was used to compare published correlations between ignition delay time obtained in 0D reactors with experimental octane ratings. Based on a literature review several arguments were brought forward why 0D correlations with the MON are not suitable for fuels with a high heat of vaporization. It was lined out why MON ratings are not a suitable fuel quality rating for direct injection spark ignited engines fuelled with oxygenated fuels such as methanol or ethanol. Based on the RON correlation two very sensitive reactions for the interaction of alkanes and aromatic species in the low temperature regime were revised. The interaction between both fuels exemplarily shows that it is not sufficient to develop multicomponent mechanisms by focusing solely on the performance of pure fuels.

A method for the formulation of ETRF gasoline surrogate mixtures was developed based on different publications and verified for measurements of TRF mixtures. Surrogate mixtures were derived from fuel data sheets for commercial gasoline and the discrepancies between them were outlined. From the compiled detailed reaction scheme different reduced schemes for specialised applications were successful generated using the proposed sequence of reduction steps. It was proven that this method can be applied to much larger reaction schemes from other authors leading to very compact reaction schemes. Further it was demonstrated that the reduction procedure can be more accurate than the experimental uncertainty of ignition delay time determination. This subsequently means that the combustion community needs more measurements of ignition delay times for engine relevant surrogate fuels and its mixtures in the temperature region between 800 and 1000 K and engine relevant pressure ranges. The published experiments to the present day show deviations which can translate up to several CAD degree of ignition onset in todays engine. Additional experiments in CFR engines or shock tubes for n-heptane / toluene mixtures with low toluene content could provide a prove for the hysteresis effect of toluene addition observed in this work.

Since this work covers various topics there are various points from which the research should be continued. The detailed chemistry model should be extended to cover additional surrogate components and recently proposed fuel decomposition pathways should be included. More over additional surrogate components would allow for a wider spread in boiling points. This would offer the possibility to also consider the boiling line of the real

fuel in the formulation of a surrogate fuel. Additional surrogate components would require to extend the mixing rules to determine the octane rating. The lumping process could be improved by using structural information in addition to the thermodynamic data and molecular formula available in the NASA format. Since data about the molecular structure are not available in standard format they could be obtained from a mechanism generator. The reduction procedure is already largely automated, however the introduction of global steps should probably be automated as well. The introduction of an additional flow and sensitivity based reaction rate reoptimisation after each reduction step or milestone would lead to even smaller reaction schemes with a higher accuracy. To shorten the CPU time needed for reaction removal, an analysis similar to the necessity analysis for species should be introduced.

13   Appendix I - Basic Equations

13.1   Thermodynamics

13.1.1   Basic Variables

13.1.1.1   Ideal Gas Law
The ideal gas law is a state equation for an ideal gas which is a good approximation for most gases. Since it neglects molecular size and intermolecular forces, the best accuracy is achieved for monomolecular gases at high temperatures and low pressures.

$$pV = nR_0T$$

Where p is the pressure, V is the volume, n the number of molecules in moles, R_0 the ideal gas constant and T the absolute temperature in Kelvin. Where R_0 can be calculated at product of $R_0 = N_A k_B$.

13.1.1.2   Molecular Mass
The molecular mass W_i of species i is given by the sum of the atomic weights of all elements j in species i, weighted by the number of elements a_{ij} in the given species i.

$$W_i = \sum_j a_{ij} W_j$$

As an example, molecular hydrogen H_2, which consists of two hydrogen atoms, will have a molecular mass of twice the molecular mass of atomic hydrogen, H. Mean molecular mass can be calculated from a given mixture of species via *Eq.* (13.1)

$$W_i = \frac{m_i}{n_i} \tag{13.1}$$

13.1.1.3   Mole Fraction
One mole is defined as 6.0236×10^{23} molecules (Avogadro's number). With n_i being the number of moles of species i in a mixture, the total number of moles, n, is defined as

$$n = \sum_i n_i$$

The mole fraction of species i is given by the fraction of moles it occupies relative to the total number of moles in the mixture:

$$X_i = \frac{n_i}{n} \tag{13.2}$$

The sum of mole fractions will necessarily become unity.

13.1.1.4   Mass Fraction
n_i moles of species i in a mixture will have the mass m_i as specified below:

$$m_i = W_i n_i$$

The total mass of the mixture is the sum of the masses of each species in the mixture.

$$m = \sum_i m_i$$

The mass fraction of species i is given by the fraction of mass it occupies relative to the total mass in the mixture. The sum of mass fractions, like the sum of mole fractions, necessarily becomes unity.

$$Y_i = \frac{m_i}{m} \tag{13.3}$$

13.1.1.5 Mean Molecular Mass
The mean molecular mass of a mixture is defined according to Eq. (13.4).

$$\overline{W} = \frac{m}{n} \tag{13.4}$$

Combining the equations for mass and mole fractions (Eqs. (13.2) and (13.3)), one obtains an expression for the relationship between mole and mass fractions:

$$Y_i = \frac{W_i}{\overline{W}} X_i$$

13.1.1.6 Concentration
The molar concentration of a species i in a mixture is defined as the quantity of moles of this species per unit volume. Concentration of species i is given as either c_i or [i].

$$c_i = \frac{n_i}{V}$$

13.1.1.7 Partial Pressure and Partial Volume
The partial pressure p_i of species i is the pressure exerted on the surroundings by that species alone. Using equations in the previous sections, it can be defined in the following ways:

$$p_i = \frac{n_i R_0 T}{V} = c_i R_0 T = \frac{\rho X_i}{\overline{W}} R_0 T = \frac{\rho Y_i}{W_i} R_0 T$$

with

$$\rho = \frac{m}{V}$$

being the mass density. The total pressure of the mixture is the sum of partial pressures:

$$p = \sum_i p_i = \frac{n R_0 T}{V}$$

The partial pressure can also be expressed using species mole fractions:

$$p_i = X_i p$$

Equivalently, the partial volume a species i occupies is given by Eq. (13.5).

$$V_i = X_i V \tag{13.5}$$

13.1.1.8   Equivalence Ratio

Equivalence ratio relates the mass fraction of fuel to oxidizer in the unburned mixture to that of complete combustion (or stoichiometric mixtures). It is calculated from the amount of carbon, hydrogen and oxygen in the mixture:

$$\Phi = \frac{\frac{Y_{(C,H)u}}{Y_{(O)u}}}{\left(\frac{Y_{(C,H)u}}{Y_{(O)u}}\right)_{\text{stoich}}}$$

where u denotes unburned.

Depending on whether a mixture is fuel lean or fuel rich, the value of Φ will vary as seen below.

$$\textit{Stoichiometric: } \xi = \xi_{\text{stoich}} \rightarrow \Phi = 1$$
$$\textit{Fuel rich: } \xi > \xi_{\text{stoich}} \rightarrow \Phi > 1$$
$$\textit{Fuel lean: } \xi < \xi_{\text{stoich}} \rightarrow \Phi < 1$$

Equivalence ratio is related to lambda,

$$\lambda = \frac{AFR}{(AFR)_{\text{stoich}}}$$

where AFR, air-fuel ratio, is defined as

$$AFR = \frac{m_{\text{air}}}{m_{\text{fuel}}}$$

through the following relation:

$$\Phi = \frac{1}{\lambda}$$

13.1.2   Transport Coefficients

The transport properties viscosity, thermal conductivity and diffusion, describe transport of physical properties due to movement in the gas. To account for intermolecular interaction the Lennard-Jones potential model is used, which is characterised by the molecular diameter σ and the depth of the intermolecular potential, ε. σ and ε are used to determine reduced collision integrals, ω, which are factors accounting for the deviation from the model of rigid elastic spheres. Values for these parameters are calculated from data in the molecular data input file (see 13.2.2.3).

13.1.2.1   Viscosity

Viscosity is momentum being transported between regions in the gas due to velocity gradients and a measure of resistance to shear stresses. It is determined by how the molecules in the gas interact, increases with temperature and is independent of pressure.

Species viscosity, η_i, is given by

$$\eta_i = 2.6693 \cdot 10^{-6} \sqrt{\frac{W_i T}{\omega_i(T)\sigma_i^2}}$$

Considering all individual viscosities, the resulting bulk viscosity is calculated as the weighted average:

$$\eta = \frac{1}{2}\left(\sum_i X_i \eta_i + \left(\sum_i \frac{X_i}{\eta_i}\right)^{-1}\right)$$

13.1.2.2   Thermal Conductivity   *Thermal conduction is energy transport due to temperature gradients and measures how well a substance conducts heat. The conductivity is determined not only by how molecules interact but also by their vibrational and rotational state (which in turn depend on the orientation of the atoms in the molecules).*

Species conductivity, λ_i, is related to species viscosity through the following expression:

$$\lambda_i = \frac{\eta_i}{W_i}\text{fact}(n)$$

Here fact(n) is a factor function calculating the net energy contained in the species and depends on excitation and the vibrational and rotational states of the molecules. It is a function of the number of atoms, n, in the species.

Overall thermal conductivity is defined as the weighted average of the species individual thermal conductivities.

$$\lambda\left(T\right) = \frac{1}{2}\left(\sum_i X_i \lambda_i + \left(\sum_i \frac{X_i}{\lambda_i}\right)^{-1}\right)$$

13.1.2.3   Diffusion   LOGESOFT *accounts for two types of diffusion; mass transport due to concentration gradients ("diffusion") and mass transport due to temperature gradients ("thermal diffusion"). Their respective expressions are given by Fick's Law and Fourier's Law.*

Binary diffusion coefficients, i.e. diffusion coefficients for a gas consisting of two species i and j where one diffuses into the other, are given by

$$d_{i,j} = 2.6693 \cdot 10^{-9} \sqrt{\frac{\left(\frac{W_i + W_j}{W_i W_j}\right) T^3}{\omega_{i,j} \; \sigma_{i,j}^2}}$$

where the collision integral and the collision diameter are weighted and averaged, depending on the dipole parameters of species i and j.

The diffusion coefficient for how species i diffuses into all other species in a mixture is calculated from the following expression:

$$d_i = \frac{(1 - X_i)}{p_{\text{ref}} \sum_j^{N_s} X_i d_{i,j}}$$

The terms $(1 - X_i)$ and p_{ref} appear due to the species diffusion being dependent on the mass of the remaining species.

Thermal diffusion coefficients are given by

$$d_i^T = \frac{1 - Y_i}{1 - X_i} \frac{X_i}{2} \sum_j \left(T_{\text{red}} X_j \frac{W_i - W_j}{W_i + W_j} \right)$$

where T_{red} is 298 K.

13.1.2.4 Lewis Number
The Lewis number, Le_i, measures the ratio of thermal diffusivity, α_i, to that of mass diffusivity, D_i;

$$Le_i = \left(\frac{\alpha_i}{D_i} \right)$$

where $\alpha_i = \frac{\lambda}{\rho c_{\mathrm{p}\,i}}$.

In a majority of combustion environments, species Lewis numbers are unity. However, for some small species, such as H and H_2 that have high diffusivity constants, the Lewis number is lower than unity. The assumption of unity for the Lewis number is very common since the it greatly simplifies energy equations.

13.1.3 State Functions

State functions describe properties that define an equilibrium state of a thermodynamic system.

13.1.3.1 Density
Mass density is the ratio between mass and volume, defining how closely packed together the molecules are. LOGESOFT calculates both species densities and overall density from the ideal gas law:

$$\rho_i = \frac{p W_i}{R_0 T}$$

$$\rho = \frac{p \overline{W}}{R_0 T}$$

13.1.3.2 Heat Capacity
Heat capacity is the measure of a system's change in temperature due to heat transfer:

$$C = \frac{dQ}{dT} \tag{13.6}$$

The heat capacity depends on whether the transferred heat is added at constant pressure or at constant volume (denoted C_{p} and C_{V} respectively).

13.1.3.3 Internal Energy
Internal energy, U, is the sum of kinetic and potential energy in a system, including energy in chemical bonds but not energy associated with the system as a whole. U_i is the corresponding internal energy of a species i in the system.

The first law of thermodynamics states that change in a system's internal energy is the sum of the heat exchange with the surroundings (δQ), the work done by the system (δW) and the energy contained in particles added to the system:

$$dU = dQ - dW + \sum_i \mu_i dn_i \tag{13.7}$$

where μ_i is the chemical potential of species i and n_i is number of moles of that species. For a closed system the last term of Eq. (13.7) is zero.

Since LOGE SOFT *only takes volume work into account, the following expression for work can be used:*

$$dW = pdV$$

For a closed system at constant volume, the work done by the system is zero and the change in internal energy is equal to heat entering or leaving the system. This makes internal energy convenient to use when defining the energy content of a closed system at constant volume:

$$dU_V = dQ \tag{13.8}$$

From Eq. (13.6) it can be seen that Eq. (13.8) is the same as $C_V dT$, which in turn leads to the following expression for the temperature dependence of the internal energy:

$$U|_V = U_{298} + \int_{298}^{T'} C_V dT$$

13.1.3.4 *Enthalpy* *Enthalpy, H, defines the energy content of a system as the sum of its internal energy and volume work, i.e. the total energy of the system:*

$$H = U + pV$$

From this definition, a change in enthalpy in a closed system can be expressed as

$$dH = dU + Vdp + pdV = dQ - pdV + Vdp + pdV = dQ + Vdp$$

Thus, at constant pressure, the change in enthalpy is equal to heat transferred to or from the system.

$$dH_p = dQ \tag{13.9}$$

From Eq. (13.6) it can be seen that this is the same as $C_p dT$, which can be used to express the temperature dependence of the enthalpy:

$$H|_p = H_{298} + \int_{298}^{T'} C_p dT$$

where H_{298} is the enthalpy of formation of the current gas mixture.

13.1.3.5 *Entropy* *Entropy, S, is a measure of the unavailability of a system's energy to perform work. The second law of thermodynamics states that the total enthalpy of a system and its surroundings can only increase or remain constant. Thus, if energy added to a system as heat is used to increase the entropy of the system, this energy can never be used by the system to perform work. Entropy is defined through*

$$dS = \frac{dQ}{T} + \frac{dW_{dis}}{T} \tag{13.10}$$

where equality holds in the case of dQ being reversible.

Similarly to internal energy and enthalpy, entropy's temperature dependence can be expressed using heat capacity:

$$S|_\text{p} = S_{298} + \int_{298}^{T'} \frac{C_\text{p}}{T} dT$$

$$S|_\text{V} = S_{298} + \int_{298}^{T'} \frac{C_\text{V}}{T} dT$$

13.1.3.6   Gibbs Free Energy

Gibbs free energy is the maximum amount of energy in a thermodynamic system available to perform mechanical work at isothermal and isobaric conditions and is defined as

$$G = H - TS \tag{13.11}$$

Using Eqs. (13.9) to (13.11), the change in Gibbs free energy at constant pressure is minimised according to

$$dG|_\text{p} = -SdT$$

which is why Gibbs free energy is a useful quantity at isobaric conditions.

Equilibrium for a constant pressure case is calculated through minimisation of Gibbs free energy for constant atomic mass fractions.

13.1.3.7   Helmholtz Free Energy

Helmholtz free energy defines the maximum amount of energy available to perform work in a thermodynamic system at isothermal and isochoric conditions and is defined as

$$A = U - TS \tag{13.12}$$

Using Eqs. (13.9), (13.10) and (13.12), the change in Helmholtz free energy at constant volume is minimized according to

$$dA|_\text{V} = -SdT$$

which is why Helmholtz free energy is a useful quantity at isochoric conditions.

Equilibrium for a constant volume case is calculated through minimisation of Helmholtz free energy for constant atomic mass fractions.

13.1.3.8   NASA Polynomials

LOGESOFT uses polynomial functions of temperature to derive state functions and heat capacity. The polynomial coefficients for each species are provided in the state function input file in standard format for NASA coefficients.

$$\frac{C_\text{p,i}}{R_0} = a_{1,i} + a_{2,i}T + a_{3,i}T^2 + a_{4,i}T^3 + a_{5,i}T^4 \tag{13.13}$$

$$\frac{H_i}{R_0 T} = a_{1,i} + \frac{a_{2,i}}{2}T + \frac{a_{3,i}}{3}T^2 + \frac{a_{4,i}}{4}T^3 + \frac{a_{5,i}}{5}T^4 + \frac{a_{6,i}}{T} \tag{13.14}$$

$$\frac{S_i}{R_0} = a_{1,i}\ln(T) + a_{2,i}T + \frac{a_{3,i}}{2}T^2 + \frac{a_{4,i}}{3}T^3 + \frac{a_{5,i}}{4}T^4 + a_{7,i} \tag{13.15}$$

All other thermodynamic properties can be derived from the above polynomials.

For each species, fourteen coefficients are provided in the state functions input file, covering the seven coefficients needed in Eqs. (13.13) to (13.15) for two consecutive temperature ranges.

13.1.4 Heat Transfer

13.1.4.1 Radiation LOGESOFT *derives thermal radiation from the Stefan-Boltzmann law, according to which the heat emitted by a blackbody per unit time is proportional to the fourth power of its absolute temperature. For non-black bodies—which do not emit radiation perfectly as black bodies do—emissivity needs to be taken into account.*

$$\dot{Q}_{rad} = \sigma \varepsilon A \left(T^4 - T_w^4 \right)$$

Here σ is the Stefan-Boltzmann constant and ε is the emissivity. T_w is the temperature of the surroundings which in LOGESOFT is assumed to be the same as the initial temperature of the gas.

Since radiation in gases is absorbed and emitted throughout the gas volume, the number of molecules along the radiation path needs to be taken into account. This depends on temperature and is proportional to the product of the species' partial pressure and the path length, i.e. $\varepsilon = f(T, p_{sl})$, where s are the radiating species. The mean path length is proportional to the mean path length of a hemispherical enclosure, $l \sim 4V / A$. The total emissivity is calculated from

$$\varepsilon = \sum_s \varepsilon_s p_s$$

where ε_s is the emissivity for the radiating species s. Only CO_2, H_2O and soot is taken into account when calculating the radiation in LOGESOFT, since these hot products of combustion make up the major part of radiation. This approximation makes the model valid only for burned gases. ε_s for CO_2 and H_2O can be seen below.

$$\varepsilon_{CO_2} = 46.241 e^{-8.888 * 10^{-4} T}$$

$$\varepsilon_{H_2O} = 22.6 e^{-1.546 * 10^{-8} T}$$

The net heat flow of radiating energy from a gas to cooler surroundings is thus given by

$$\dot{Q}_{rad} = 4 \sigma V \left(T^4 - T_w^4 \right) \varepsilon$$

13.2 Chemical Kinetics

The quality of the results from LOGESOFT depends on the quality of the chemical model used. Each chemical model is based on the fuel and oxidizer it is developed for. Typically the more complex the fuel, the more complex the chemical model will be. This implies that a small fuel species like hydrogen has a chemical model of less than ten species and that more complex fuel species like iso-octane might have several hundred species. The complexity of the fuel is not the only thing dictating the size of the chemical model; if emissions such as NO_x and soot are to be calculated, chemical submodels with relevant species and reactions need to be included. Typically the size of the chemical model gives an exponential increase of computational time.

13.2.1   Basics of Chemical Kinetics

Any elementary chemical reaction can be represented by the general equation

$$v'_A A + v'_B B + \ldots = v''_C C + v''_D D + \ldots$$
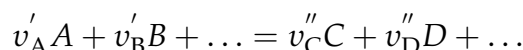
where the v are known as stoichiometric coefficients, defining how many moles of the given species take part in the reaction. Superscript $'$ indicates reactants and $''$ indicates products.

A net stoichiometric coefficient, v_S, gives the total number of moles of species S that is produced or consumed by a reaction.

$$v_S = v''_S - v'_S$$

The production (or consumption) rate of a species S, $\dot{\omega}_S$, depends on the reaction rates of the reactions producing and consuming the species, and on the concentration of all species participating in those reactions. In 13.17 and 13.16, $r\,(= 1, 2, \ldots R)$ denotes reactions and s denotes species.

$$\dot{\omega}_S = \frac{d\,[s]}{d\,[t]} = \sum_{r=1}^{R} v_{r,S} q_r \tag{13.16}$$

$$q_r = k_{f,r} \prod_s [S]^{v'_{r,s}} - k_{b,r} \prod_s [S]^{v''_{r,s}} \tag{13.17}$$

13.2.1.1   Third-body Species   LOGESOFT *considers reactions including third-body species, denoted with the symbol M. These species are needed in certain reactions to provide necessary energy or carry away excess energy in order for the reaction to proceed, but do not change the chemical composition in the process. The recombination of H_2O below is an example of when third body species are used.*

$$H + OH + M1 = H_2O + M1 \tag{13.18}$$

When third-body species are taken into account the reaction progress rate variable q_r in 13.17 is modified to

$$q_r = \left(\sum_s \alpha_{r,s} [s] \right) \left(k_{f,r} \prod_s [s]^{v'_{r,s}} - k_{b,r} \prod_s [s]^{v''_{r,s}} \right) \tag{13.19}$$

where $\alpha_{r,s}$ is the enhancement factor for species s in reaction r. If all species contribute equally as third-body species all $\alpha_{r,s} = 1$, which makes the first factor in 13.19 the total concentration of the mixture. Certain species may have higher impact on the reaction and can thus be given a higher enhancement factor (see 13.2.2.2 for information on how to set this factor).

13.2.1.2   Pressure Dependent Fall-Off Reactions   *Dissociation and recombination reactions are not elementary but rather a sequence of reactions, which is reflected in their pressure dependence. According to the Lindemann model [150], these reactions require energy to be added or carried away by a third body, the concentration of which depends on the pressure. The sequence of*

reactions is made from three kinds of reactions:

$$\text{S} + \text{M} \xrightarrow{k_\text{a}} \text{S}* + \text{M} \tag{13.20}$$

$$\text{S}* \xrightarrow{k_\text{u}} \text{P} \tag{13.21}$$

$$\text{S}* + \text{M} \xrightarrow{k_{-\text{a}}} \text{S} + \text{M} \tag{13.22}$$

where S represents a species, M a third-body molecule and P the products. k_a is the rate coefficient for the activation reaction (Eq. (13.20)), k_u the rate coefficient for the unimolecular reaction (Eq. (13.21)) and $k_{-\text{a}}$ the rate coefficient for the deactivation reaction (Eq. (13.22)). The concentration of $S*$ can be assumed to be in a quasi-steady state which yields

$$\frac{d\,[\text{S}*]}{dt} \approx 0 \tag{13.23}$$

Using Eq. (13.16) and Eq. (13.23) for $S*$ and P gives

$$\frac{d\,[\text{P}]}{dt} = \frac{k_\text{u}k_\text{a}\,[\text{S}]\,[\text{M}]}{k_{-\text{a}}\,[\text{M}] + k_\text{u}}$$

At low pressures the concentration of M is small and $k_{-\text{a}}[M] \ll k_\text{u}$, which leads to Eq. (13.24).

$$\frac{d\,[\text{P}]}{dt} = k_\text{a}\,[\text{S}]\,[\text{M}] \equiv k_0\,[\text{S}]\,[\text{M}] \tag{13.24}$$

At high pressures the concentration of M is high and $k_{-\text{a}}[M] \gg k_\text{u}$, which leads to Eq. (13.25).

$$\frac{d\,[\text{P}]}{dt} = \frac{k_\text{u}k_\text{a}\,[\text{S}]}{k_{-\text{a}}} \equiv k_\infty\,[\text{S}] \tag{13.25}$$

The rate coefficients k_0 and k_∞ are supplied to LOGESOFT *in the form*

$$k_0 = A_0 T^{n_0} e^{-\frac{E_0}{R_0 T}} \tag{13.26}$$

$$k_\infty = A_\infty T^{n_\infty} e^{-\frac{E_\infty}{R_0 T}} \tag{13.27}$$

The Lindemann approach as was explained above results in an error caused by inefficient collisions and non-steady state behaviour. Troe introduced a temperature dependent symetric F_cent. Studying the rate law on the form $d[P]/dt = k[A]$, the pressure dependence of k is drawn as fall-off curves (also depending on temperature). Using the formalism of Troe et al [151] these fall-off curves can be described using four parameters determining the center of the fall-off range: (a, T^{***}, T^* and T^{**})

$$F_\text{cent} = (1-a)\,e^{-T/T^{***}} + a e^{-T/T^*} + e^{-T^{**}/T}$$

The center of the fall-off range can in turn be used to calculate a factor F which modifies the rate coefficient for weak colliders according to Eq. (13.28)

$$k = k_\infty \left(\frac{P_\text{r}}{1 + P_\text{r}} \right) F \tag{13.28}$$

where

$$\log(F) = \left\{ 1 + \left[\frac{\log\left(P_{\mathrm{r}}\right) + c}{n - d\left(\log\left(P_{\mathrm{r}}\right) + c\right)} \right]^2 \right\}^{-1} \cdot \log(F_{\mathrm{cent}})$$

$$c = -0.4 - 0.67 \log\left(F_{\mathrm{cent}}\right)$$

$$n = 0.75 - 1.27 \log\left(F_{\mathrm{cent}}\right)$$

$$d = 0.14$$

$$P_{\mathrm{r}} = \frac{k_0\left[M\right]}{k_\infty}$$

Another way to modify the rate coefficients is the standard of SRI International [152], which calculates F slightly differently:

$$F = d \left[a e^{-b/T} + e^{-T/c} \right]^X T^e$$

where

$$X = \frac{1}{1 + \log^2(P_{\mathrm{r}})}$$

P_r *is calculated in the same manner as for the Troe formalism.*

13.2.1.3 Pressure Dependence Through Logarithmic Interpolation *In a reaction mechanism, multiple reaction coefficients that are valid at different pressures may be given for a single reaction.* LOGESOFT *can logarithmically interpolate for the actual pressure based on the given coefficients.*

13.2.2 Reaction Mechanisms

13.2.2.1 Gas Phase Data *The gas phase data files state which chemical elements that are included in the mechanism as well as the chemical species these elements make up. Thereafter the data files present a list of reactions the species may participate in and corresponding coefficients, A, n and E_a, used in the Arrhenius law reaction rate calculation (see Section 13.2.1 and Eq. (13.26)). Variables for calculating the rate of the backwards reactions are also stated in the gas phase file.*

13.2.2.2 Third-Body Reactions *Third-body reactions are written with a species M as reactant or product (normally it appears as both). Auxiliary information regarding enhanced third-body efficiencies of certain species may be given on the line below the reaction. This information is given with the name of the species followed by the enhancement factor within slashes. For more information about enhancement factors, see 13.2.1.1. Below is an example of a third-body reaction.*

```
O+CO+M<=>CO2+M            1.800E+10    0.00    8600.00
H2/2.00/ O2/6.00/ H2O/6.00/ CO/1.50/ CO2/3.50/ AR/0.50/
```

13.2.2.3 Molecular Data *The molecular data files list the following seven variables for each species in the mechanism:*

- *chemical name*

- *indicator for the structure of the species (0 = atom, 1 = linear molecule, 2 = non-linear molecule)*

- *two parameters describing the shape of the Lennard-Jones potential well: well depth divided by Boltzmann's constant [K] and collision diameter [Å], i.e. the (finite) distance at which the interparticle potential is zero.*

- *the bond dipole moment [Debye]*

- *the polarisability [Å]*

- *the rotational collision number (Z_{ROT}) at 298 K*

Since the molecular data is species specific, any file that contains data for all species in the gas phase or solid state phase files can be used. Below is an example of the structure of a molecular data file.

```
H              0 0.145E+03 0.205E+01 0.000E+00 0.000E+00 0.000E+00
O              0 0.800E+02 0.275E+01 0.000E+00 0.000E+00 0.000E+00
OH             1 0.800E+02 0.275E+01 0.000E+00 0.000E+00 0.000E+00
HO2            2 0.107E+03 0.346E+01 0.000E+00 0.000E+00 0.100E+01
H2O2           2 0.107E+03 0.346E+01 0.000E+00 0.000E+00 0.380E+01
CH             1 0.800E+02 0.275E+01 0.000E+00 0.000E+00 0.000E+00
HCO            2 0.498E+03 0.359E+01 0.000E+00 0.000E+00 0.000E+00
...
```

13.3 Homogeneous Reactor Models

Combustion processes obey the laws of thermodynamics. Hence, for each simulation in LOGEsoft, *the balance equations for mass, energy and momentum need to be solved. All balance equations are based on the Navier-Stokes equation for reactive flow:*

$$\frac{\partial W}{\partial t} + \frac{\partial J}{\partial x} = Q$$

For any variable V, W is the density of V, Q is a source or sink term describing production or consumption of V and J is the flux density of V.

All reactor specific equations can be derived from the Navier-Stokes equation (see for example [44], [153]).

13.3.1 Constant Volume Reactor

A Constant Volume reactor consists of a closed rigid vessel in which the volume is kept constant during combustion, allowing the pressure to increase. Although this device is used in research much less than the Perfectly Stirred Reactor (PSR) or the Plug Flow Reactor (PFR), it is often employed for calorimetric studies to determine the heats of formation for various fuels.

As the constant volume reactor is a closed system, the balance equations can be simplified to conservation equations. Since no mass flows into or out of the system and since mass is preserved, the mass conservation equation reads

$$\frac{dm}{dt} = 0 \tag{13.29}$$

Since $Y_{i,l} = Y_i$, the conservation equation for a species mass fraction becomes

$$\frac{dY_i}{dt} = \frac{\omega_i W_i}{\rho} \tag{13.30}$$

The energy conservation equation is expressed in terms of specific internal energy since the volume is constant. With appropriate simplifications, such as $u_{i,l} = u_i$, one obtains

$$\rho c_{\mathrm{v}} \frac{dT}{dt} = \sigma \varepsilon \frac{A}{V} (T^4 - T_{\mathrm{w}}^4) - \sum_i^{N_{\mathrm{s}}} \omega_i U_i \tag{13.31}$$

As the system is assumed to be stationary and homogeneous, the momentum is zero and no momentum balance equation needs to be solved.

13.3.2   Constant Pressure Reactor

The Constant Pressure reactor represents a gas that is allowed to expand freely. Such a reactor can consist of for instance a tube, closed at one end and with a movable piston at the other, assuring a constant pressure during combustion.

Like the constant volume reactor, the constant pressure reactor is assumed to be a closed system, hence there is no inflow or outflow and the balance equations become simple conservation equations, see *Eqs.* (13.29) *and* (13.30).

The energy conservation equation is expressed in terms of specific enthalpy. Since $h_{i,l} = h_i$, the energy equation becomes

$$\rho c_{\mathrm{p}} \frac{dT}{dt} = \sigma \varepsilon \frac{A}{V} (T^4 - T_{\mathrm{w}}^4) - \sum_i^{N_{\mathrm{s}}} \omega_i H_i \tag{13.32}$$

13.3.3   Perfectly Stirred Reactor

The Perfectly Stirred Reactor model (PSR) is often employed to simulate toroidal jet-stirred reactors, which are practical laboratory devices for research of ignition processes. Experimental reactors employing high velocity inlet jets approach this ideal reactor and have been used to study many aspects of combustion, such as flame stabilization and NO_x formation.

The PSR consists of a constant pressure vessel with inlet and outlet ducts, and may or may not be thermally insulated. A steady flow of gas with a certain composition and temperature is introduced through the inlets. The gas undergoes chemical reactions and eventually exits the chamber through the outlets. The PSR can be regarded as a vessel in which there is extremely strong mixing, giving rise to steady-state solutions of the balance equations.

$$\frac{dm}{dt} = \sum_l^{N_{\mathrm{in}}} \dot{m}_l - \sum_k^{N_{\mathrm{out}}} \dot{m}_k \tag{13.33}$$

Since fresh gas continuously enters the reactor, the PSR contains a mixture of burned and unburned gas. The assumption of homogeneity implies that the gas exiting the vessel must be of the same composition as the gas inside the reactor, i.e. $Y_{i,l} = Y_i$ for all outlets. Following this, the balance equation for a species mass fraction becomes

$$\frac{dY_i}{dt} = \frac{\omega_i W_i}{\rho} + \frac{1}{\rho V} \sum_l^{N_{\text{in}}} \dot{m}_l (Y_{i,l} - Y_i) = \frac{\omega_i W_i}{\rho} + \sum_l^{N_{\text{in}}} \frac{1}{\tau_l} (Y_{i,l} - Y_i) \tag{13.34}$$

where $\tau_l = \frac{m}{\dot{m}_l}$ is the residence time, in practice interpreted as the ratio between the volume flow and vessel volume, which determines the influence of mixing. Since the pressure in the PSR is assumed to be constant, the energy conservation equation is expressed in terms of specific enthalpy:

$$\begin{aligned} \rho c_{\text{p}} \frac{dT}{dt} = &\frac{1}{V} \sum_l^{N_{\text{in}}} \dot{m}_l \sum_i^{N_{\text{s}}} Y_{i,l} (h_{i,l} - h_i) - \sum_i^{N_{\text{s}}} \omega_i H_i \\ &+ \frac{h_{\text{c}} A}{V} (T - T_{\text{w}}) + \sigma \varepsilon \frac{A}{V} (T^4 - T_{\text{w}}^4) \end{aligned} \tag{13.35}$$

The change in energy thus corresponds to the change in enthalpy due to mass influx, chemical reactions and heat losses.

13.3.4 Plug Flow Reactor

The Plug Flow Reactor model (PFR) is an idealised one dimensional model of a tubular reactor, with support for surface chemistry. Gas travelling through the tube is modelled as a series of "plugs": thin discs in each of which the gas is homogeneous. The flow is under steady-state conditions, i.e. it is constant in time and species on the tube walls are in a quasi-steady state. Furthermore, information can only travel in the direction of the flow so all reactor properties can be calculated as functions of distance from the inlet.

The PFR model can be used to simulate for example a catalyst channel or the gas flow in a pipe. Initial values are used at the entrance of the pipe and species, temperature, velocity and density values throughout the rest of the pipe are calculated. The following equation for conservation of mass is obtained:

$$\frac{d(\rho v_x A)}{dx} = \sum_s^{N_{\text{surf}}} \frac{A_s}{V} \sum_i^{N_{\text{s}}} \omega_{i,s} W_i A \tag{13.36}$$

where v_x is the flow velocity, A_s is the area of surface s, A is the cross-sectional area of the reactor and $\omega_{i,s}$ is the production or consumption of species i at surface s. In this setup, mass can be added to the gas as molecules change phase from surface to gas. The conservation of gas phase species mass fractions is given by

$$\rho v_x \frac{dY_i}{dx} = \sum_s^{N_{\text{surf}}} \frac{A_s}{V} \sum_i^{N_{\text{s}}} W_i \omega_{i,s} + W_i \omega_{i,g} - Y_i \sum_s^{N_{\text{surf}}} \frac{A_s}{V} \sum_s^{N_{\text{surf}}} W_i \omega_{i,s} \tag{13.37}$$

The conservation of surface site fractions, θ_i, is given by

$$v_x \frac{d\theta_i}{dx} = \sum_{s}^{N_{\text{surf}}} W_{i,s} \omega_{i,s} \frac{\sigma_{i,s}}{\Gamma_s} \tag{13.38}$$

where Γ_s is site density (assumed constant) and $\sigma_{i,s}$ is the site occupancy number of species i on surface site s.

The energy balance equation is derived from the Navier-Stokes equations as

$$\frac{d(\frac{EAv_x}{V})}{dx} = \frac{dQ}{dx} - \frac{dQ}{dx} + \sum_{i}^{N_s} W_i h_i \sum_{s}^{N_{\text{surf}}} \frac{A_s}{V} \omega_{i,s} A \tag{13.39}$$

The change in momentum is equal to the forces acting on the fluid so the momentum equation can be expressed as

$$\frac{d(A\rho v^2 + A\rho)}{dx} = \sum F_x \tag{13.40}$$

Since the reactor wall has zero velocity, there is no increase of momentum due to transfer of species and energy from the walls to the gas. Expanding the left hand side of *Eq.* (13.40) and substituting *Eq.* (13.39) gives

$$A\rho v_x \frac{dv_x}{dx} = -Fa - A\frac{dp}{dx} - p\frac{dA}{dx} - v_x \sum_{i}^{N_s} W_i \sum_{s}^{N_{\text{surf}}} \frac{A_s}{V} \omega_{i,s} A \tag{13.41}$$

The second term on the right hand side of *Eq.* (13.41) represents the pressure drop through the pipe and the third term discribes momentum changes due to changes in the cross-sectional area. If the tube is uniform, the term from the cross-sectional area disappears.

13.4   Flames

LOGESOFT *defines a flame as a self-sustaining propagation of a localised combustion zone at subsonic velocities (deflagration). The structure of a flame can vary from laminar to turbulent, from premixed to non-premixed, from co-flow to counter-flow etc. All flames in* LOGESOFT *are one dimensional, stationary, with a z-axis perpendicular to the flame front and evaluated at constant pressure.*

13.4.1   Premixed Flames

For a premixed laminar flame, the fuel and oxidant mixture move in the z direction with the unburned mixture at $z \to -\infty$ and the burned mixture at $z \to \infty$. Conservation equations are given as follows, starting with the continuity equation

$$\frac{d(\rho u)}{dz} = 0 \tag{13.42}$$

The species conservation equation is given by

$$\rho u \left(\frac{dY_i}{dz} \right) = - \left(\frac{dj_i}{dz} \right) + \omega_i \tag{13.43}$$

The energy conservation equation is given by

$$\rho u c_{\mathrm{P}} \left(\frac{dT}{dz} \right) = \frac{d}{dz} \left(\lambda \left(\frac{dT}{dz} \right) \right) - \sum_{i=1}^{N_{\mathrm{s}}} h_i \omega_i - \sum_{i=1}^{N_{\mathrm{s}}} c_{\mathrm{P}} j_i \frac{dT}{dz} - 4\alpha\sigma(T^4 - T_0^4) f_{\mathrm{r}} \qquad (13.44)$$

where ρ is the density, u is the gas velocity component, Y_i is the mass fraction of species i, j_i is the diffusion flux, ω_i is the net production rate of species i, c_{P} is the heat capacity at constant pressure, λ is the thermal conductivity, h_i is the specific enthalpy and N_{s} is the number of species. α is Planck's constant, σ the Stefan Boltzmann constant, T_0 the temperature of the surroundings and f_{r} a radiation factor.

The overall mass conservation is represented by the continuity equation (Eq. (13.42)) and yields for moving flows. The species mass conservation equation Eq. (13.43) describes the rate of change of the mass fraction of species i in the flow field due to the diffusion j_i over the flame zone and the production rate ω_i. The energy conservation equation Eq. (13.44) originates from the general assumption that the total energy in the system is unchanged. In Eq. (13.44), the rate of change of the heat transported by convection of the gas is equal to the heat transfer due to conductivity (first term on the right-hand side), the rate of change due to enthalpy release through production of the species (second term on the right-hand side), thermodiffusion (third term on the right-hand side) and radiation (last term on the right-hand side).

The species taken into account for radiation are CO_2 and H_2O. If calculating with soot, soot radiation effects can also be applied. The radiation factor, f_{r}, represents the fraction of volume of burned gas (high temperature) to unburned gas (low temperature). In the hypothetical situation of an infinite flame front this fraction is 0.5 but this value can be changed to match the simulation to experimental results.

13.4.1.1 Freely Propagating Flame

For a flat, freely propagating flame, the appropriate reference system is fixed to the propagating flame. Thus any observer following the flame would experience the unburned mixture of fuel and oxidants approaching at the (laminar) burning velocity, s_{L}. The continuity equation describes the conservation of momentum, ρu, over the flame zone and, since the density of the burned (hot) gases is lower, continuity requires that the speed of the burned gases is higher than that of the unburned gases. Integration of Eq. (13.42) yields

$$\rho_{\mathrm{u}} u_{\mathrm{u}} = \rho_{\mathrm{u}} s_{\mathrm{L}} = \rho_{\mathrm{b}} u_{\mathrm{b}}$$

The fundamental property of a premixed flame, the laminar flame speed, can be found by solving the conservation equations above. s_{L} is strongly dependent on the fuel mixture and the equivalence ratio. The burning velocity is at its maximum close to stoichiometric conditions and falls off as the mixture becomes leaner or richer as these conditions yield a lower flame temperature.

13.4.1.2 Burner Stabilised Flame

The burner stabilised flame is a premixed flame that originates from a burner consisting of a multiple of small pipes through which the premixed gas flows.

A solution is defined at $z \in [0, \infty)$ where $z = 0$ defines the burner surface. The model includes

radical recombination of the radical species O, OH, HO$_2$ and H at the burner surface:

$$Y_i(0) = 0, \qquad i = i_O, i_{OH}, i_{HO_2}, i_H$$

13.5   Mechanism Analysis

13.5.1   Reaction Flow Analysis

The reaction flow analysis describes the importance of reaction paths in the mechanism under the specified conditions. The analysis is performed through calculation of the transfer rate of elements between molecular species. LOGEsoft analyses all elements present in the chemical mechanism. The flow of atoms between the reacting molecules is used as a measure of the relevance of the species in the reaction mechanism. The reaction flow of atom a between species i and species j can be described very simply [154]:

$$f_{i,j}^a = \sum_{k=1}^{N_r} \omega_k \left(n_i^a \nu_{i,k} - n_j^a \nu_{j,k} \right) \tag{13.45}$$

The sum in Eq. (13.45) is carried out over the set of N_r irreversible reactions with reaction rate ω_k. n_i^a and n_j^a are the numbers of atom a in moleculrs i and j and $\nu_{i,k}$ and $\nu_{j,k}$ are the stoichiometric coefficients for the molecules i and j in reaction k.

In LOGEsoft, forward and backward reactions are treated separately so as to capture reversible reaction pairs in which the flow of atoms is high in both directions but where the net flow is not necessarily high. This procedure results in the two new flow parameters shown below (13.46, 13.47) in which $f_{i,j}^a$ is the flow of atom a by the formation of species i from species j and $c_{i,j}^a$ is the flow of atom a by the consumption of species i to species j

$$f_{i,j}^a = \sum_{k_f=1}^{N_r} \left(\omega_{k_f} \nu'_{j,k_f} \nu''_{i,k_f} \right) \frac{n_i^a}{\Delta n_{k_f}^a} \tag{13.46}$$

$$c_{i,j}^a = \sum_{k_b=1}^{N_r} \left(\omega_{k_b} \nu''_{j,k_b} \nu'_{i,k_b} \right) \frac{n_j^a}{\Delta n_{k_b}^a} \tag{13.47}$$

where subscript f denotes a forward reaction and subscript b denotes a backward reaction. The number of atoms n_j^a is normalised to the total number of atoms transported in the reaction, $\Delta n_{k_f}^a = \sum_{i=1}^{N_s} \nu'_{i,k_f} n_i^a$. To obtain a flow value representative of the full ignition process, the integral over time is calculated. The net flow is calculated for each species combination and atom:

$$F_{i,j}^a = \int_{t=t_0}^{t_1} f_{i,j}^a dt - \int_{t=t_0}^{t_1} c_{i,j}^a dt$$

The LOGEsoft GUI creates a flow path graph of the integral net flows, $F_{i,j}$. If $F_{i,j} > 0$, the arrow points from species j to species i. The flow values are given in mole/m^3 for gas phase reactions and mole/m^2 for surface reactions. An example graph is given in 110, which shows the flow of C atoms in a reaction mechanism for an n-heptane fuelled homogeneous reactor. Major reaction flows are marked by thick arrows and the minor flows by thin arrows.

13.5.2 Sensitivity Analysis

A chemical system consists of a mechanism containing a set of differential equations. The equations describe the evolution of the concentrations of the various species during the combustion process, thus representing the species conservation equations. The system itself is most often defined in terms of mole or mass fractions of the following form

$$\frac{\partial Y}{\partial t} = P(Y, u, T) + \omega(Y, T) \tag{13.48}$$

Here $P(Y, u, T)$ represents the spatial differential operator (advection, convection and diffusion) thus dependent on the velocity field, u, and the temperature T, and $\omega(Y, T)$ represents the chemical source term, which includes chemical production and consumption of the species. Y is the N_s-dimensional vector of mass fractions of a mechanism containing N_s species. Sensitivity analysis involves investigation of the change in a quantity of interest due to small changes in the controlling parameters [155]. The investigation is of interest in itself for gaining insight into the reaction model but is in addition a very useful tool for reduction of reaction mechanisms. After the minor flows have been detected by reaction flow analysis, it is important to ensure that the species involved in the minor flows do not influence the result significantly as they in that case should be included in further investigations. In local sensitivity analysis, the sensitivity is described by the partial derivative of the investigated quantity with respect to the controlling parameters.

Starting from Eq. (13.48), investigation of how the concentration of a species i is influenced by a perturbation, Δk, of the rate coefficient k can be expressed through differentiation of the original set of chemical differential equations with respect to k_j and expansion of the right hand side. This gives the following equation:

$$\frac{d}{dt}\left(\frac{\partial Y}{\partial k_j}\right) = \frac{\partial P}{\partial Y}\frac{\partial Y}{\partial k_j} + \frac{\partial P}{\partial k_j} + \frac{\partial \omega(t)}{\partial Y}\frac{\partial Y}{\partial k_j} + \frac{\partial \omega(t)}{\partial k_j}, \qquad j = 1, \ldots, N_s \tag{13.49}$$

For a homogeneous system $P = 0$ and Eq. (13.49) is reduced to

$$\frac{d}{dt}\left(\frac{\partial Y}{\partial k_j}\right) = J(t)\frac{\partial Y}{\partial k_j} + \frac{\partial \omega(t)}{k_j}, \qquad j = 1, \ldots, N_s \tag{13.50}$$

where $J(t) = \partial \omega(t)/\partial Y$ is the Jacobian matrix and the initial condition for $\partial Y/\partial k_j$ (recognised as the sensitivity matrix) is a vector containing only zeroes [156].

The same method can be applied to investigate the sensitivities of parameters such as flame temperature for premixed flames or ignition timing in engine simulations. The information obtained through analysis acts as basis for reduction of the mechanism.

In LOGESOFT, the sensitivity analysis is a representation of a simultaneous reaction flow and sensitivity analysis. Sensitivities are transported through the mechanism in the sense that a species is rated according to its own importance and its involvement in the production or consumption of important species [155]. The species sensitivity, defined for each species, represents the species' sensitivity towards a chosen parameter A, and is the sum of the reaction sensitivities in which the species

participates:

$$S^S_{A,i} = \frac{\partial \psi_A}{\partial c_i} \approx \sum_{k=1}^{N_r} \frac{\partial \psi_A}{\partial r_k} \frac{\partial r_k}{\partial c_i} \tag{13.51}$$

With $c_i = c_{i0} + \epsilon_i$. Here $S^S_{A,i}$ contains the information on how sensitive an arbitrary parameter A in the vector of unknowns, ψ_A is to species i. By differentiating the last term of Eq. (13.51)

$$\frac{\partial r_k}{\partial c_i} = v'_{i,k} c_i^{|v'_{i,k}-1|} \prod_{\substack{j=1 \\ j \neq i}}^{N_s} c_j^{v'_{j,k}} k_k = \frac{v'_{i,k}}{c_{i0}} r_k$$

one obtains the final expression for the species sensitivity:

$$S^S_{A,i} = \left| \sum_{k=1}^{N_r} \frac{\partial \psi_A}{\partial r_k} \frac{v'_{i,k}}{c_i} r_k \right| \tag{13.52}$$

A species is assigned a relative redundancy index which represents how important the species is for changes in parameter A relative to the other species. The redundancy index is based on the species sensitivity according to Eq. (13.52).

$$I_i = \frac{S^S_{A,i}}{\max_{k=1,N_s}(S^S_{A,k})}$$

Even if a species has a low redundancy it can be assigned a high overall redundancy index if there is a significant flow of atoms from this species to or from an important species. The overall redundancy is determined by Eq. (13.53).

$$\bar{I}_i = \max(I_j f^a_{i,j}, \quad I_j c^a_{i,j}, \quad I_i; \quad j = 1, N_s, a = 1, N_a) \tag{13.53}$$

Eq. (13.53) needs to be solved iteratively with a preset value of $\bar{I}_i$. Species with a low overall $\bar{I}_i$ are considered to be redundant.

13.5.3   Necessity Analysis

A necessity analysis takes both flow analysis and sensitivity analysis into account to give an improved tool for reduction. This concept was introduced by Soyhan et al. [155, 27] and sucessfully applied in mechanism reduction [134, 82]. The analysis regards a number of user-defined species — necessity analysis targets — to find the reactions and species most necessary for the formation and consumption of said targets. This analysis can be very useful for instance when investigating the emissions of combustion of a certain fuel.

A detailed description can be found in the chapter about the reduction methods: 10.1.2.

13.5.4   Lifetime Analysis

The lifetime analysis method concerns the chemical lifetime of an individual species. Lifetime analysis is used for finding species eligible for the quasi steady state assumption, i.e. species for which the reactions consuming them are much faster than the reactions producing them. Species having much

faster consumption than production are very short lived and low in concentration.

Since a chemical system is strongly non-linear, carrying out a lifetime analysis requires that the system is linearised around a starting point Y_0. This results in Eq. (13.54), which corresponds to Eq. (13.48) with the spatial operator neglected.

$$\frac{dY}{dt} = \omega(Y) \rightarrow \frac{d}{dt}(Y - Y_0) = \omega_0 + J(Y - Y_0) \tag{13.54}$$

Here $Y - Y_0 \rightarrow 0$ and J is the Jacobian matrix with respect to the chemical source terms ω. The Jacobian matrix holds information regarding the rate of change in the source terms of the species when a change in species concentrations occurs. The error, ΔY_i, introduced by the steady state approximation of a species is calculated as [156]:

$$\Delta Y_i = \frac{1}{J_{i,i}} \frac{dY_i}{dt} \tag{13.55}$$

The dimension of $J_{i,i}$ is 1/time which means that the inverse of the Jacobian elements can be interpreted as the characteristic timescale of the species in question. From Eq. (13.55) it can be seen that a short lifetime, i.e. a small $\frac{1}{J_{i,i}}$ or a slow rate of change for a species, results in a small error in the calculated concentration.

In line with the reasoning above and expanding the Jacobi elements accordingly, the chemical lifetime can be expressed as

$$\tau_i = \frac{1}{\frac{d\omega_i}{dc_i}} = \frac{dc_i}{d\omega_i} = \frac{\int dci}{\int d\omega_i} = \frac{c_i}{\sum_{k=1}^{N_r} \left(v'_{i,k} - v''_{i,k} \right)} v'_{i,k} r'_k$$

where ω_i represents the species source term in terms of concentrations, c_i, $v_{i,k}$ is the stoichiometric coefficient (the prime denoting reactant properties, the double prime denoting product values) and r_k is the reaction rate for reaction k. In these terms, the chemical lifetime can be interpreted as a measure of how fast a particular species is consumed after being produced. The species with the shortest lifetimes are appropriate to set as steady state species.

14   Appendix II

14.1   List of Different Multicomponent Mixtures in Different Fractions

The conversion mixtures fractions in different fraction can be very confusing and lead to miss understandings. Fuel mixtures are often given in molar fraction (among chemists), liquid volume fraction (used by most humans) or even mass fraction. The table below may spare the reader the conversion.

Fuels	Liquid volume fraction	Molar fraction
n-Heptane / Toluene	90 / 10	88.5 / 11.5
n-Heptane / Toluene	35 / 65	28.0 / 72.0
n-Heptane / Toluene	40 / 60	43.9 / 56.1
iso-octane / Toluene	90 / 10	89.9 / 10.1
iso-octane / Toluene	40 / 60	40.3 / 59.7
iso-octane / n-heptane	10 / 90	10.2 / 89.8
iso-octane / n-heptane	50 / 50	50.5 / 49.5
iso-octane / n-heptane	60 / 40	60.4 / 39.6
iso-octane / n-heptane	75 / 25	75.3 / 24.7
iso-octane / n-heptane	80 / 20	80.3 / 19.7
iso-octane / n-heptane	90 / 10	90.2 / 9.8
iso-octane / n-heptane	95 / 5	95.1/ 4.9

Table 34: Different multicomponent fuels in liquid volume and molar fraction.

14.2   Ignition Delay Times of n-Heptan/Toluene and iso-Octane/Toluene mixtures

The 2 figures below show the predicted ignition delay for stoechiometric n-heptane/toluene / air and iso-octane/toluene / air mixtures at 40 bar.

(a) n-heptane/toluene

(b) iso-octane/toluene
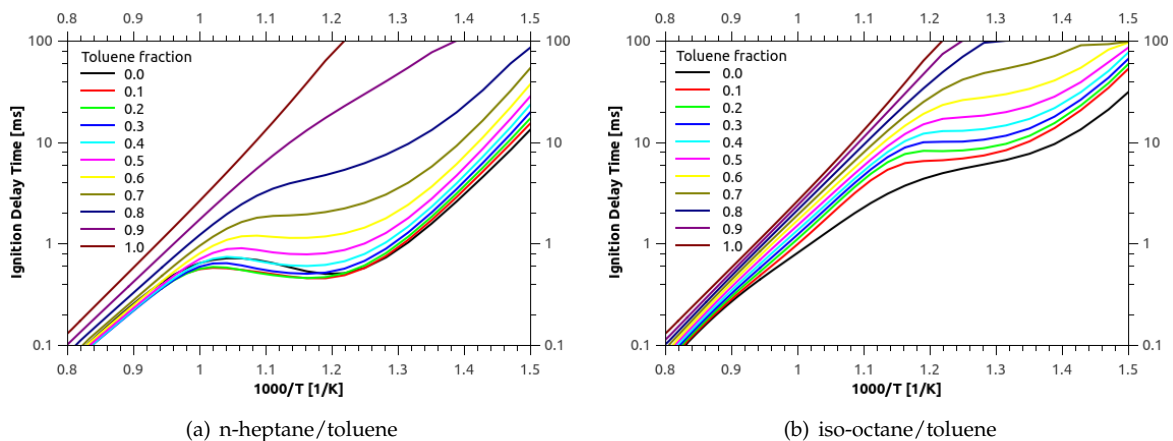
Figure 120: Predicted ignition delay for stoechiometric n-heptane/toluene / air and iso-octane/toluene / air mixtures at 40 bar using the modified scheme. Mixtures in molar fractions.

14.3 Calculation of the liquid volume fraction

The liquid volume fraction was calculated as follows:

$$L_i = \frac{\frac{Y_i}{\rho_i}}{\frac{Y_e}{\rho_e} + \frac{Y_{tol}}{\rho_{tol}} + \frac{Y_{iO}}{\rho_{iO}} + \frac{Y_{nH}}{\rho_{nH}}}. \tag{14.1}$$

14.4 Additional Plots from the NACA Report 812

Pressure in inches Hb abs	Pressure in bar	BP Methanol [K]	BP Water [K]
60	≈ 2.0	≈ 356	≈ 399
70	≈ 2.3	≈ 360	≈ 398
100	≈ 3.4	≈ 371	≈ 410
150	≈ 5.0	≈ 385	≈ 425

Table 35: Boiling temperature was obtained from Refrop. The preheating temperatures of 250° Fahrenheit correspond to 121.1° Celsius or 394.2 Kelvin. Preheating Temperatures of 150° Fahrenheit correspond to 65.6° Celsius or 338.7 Kelvin or 21.6 ° Newton.
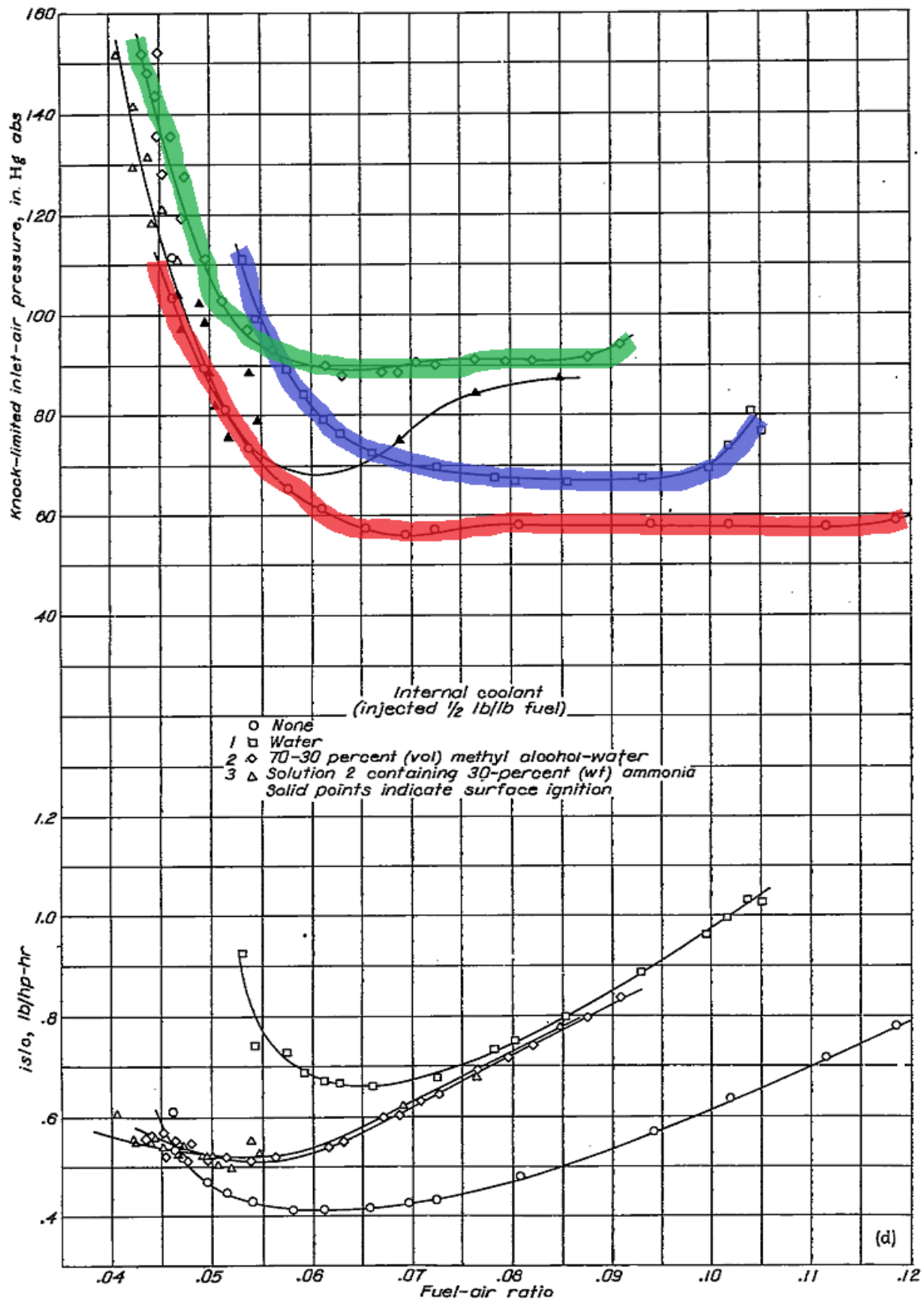
Figure 121: Fig 5d) from NACA Report 812 [64]. Colouring added by author for eye guidance. Original citation from [64]: *Figure 5 - Effect of internal coolants 1,2, and 3 on knock-limited engine performance. CFR engine; fuel, AN-F-28, compression ratio 7.0; inlet-coolant temperature, 250° F; spark advance, 30° B.T.C.; engine speed, 2500 rpm. Variation of indicated specific fuel consumptionand knock-limited inlet-air pressure with fuel-air ratio at temperature of 150° F.*
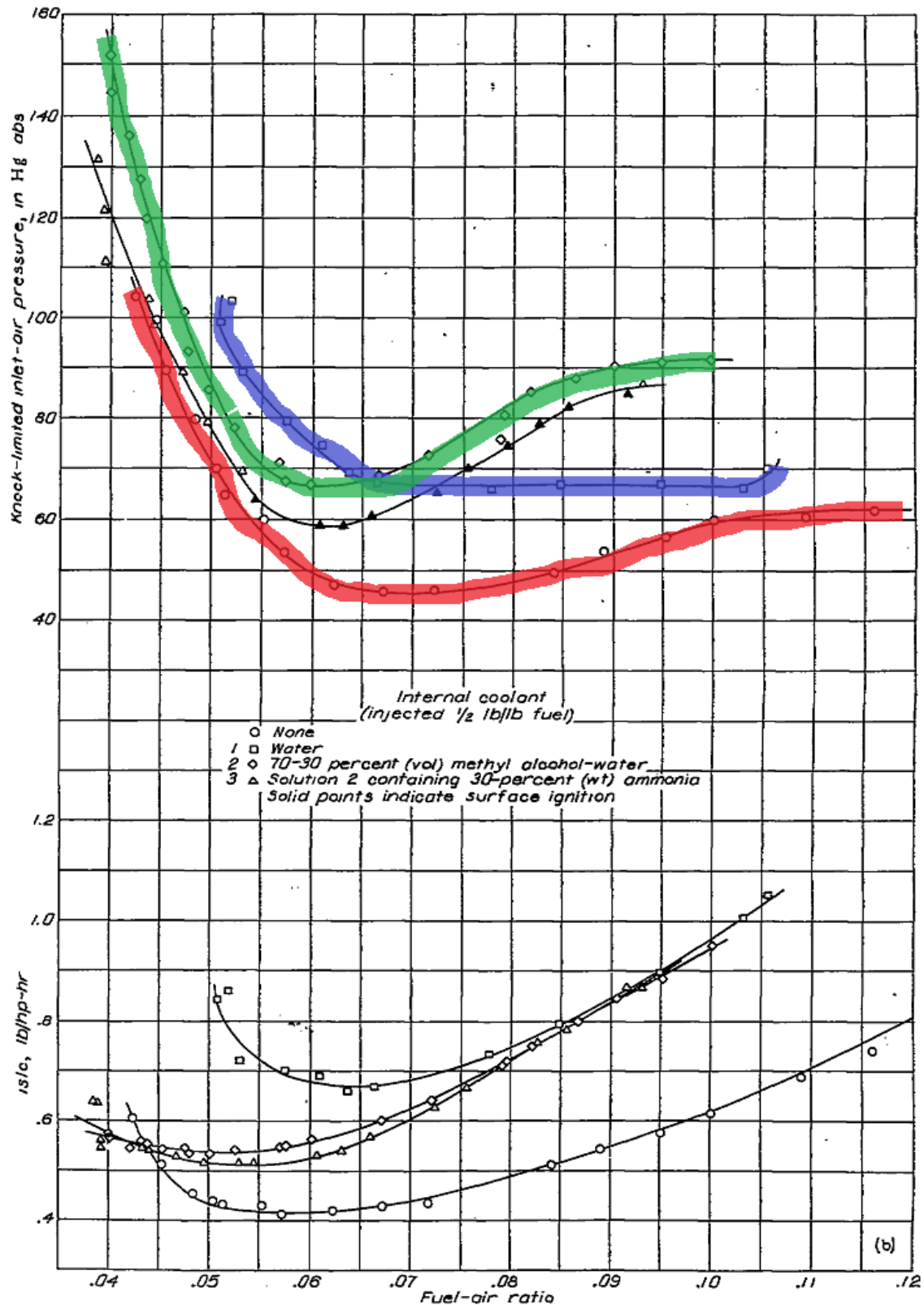
Figure 122: Fig 5b) from NACA Report 812 [64]. Colouring added by author for eye guidance. Original citation from [64]: *Figure 5 - Effect of internal coolants 1,2, and 3 on knock-limited engine performance. CFR engine; fuel, AN-F-28, compression ratio 7.0; inlet-coolant temperature, 250° F; spark advance, 30° B.T.C.; engine speed, 2500 rpm. Variation of indicated specific fuel consumptionand knock-limited inlet-air pressure with fuel-air ratio at temperature of 250° F.*

14.5 Nomenclature

| Symbol	Units	Description
AFR	-	Air - fuel ratio
c_p	$J/(kgK)$	Heat capacity (per unit mass)
d	m^2/s	Diffusion coefficient
h_{298}	J/kg	Enthalpy at 298K
k	mol, m^3, s	Reaction rate constant (unit depends on reaction type)
L_e	-	Liquid volume fraction of ethanol
L_{io}	-	Liquid volume fraction iso-octane
L_{nh}	-	Liquid volume fraction n-heptane
L_{tol}	-	Liquid volume fraction toluene
M or ω	kg/mol	Molar mass
N_a		Total number of elements
N_S		Total number of species
N_R		Total number of reactions
n	mol	Amount of substance
P	N/m^2	Pressure
R_0	$8.314 J/(molK)$	Ideal gas constant
$[S]$	mol/m^3	Species concentration
T	K	Temperature
V	m^3	Volume
V_a	-	Volume fraction aromatic species
V_a	-	Volume fraction ethanol
V_{io}	-	Volume fraction iso-octane
V_{nh}	-	Volume fraction n-heptane
V_{tol}	-	Volume fraction toluene
vapH	J/mol	Enthalpy of vaporisation
X_e	-	Molar fraction of ethanol
X_i	-	Molar fraction of species i
X_{io}	-	Molar fraction iso-octane
X_{nh}	-	Molar fraction n-heptane
X_{tol}	-	Molar fraction toluene
Y_e	-	Mass fraction of ethanol
Y_i	-	Mass fraction of species i
Y_{io}	-	Mass fraction iso-octane
Y_{nh}	-	Mass fraction n-heptane
Y_{tol}	-	Mass fraction toluene
α	$W/(m^2 s)$	Convective heat transfer coefficient
ϵ	-	Emissivity
λ	$W/(mK)$	Thermal conductivity
λ	-	Air -fuel equivalence ratio
ν	-	Stoichiometric coefficient
ρ	kg/m^3	Density
σ	$W/(m^2 K^4)$	Stefan-Boltzmann constant
σ	Å	Collision diameter
τ	s	Ignition delay time or residence time
ϕ or Φ	-	Fuel -air equivalence ratio
Ω or ω	-	Collision integral

Table 36: Nomenclature

References

[1] D.L. Baulch, C.J. Cobos, R.A. Cox, C. Esser, P. Frank, Th. Just, J.A. Kerr, M.J. Pilling, J. Troe, R.W. Walker, et al. Evaluated kinetic data for combustion modelling. *Journal of Physical and Chemical Reference Data*, 21(3):411–734, 1992.

[2] D.L. Baulch, C.J. Cobos, R.A. Cox, P. Frank, G. Hayman, Th. Just, J.A. Kerr, T. Murrells, M.J. Pilling, J. Troe, R.W. Walker, and J. Warnatz. Summary table of evaluated kinetic data for combustion modeling: Supplement 1. *Combustion and Flame*, 98(1-2):59–79, 1994.

[3] D.L. Baulch, C.T. Bowman, and C.J. Cobos. Evaluated kinetic data for combustion modeling: Supplement II. *Journal of Physical and Chemical Reference Data*, 34(3):757, 2005.

[4] W. Tsang. Chemical Kinetic Data Base for Combustion Chemistry. Part 2. Methanol. *Journal of Physical and Chemical Reference Data*, 16(3):471–508, 1987.

[5] W. Tsang. Chemical Kinetic Data Base for Combustion Chemistry. Part 3: Propane. *Journal of Physical and Chemical Reference Data*, 17(2):887–951, 1988.

[6] W. Tsang. Chemical Kinetic Data Base for Combustion Chemistry. Part 4: Isobutane. *Journal of Physical and Chemical Reference Data*, 19(1):1–68, 1990.

[7] W. Tsang. Chemical Kinetic Data Base for Combustion Chemistry. Part 5: Propene. *Journal of Physical and Chemical Reference Data*, 20(2):221–273, 1991.

[8] D.L. Allara and R. Shaw. A compilation of kinetic parameters for the thermal degradation of n-alkane molecules. *Journal of physical and chemical reference data*, 9(3):523–560, 1980.

[9] J.A. Badra, N. Bokhumseen, N. Mulla, S.M. Sarathy, A. Farooq, G. Kalghatgi, and P. Gaillard. A methodology to relate octane numbers of binary and ternary n-heptane, iso-octane and toluene mixtures with simulated ignition delay times. *Fuel*, 160:458–469, 2015.

[10] M. Olzmann and K. Scherzer. Zur unimolekularen beta-Spaltung großer n-Alkylradikale. *Berichte der Bunsengesellschaft für Physikalische Chemie*, 92:908–916, 1988.

[11] H.J. Curran, P. Gaffuri, W.J. Pitz, and C.K. Westbrook. A comprehensive modeling study of n-heptane oxidation. *Combustion and flame*, 114(1):149–177, 1998.

[12] S.M. Sarathy, C.K. Westbrook, M. Mehl, W.J. Pitz, C. Togbe, P. Dagaut, H. Wang, M.A. Oehlschlaeger, U. Niemann, K. Seshadri, P.S. Veloo, C. Ji, F.N. Egolfopoulos, and T. Lu. Comprehensive chemical kinetic modeling of the oxidation of 2-methylalkanes from C7 to C20. *Combustion and Flame*, 158(12):2338–2357, 2011.

[13] C.K. Westbrook, W.J. Pitz, O. Herbinet, J. Curran, and E.J. Silke. A comprehensive detailed chemical kinetic reaction mechanism for combustion of n-alkane hydrocarbons from n-octane to n-hexadecane. *Combustion and Flame*, 156(1):181–199, 2009.

[14] S.S. Ahmed, F. Mauss, G. Moréac, and T. Zeuch. A comprehensive and compact n-heptane oxidation model derived using chemical lumping. *Physical Chemistry Chemical Physics*, 9:1107–1126, 2007.

[15] O. Herbinet, B. Husson, Z. Serinyel, M. Cord, V. Warth, R. Fournet, P.-A. Glaude, B. Sirjean, F. Battin-Leclerc, Z. Wang, M. Xie, Z. Cheng, and F. Qi. Experimental and modeling investigation of the low-temperature oxidation of n-heptane. *Combustion and Flame*, 159(12):3455–3471, 2012.

[16] M. Pelucchi, M. Bissoli, C. Cavallotti, A. Cuoci, T. Faravelli, A. Frassoldati, E. Ranzi, and A. Stagni. Improved Kinetic Model of the Low-Temperature Oxidation of n - Heptane. *Energy & Fuels*, 28(11):7178–7193, 2014.

[17] C. Chevalier, W.J. Pitz, J. Warnatz, C.K. Westbrook, and H. Melenk. Hydrocarbon ignition: Automatic generation of reaction mechanisms and applications to modeling of engine knock. *Symposium (International) on Combustion*, 24(1):93–101, 1992.

[18] E. Ranzi, T. Faravelli, P. Gaffuri, and A. Sogaro. Low-temperature combustion: Automatic generation of primary oxidation reactions and lumping procedures. *Combustion and Flame*, 102(1-2):179–192, 1995.

[19] V. Warth, F. Battin-Leclerc, R. Fournet, P.A. Glaude, G.M. Côme, and G. Scacchi. Computer based generation of reaction mechanisms for gas-phase oxidation. *Computers and Chemistry*, 24(5):541–560, 2000.

[20] E.S. Blurock. Detailed mechanism generation. 1. Generalized reactive properties as reaction class substructures. *Journal of chemical information and computer sciences*, 44(4):1336–47, 2004.

[21] G. Moréac, E.S. Blurock, and F. Mauss. AUTOMATIC GENERATION OF A DETAILED MECHANISM FOR THE OXIDATION OF n-DECANE. *Combustion Science and Technology*, 178:2025–2038, 2006.

[22] K.M. Van Geem, M.F. Reyniers, G.B. Marin, J. Song, W.H. Green, and D.M. Matheu. Automatic reaction network generation using RMG for steam cracking of n-hexane. *AIChE Journal*, 52(2):718–730, 2006.

[23] M. Hilbig, L. Seidel, X. Wang, F. Mauss, and T. Zeuch. Computer aided detailed mechanism generation for large hydrocarbons: n-decane. *23rd ICDERS*, pages 24–27, 2011.

[24] R. Van de Vijver, N.M. Vandewiele, P.L. Bhoorasingh, B.L. Slakman, F. Seyedzadeh Khanshan, H.-H. Carstensen, M.-F. Reyniers, G.B. Marin, R.H. West, and K.M. Van Geem. Automatic Mechanism and Kinetic Model Generation for Gas- and Solution-Phase Processes: A Perspective on Best Practices, Recent Advances, and Future Challenges. *International Journal of Chemical Kinetics*, 47:199–231, 2015.

[25] T. Tsurushima. A new skeletal PRF kinetic model for HCCI combustion. *Proceedings of the Combustion Institute*, 32(2):2835–2841, 2009.

[26] C.V. Naik, C.K. Westbrook, O. Herbinet, W.J. Pitz, and M. Mehl. Detailed chemical kinetic reaction mechanism for biodiesel components methyl stearate and methyl oleate. *Proceedings of the Combustion Institute*, 33(1):383–389, 2011.

[27] H.S. Soyhan, F. Mauss, and C. Sorusbay. Chemical kinetic modeling of combustion in internal combustion engines using reduced chemistry. *Combustion Science and Technology*, 174(11-12):73–91, 2002.

[28] T. Lu and C.K. Law. A directed relation graph method for mechanism reduction. *Proceedings of the Combustion Institute*, 30(1):1333–1341, 2005.

[29] P. Pepiot-Desjardins and H. Pitsch. An efficient error-propagation-based reduction method for large chemical kinetic mechanisms. *Combustion and Flame*, 154(1-2):67–81, 2008.

[30] X.L. Zheng, T.F. Lu, and C.K. Law. Experimental counterflow ignition temperatures and reaction mechanisms of 1,3-butadiene. *Proceedings of the Combustion Institute*, 31(1):367–375, 2007.

[31] T. Turanyi and A.S. Tomlin. *Analysis of Kinetic Reaction Mechanisms*. Springer-Verlag Berlin Heidelberg, 1 edition, 2014.

[32] A. Matrisciano, A. Borg, C. Perlman, H. Lehtiniemi, M. Pasternak, and F. Mauss. Soot source term tabulation strategy for diesel engine simulations with srm. *SAE Technical Papers*, 2015, 2015.

[33] E.L. Petersen and R.K. Hanson. Nonideal effects behind reflected shock waves in a high-pressure shock tube. *Shock Waves*, 10(6):405–420, 2001.

[34] K. Heufer and H. Olivier. Determination of ignition delay times of different hydrocarbons in a new high pressure shock tube. *Shock Waves*, 20(4):307–316, 2010.

[35] Y.B. Zeldovich and Y.P. Raizer. *Physics of Shock Waves and High-Temperature Hydrodynamic Phenomena*. Dover Publications, INC Mineola, New York, dover edition, republication of 1966 edition, 2002.

[36] J. Herzler, M. Fikri, K. Hitzbleck, R. Starke, C. Schulz, P. Roth, and G.T. Kalghatgi. Shock-tube study of the autoignition of n-heptane/toluene/air mixtures at intermediate temperatures and high pressures. *Combustion and Flame*, 149(1-2):25–31, 2007.

[37] M. Hartmann, I. Gushterova, M. Fikri, C. Schulz, R. Schiessl, and U. Maas. Auto-ignition of toluene-doped n-heptane and iso-octane/air mixtures: High-pressure shock-tube experiments and kinetics modeling. *Combustion and Flame*, 158(1):172–178, 2011.

[38] K. Fieweger, R. Blumenthal, and G. Adomeit. Self-Ignition of S.I. engine Model Fuels: A Shock Tube Investigation at High Pressure. *Combustion and Flame*, 109:599–619, 1997.

[39] M. Hartmann and R. Starke. Untersuchung der Zündverzugszeiten im Stoßwellenrohr - Abschlussbericht. *Kraftstoffkenzahlen - TP 1 Stoßwellenrohr*, 2009.

[40] P. Dagaut, M. Reuillon, and M. Cathonnet. Experimental study of the oxidation of n-heptane in a jet stirred reactor from low to high temperature and pressures up to 40 atm. *Combustion and Flame*, 101(1-2):132–140, 1995.

[41] P. Osswald, K. Kohse-Hoinghaus, U. Struckmeier, T. Zeuch, L. Seidel, L. Leon, and F. Mauss. Combustion chemistry of the butane isomers in premixed low-pressure flames. *Zeitschrift fuer physikalische Chemie*, 225(9-10):1029–1054, 2011.

[42] M. Schenk, L. Leon, K. Moshammer, P. Osswald, T. Zeuch, L. Seidel, F. Mauss, and K. Kohse-Hoinghaus. Detailed mass spectrometric and modeling study of isomeric butene flames. *Combustion and Flame*, 160(3):487–503, 2013.

[43] L. Seidel, K. Moshammer, X. Wang, T. Zeuch, K. Kohse-Höinghaus, and F. Mauss. Comprehensive kinetic modeling and experimental study of a fuel-rich, premixed n-heptane flame. *Combustion and Flame*, 162(5):2045–2058, 2015.

[44] *SCIENTIFIC SOFTWARE FOR MODELLING OF CHEMICAL KINETIC SYSTEMS*. LOGE AB, Lund, Sweden, book 1-5 edition, 2016.

[45] B.M. Gauthier, D.F. Davidson, and R.K. Hanson. Shock tube determination of ignition delay times in full-blend and surrogate fuel mixtures. *Combustion and Flame*, (139):300–311, 2004.

[46] G. Kalghatgi. Auto-Ignition Quality of Practical Fuels and Implications for Fuel Requirements of Future SI and HCCI Engines. *SAE Technical Paper 2005-01-0239*, 2005.

[47] T.M. Foong, K.J. Morganti, M.J. Brear, G. da Silva, Y. Yang, and F.L. Dryer. The octane numbers of ethanol blended with gasoline and its surrogates. *Fuel*, 115:727–739, 2014.

[48] J.E Anderson, T.G. Leone, M.H. Shelby, T.J. Wallington, J.J. Bizup, M. Foster, M.G. Lynskey, and D. Polovina. Octane Numbers of Ethanol-Gasoline Blends: Measurements and Novel Estimation Method from Molar Composition. *SAE Technical Paper 2012-01-1274*, 2012.

[49] T. Midgley. Problem + research + capital=progress. *Industrial & Engineering Chemistry*, 31(5):504–506, 1939.

[50] E. Graham. Detonation specifications for automotive fuels. *SAE Technical Paper 270006*, 1927.

[51] F. Spausta. *Eigenschaften und Untersuchungen der flüssigen Treibstoffe. Die gasförmigen Treibstoffe.* Springer-Verlag Wien, 2 edition, 1953.

[52] J.B. Heywood. *Internal Combustion Engine Fundamentals*. McGraw Hill, 1988.

[53] H.R. Ricardo. *Schnellaufende Verbrennungsmaschinen*. Springer-Verlag Berlin Heidelberg, 1926.

[54] D. Bradley, C. Morley, and H. Walmsley. Relevance of research and motor octane numbers to the prediction of engine autoignition. *SAE Technical Paper 2004-01-1970*, 2004.

[55] J.C.G. Andrae, P. Björnbom, R.F. Cracknell, and G.T. Kalghatgi. Autoignition of toluene reference fuels at high pressures modeled with detailed chemical kinetics. *Combustion and Flame*, 149(1-2):2–24, 2007.

[56] K. Kohse-Höinghaus, P. Osswald, T.A. Cool, T. Kasper, N. Hansen, F. Qi, C.K. Westbrook, and P.R. Westmoreland. Biofuel combustion chemistry: from ethanol to biodiesel. *Angewandte Chemie (International ed. in English)*, 49(21):3572–97, 2010.

[57] N. Morgan, A. Smallbone, A. Bhave, M. Kraft, R. Cracknell, and G. Kalghatgi. Mapping surrogate gasoline compositions into RON/MON space. *Combustion and Flame*, 157(6):1122–1131, 2010.

[58] J.E. Anderson, U. Kramer, S.A. Mueller, and T.J. Wallington. Octane Numbers of Ethanol- and Methanol- Gasoline Blends Estimated from Molar Concentrations. *Energy & Fuels*, 24(12):6576–6585, 2010.

[59] T. Wallner, A. Ickes, and K. Lawyer. Analytical Assessment of C2–C8 Alcohols as Spark-Ignition Engine Fuel. *Proceedings of the FISITA 2012 World Automotive Congress*, pages 365–376, 2013.

[60] H.C. Barnet. Antiknock Evaluation Of Hydrocarbons And Ethers As Aviation Fuel Components. Technical report, Lewis Flight Propulsion Laboratory, Cleveland, Ohio, 1950.

[61] V. Knop, M. Loos, C. Pera, and N. Jeuland. A linear-by-mole blending rule for octane numbers of n-heptane/iso-octane/ toluene mixtures. *Fuel*, 115:666–673, 2014.

[62] Bruce Hamilton. FAQ: Automotive Gasoline, 1997.

[63] F.M. Haas and F.L. Dryer. Application of blending rules for ignition quality metrics: A comment on "A linear-by-mole blending rule for octane numbers of n-heptane/iso-octane/toluene mixtures". *Fuel*, 120:240–242, 2014.

[64] D.R. Bellman and J.C Evvard. Knock-Limited Performance of several Internal Coolants. Technical report, Aircraft Engine Research Laboratory, Cleveland, Ohio, 1944.

[65] G. Merker, C. Schwarz, G. Stiesch, and F. Otto. *Verbrennungsmotoren. Simulation der Verbrennung und Schadstoffbildung*. Teubner Verlag Wiesbaden, 3 edition, 2006.

[66] C. Pera and V. Knop. Methodology to define gasoline surrogates dedicated to autoignition in engines. *Fuel*, 96:59–69, 2012.

[67] G. Kalghatgi, H. Babiker, and J. Badra. A Simple Method to Predict Knock Using Toluene, N-Heptane and Iso-Octane Blends (TPRF) as Gasoline Surrogates. *SAE Int. J. Engines 8(2):505-519*, 2015.

[68] American Society of Testing Materials. *Annual book of ASTM Standards Vol. 5.01-5.05.*

[69] G. Kalghatgi, P. Risberg, and H.-E. Angstrom. A method of defining ignition quality of fuels in HCCI engines. *SAE Technical Paper 2003-01-1816*, 2003.

[70] C.M. Coats and A. Williams. Investigation of the ignition and combustion of n-heptane-oxygen mixtures. *Symposium (International) on Combustion*, 17(1):611–621, 1979.

[71] J. Warnatz, U. Maas, and R. W. Dibble. *Combustion: Physical and Chemical Fundamentals, Modeling and Simulation Experiments, Pollutant Formation*. Springer-Verlag, 2001.

[72] N. Semenov. Some problems relating to chain reactions and to the theory of combustion. *Nobel Lecture*, 1956.

[73] A. Nawdiyal, N. Hansen, T. Zeuch, L. Seidel, and F. Mauss. Experimental and modelling study of speciation and benzene formation pathways in premixed 1-hexene flames. *Proceedings of the Combustion Institute*, 35(1):325 – 332, 2015.

[74] K. Hoyermann, F. Mauß, and T. Zeuch. A detailed mechanism for the oxidation of hydrocarbons and its application to the analysis of benzene formation in fuel rich premixed laminar acetylene and propene flames. *Physical Chemistry Chemical Physics*, 6(14):3824–3835, 2004.

[75] T. Zeuch. *Reaktionskinetik von Verbrennungsprozessen in der Gasphase: Spektroskopische Untersuchungen der Geschwindigkeit, Reaktionsprodukte und Mechanismen von Elementarreaktionen und die Modellierung der Oxidation von Kohlenwasserstoffen mit detaillierten Reaktionsmechanismen*. PhD thesis, Georg-August-Universität zu Göttingen, 2003.

[76] F. Mauss. Entwicklung eines kinetischen modells der rußbildung mit schneller polymerisation. *Ph. D. Thesis RWTH Aachen University*, 1997.

[77] G. Vourliotakis, G. Skevis, and M.A. Founti. Detailed kinetic modelling of non-catalytic ethanol reforming for SOFC applications. *International Journal of Hydrogen Energy*, 34(18):7626–7637, 2009.

[78] N.M. Marinov. A Detailed Chemical Kinetic Model for High Temperature Ethanol Oxidation. *International Journal of Chemical Kinetics*, 31(3):183–220, 1999.

[79] J. Park, Z.F. Xu, and M.C. Lin. Thermal decomposition of ethanol. II. A computational study of the kinetics and mechanism for the H+C2H5OH reaction. *Journal of Chemical Physics*, 118(22):9990–9996, 2003.

[80] C.W. Wu, Y.P. Lee, S. Xu, and M.C. Lin. Experimental and Theoretical Studies of Rate Coefficients for the Reaction O (3P) + C2H5OH at High Temperatures. *Journal of Physical Chemistry A*, (11):6693–6703, 2007.

[81] S. Xu and M.C. Lin. Theoretical study on the kinetics for OH reactions with CH3OH and C2H5OH. *Proceedings of the Combustion Institute*, 31(1):159–166, 2007.

[82] T. Zeuch, G. Moréac, S.S. Ahmed, and F. Mauss. A comprehensive skeletal mechanism for the oxidation of n-heptane generated by chemistry-guided reduction. *Combustion and Flame*, 155(4):651–674, 2008.

[83] S.S. Ahmed, F. Mauß, and T. Zeuch. The Generation of a Compact n-Heptane / Toluene Reaction Mechanism Using the Chemistry Guided Reduction (CGR) Technique. *Zeitschrift für Physikalische Chemie International journal of research in physical chemistry and chemical physics*, 233(4-5):551–563, 2009.

[84] R. Bounaceur, I. Da Costa, R. Fournet, F. Billaud, and F. Battin-Leclerc. Experimental and modeling study of the oxidation of toluene. *International journal of chemical kinetics*, 37(1):25–49, 2005.

[85] H. Hippler, C. Reihs, and J. Troe. Shock tube UV absorption study of the oxidation of benzyl radicals. 23(1):37–43, 1991.

[86] J.L. Emdee, K. Brezinsky, and I. Glassman. A kinetic model for the oxidation of toluene near 1200 K. *The Journal of Physical Chemistry*, 96(15):2151–2161, 1992.

[87] L. Seidel, C. Netzer, M. Hilbig, F. Mauss, C. Klauer, M. Pasternak, and A. Mastrisciano. SYSTEMATIC REDUCTION OF DETAILED CHEMICAL REACTION MECHANISMS FOR ENGINE APPLICATIONS. *Proceedings of the ASME 2016 Internal Combustion Fall Technical Conference*, (ICEF2016-9304), 2016.

[88] A. Matrisciano, L. Seidel, C. Klauer, H. Lehtiniemi, and F. Mauss. An a priori thermodynamic data analysis based chemical lumping method for the reduction of large and multi-component chemical kinetic mechanisms. *Proceedings of the 5th International Workshop on Model Reduction in Reaction Flows*, 2015.

[89] A. Matrisciano, L. Seidel, C. Klauer, F. Mauss, and H. Lehtiniemi. An a priori thermodynamic data analysis based on chemical lumping method for the reduction of large and multi-component chemical kinetic mechanisms. *Presentation 3rd Topical Workshop: Taming uncertainty in combustion chemistry: experiments and models, Budapest, Hungary*, 2015.

[90] H.K. Ciezki and G. Adomeit. Shock-tube investigation of self-ignition of n-heptane-air mixtures under engine relevant conditions. *Combustion and Flame*, 93(4):421–433, 1993.

[91] A.P. Kelley, A.J. Smallbone, D.L. Zhu, and C.K. Law. Laminar flame speeds of C5 to C8 n-alkanes at elevated pressures: Experimental determination, fuel similarity, and stretch sensitivity. *Proceedings of the Combustion Institute*, 33(1):963–970, 2011.

[92] A.J. Smallbone, W. Liu, C.K. Law, X.Q. You, and H. Wang. Experimental and modeling study of laminar flame speed and non-premixed counterflow ignition of n-heptane. *Proceedings of the Combustion Institute*, 32(1):1245–1252, 2009.

[93] K. Kumar, J.E. Freeh, C.J. Sung, and Y. Huang. Laminar Flame Speeds of Preheated iso-Octane/O2/N2 and n-Heptane/O2/N2 Mixtures. *Journal of Propulsion and Power*, 23(2):428–436, 2007.

[94] C. Ji, E. Dames, Y.L. Wang, H. Wang, and F.N. Egolfopoulos. Propagation and extinction of premixed C5-C12 n-alkane flames. *Combustion and Flame*, 157(2):277–287, 2010.

[95] S.G. Davis and C.K. Law. Laminar flame speeds and oxidation kinetics of iso-octane-air and n-heptane-air flames. *Symposium (International) on Combustion*, 27(1):521–527, 1998.

[96] P. Dirrenberger, P. Glaude, R. Bounaceur, H. Le Gall, Pires da Cruz, A.A. Konnov, and F. Battin-Leclerc. Laminar burning velocity of gasolines with addition of ethanol. *Fuel*, 115:162–169, 2014.

[97] J.P.J. van Lipzig, E.J.K. Nilsson, L.P.H. de Goey, and A.A. Konnov. Laminar burning velocities of n-heptane, iso-octane, ethanol and their binary and tertiary mixtures. *Fuel*, 90(8):2773–2781, 2011.

[98] S. Jerzembeck, N. Peters, P. Pepiot-Desjardins, and H. Pitsch. Laminar burning velocities at high pressure for primary reference fuels and gasoline: Experimental and numerical investigation. *Combustion and Flame*, (156):292–301, 2009.

[99] G. Broustail, P. Seers, F. Halter, G. Moréac, and C. Mounaim-Rousselle. Experimental determination of laminar burning velocity for butanol and ethanol iso-octane blends. *Fuel*, 90(1):1–6, 2011.

[100] B. Galmiche, F. Halter, and F. Foucher. Effects of high pressure, high temperature and dilution on laminar burning velocities and Markstein lengths of iso-octane/air mixtures. *Combustion and Flame*, 159(11):3286–3299, 2012.

[101] L. Sileghem, V.A. Alekseev, J. Vancoillie, K.M. Van Geem, E.J.K. Nilsson, S. Verhelst, and A.A. Konnov. Laminar burning velocity of gasoline and the gasoline surrogate components iso-octane, n-heptane and toluene. *Fuel*, 112:355–365, 2013.

[102] D. Bradley, R.A. Hicks, M. Lawes, C.G.W. Sheppard, and R. Woolley. The measurement of laminar burning velocities and Markstein numbers for iso-octane-air and iso-octane-n-heptane-air mixtures at elevated temperatures and pressures in an explosion bomb. *Combustion and Flame*, 115(1-2):126–144, 1998.

[103] E. Varea, V. Modica, B. Renou, and A.M. Boukhalfa. Pressure effects on laminar burning velocities and Markstein lengths for Isooctane-Ethanol-Air mixtures. *Proceedings of the Combustion Institute*, 34(1):735–744, 2013.

[104] M.P. Dunphy and J.M. Simmie. High-temperature oxidation of ethanol. part 1.-ignition delays in shock waves. *J. Chem. Soc., Faraday Trans.*, 87:1691–1696, 1991.

[105] M.P. Dunphy, P.M. Patterson, and J.M. Simmie. High-temperature oxidation of ethanol. part 2.-kinetic modelling. *J. Chem. Soc., Faraday Trans.*, 87:2549–2559, 1991.

[106] P.S. Veloo, Y.L. Wang, F.N. Egolfopoulos, and C.K. Westbrook. A comparative experimental and computational study of methanol, ethanol, and n-butanol flames. *Combustion and Flame*, 157(10):1989–2004, 2010.

[107] D. Bradley, M. Lawes, and M.S. Mansour. Explosion bomb measurements of ethanol-air laminar gaseous flame characteristics at pressures up to 1.4 MPa. *Combustion and Flame*, 156(7):1462–1470, 2009.

[108] G. Broustail, F. Halter, P. Seers, G. Moréac, and C. Mounaïm-Rousselle. Experimental determination of laminar burning velocity for butanol/iso-octane and ethanol/iso-octane blends for different initial pressures. *Fuel*, 106:310–317, 2013.

[109] H.S. Shen, J. Steinberg, J. Vanderover, and M.A. Oehlschlaeger. A shock tube study of the ignition of n-heptane, n-decane, n-dodecane, and n-tetradecane at elevated pressures. *Energy & Fuels*, 23(5):2482–2489, 2009.

[110] S.G. Davis and C.K. Law. Determination of and Fuel Structure Effects on Laminar Flame Speeds of C1 to C8 Hydrocarbons. *Combustion Science and Technology*, 140(1-6):427–449, 1998.

[111] T. Hirasawa, C.J. Sung, A. Joshi, Z. Yang, H. Wang, and C.K. Law. Determination of laminar flame speeds using digital particle image velocimetry: Binary Fuel blends of ethylene, n-Butane, and toluene. *Proceedings of the Combustion Institute*, 29(2):1427–1434, 2002.

[112] R.J. Johnston and J.T. Farrell. Laminar burning velocities and Markstein lengths of aromatics at elevated temperature and pressure. *Proceedings of the Combustion Institute*, 30(1):217–224, 2005.

[113] M. Fikri, J. Herzler, R. Starke, C. Schulz, P. Roth, and G.T. Kalghatgi. Autoignition of gasoline surrogates mixtures at intermediate temperatures and high pressures. *Combustion and Flame*, (152):276–281, 2008.

[114] U. Burke, W.K. Metcalfe, S.M. Burke, K.A. Heufer, P. Dagaut, and H.J. Curran. A detailed chemical kinetic modeling, ignition delay time and jet-stirred reactor study of methanol oxidation. *Combustion and Flame*, 165:125–136, 2016.

[115] K.E. Noorani, B. Akih-Kumgeh, and J.M. Bergthorson. Comparative High Temperature Shock Tube Ignition of C1-C4 Primary Alcohols. *Energy & Fuels*, 24(11):5834–5843, 2010.

[116] L. Sileghem, V.A. Alekseev, J. Vancoillie, E.J.K. Nilsson, S. Verhelst, and A.A. Konnov. Laminar burning velocities of primary reference fuels and simple alcohols. *Fuel*, 115:32–40, 2014.

[117] F.N. Egolfopoulos, D.X. Du, and C.K. Law. A study on ethanol oxidation kinetics in laminar premixed flames, flow reactors, and shock tubes. *Symposium (International) on Combustion*, 24(1):833–841, 1992.

[118] K. Saeed and C.R. Stone. Measurements of the laminar burning velocity for mixtures of methanol and air from a constant-volume vessel using a multizone model. *Combustion and Flame*, 139(1-2):152–166, 2004.

[119] F. Halter, T. Tahtouh, and C. Mounaïm-Rousselle. Nonlinear effects of stretch on the flame front propagation. *Combustion and Flame*, 157(10):1825–1832, 2010.

[120] O. Park, P.S. Veloo, N. Liu, and F.N. Egolfopoulos. Combustion characteristics of alternative gaseous fuels. *Proceedings of the Combustion Institute*, 33(1):887–894, 2011.

[121] K.J. Bosschaart and L.P.H. de Goey. The laminar burning velocity of flames propagating in mixtures of hydrocarbons and air measured with the heat flux method. *Combustion and Flame*, 136(3):261–269, 2004.

[122] K. Kumar, G. Mittal, C. Sung, and C. Law. An experimental investigation of ethylene/O2/diluent mixtures: Laminar flame speeds with preheat and ignition delays at high pressures. *Combustion and Flame*, 153(3):343–354, 2008.

[123] P.S. Veloo and F.N. Egolfopoulos. Studies of n-propanol, iso-propanol, and propane flames. *Combustion and Flame*, 158(3):501–510, 2011.

[124] S.Y. Liao, D.M. Jiang, Z.H. Huang, K. Zeng, and Q. Cheng. Determination of the laminar burning velocities for mixtures of ethanol and air at elevated temperatures. *Applied Thermal Engineering*, 27(2-3):374–380, 2007.

[125] M. Christensen, M.T. Abebe, E.J.K. Nilsson, and A.A. Konnov. Kinetics of premixed acetaldehyde+air flames. *Proceedings of the Combustion Institute*, 35(1):499–506, 2015.

[126] S.G. Davis, H. Wang, K. Breinsky, and C.K. Law. Laminar flame speeds and oxidation kinetics of benene-air and toluene-air flames. *Symposium (International) on Combustion*, 26(1):1025–1033, 1996.

[127] N. Lamoureux, H. El Merhubi, L. Pillier, S. de Persis, and P. Desgroux. Modeling of NO formation in low pressure premixed flames. *Combustion and Flame*, 163:557–575, 2016.

[128] G.P. Smith, D.M. Golden, M. Frenklach, N.W. Moriarty, B. Eiteneer, M. Goldenberg, C.T. Bowman, R.K. Hanson, S. Song, William C. Gardiner J., et al. GRI-Mech 3.0. *http://www. me. berkeley. edu/gri_mech*.

[129] P. Klaus. *Entwicklung eines detailierten Reaktionsmechanismus zur Modellierung der Bildung von Stickoxiden in Flammenfronten*. PhD thesis, Ruprecht-Karls-Universität Heidelberg 1997, 1997.

[130] A. Ahmed, G. Goteng, V.S.B. Shankar, K. Al-Qurashi, W.L. Roberts, and S.M. Sarathy. A computational methodology for formulating gasoline surrogate fuels with accurate physical and chemical kinetic properties. *Fuel*, 143:290–300, 2015.

[131] M. Mehl, W.J. Pitz, C.K. Westbrook, and H.J. Curran. Kinetic modeling of gasoline surrogate components and mixtures under engine conditions. *Proceedings of the Combustion Institute*, 33(1):193–200, 2011.

[132] E. Ranzi, C. Cavallotti, A. Cuoci, A. Frassoldati, M. Pelucchi, and T. Faravelli. New reaction classes in the kinetic modeling of low temperature oxidation of n-alkanes. *Combustion and Flame*, 162(5):1679–1691, 2014.

[133] R. Goscinny and A. Uderzo. Asterix the Gaul. 1961.

[134] T. Løvås, P. Amnéus, F. Mauss, and E. Mastorakos. Comparison of automatic reduction procedures for ignition chemistry. *Proceedings of the Combustion Institute*, 29(1):1387–1393, 2002.

[135] C. Olm, I.G. Zsély, T. Varga, H.J. Curran, and T. Turányi. Comparison of the performance of several recent syngas combustion mechanisms. *Combustion and Flame*, 162(5):1793–1812, 2014.

[136] A. Stagni, A. Frassoldati, A. Cuoci, T. Faravelli, and E. Ranzi. Skeletal mechanism reduction through species-targeted sensitivity analysis. *Combustion and Flame*, 163:382–393, 2016.

[137] M. Tunér. *Stochastic Reactor Models for Engine Simulations*. PhD thesis, Lund University, 2008.

[138] M. Pasternak, F. Mauss, A. Matrisciano, and L. Seidel. Simulation of Diesel surrogate fuels performance under engine conditions using 0D engine – fuel test bench. *Proc. COMODIA Conf.*, 8:536–541, 2012.

[139] C. Perlman, K. Frojd, L. Seidel, and F. Mauss. A Fast Tool for Predictive IC Engine In-Cylinder Modelling with Detailed Chemistry. *SAE 2012-01-1074*, 2012.

[140] M. Pasternak, F. Mauss, G. Janiga, and D. Thévenin. Self-calibrating model for diesel engine simulations. *SAE 2012-01-1072*, 2012.

[141] M. Pasternak, F. Mauss, C. Perlman, and H. Lehtiniemi. Aspects of 0D and 3D Modeling of Soot Formation for Diesel Engines. *Combustion Science and Technology*, 186(10-11):1517–1535, 2014.

[142] A. Matrisciano, M. Pasternak, X. Wang, O. Antoshkiv, F. Mauss, and P. Berg. On the Performance of Biodiesel Blends - Experimental Data and Simulations Using a Stochastic Fuel Test Bench. *SAE Technical Paper 2014-02-1115*, 2014.

[143] M. Tuner, K. Fröjd, L. Seidel, and F. Mauss. Diesel-PPC engine: Predictive Full Cycle Modeling with Reduced and Detailed Chemistry. *JSAE*, 01(1787):1–14, 2011.

[144] S. Pope. PDF methods for turbulent reactive flows. *Progress in Energy and Combustion Science*, 11(2):119–192, 1985.

[145] LOGEengine v1.04. Lund Combustion Engineering Loge AB, Lund, Sweden, 2015.

[146] H. Lehtiniemi, Y. Zhang, R. Rawat, and F. Mauss. Efficient 3-D CFD Combustion Modeling with Transient Flamelet Models. *SAE 2008-01-0957*, 2009.

[147] K. Netzell. *Development and Applications of Detailed Kinetic Models for the Soot Particle Size Distribution Function*. PhD thesis, Lund University, 2006.

[148] Y. Pei, M. Mehl, W. Liu, T. Lu, W.J. Pitz, and S. Som. A Multicomponent Blend as a Diesel Fuel Surrogate for Compression Ignition Engine Applications. *Journal of Engineering for Gas Turbines and Power*, 137(11):111502, 2015.

[149] L. Cai and H. Pitsch. Optimized chemical mechanism for combustion of gasoline surrogate fuels. *Combustion and Flame*, 162(5):1623–1637, 2015.

[150] F.A. Lindemann, S. Arrhenius, I. Langmuir, N.R. Dhar, J. Perrin, and W.C.McC. Lewis. Discussion on the radiation theory of chemical action". *Trans. Faraday Soc.*, 17(598), 1922.

[151] R.G. Gilbert, K. Luther, and J. Troe. Theory of thermal unimolecular reactions in the fall-off range. ii. weak collision rate constants. *Berichte der Bunsengesellschaft für physikalische Chemie*, 87(2):169–177, 1983.

[152] D. M. Golden P.H. Stewart, C. W. Larson. Pressure and temperature dependence of reactions proceeding via a bound complex. 2. application to 2CH3 $\rightarrow$ C2H5 + H. *Combustion and Flame*, 75:25–31, 1989.

[153] R. Bellanca. *BlueBellMouse - A Tool for Kinetic Model Development*. PhD thesis, Lund University, 2004.

[154] D. Nilsson. *Analysis and Reduction of Fuel and Pollutant Chemistry in Combustion Systems*. PhD thesis, Lund University, 2000.

[155] H. Soyhan, P. Amnéus, F. Mauss, and C. Sorusbay. A Skeletal Kinetic Mechanism for the Oxidation of Iso-Octane and N-Heptane Validated Under Engine Knock Conditions. *SAE Technical Paper 1999-01-3484*.

[156] A.S. Tomlin, T. Turányi, and M.J. Pilling. Mathematical tools for construction, investigation and reduction of combustion mechanisms. *Low-Temperature Combustion and Autoignition, Comprehensive Chemical Kinetics*, 35, 1997.